Analysis of CdgC as the major diguanylate cyclase in *S. venezuelae*

DISSERTATION

fulfillment of the requirements for the degree

DOCTOR RERUM NATURALIUM

(Dr. rer. nat.)

in the field of biology

submitted at the life science faculty

at the Humboldt University of Berlin

by

Sara Alina Neumann

President of the Humboldt University of Berlin

Prof. Dr.-Ing. Dr. Sabine Kunst

Dean of the life science faculty

Prof. Dr. Dr. Christian Ulrichs

Reviewers:

1. Prof. Dr. Natalia Tschowri
2. Prof. Dr. Regine Hengge
3. Prof. Dr. Kürşad Turgay

Date of the oral examination: 10.06.2021

This thesis was developed in the period between July 2016 and March 2020 in the laboratory of Prof. Dr. Natalia Tschowri at Humboldt University of Berlin.

Publications

Parts of the thesis have been published in:

M.M. Al-Bassam, J. Haist, **S.A. Neumann**[1], S. Lindenberg, and N. Tschowri. (2018). Expression Patterns, Genomic Conservation and Input Into Developmental Regulation of the GGDEF/EAL/HD-GYP Domain Proteins in *Streptomyces*. Frontiers in Microbiology. 9:2524. doi: 10.3389/fmicb.2018.02524. https://www.frontiersin.org/articles/10.3389/fmicb.2018.02524/full

J. Haist, **S.A. Neumann**[1], M.M. Al-Bassam, S. Lindenberg, M.A. Elliot, and N. Tschowri. (2020). Specialized and shared functions of diguanylate cyclases and phosphodiesterases in *Streptomyces* development. Molecular Microbiology, 114: 808–822. doi: 10.1111/mmi.14581. https://onlinelibrary.wiley.com/doi/full/10.1111/mmi.14581

[1]J. Haist and S.A. Neumann contributed equally to this work.

Acknowledgments

My fascination for molecular microbiology was first peaked during my time as a student assistant, where I prepared and supported courses in the department of microbiology at the Humboldt University in Berlin. For giving me this opportunity to learn while supporting the process of teaching, I want to thank Prof. Dr. Regine Hengge and Prof. Dr. Thomas Eitinger.

I am deeply indebted to my supervisor Prof. Dr. Natalia Tschowri, who allowed me to work on this exciting topic in her laboratory. She opened up this new universe for me, enriched my progress with stimulating discussions and encouraged me in my scientific life to this very day. Thanks to her constant support, I was able to present my work at international conferences and had the opportunity to continue working on my project in the laboratory of Prof. Dr. Marie A. Elliot (McMaster University, Hamilton, ON, Canada).

I was very lucky to be warmly welcomed by Prof. Elliot and her group, who broadened my methodical spectrum, gave me the opportunity to look at my project from another perspective and made me feel at home in her group.

At this point, I would like to thank the German Academic Exchange Service (DAAD) sincerely for awarding me with the doctoral fellowship, that enabled me to make this invaluable scientific and personal experience, enriching my PhD.

I feel a great urge to thank my external coauthors outside the research group surrounding Prof. Tschowri: Dr. Mahmoud M. Al-Bassam (University of California, San Diego, CA, USA) and Prof. Elliot. I want to thank my colleagues and former colleagues (in no particular order) Dr. Julian Haist, Dr. Sandra Lindenberg, Dr. Mirka Wörmann, Thi Kim Loan Nguyen, Dr. Diego Serra, Dr. Susanne Herbst, Dr. Friedrich Finkenwirth, Dr. Gisela Klauck, Franziska Skopp, Dr. Franziska Mika, Dr. Martin Lorkowski, Dr. Vanessa Pfiffer, Dr. Skander Hathroubi, Ronja Offer, Eike Junkermeier, Amita Bhatti, Jared Cocke, Dr. Katherina Preßler, Sinah Noemie Pecina, Mario Gäde, Maxim Bogisch, Victoria Riebe, Mandy Lawrenz, Cristina Martínez Reig, Jakob Johann Wiese, Julia Schneider, Dr. Mihaela Pruteanu, Felicitas Reindl, Dr. Christine Kanow-Scheel, Niclas Barke, Clara Missiha, Janina Krambrich and all I may have forgotten, for creating a pleasant and light work atmosphere.

Additionally, I want to give special thanks to Alexandra Poßling for uncountable, delightful morning coffee breaks, providing me with laughter and troubleshooting ideas in and outside the laboratory. In this context, I wish to give huge thanks to Raúl Trepel, who I am proud to call my friend: live long and prosper! For broadening my horizon regarding heavy metal in ions and notes, I would like to thank my dear college Dr. Andreas Latoscha: Merci!

I wish to extend my thanks to my family, my friends and my partner for all their love, moral support and joyful distractions exactly when needed.

Finally, I want to thank my reviewers for taking the time to review my thesis.

Contents

List of Figures

List of Tables

Abbreviations

APS	ammonium persulfate
A-site	active site
BGC	biosynthetic gene cluster
bp	base pairs
C-terminal	carboxy–terminal
c-di-GMP	bis-(3'-5')-cyclic dimeric guanosine monophosphate
CTD	carboxy–terminal domain
Da	Dalton
DBD	DNA-binding domain
dest.	distilled
DGC	diguanylate cyclase
DMSO	dimethyl sulfoxide
DNA	deoxyribonucleic acid
dNTP	desoxyribonucleoside triphosphate
$\texttt{EAL}_{\text{deg}}$	degenerate `EAL` domain
EDTA	ethylenediaminetetraacetic acid
EMSA	Electrophoretic mobility shift assay
gDNA	genomic DNA
GTP	guanosine triphosphate
i.a.	inter alia
IPTG	isopropyl-β-D-thiogalactopyranoside
I-site	inhibitory site
Kan	Kanamycin
LB	Lysogeny broth
M	molar
$MgCl_2$	magnesium chloride
$MgSO_4$	magnesium sulfate
mRNA	messenger RNA
N-terminal	amino–terminal
NaCl	sodium chloride
ODλ	optical density at a wavelength λ
oN	overnight
PAGE	polyacrylamide gel electrophoresis
PCR	polymerase chain reaction
PDE	phosphodiesterase
pH	*potentia hydrogenii*
(p)ppGpp	guanosine (penta)tetraphosphate
PVDF	polyvinylidene fluoride
RNA	ribonucleic acid

RNAP	RNA polymerase
rpm	revolutions per minute
RT	room temperature
SEM	scanning electron micrographs
TAE	Tris-Acetate-EDTA
Taq polymerase	polymerase from the bacteria *Thermus aquaticus*
TBE	Tris-borate-EDTA
TBST	Tris-buffered saline and tween 20
TCE	2,2,2-Trichloroethanol
TRIS	Tris(hydroxymethyl)-aminomethane
TSS	transformation and storage solution
WT	wild type
X-Gal	5-Bromo-4-chloro-3-indolyl-β-D-galactopyranoside

Summary

The Gram-positive soil bacteria *Streptomyces* represent the main source of bioactive secondary metabolites. Their proliferation is temporally and genetically coordinated with a complex developmental life cycle, including three main stages of differentiation: vegetative hyphal growth, formation of aerial mycelium and sporulation. The key factor of *Streptomyces* developmental control is c-di-GMP with to-date two identified effector proteins: the master regulator BldD, which binds tetrameric c-di-GMP, enabling repression of reproductive genes during the vegetative phase, and the recently discovered anti-sigma factor RsiG, which binds c-di-GMP, supporting complex formation with its corresponding sigma factor σ^{WhiG}. The sequestration of σ^{WhiG} inhibits the expression of genes, that are important for late sporulation.

In this thesis, one of ten c-di-GMP turnover proteins encoded in *S. venezuelae*, the membrane-associated `GGDEF-EAL` protein CdgC, was identified as a major active diguanylate cyclase (DGC), highly conserved in the genus *Streptomyces*. Deletion of *cdgC* results in the unique flat gray colony morphology with radial wrinkles and a hydrophilic surface, that shows enhanced sporulation without forming aerial hyphae. Phenotypic analyses comparing Δ*cdgC*, a variant with inactive `GGDEF` domain (*cdgC*$^{\texttt{ALLEF}}$) and a strain overexpressing the heterologous *S. coelicolor* DGC CdgB in Δ*cdgC* to the wild type (WT) suggest, that the DGC activity is essential for its biological role, but hint to an additional protein specific role. The protein levels of CdgC-FLAG were found to accumulate during the life cycle of *S. venezuelae*, which is in line with microarray data on *cdgC* expression, and showed a degradation pattern not associated with any tested protease. Further investigation of CdgC-FLAG in a strain carrying a DNA-binding deficient BldD_`D116A` allele indicated, that BldD represses the expression of CdgC in a regulatory feedback loop along with the DGCs CdgA, CdgB and CdgE. Enzymatic activities of the individual domains of CdgC were determined by using *in vitro* enzyme assays.

RNA-sequencing data indicated that reduced expression levels of chaplin and rodlin proteins, the major compounds of the hydrophobic sheath, result in the initiation of sporulation out of the vegetative mycelium. These results were verified by quantifying transcription levels of representative chaplins and their regulator σ^{BldN} via qRT-PCR. Furthermore, it was discovered that overexpressing ChpC/ChpE in Δ*cdgC* only partially restores the wild type phenotype. Confocal microscopic imaging of the bacterial tubulin homolog FtsZ fused to the YPet protein indicated a contribution of CdgC via its DGC activity in coordination of the cell division. This helps elucidate the importance and functional mechanism by which CdgC contributes to the coordination of the timing and location of the sporulation, affecting ∼20% of all *S. venezuelae* genes.

In addition, BTH screenings revealed self-interaction and identified three membrane associated interaction partners. One of them, Vnz08595, has an ortholog in *S. coelicolor*, which is known to influence cell division. This interplay might indirectly add to the c-di-GMP-sensitive influence on cell division proteins, like FtsZ, resulting in an alteration of sporulation initiation.

In conclusion, this study introduces the `GGDEF-EAL` tandem protein CdgC, whose specific knockout phenotype is governed by its DGC activity and membrane association. CdgC seems to drive timing and mode of sporulation in response to an unknown signal to a major extend.

Zusammenfassung

Streptomyceten sind grampositive Bodenbakterien und stellen die Hauptquelle für bioaktive Sekundärmetabolite dar. Ihre Entwicklung ist in einem komplexen Lebenszyklus koordiniert, der in drei Hauptentwicklungsstufen eingeteilt wird: vegetatives Hyphenwachstum, Bildung des Luftmycelen und Sporulation. C-di-GMP beeinflusst entscheidend die Entwicklung von *Streptomyces* über zwei Effektorproteine: dem Masterregulator der Entwicklung BldD und dem Anti-Sigmafaktor RsiG. Letzterer kann c-di-GMP-vermittelt effektiv an seinen Sigmafaktor σ^{WhiG} binden und die Expression der σ^{WhiG}-abhängig regulierten, späten Sporulationsgene inhibieren.

Im Rahmen dieser Doktorarbeit gelang es, eines der zehn im *S. venezuelae*-Genom kodierten c-di-GMP metabolisierenden Proteine, das membranständige `GGDEF-EAL` Protein CdgC, als eine der wichtigsten aktiven Diguanylatzyklasen (DGC) zu identifizieren. Eine chromosomale Deletion oder enzymatische Inaktivierung der Diguanylatzyklaseaktivität des in *Streptomyces* hoch konservierten *cdgC* Gens führten jeweils zu einer flachen, gräulich erscheinenden Koloniemorphologie mit radialen Stegen und einer hydrophilen Oberfläche. Dabei war eine verstärkte Sporulation ohne Lufthyphenbildung zu erkennen. Transkriptomischen Analysen zufolge waren etwa 20% aller offenen Leseraster in $\Delta cdgC$ beeinflusst. Trotz der Tatsache, dass die DGC-Aktivität von CdgC essentiell für dessen biologische Rolle scheint, deutet die nur teilweise Komplementierbarkeit des Wildtyp-Phänotyps durch die Überexpression der heterologen DGC CdgB aus *S. coelicolor* auf einen Protein-spezifischen morphologischen Effekt von CdgC hin. Die bereits auf transkriptioneller Ebene gezeigte Akkumulation von *cdgC* entlang des Lebenszyklus konnte auf translationellem Level bestätigt werden. Dabei zeigte sich ein Abbaumuster, welches mit keiner getesteten Protease spezifisch assoziiert werden konnte. Zudem scheint die Expression von CdgC BldD-abhängig mittels einer c-di-GMP vermittelten Feedbackschleife reguliert zu werden. Diese war in früheren Publikationen bereits für die DGC-kodierenden Gene *cdgA*, *cdgB* und später, parallel zu dieser Arbeit, für *cdgE* gezeigt worden.

CdgC trägt zur Koordination von Zellteilungs- und hydrophoben Zelloberflächenproteinen bei und beeinflusst damit c-di-GMP-abhängig den Zeitpunkt der Sporenbildung. Diesbezüglich deuteten frühere RNA-seq Analysen eine differentielle Expression der wichtigsten Bestandteile des hydrophoben Mantels, der Chaplin- und Rodlin-Proteine, an, was durch eine Quantifizierung der Transkriptmengen repräsentativer Chaplin-Gene und dem sie kontrollierenden σ^{BldN} verifiziert werden konnte. Überraschenderweise führte eine Überexpression von σ^{BldN} in $\Delta cdgC$ nur zu einem minimalen Anstieg der Hydrophobizität der Oberfläche, was auf den Einfluss weiterer Faktoren auf die Lokalisation der Sporulation hindeutet. Konfokalmikroskopische Aufnahmen des bakteriellen Tubulin-Homologons FtsZ deuten einen c-di-GMP-sensitiven Einfluss von CdgC auf die Koordination der Zellteilung an.

Zudem konnte nachgewiesen werden, dass CdgC, neben zwei weiteren potentiellen Membranproteinen, auch direkt mit Vnz08595 interagiert, dessen Orthologon in *S. coelicolor* bekanntermaßen die Zellteilung beeinflusst. Diese Interaktion könnte den c-di-GMP-abhängigen Einfluss von CdgC auf Zellteilungsproteine wie FtsZ indirekt ergänzen, was ein verändertes Einsetzen der Sporulation zur Folge hätte.

Insgesamt führt diese Studie CdgC als GGDEF-EAL-Tandemprotein mit spezifischem Knockout-Phänotyp ein, der von seiner DGC-Aktivität sowie seinem Membrananker bestimmt wird. Die Ergebnisse dieser Studie zeigen, dass CdgC, als Reaktion auf eine noch unbekannte Signalübertragungskaskade, an der Koordinierung von Zeitpunkt und Verlauf der Sporulation ausschlaggebend beteiligt ist.

Chapter 1

Introduction

1.1 *Streptomyces* as producers of bioactive compounds

When thinking of the GC-rich Gram-positive soil-dwelling organisms *Streptomyces* (family of Actinobacteria), the first key word that comes to mind is "antibiotics". Since the middle of the golden age of antibiotics, this class of the Actinobacteria represents the most abundant source of natural antibiotics and other medically relevant secondary metabolites. This ability to provide antibacterial compounds, and many other important agents such as anticancer and antifungal drugs, makes them especially interesting for medicine and industry (Hopwood, 2007). Some of them, like the chloramphenicol producing *S. venezuelae*, the actinorhodin and undecylprodigiosin producing *S. coelicolor* (Bentley et al., 2002) or the streptomycin encoding *S. griseus*, emerged as model organisms for *Streptomyces* research (Ohnishi et al., 2008).

To date, the rising number of pathogens showing a broad spectrum of resistances against regularly used antibiotics increases the pressure to discover new antibiotics and treatment options. One source of novel metabolites is the isolation of exceptional classes of antibiotics from more uncommon *Streptomyces* species (Vasilchenko et al., 2020). Bioinformatic analysis of the linear *Streptomyces* chromosome (Bentley et al., 2002), called "genome mining", revealed a multitude of natural products encoding gene clusters. The majority of them are transcriptionally silent under laboratory conditions, which led to them being called silent "biosynthetic gene clusters" (BGC) (Rigali et al., 2018). Keeping in mind that Actinobacteria, like *Streptomyces*, exist in manifold symbioses with all kingdoms of life in their natural habitat, this comes as no surprise. Its interactions with other organisms range from parasitic and pathogenic to beneficial and growth promoting (Seipke et al., 2012; Vurukonda et al., 2018). The influence of *Streptomyces*-produced secondary metabolites on other bacteria, fungi, plants, and animals remains unknown. These secondary metabolites might equip against the upcoming problem of antibiotic resistance as one of the major threats for global public health in the current century (Rigali et al., 2018).

Various attempts have been made to activate the expression of these silent BGCs using classical cloning or CRISPR-Cas9 mediated site-specific insertion of a constitutively active promoter (Ma et al., 2020; Tao et al., 2018). A more common approach to improve the yield of antibiotic production and decrypt silent BGCs in *Streptomyces* aims at a better understanding of their regulatory networks (Sánchez de la Nieta et al., 2020). Deeper insights into how *Streptomyces* regulators fine-tune the complex developmental life cycle and coordinate the interplay with plants, as well as their role as destruent recycling nutrients in terrestrial habitats, will improve our understanding of the production of cryptic metabolites.

1.2 More than "Divide and conquer" – the life cycle of *Streptomyces*

The proliferation of *Streptomyces* is temporally and genetically coordinated with a complex life cycle. It includes three main stages of differentiation: vegetative hyphal growth, formation of aerial mycelium and sporulation, as displayed in Fig. 1.1 (Flärdh et al., 2000; Bush et al., 2015). This life cycle is preeminent in the bacterial kingdom.

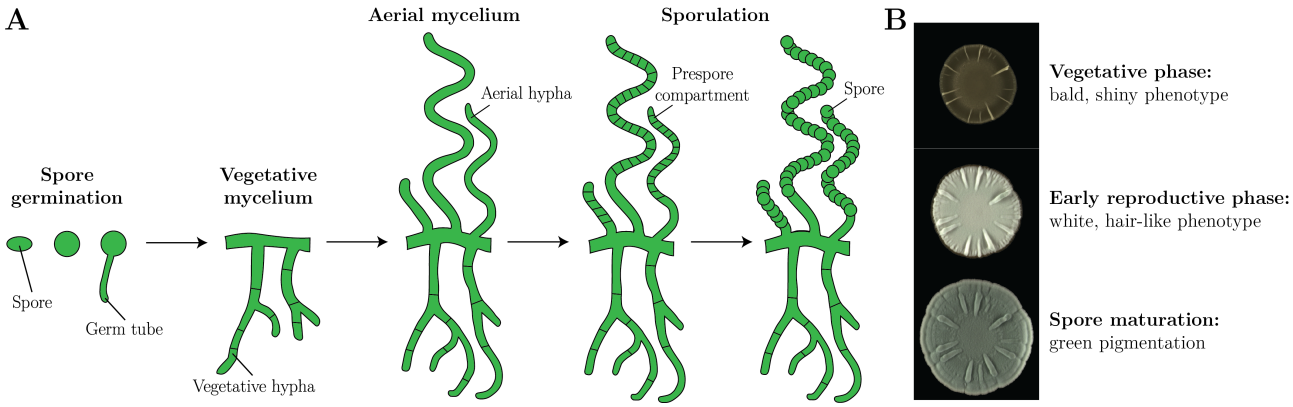

Fig. 1.1 The life cycle of *Streptomyces* (A) illustrated schematically and (B) macrocolonies (strain: SVSN6; see Table 6.4) of the distinct growth stages.

Germination. Unigenomic spores germinate under favorable conditions. The speed and effectiveness of germination varies highly within a population and between different *Streptomyces* species. Compared to other *Streptomyces*, *S. venezuelae* germinates rather slowly and incoherently. (Bobek et al., 2017; Wright & Vetsigian, 2019)

Hardisson et al. (1978) divide the process of germination into three distinct stages: darkening, swelling and emergence of the germ tubes. The first step is initiated by the loss of hydrophobicity of the spores. As a result, the cytoplasm rehydrates due to entering water, causing a swelling of the spore and the reactivation of the cell metabolism (Strakova et al., 2013). With the awakening of the cell metabolism, chaperons take over the protection of the cellular macromolecules, enabling proteins to refold into their functional conformation state (Bobek et al., 2004).

In parallel or shortly after the first DNA replication, the spore releases one or two not yet septated germ tubes originating from a location at the inner spore wall, determined by the chaperon-like SsgA protein (see Fig. 1.1) (Mikulík et al., 2002; Bobek et al., 2017). The accumulation of the DivIVA protein at the tip of the germ tubes is crucial for the beginning of vegetative growth (Bobek et al., 2017).

Vegetative growth. Processes of cell wall synthesis at the hyphal tips and *de novo* at lateral branching sites culminate into formation of a vegetative mycelium (Bush et al., 2015). The location and frequency of these growth sites are directed by the polarisome, which consists at its core of three coiled-coil proteins: DivIVA, Scy and FilP (Holmes et al., 2013).

DivIVA is the only essential protein and it localizes at growing hyphal tips and future branching sites (Flärdh, 2003). It recruits the cell wall biosynthetic machinery and Scy to newly established tip locations (Hempel et al., 2008; Holmes et al., 2013). Regarding the recognition of hyphal tips and new branching sites, DivIVA seems to bind preferably to curved cell walls, stabilized in a still unknown manner (Flärdh et al., 2012). Scy is suggested to act as a scaffold protein for DivIVA and further proteins of the polarisome, like FilP, by direct protein-protein interaction. The latter was shown to build a net-like structure at the cytosol-facing site of DivIVA, enhancing the rigidity and shape of the hyphae. (Bagchi et al., 2008) The localization of FilP has a dynamic and rapid turnover, culminating in a redistribution to newly formed hyphal tips, in contrast to DivIVA (Fröjd & Flärdh, 2019). Furthermore, FilP seems to play a major role in shaping and structuring the DivIVA polarisome, hinting at a more indirect effect on cell shape via DivIVA concentration that requires more detailed investigations (Fröjd & Flärdh, 2019).

Another protein, associated to the polarisome, is the chromosome segregation protein ParA (Ditkowski et al., 2013). Each chromosome has a ParB protein attached to the origin of replication (OriC) and ParA interacts with the ParB-OriC complex of one chromosome, locating it to the growing hyphal tip (Kois-Ostrowska et al., 2016). Meanwhile, any daughter chromosome is segregated from the hyphal tip after replication. This ParAB interplay is unique in bacteria. It allows sequestering of a chromosome to the growing hyphae as well as into new branch tubes and causes the replication of the GC-rich genome to be temporally dissociated from cell division in the multinucleate vegetative hyphae. (Kois-Ostrowska et al., 2016)

During vegetative phase, cell division occurs via sporadic cross-wall formation. These cross walls divide the hyphae into approximately 10 µm long, multigenomic compartments which are still physically connected. It has been conjectured that cross-membranes separate them further in 1 µm subcompartments, but experimental evidence is still lacking. (Bush et al., 2015; Yagüe et al., 2016; Sexton & Tocheva, 2020) The peptidoglycan wall is thicker at the apex compared to the lateral regions, which is presumably caused by enhanced amounts of polysaccharides and teichoic acids. However, the cell walls are evenly thick. (Sexton & Tocheva, 2020; Ultee et al., 2020) The formed vegetative network presents a compact state of growth that allows *Streptomyces* to exploit nutrient sources and spread in its terrestrial surrounding.

Reproductive phase. When facing nutrient depletion, *Streptomyces* initiates reproductive growth, enabling it to morphologically adapt and form resilient hydrophobic spores. In order to escape its aqueous substrate into the air, *Streptomyces* covers its previously smooth and plain surface with a very hydrophobic layer. This layer consists of three distinct groups of proteins: chaplin, rodlin and the surfactant protein SapB. (Willey et al., 1991; Claessen et al., 2002; Elliot et al., 2003) Their development-specific expression regulation is discussed in more detail in

Section 1.4. The chaplins and rodlins are highly hydrophobic, secreted and self-aggregating proteins. The chaplins contain a characteristic, circa 40 hydrophobic residues long chaplin domain. The protein class is divided into short and long chaplins according to the number of chaplin domains: While short ones only contain a single chaplin domain, long ones contain two chaplin domains and a carboxy terminal located sorting signal. This signal marks the long chaplins for attachment to the cell wall by sortase enzymes. (Elliot et al., 2003) The sortase-mediated attachment of long chaplin proteins to the cell wall was proven for ChpC and, therefore, assumed for the other long chaplin proteins (Duong et al., 2012). Once the chaplin proteins have been secreted in a sufficient amount, the rodlin protein RdlB self-assembles to rodlin fibrils. This process is essentially supported by RdlA, in a still unknown manner, and forms what in recent studies is suggested to be a second independent rodlet layer, which covers the surface of the aerial hyphae. (Claessen et al., 2003; Elliot et al., 2003; Yang et al., 2017; Dragoš et al., 2017) *In vitro* approaches provided convincing evidence that self-assembled chaplin fibrils form amphipathic membranes. This led to the hypothesis that the chaplin proteins might form layers similiar to the rodlet layer with its hydrophilic site facing the cell wall, while the hydrophobic surface is oriented towards the aqueous environment. (Bokhove et al., 2013)

Under high osmotic conditions, the surfactant protein SapB additionally reduces the surface tension (de Jong et al., 2012). In such a manner, coated hyphae rise in the air and form the non-branching aerial mycelium (Bush et al., 2015). Additionally, recent approaches propose a function of chaplin proteins in *S. mobaraensis* as a new translocase, facilitating the passage of metal ions through the cell wall (Anderl et al., 2020). To provide the nutrients and compartments, which are essential to undergo this harsh transition in pivotal mycelial organization and surface properties, parts of the vegetative mycelium are lysed by programmed cell death (Claessen et al., 2014). Among other factors, programmed cell death can be triggered by the production of DNA-damaging prodiginines, a family of tripyrrole (Tenconi et al., 2018). Additionally, the reproductive phase is characterized by a tremendous alteration in the peptidoglycan composition, enhancing its thickness and composition (van der Aart et al., 2018; Sexton & Tocheva, 2020).

In *S. venezuelae*, the shift from vegetative to reproductive phase is accompanied by a shift between two distinct modes of cell division: from vegetative cross wall formation to sporulation-specific septation. The latter takes place in a synchronous septation event during which multinucleoid *Streptomyces* hyphae are divided into unigenomic prespore compartments. This septation event marks the onset of sporulation. It initiates with the interaction of SsgA and SsgB, resulting in the recruitment of the highly conserved FtsZ to future cell division sites in proximity to the membrane by direct interaction with SsgB. (Willemse et al., 2011) The positioning mechanism that determines the localization of SsgA and SsgB to these future cell division sites in *S. venezuelae* is, however, still unknown (Willemse et al., 2011). The tubulin-like FtsZ functions as a GTPase by polymerizing into short filaments at the cytoplasmic membrane, forming the cytokinetic Z-rings (Bi & Lutkenhaus, 1991; Löwe & Amos, 1998). The Z-ring is a cytoskeletal element analogous to the eukaryotic contractile ring needed for both types of septation (McCormick et al., 1994; Lutkenhaus & Addinall, 1997). Localization of FtsZ to the

future septation site initiates the recruitment of further cell division proteins, thus, forming the multi-protein complex named the "divisome". Herein, the GTPases DynA and DynB, members of the multidomain GTPase dynamin family, localize FtsZ-dependently and play a crucial role in stabilizing the *de novo* formed, cyokinetic Z-ring. (Haeusser & Margolin, 2016; Schlimpert et al., 2017) The Z-ring forming FtsZ colocalizes with both dynamin proteins and shows direct interaction with SsgB and SepF, a protein of unknown function in *Streptomyces* with two homologs SepF2 and SepF3 in *S. coelicolor* (see Fig. 1.2 B and C) (Schlimpert et al., 2017). Within the divisome, SsgB seems to bridge FtsZ to DynA, DynB and SepF2. Additional interactions between these members of the divisome seem to stabilize the complex, supporting the coordination of peptidoglycan synthesis (Xiao & Goley, 2016; Schlimpert et al., 2017). In *Streptomyces*, the *ftsZ* gene is encoded in the "division and cell wall" (dcw) cluster, together with a number of additional cell division genes like *divIVA*, *ftsILQW* and the *mur* genes (see Fig. 1.2 A) (Schlimpert et al., 2017).

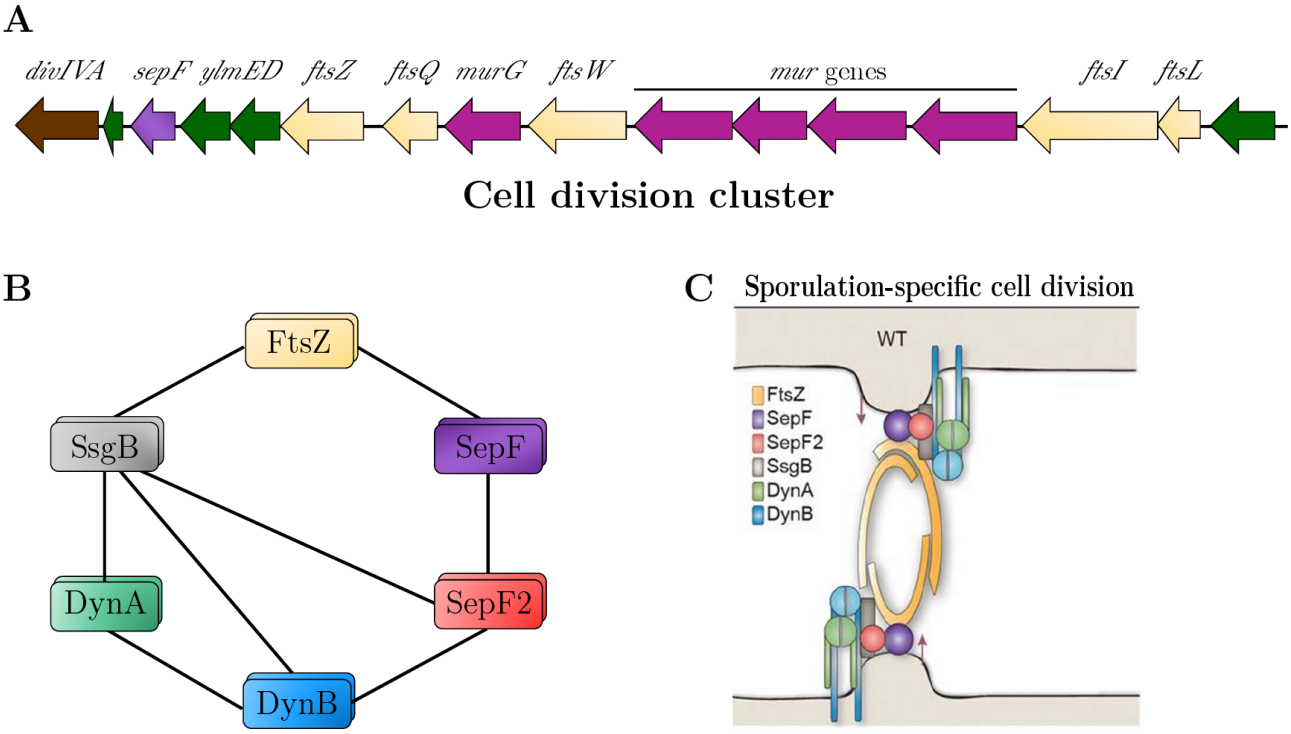

Fig. 1.2 The tubulin-like FtsZ polymerizes into short filaments at the cytoplasmic membrane, forming the cytokinetic Z-rings. (A) Organization of *ftsZ* in *Streptomyces* in the *dcw* gene cluster, together with a number of additional cell division genes like *divIVA*, *ftsILQW* and the *mur* genes (StrepDB). (B) Schematic model of the protein interactions between FtsZ and other associated components of the *Streptomyces* divisome based on two-hybrid results by Schlimpert et al. (2017). (C) Schematic model of the FtsZ-dependent divisome in *Streptomyces*. SsgB localizes at the future division sites via a to date unknown position determination mechanism and recruits FtsZ, initiating the massive septation event at the onset of sporulation (Willemse et al., 2011). Localization of FtsZ to the future septation site initiates the recruitment of further cell division proteins, forming the divisome to which DynA and DynB localize FtsZ-dependently (Haeusser & Margolin, 2016; Schlimpert et al., 2017). Additional interactions between these members of the divisome seem to stabilize the complex supporting the coordination of peptidoglycan synthesis. Part B and C of this figure were modified after Schlimpert et al. (2017); published in PNAS freely available online through the PNAS open access option and is not covered by the CC BY-NC-ND license Attribution-NonCommercial-NoDerivatives 4.0 International License of this thesis.

Sporulation. During the process of differentiation, the sporulation commences with an enormous, synchronous cell division event in the aerial hyphae, comparting them into long strings of pre-spores (Bush et al., 2015). Maturation processes result in thick-walled, dormant exospores that recent studies ascertained in *S. albus* to be no longer surrounded by the hydrophobic coat but instead by a more dense layer, called the "spore coat" (Sexton & Tocheva, 2020). Due to the biosynthesis of spore-specific polyketides, i.a. jadomycin in *S. venezuelae*, mature spores can be determined by the species-specific color change of the colonies (Han et al., 1994). Furthermore, *Streptomyces* are able to produce protective heat shock proteins to enhance the resilience of the spores (Bobek et al., 2017; McCormick & Flärdh, 2012).

Once detached from the spore chain into the environment, spores are able to spread by direct interaction of the rodlins with the motility machinery of other soil bacteria (Muok et al., 2020). The characteristic soil-like odor, perceptible by humans and several other species at minimum doses, is caused by secreted metabolites of *Streptomyces*, like geosmin or 2-methylisoborneol (Ruddick & Williams, 1972). Recent studies provided evidence that this smell attracts soil arthropods, promoting the attachment to their surface to facilitate spore dispersal (Becher et al., 2020).

Conditional growth modes. *Streptomyces* exist in their natural environment in a complex interplay with other organisms, which is why the good laboratory practice of analyzing bacterial strains in pure culture has recently been questioned in this context. Attempts to shift to mixed cultures, growing *S. venezuelae* in the presence of the yeast strain *Saccharomyces cerevisiae* caused a switch to a hitherto unprecedented growth strategy named "exploration" (Jones et al., 2017). This notation is derived from its expeditious spread, whose speed reminds of a motility mode. Glucose depletion and presence of the volatile organic compound, trimethylamine (TMA), induces this switch to exploration growth. Secretion of the latter raises the environmental pH and acts as a *Streptomyces* intraspecies communication signal to other colonies over physical distance (Jones et al., 2017). Additionally, TMA synthesis reduces the survival of other nearby bacteria and fungi by pirating their vital iron sources while enhancing exploration growth and, thereby, siderophore secretion and iron uptake (Jones et al., 2017, 2018).

Recent studies discovered another cell wall deficient developmental growth mode, functioning as an adaptation to hyperosmotic conditions. The so-called "S-cells" are repelled from vegetative hyphae tips, which are highly osmo-resistant and capable of re-transformation into a vegetative mycelium under favorable conditions. Depending on the cell size, S-cells contain one or several chromosomes. (Ramijan et al., 2018)

Historically, *S. coelicolor* is the best understood model organism of the genus *Streptomyces* in which many major developmental regulators were identified. However, recent research on *Streptomyces* developmental regulation focuses on *S. venezuelae* which, in contrast to *S. coelicolor*, is able to undergo the full life cycle, including sporulation, in liquid culture media (Bush et al., 2017).

1.3 The second messenger c-di-GMP – "one ring to rule them all"

Bis-(3´-5´)-cyclic dimeric guanosine monophosphate (c-di-GMP) is a signaling molecule that is almost ubiquitous in the bacterial kingdom (Schirmer & Jenal, 2009). Having first been described as an allosteric activator of the cellulose synthase in *Gluconoacetobacter xylinus*, c-di-GMP drifted out of focus for a long time (Ross et al., 1987, 1991). Only several years later, the central role of this second messenger in the induction of biofilm formation and control of the cell cycle was discovered and c-di-GMP became a well-studied nucleotide second messenger in bacteria. Many pathogenic bacteria regulate the expression of their virulence factors c-di-GMP-dependently. (Valentini & Filloux, 2019) In unicellular Gram-negative bacteria like, for example *Escherichia coli*, local and global increase of c-di-GMP levels initiate the coordinated switch from the flagellar, motile stage of life typical for exponential growth, to an extracellular matrix producing physiology, which is associated with biofilm formation and the stationary phase (Jenal et al., 2017).

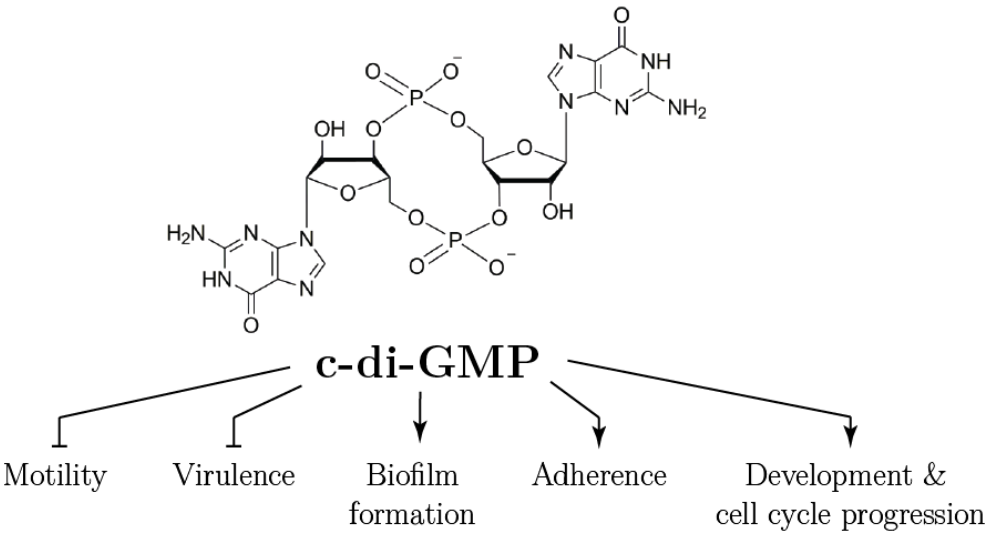

Fig. 1.3 Chemical structure of c-di-GMP and its impact on physiological networks. This figure was modified with permission after Hengge (2009) published in Nature Reviews Microbiology with license granted at the 5th of January 2021 under the license number: 4982410450133 and is not covered by the CC BY-NC-ND license Attribution-NonCommercial-NoDerivatives 4.0 International License of this thesis.

Molecular structure. The nucleotide second messenger c-di-GMP consists of two guanosine monophosphate molecules that are organized in a circle and connected via the phosphate group at the third and fifth carbon atom of both ribose molecules (see Fig. 1.3). To fulfill its diverse functional requirements, this cyclic molecule has a high conformational flexibility and binds, in different stoichiometric ratios, a huge amount of effectors. In doing so, c-di-GMP influences the orchestration of several physiological processes on the transcriptional, translational as well as the post-translational level by controlling the expression, enzymatic activity or induction of protein-complex formation. (Schirmer & Jenal, 2009; Boyd & O'Toole, 2012; Römling et al., 2013; Jenal et al., 2017)

C-di-GMP sensing effectors. Effector components that interact with c-di-GMP can function as transcription factors in two-component systems or riboswitches (Tschowri, 2016). By binding the latter in mRNAs, c-di-GMP regulates their stability and translation (Sudarsan et al., 2008). As proteins, c-di-GMP effector components contain one of many c-di-GMP binding motifs that, upon binding, alters their conformation and activity. Between the numerous `GGDEF`/`EAL` domain proteins, several are enzymatically inactive because of degeneration in their catalytic site and can act as effector proteins by binding c-di-GMP (Jenal & Malone, 2006; Bordeleau et al., 2011).

The probably most famous and best studied c-di-GMP binding domain is PilZ, named after the first described effector protein PilZ in *Pseudomonas aeruginosa* (Amikam & Galperin, 2005; Ryjenkov et al., 2006). Here, c-di-GMP binds to two highly conserved motifs: (`Q`/`E`)`RRxxxR` and `D`/`NxSxxG` followed by an allosteric modulation of the effector protein (Amikam & Galperin, 2005; Ryjenkov et al., 2006; Benach et al., 2007). While many effector proteins bind c-di-GMP specifically, the small-molecule-binding protein SmbA in *Caulobacter cresentus* is reciprocally regulated by competitively binding the molecules ppGpp and c-di-GMP. This regulatory mechanism impacts the growth on glucose as a carbon source. (Shyp et al., 2020) Recently, c-di-GMP sequestering, artificial CheY-like peptide was developed, which is optimized to a minimal size of 19 residues. This peptide skims off cellular c-di-GMP by binding it at low-nanomolar affinity in *P. aeruginosa*, resulting in significantly reduced biofilm formation. (Hee et al., 2020) Altogether, c-di-GMP interacts with divers effectors, leading to a multistage, specific and fine-tuned physiological response to cellular or environmental stimuli.

Local c-di-GMP signaling. Despite the fact that in many bacteria multiplicities of c-di-GMP turnover proteins and effectors components are bridged by one and the same second messenger, studies provided evidence that these various signaling pathways are orchestrated in a highly specific manner (Schirmer & Jenal, 2009; Römling et al., 2013). Several of those c-di-GMP turnover proteins have characteristic knockout phenotypes, which connect them to a specific effector pathway, like the active DGC PleD in *C. cresentus* that specifically controls the processes at the origin of replication (Kaczmarczyk et al., 2020). These findings suggest local c-di-GMP effector modules that respond to a specific stimulus. The concept of local c-di-GMP signaling describes the spatial proximity of c-di-GMP turnover, sensor and effector proteins to larger complexes in which local c-di-GMP concentrations alter in response to a specific environmental signal, without affecting the cellular c-di-GMP concentrations, first described by Lindenberg et al. (2013). A recent study, analyzing the interactome of all c-di-GMP turnover proteins in *E. coli*, describes that a specific local signaling module often consists of a DGC, its antagonistic PDE and effector components and requires direct protein-protein interactions (Sarenko et al., 2017). From their insights in *E. coli*, the authors deduced a new concept of local c-di-GMP signaling, named the fountain model. It is based on the fact that the dissociation constant (K_d) of some c-di-GMP effector components is significantly higher than the average cellular c-di-GMP level in the concerned species, thus binding its ligand with a quite low affinity (Pultz et al., 2012). As global c-di-GMP levels are insufficient to provide effective binding, the fountain model suggests a combined presence of one or more global acting c-di-GMP turnover proteins, counteracting

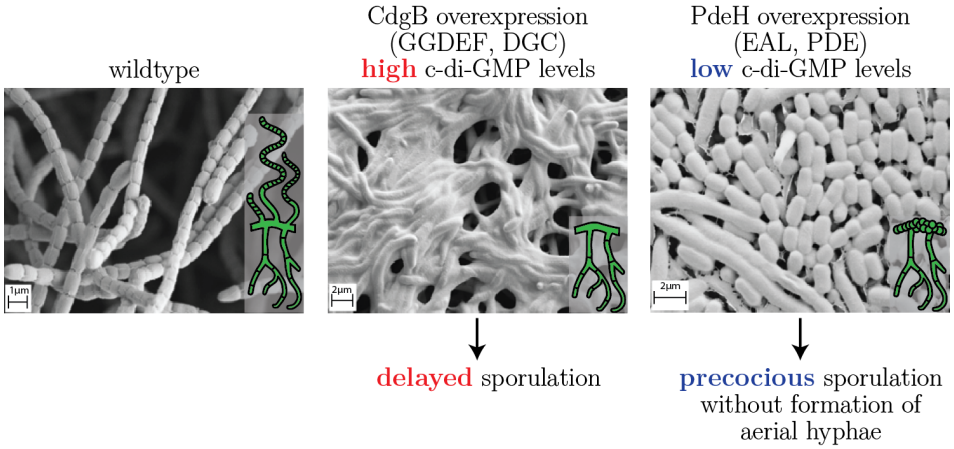

Fig. 1.4 Altered c-di-GMP levels influence *S. venezuelae* development. Overexpression of CdgB arrests the development in the vegetative phase, while PdeH overexpression (right) leads to precocious sporulation without aerial hyphae formation. In comparison, the wild type grows sporulating aerial hyphae (left). Scanning electron micrographs (SEM) show cells grown on maltose-yeast extract-malt extract (MYM) solid medium for 4 d at 30 °C. The schematic illustration in the lower right corner of the images indicates the growth stages of the strain. The SEM images shown in this figure were originally published in Tschowri et al. (2014); published in Cell under the CC BY license Attribution 3.0 Unported License.

each other to regulate the cellular c-di-GMP levels, and several stimulus-specific local acting signal transduction pathways (Sarenko et al., 2017). A recent study characterized another local signaling module in *E. coli*, where the interacting DGC-PDE pair DgcC and PdeK co-localize with the cellulose synthase complex by directly interacting with the subunit BcsB, establishing a delicately calibrated local c-di-GMP pool in direct proximity of the biosynthesis complex of the biofilm exopolysaccharide pEtN-cellulose (Richter et al., 2020). Here, mathematical modeling and simulations confirmed that local c-di-GMP signaling is possible, independent of spatial compartmentalization. These studies defined the criteria and provided the methods to predict and identify putative local c-di-GMP signaling modules in other species like *S. venezuelae*.

C-di-GMP in *Streptomyces*. In these soil bacteria, the life cycle progression involves a distinct succession of growth stages, explained in detail in Section 1.2. Early studies identified a number of potential c-di-GMP turnover proteins in *S. coelicolor*, hinting at a regulatory impact of c-di-GMP in *Streptomyces* (Tran et al., 2011). Later studies revealed that artificial elevation of the cellular c-di-GMP levels, caused by overexpression of the *S. coelicolor* `GGDEF` domain containing DGC CdgB in *S. venezuelae*, arrested the cells in the vegetative stage (see Fig. 1.4 middle). As a result, the strain had a bald and shiny colony morphology and showed delayed aerial hyphae and spore formation (Tschowri et al., 2014). In contrast, reduction of cellular c-di-GMP levels by overexpression of the *E. coli* phosphodiesterase (PDE) PdeH in *S. venezuelae* led to precocious sporulation with a deficiency in aerial hyphae formation, exhibiting an irregular spore mass in SEM images and a bald but matte colony phenotype (see Fig. 1.4 right) (Tschowri et al., 2014). These results suggested that c-di-GMP plays a central role as a "brake" for the developmental progression, impacting the expression of reproductive genes during the vegetative phase and, later on, in the timing of sporulation. C-di-GMP was, therefore, assumed to interact with major developmental regulators in *S. venezuelae*.

1.4 The role of Bld and Whi regulators in *Streptomyces*

To date, two effector proteins are associated with the key factor of *Streptomyces* developmental regulation, c-di-GMP: the developmental master regulator BldD and the anti-σ factor RsiG, supporting the σ^{WhiG}-RsiG complex formation (Tschowri et al., 2014; Gallagher et al., 2020).

BldD acts as a transcriptional regulator during the vegetative phase (see Fig. 1.5) and sits, as a repressor, on top of the sporulation regulatory cascade (Den Hengst et al., 2010). BldD is a member of the GntR family of regulators, a broadly distributed family of Helix-Turn-Helix transcription factors. GntR family regulators typically consist of a DNA-binding domain (DBD) and a domain for effector binding/oligomerization, which is responsive to cellular nutrient states. In general, effector binding leads to conformational alterations in members of this regulator class. These impact the DNA binding affinity and, thereby, activity of the transcription factor (Hoskisson & Rigali, 2009).

The effective DNA binding activity of BldD depends on sequential binding of tetrameric c-di-GMP via its carboxy-terminal domain (CTD), as illustrated in Fig. 1.5 (Schumacher et al., 2017; Tschowri et al., 2014). Herein, a BldD protomer binds one c-di-GMP dimer resulting in the ability to form weak dimers with another BldD protomer, both via the motif 2 (`RXXD`). With increasing c-di-GMP concentrations, a second c-di-GMP intercalated dimer binds the motif 1 (`RXD`) of both BldD protomers (Schumacher et al., 2017; Tschowri et al., 2014).

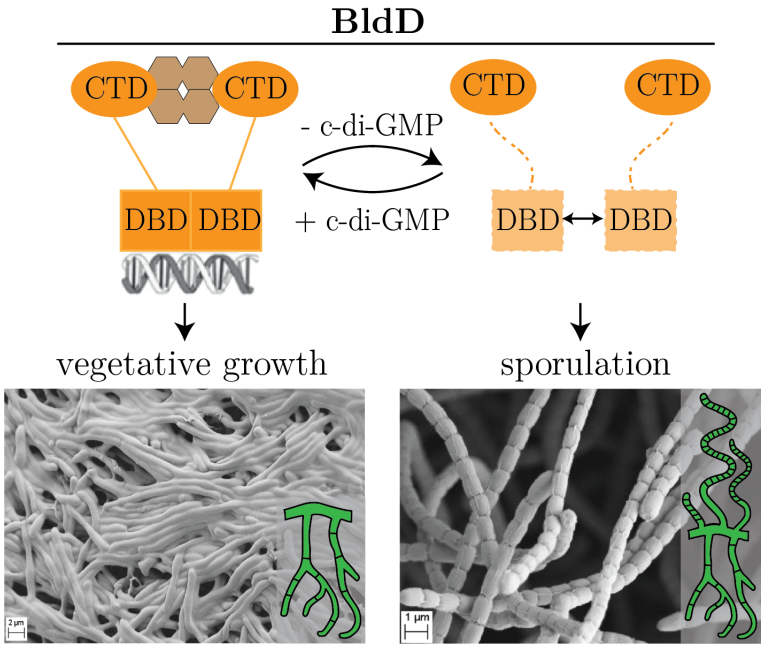

Fig. 1.5 BldD represses c-di-GMP-mediated the developmental gene cascade. Upon c-di-GMP-binding, BldD develops a high affinity DNA binding activity, resulting in the repression of *Streptomyces* development. At low c-di-GMP (beige hexagon) levels, the BldD DBDs (orange squares) show only weak interactions *in vivo* (right side; dashed lines and the double-headed arrow). Increases in c-di-GMP concentrations bridge the dimerization of the BldD CTDs (orange ovals) stabilizing the conformation of the DBDs in local proximity. Thereby, DBDs are able to dimerize effectively when close to DNA, leading to a high DNA binding affinity and repression of the targeted developmental genes during vegetative growth. This figure was modified with permission and the SEM images were originally published in Tschowri et al. (2014); published in Cell under the CC BY license Attribution 3.0 Unported License.

The second c-di-GMP effector protein, RsiG, was identified as the anti-σ factor of σ^{WhiG}, which activates late sporulation genes via WhiI and WhiH expression control (Gallagher et al., 2020). Upon binding c-di-GMP, RsiG is able to form a stable complex with σ^{WhiG}, preventing it from forming a stable holoenzyme with the RNA polymerase (RNAP) (see Fig. 1.6). Thus, RsiG is active in the early reproductive phase and releases σ^{WhiG}, presumably caused by a further decrease in c-di-GMP concentration, as BldD shows a significantly higher K_d towards c-di-GMP than RsiG (Tschowri et al., 2014; Gallagher et al., 2020). This explanation is supported by a drop of c-di-GMP levels at the onset of the reproductive phase (J. Haist, unpublished).

The BldD-(c-di-GMP) regulon. At the beginning of the life cycle, the $\mathrm{BldD}_2(\text{c-di-GMP})_4$ complex acts as an active, DNA-binding transcription factor, repressing most of its 282 target transcriptional units in *S. venezuelae* (Elliot et al., 2001; Den Hengst et al., 2010; Tschowri et al., 2014). Its expression is directly regulated by the two-component system MtrAB in *S. coelicolor*, but could not be verified in *S. venezuelae* so far (Som et al., 2017a,b). BldD was shown to directly activate antibiotic production in *S. roseosporus*, *S. avermitilis* and *S. lincolnensis* (Li et al., 2019; Yan et al., 2020), while the BldD-dependent developmental regulon was repressed during vegetative growth, as shown by Den Hengst et al. (2010) (see Fig. 1.7). BldD sits on top of two fundamental regulatory classes controlling the transition from vegetative growth to sporulation (*bld* and *whi* regulators), as well as further cell division and chromosome segregation genes. (Elliot et al., 2001; Den Hengst et al., 2010; Tschowri et al., 2014; Bush et al., 2015)

Bld regulators. The deletion of any *bld* gene results in the "bald" colony phenotype that fails to produce the characteristically hair-like appearing aerial hyphae, as described by Merrick (1976) (see Fig. 1.1 B top). These *bld* mutants can be divided into two classes, according to their phenotype. Both *bld* mutant classes appear bald and shiny at macroscopic scale, but alter in the surface texture and microscopic structure. One class represented by Δ*bldN* and Δ*bldM* results from cells that are arrested in the vegetative stage and, thus, stay bald and shiny. In contrast, the deletion of *bldD* or *bldO* results in a morphological, developmental phenotype, where the formation of the aerial mycelium is bypassed. Here, sporulation initiates directly in the vegetative mycelium. This phenotype, called hypersporulation, represents the second class of *bld* mutants (Bush et al., 2017; Kim et al., 2006).

Whi regulators. The *whi* genes encode a class of regulators, named after the characteristic "white" and fuzzy colony appearance of their knockout mutants (see Fig. 1.1 B middle) that orchestrate the accurate spore maturation (Bush et al., 2015). The *whi* knockout mutants are deficient in their spore pigmentation, which is genetically correlated with mature wild type spores (Chater, 1972). Like the *bld* regulators, *whi* regulators are categorized in two different manifestations, based on the physiology of their knockout mutants. The first form is arrested in the early reproductive stage with aerial hyphae, but deficient in sporulation as seen in the knockout mutant of *whiA* or *whiG* (Chater, 1972). The second variant produces spores that do not mature properly. The spores appear deformed and colonies lack pigmentation, a phenotype that can be found in Δ*whiD* for example (Yan et al., 2017).

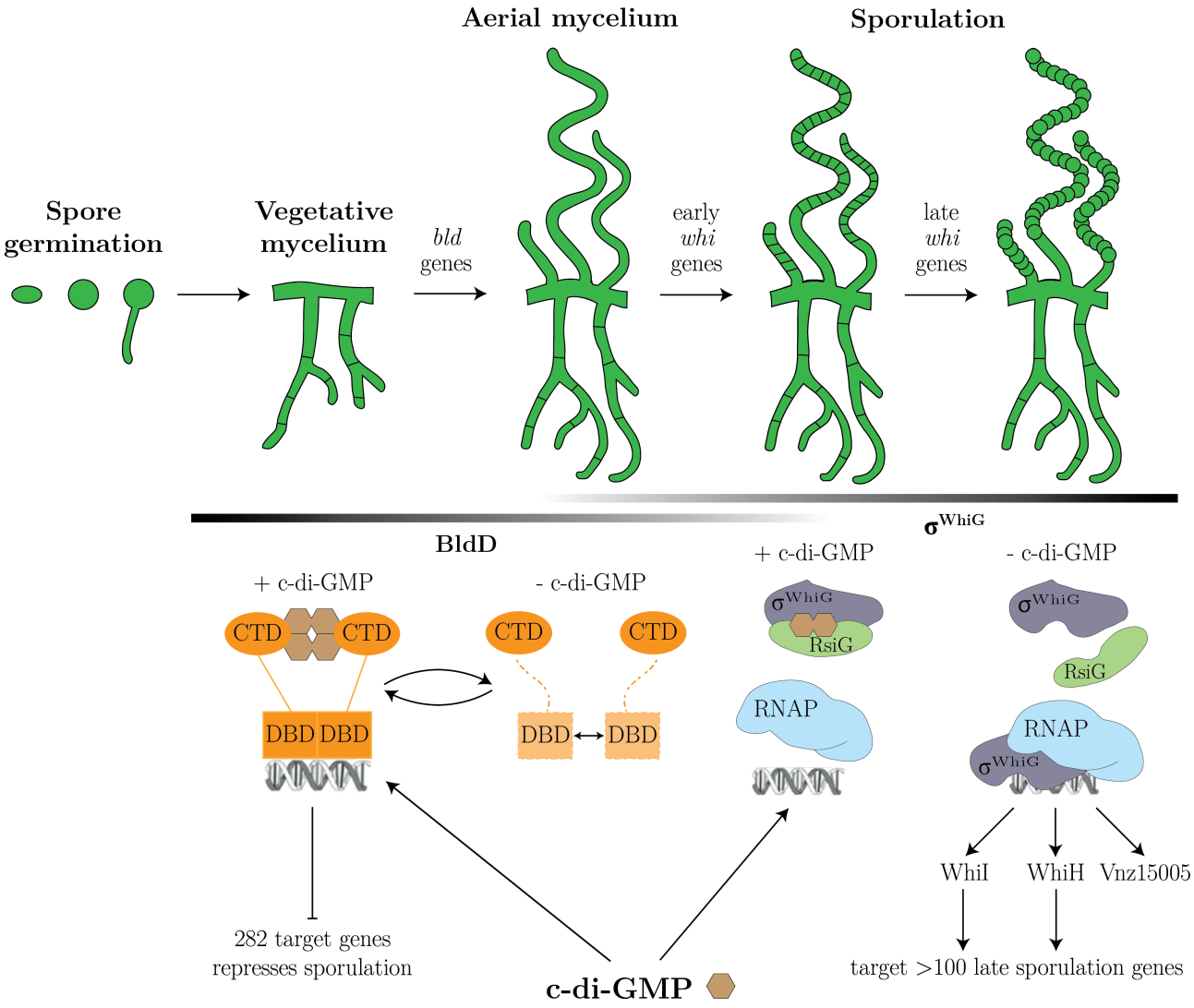

Fig. 1.6 C-di-GMP-mediated orchestration of the developmental regulation genes in *Streptomyces* life cycle. High c-di-GMP (beige hexagon) levels during the vegetative phase support repression of the sporulation cascade by BldD. A decrease of c-di-GMP inactivates BldD, initiating the expression of *bld* genes as well as, later on, early *whi* genes and, thus, differentiation. Upon the expression of the late sporulation σ^{WhiG}, c-di-GMP levels seem to still be sufficient to mediate σ-anti-σ complex formation between σ^{WhiG} and its anti-σ, RsiG. Decreasing c-di-GMP levels result in the release of σ^{WhiG}, activating the late sporulation regulators WhiH, WhiI and Vnz15005. This figure was modified with permission after Tschowri et al. (2014); published in Cell under the CC BY license Attribution 3.0 Unported License and Gallagher et al. (2020).

Early sporulation genes. The reproductive phase is initiated by the inactivation of BldD, presumably through a global or local drop in c-di-GMP levels, but the mechanism is still unknown. After BldD inactivation, the first steps of the sporulation cascade are activated, causing the inhibition of DNA replication as well as the formation of a reproductive mycelium. These steps are controlled in parallel by the interplay of BldH and BldA and the expression of the σ factor BldN as well as its anti-σ factor RsbN, as illustrated in Fig. 1.7 (Merrick, 1976; Bibb et al., 2012). All of them have been identified as direct target genes of BldD-(c-di-GMP), presumably repressing their transcription (Den Hengst et al., 2010; Schumacher et al., 2017).

The developmental transcription regulator BldH, among others, is controlling the developmental chromosomal replication (Higo et al., 2012). Therefore, BldH binds atypically to the 5'-region of the origin of replication (*oriC*), which is located in one operon with *dnaA* and *dnaN*. This operon is also repressed by the two-component system MtrAB in a presumably biphasic manner during vegetative phase and again, later on, during sporulation (Som et al., 2017b). BldH and BldA together control the expression of AmfR, the regulator of SapB (Ueda et al., 2005; Higo et al., 2011).

SapB is a surfactant peptide and present when cells are grown on a rich medium (Capstick et al., 2007). Simultaneously, the extracytoplasmic function (ECF) σ factor BldN activates the transcription of chaplin (*chp*) and rodlin (*rdl*) genes. The *chp* and *rdl* genes encode strongly hydrophobic proteins that are secreted and self-assemble on the cell surface together with SapB to form a hydrophobic, basket-like layer around the mycelium, as described in detail in Section 1.2 (Claessen et al., 2004). This hydrophobic layer enables the hyphae to break the air-water interface as aerial hyphae, escape the aqueous environment and, most likely, enhance their stress resistance in this new environment (McCormick & Flärdh, 2012).

Additionally to the transcriptional repression by BldD, the activity of *S. venezuelae* σ^{BldN} is regulated by its anti-σ factor RsbN. Recent structural analysis of the crystal structure unveiled the underlying mechanism. The membrane-standing RsbN, member of a new structural class of anti-σ factors, sequesters σ^{BldN} upon binding at the cytoplasmic side of the cell membrane during the vegetative phase. A to-date unknown signal causes RsbN to release σ^{BldN} into the cytoplasm. Here, σ^{BldN} forms a holoenzyme with the RNAP and activates the transcription by binding the promoter region of the *chp* and *rdl* genes as well as *bldM*. (Tschowri et al., 2014; Schumacher et al., 2018)

Like many other members of the *bld* regulator family, *bldM* is a direct BldD target gene and is, most likely, repressed by the $\mathrm{BldD_2}$(c-di-GMP)$_4$ complex, but also autoregulated in a negative feedback loop (Al-Bassam et al., 2014; Tschowri et al., 2014). Bioinformatic analyses revealed BldM to be perfectly conserved across all sequenced *Streptomyces*. In the early reproductive phase, the BldM protomer forms a homodimer regulating early sporulation genes like *ssgR* and *ssgB*, encoding cell division initiating proteins and *whiB* (Al-Bassam et al., 2014). Furthermore, recent studies discovered that BldM directly activates the *eshA-mishA-mishB* operon encoding the volatile 2-methylisoborneol (mentioned in Section 1.2). Thereby, the attraction of potential spore dispersers is integrated in the developmental differentiation (Becher et al., 2020).

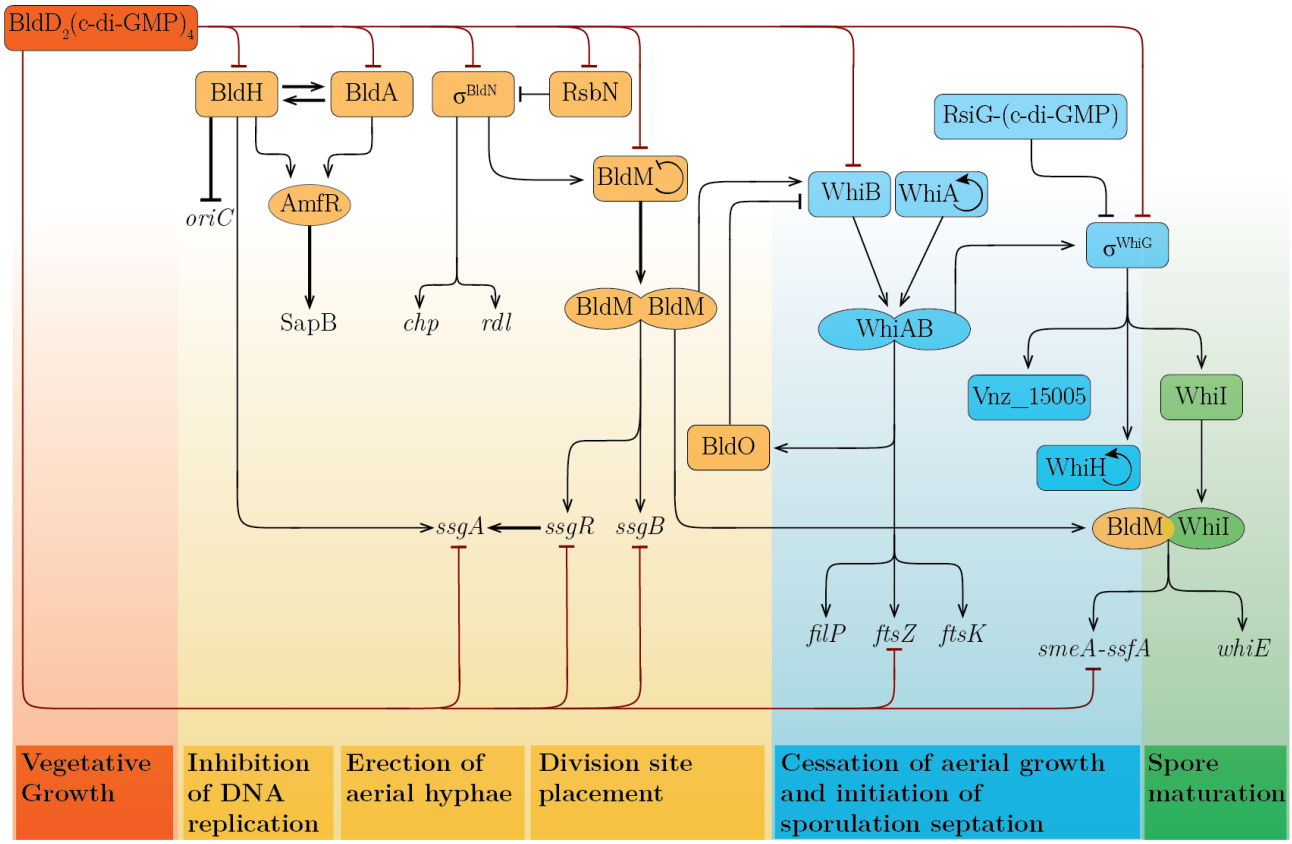

Fig. 1.7 $BldD_2$(c-di-GMP)$_4$ sits on top of the developmental cascade in streptomycetes (modified after Persson et al. (2013); Bush et al. (2015, 2016, 2017); Gallagher et al. (2020) compiled from findings in *S. venezuelae*, *S. coelicolor* and *S. griseus* some variations in the detailed linking between the species). BldD–cyclic di-GMP ($BldD_2$(c-di-GMP)$_4$) represses a huge network of developmental and sporulation genes facilitating a sufficient period of vegetative growth. The vast majority of genes, encoding pivotal developmental transcriptional regulators (upper red lines), are targets of $BldD_2$(c-di-GMP)$_4$-mediated repression. Affected are *bld* genes encoding regulators like BldH, BldA, σ^{BldN} and BldM as well as *whi* genes encoding regulators WhiB and σ^{WhiG}. The former prepares the transition to the reproductive phase via the regulation of DNA replication by *oriC* inhibition by BldH which, combined with BldA, also activates the AmfR-mediated expression of the surfactant peptide SapB. Like SapB, the σ^{BldN} controlled expression of the *chp* and *rdl* genes is necessary for the formation of the hydrophobic layer and the breaking of the water-air barrier by the aerial mycelium. The likewise σ^{BldN} controlled homodimeric transcriptional regulator BldM impacts the division site placement via *ssgR* and *ssgB* and activates the expression of WhiB. The latter is tightly repressed by BldD and BldO and interacts with WhiA in the heterodimeric transcription factor WhiAB, controlling further genes required for the differentiation of aerial hyphae. Activation of σ^{WhiG} is subject to multilayered c-di-GMP-mediated regulation. On the transcriptional level, *whiG* is a direct target gene of $BldD_2$(c-di-GMP)$_4$-mediated repression as well as activation via WhiAB. On post-translational level, the activity of σ^{WhiG} is directly controlled via c-di-GMP-dependent release from its anti-σ RsiG. This σ factor impacts the initiation of spore maturation via WhiI, WhiH and Vnz15005. WhiI controls a set of late sporulation genes forming a heterodimeric transcriptional regulator with BldM. Furthermore, the BldD regulon includes the direct repression of central factors involved in all stages of differentiation like SsgA, SsgB, FtsZ and SffA (lower red lines). This figure was modified after Bush et al. (2015); published in Nature Reviews Microbiology with license granted at the 4th of January 2021 under the license number: 4982000052251 and is not covered by the CC BY-NC-ND license Attribution-NonCommercial-NoDerivatives 4.0 International License of this thesis.

Sporulation septation. Marking the initiation of sporulation septation, the expression of *whiB* is tightly regulated (see Fig. 1.7). BldD was shown to directly bind the promoter region of *whiB* and presumably repress its transcription (Den Hengst et al., 2010). Additionally, BldO and MtrAB were shown to act as transcription repressors and *whiB* is the only known target gene of the transcriptional regulator BldO (Bush et al., 2017; Som et al., 2017a,b). Since WhiB is pivotal in the transition from vegetative growth to developmental septation, deletion of *bldD* and *bldO* as well as the overexpression of WhiB all result in hypersporulation (Bush et al., 2017). The repression of BldD and BldO together time the duration of vegetative growth before the differentiation of spores (Bush et al., 2017).

WhiB interacts with WhiA to function as a heterodimeric transcription regulator (Bush et al., 2016). Contrary to WhiB, WhiA is BldD-independently expressed, constitutively present at all time points examined and autoregulated via a positive feedback loop activating its own expression (Bush et al., 2013). The WhiAB heterodimer binds directly to a highly conserved GACAC motif in the promoter region, predominantly at the onset of sporulation during the fragmentation phase. WhiA and WhiB coactivate the expression of pivotal cell division genes like *ftsK*, *ftsW* and *ftsZ* (Bush et al., 2016). In *S. coelicolor* and *S. venezuelae*, reflecting its distinct requirements in the life cycle of *S. venezuelae*, *ftsZ*-expression is regulated by three promoters (Flärdh et al., 2000; Haist et al., 2020). The vegetative promoter realizes a basal level of FtsZ in the cells, which is needed for the infrequent cross-wall formation. The onset of sporulation coincides with a strong upregulation of *ftsZ* transcription that is regulated by a second FtsZ promoter. This increased expression is crucial for sporulation septation. (Flärdh et al., 2000) Furthermore, $BldD_2$(c-di-GMP)$_4$ directly binds to the *ftsZ* promoter region both in *S. coelicolor* and *S. venezuelae* at a conserved site, thereby, bridging *ftsZ* transcription to the cellular c-di-GMP level (Tschowri et al., 2014; Den Hengst et al., 2010). The expression of BldO is activated by WhiAB. BldO represses the *whiB* transcription, which causes a negative feedback loop on the expression of *whiB*, whose importance remains to be investigated. (Bush et al., 2017)

The second gatekeeper of proliferation. The expression of the late sporulation σ factor σ^{WhiG} is essential for maturation of aerial hyphae and initially inhibited directly by BldD (Den Hengst et al., 2010). The inactivation of BldD results in the expression of WhiB which then contributes in the WhiAB heterodimer in the activation of *whiG* transcription, leading to a constant presence of σ^{WhiG}. This created a time gap between the presence and activity of σ^{WhiG} that remained obscure until the identification of its anti-σ factor RsiG. As described above, c-di-GMP arms RsiG to sequesters σ^{WhiG}. This complex formation prevents σ^{WhiG} from forming holoenzymes with the RNAP (Gallagher et al., 2020). So far, σ^{WhiG} controls the expression of *whiI* and *vnz15005* completely and *whiH* partially (Bush et al., 2013; Gallagher et al., 2020).

The GntR-family transcriptional regulator WhiH was indicated to control a large regulon of sporulation genes (Persson et al., 2013; Gallagher et al., 2020). Early studies were not able to identify a WhiH target gene (Persson et al., 2013). To date, the only identified direct target gene of WhiH is the VOC geosmin encoding *geoA*, thus, coordinating its expression to the spore differentiation (Becher et al., 2020).

WhiI interacts with BldM to form a heteromeric transcriptional regulator that activates the *smeA-sffA* operon and the *whiE* gene cluster (Al-Bassam et al., 2014). The small membrane associated SmeA protein is essential for the navigation of putative DNA translocase SffA to the spore septa (Ausmees et al., 2007). Hidden behind the gene name *whiE* is a large intricate locus of genes, playing a pivotal role in spore polyketide pigment specification (Kelemen et al., 1998).

Summary. Taken together, alterations in the cellular c-di-GMP levels interfere with the developmental progression at two stages: the initiation of reproductive growth and the differentiation of spore chains. By binding the effector protein BldD, c-di-GMP controls the repression of sporulation genes during the vegetative phase. Decreasing cellular c-di-GMP levels initiate the sporulation cascade, while still arming RsiG to occupy σ^{WhiG}. In the late reproductive phase, a final drop of the cellular c-di-GMP levels causes RsiG to release σ^{WhiG}, which then forms a holoenzyme with RNAP, transcribing late sporulation genes. (Tschowri et al., 2014; Schumacher et al., 2017; Gallagher et al., 2020) In order to meet these physiological requirements, the cellular c-di-GMP concentration is fine-tuned throughout the life cycle by a dynamic equilibrium between making and breaking.

1.5 Molecular mechanisms of c-di-GMP turnover

The c-di-GMP turnover is mediated by synthesis via diguanylate cyclases (DGCs) and degradation via specific phosphodiesterases (PDEs) (Ross et al., 1987, 1991).

Synthesis. The synthesis of c-di-GMP from two molecules guanosine triphosphate (GTP) is catalyzed at the enzymatically active center (A-site) by the interplay of two `GGDEF` domains. The domain is named after its highly conserved signature amino acid motif `Gly-Gly-Asp-Glu-Phe` (`GGDEF`/in some cases `GGEEF`), each binding one GTP molecule, as exhibited in Fig. 1.8. (Ross et al., 1987, 1991; Paul et al., 2004; Chan et al., 2004) The first described `GGDEF`-containing protein is PleD in *C. cresentus*, which is activated by the phosphorylation of its receiver domain functioned as a role model to investigate mechanisms of substrate binding, enzymatic activity and regulation (Paul et al., 2004; Chan et al., 2004). In order to bind GTP and Mg^{2+} as an essential cofactor for the enzymatic activity, the `GGDEF` domain needs to contain an asparagine and two aspartic acids (Ausmees et al., 2001; Chan et al., 2004; Paul et al., 2007).

Furthermore, these `GGDEF` domains are usually found in large protein with a complex structural architecture, containing a number of accessory domains with regulatory and sensory functions. The most common regulator of enzymatic activity of the DGC is provided by another c-di-GMP binding domain with a conserved `RxxD` motif, functioning as an inhibitory "set screw" for DGC activity and is therefore called "inhibitory site" (I-site). Binding of c-di-GMP at this site causes an allosteric conformational change of the protein responsible for a negatively regulating feedback loop, controlling the DGC activity at the A-site (Chan et al., 2004; Christen et al., 2005). Therefore, the enzymatic activity of a DGC can be so far regulated by its expression levels, dimerization efficiency and allosteric product inhibition within the `GGDEF` domain.

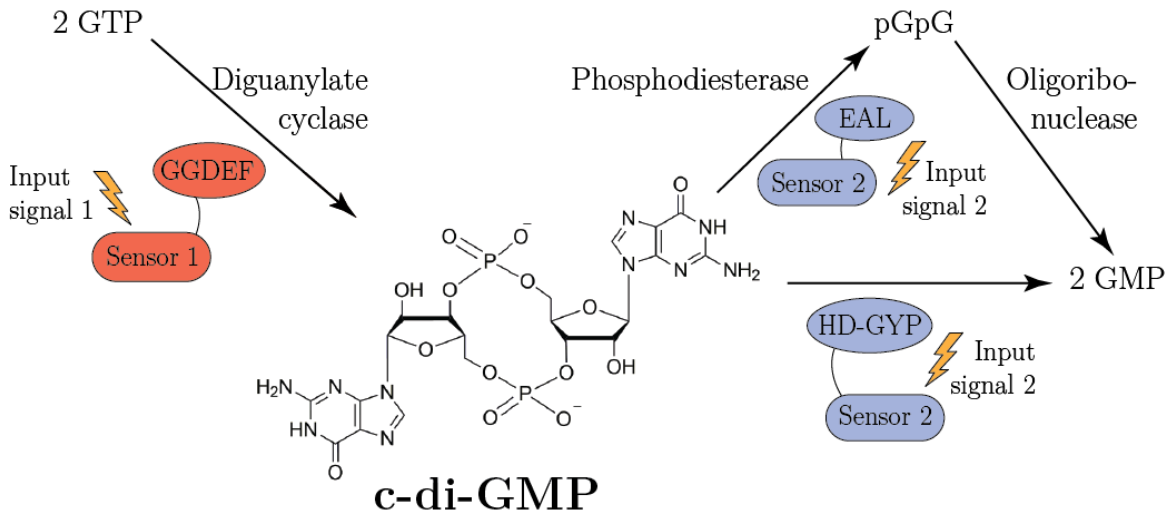

Fig. 1.8 Making and breaking of c-di-GMP. Diguanylate cyclase synthesizes c-di-GMP from two GTP molecules at the enzymatically active site at the `GGDEF` motif regulated by environmental or cellular stimuli. The degradation of c-di-GMP is provided via hydrolysis to pGpG or directly GMP mediated by `EAL` or `HD-GYP` domain containing phosphodiesterases. `EAL` domain phosphodiesterases have pGpG as a product, which, in some bacterial species, is substrate of non-specific oligoribonucleases that degrade it further to GMP. This figure was modified with permission after Hengge (2009) published in Nature Reviews Microbiology with license granted at the 5th of January 2021 under the license number: 4982410450133 and is not covered by the CC BY-NC-ND license Attribution-NonCommercial-NoDerivatives 4.0 International License of this thesis.

Degradation. Phosphodiesterases contain either an `EAL` or a `HD-GYP` domain hydrolyzing c-di-GMP specifically, but in distinct mechanistic manners, described in Ross et al. (1987, 1991) (see Fig. 1.8). While `HD-GYP` domains hydrolyze c-di-GMP to two GMP molecules, an `EAL` domain attacks one ester bond using Mg^{2+} or Mn^{2+} as essential cofactors leading initially to a linearization of c-di-GMP to the dinucleotide 5'-phosphoguanylyl-(3'-5')-guanosine (pGpG). Since not every c-di-GMP regulating bacterial species encodes `HD-GYP` domain proteins the mechanism of degrading pGpG to GMP remained unknown for a long time. More recently, a study provided evidences that the oligoribonuclease Orn in *P. aeruginosa*, a ribonuclease responsible for the hydrolysis of short (2-5 bp) RNA, is able to cleave pGpG further into two GMP molecules (Orr et al., 2015; Cohen et al., 2015).

The role of sensory domains. The redundant presence of synthesizing and degrading proteins hints towards a specific regulation of global and local c-di-GMP levels in response to distinct environmental stimuli. These can be sensed in one or more associated domains like GAF (c**G**MP-specific phosphodiesterases, **a**denylyl cyclases and **F**hlA), PAS (**P**er-**A**RNT-**S**im) or PAC (motif **C**-terminal to **PAS**), linked to the catalytic domains of both diguanylate cyclases and phosphodiesterases and integrated in large, highly structured proteins (Ponting & Aravind, 1997; Ho et al., 2000; Römling et al., 2013).

The regulatory input domain GAF is mainly associated with active DGCs. The high specificity regarding the temporal and spatial impact of single c-di-GMP turnover proteins enables a strictly circumscribed functionality of c-di-GMP on the local and cellular level (Lindenberg et al., 2013). C-di-GMP turnover proteins are regulated regarding their expression

as well as their specific activity and impact on the physiological morphology (Jenal et al., 2017). In *E. coli*, the DGC and constitutive dimer DgcZ is allosterically inhibited by its ligand zinc binding to the amino-terminal (N-terminal) zinc binding domain (CZB). Thereby, the protein conformation is changed to an enzymatically inactive state, although the `GGDEF` domains are still facing each other. (Zähringer et al., 2013) In addition, gaseous molecules can also act as ligands. In *Azotobacter vinelandii*, the DGC AvGReg binds oxygen via its globin coupled sensors (GCS), which leads to a closed conformation that enables DGC activity (Germani et al., 2020). The DGC CdgC is the main research subject of this thesis, wherefore the sensory PAS and PAC domain present in CdgC will be discussed in more detail in Section 5.1.1 in the discussion.

Summary. In *S. venezuelae* c-di-GMP levels have to be perfectly, dynamically balanced within the cell in order to orchestrate its elaborate differentiation system. This is implemented in *Streptomyces* by to-date ten `GGDEF`/`EAL`/`HD-GYP` domain proteins encoded in the genome, indicating the importance of this signaling molecule in the regulation of developmental cell cycle progression. Analyzing the target cluster of the developmental master regulator BldD revealed several putative c-di-GMP turnover proteins giving the first hint that altered c-di-GMP levels might influence the coordinated progression of the *Streptomyces* life cycle (Den Hengst et al., 2010).

1.6 CdgC influences morphological differentiation in *S. venezuelae*

S. venezuelae encodes ten `GGDEF-EAL` domain proteins. Previous analyses addressed the morphological effects of the individual putative c-di-GMP turnover proteins on the development of *S. venezuelae*. The developmental progression of their deletion strains was therefore compared to the wild type via phenotypic analysis of macrocolonies. This experiment showed a morphological influence of four out of ten proteins compared to the wild type: CdgB, CdgC, RmdA and RmdB, shown in Fig. 1.9 (Al-Bassam et al., 2018). Previous studies in *S. coelicolor* identified and characterized three of them to be involved in c-di-GMP-dependent developmental processes: the functional DGC CdgB and the active PDEs RmdA and RmdB (Den Hengst et al., 2010; Tran et al., 2011). The deletion of *rmdA* and *rmdB* resulted in a delayed and deletion of *cdgB* accelerated progress version of the wild type phenotype, as exhibited in Fig. 1.9 (Al-Bassam et al., 2018; Haist et al., 2020). In *S. coelicolor*, CdgD was shown to function as an active DGC. Here, its deletion leads to no alteration of the phenotype, but the overexpression blocks the developmental progression and the antibiotic biosynthesis (Liu et al., 2009). In contrast, deletion of *cdgC* led to a most striking gray phenotype called hypersporulation, which is verified several times in this thesis. During its growth, this strain skipped the white stage and remained gray, failing to turn green even after prolonged incubation, as illustrated in Fig. 1.10 left row (Al-Bassam et al., 2018). The white colony morphology is known, from studies of *S. venezuelae* WT, to represent the initiation of the reproductive phase with aerial hyphae formation (see Fig. 1.1). The latter indicates the maturation of the spores.

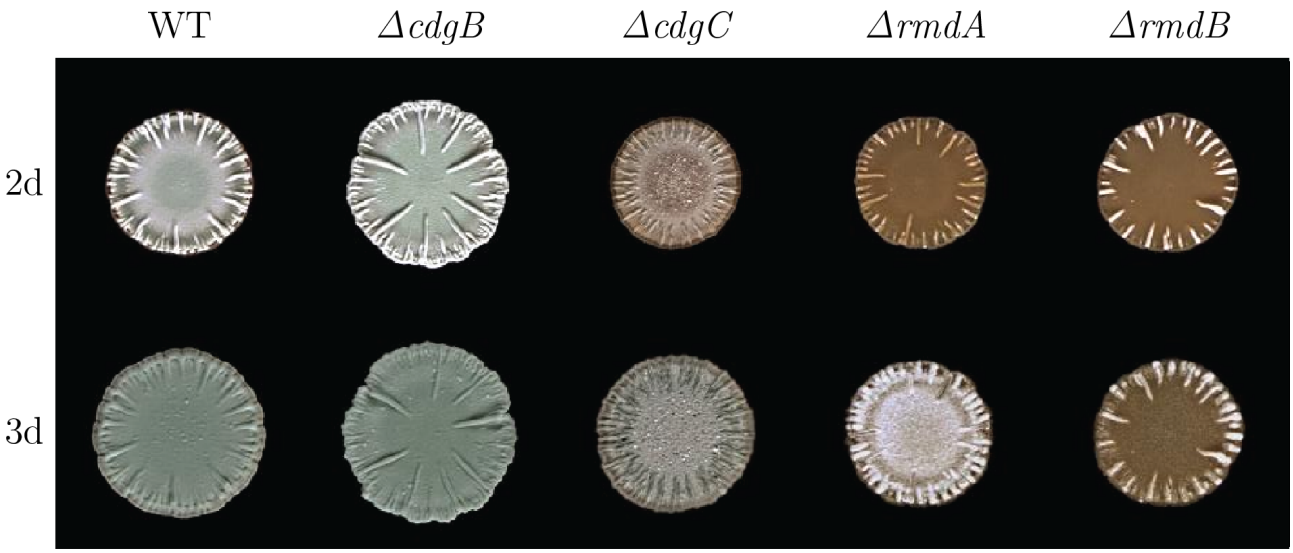

Fig. 1.9 The deletion of *cdgB* and *cdgC* accelerated the morphological progression in *S. venezuelae* while the deletion of *rmdA* and *rmdB* delayed it. Macrocolonies of these strains were created through drip of 12 µL $2 \cdot 10^5$ CFU/µL spores on MYM agar and plates were incubated for 4 d at 30 °C. This figure was modified with permission after Al-Bassam et al. (2018); published in Frontiers of Microbiology under the CC BY license Attribution 4.0 International License.

Further analysis via scanning electron microscopy taken from solid medium after four days of incubation revealed a precocious sporulating mass lacking aerial hyphae in the absence of *cdgC* compared to the wild type (see Fig. 1.10 middle row). Phase contrast documentation of samples taken from these strains after 12 h in liquid MYM medium supplement the picture of Δ*cdgC*, being a precocious sporulating strain lacking the ability to form aerial hyphae (see Fig. 1.10 right row). The hypersporulation phenotype is strongly reminiscent of the phenotype known from a strain overexpressing, the *E. coli* PDE PdeH, the *bldD* deletion strain and the WhiG overexpression strain (Tschowri et al., 2014; Gallagher et al., 2020). The unique nature of this phenotype among the c-di-GMP-turnover proteins raised the question, whether the c-di-GMP synthesized by CdgC feeds the local pool sensed by BldD or WhiG in a more direct manner. Possible hypotheses e.g. local signaling between BldD/RsiG and CdgC or correlating expression/activity of the proteins were addressed in this thesis.

Additionally, CdgC was shown to be present in 91 of 93 *Streptomyces* strains during a pangenomic analysis making it strongly conserved, but its enzymatic activity and physiological function remained unknown and are addressed extensively in this thesis (Al-Bassam et al., 2018).

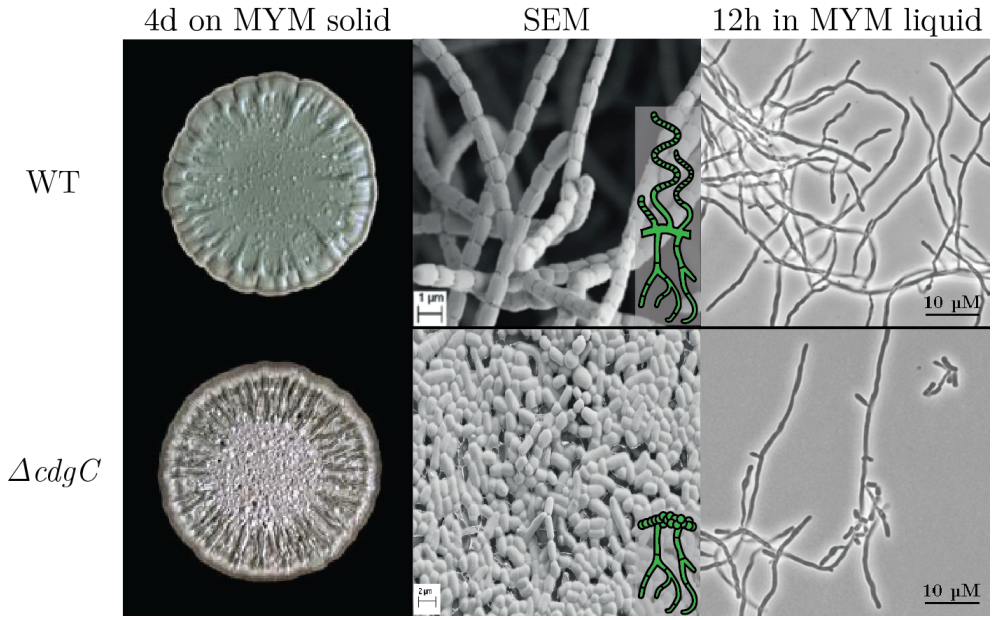

Fig. 1.10 CdgC shows a most striking knockout phenotype. The *cdgC* mutant shows a gray morphology and does not form aerial mycelium. Macrocolonies of these strains were created through drip of 12 µL $2 \cdot 10^5$ CFU/µL spores on MYM agar and plates were incubated for 4 d at 30 °C. For microscopic analysis of these strains liquid cultures of these strains initiated with $1{\cdot}10^6$ CFU/mL spores in MYM medium supplemented with Trace Element (2 mL/L) and samples were taken after 12 h. The SEM image of the *S. venezuelae* WT was modified after Tschowri et al. (2014); published in Cell under the CC BY license Attribution 3.0 Unported License, and the SEM image of the Δ*cdgC* was kindly provided by N. Tschowri, unpublished.

Chapter 2

Objectives

CdgC is a composite protein, containing a `GGDEF` and an `EAL` domain in tandem. One of the central goals of this work was to determine the enzymatic activities of the individual domains by using *in vitro* enzyme assays. The specific knockout phenotype of CdgC is characterized by precocious sporulation on vegetative mycelium without aerial hyphae formation. This indirectly reflects the morphological influence of CdgC on the c-di-GMP-mediated coordination of the developmental differentiation in *S. venezuelae*. Mutagenesis techniques were used to uncover the key residues relevant for the *in vivo* function of CdgC.

Furthermore, immunodetection of FLAG-tagged CdgC in *S. venezuelae* shall be used to characterize its expression patterns and activity control, pinpointing the activity of CdgC throughout the life cycle. In the light of previous characterizations of developmental master regulator and c-di-GMP effector protein BldD and its regulon, the DGC encoding genes *cdgA*, *cdgB*, *cdgC* and *cdgE* were indicated as direct BldD-target genes (Tschowri et al., 2014; Haist et al., 2020). In this study, the indicated role of *cdgC* as direct BldD-target gene in a regulatory feedback loop along with the other BldD-dependent DGCs shall be investigated using immunodetection and qRT-PCR analysis.

The specific hypersporulation phenotype of Δ*cdgC* that strongly resembles the low c-di-GMP level state of both to-date identified c-di-GMP effector proteins (deletion of *bldD* or overexpression of WhiG) fulfills one of three postulated criteria of local c-di-GMP signaling modules (Tschowri et al., 2014; Gallagher et al., 2020). Using Bacterial-Two-Hybrid (BTH) and pulldown assays, a second criterion shall be analyzed, testing for direct protein-protein interactions between CdgC and its potential effector compounds. Moreover, BTH screenings shall be used to investigate the interactome of CdgC and identify specific molecular targets causing hypersporulation in the *cdgC* mutant.

The lack of the characteristic surface hydrophobicity in Δ*cdgC* indicates that the location of spore formation on vegetative or aerial mycelium correlates indirectly with the differential expression of major hydrophobins and their regulating σ^{BldN}. Accordingly, preliminary RNA-seq data indicated reduced expression levels of major compounds of the hydrophobic sheath in Δ*cdgC* compared to the wild type. A central objective of this study is the validation of the RNA-seq data with results received from qRT-PCR analyses.

Finally, precocious sporulation observed in the *cdgC* knockout mutant suggests an impact of CdgC on the coordination of the cell division and timing of sporulation septation. This shall be verified using confocal microscopy and immunodetection to illuminate the expression and Z-ring formation of the bacterial tubulin homolog FtsZ.

Chapter 3

Material and methods

3.1 Chemicals and materials

All chemicals utilized in this study are listed in Table 6.1 with their corresponding manufacturer in the appendix. All unlisted chemicals were obtained in the quality pro analysis (p.a.) by the manufacturers AppliChem, Millipore, Merck, Carl Roth, Roche, Sarstedt, Sigma-Aldrich and VWR. All technical devices relevant for experimentation of this thesis are mentioned with the corresponding manufacturers in Table 6.2 in the appendix. All buffers utilized in this study and their compositions are listed in Table 6.3 in the appendix.

3.2 Media and supplements

If not described otherwise, solutions were solved in Aqua bidest. (H. Kerndl GmbH). All used media were sterilized as described in Section 3.4.1 and supplements added after sterilization.

3.2.1 Liquid media

Lysogeny Broth media (LB)	Tryptone	10 g/L
	Yeast extract	5 g/L
	NaCl	5 g/L
2x TSS media	PEG-6000	20%
	$MgSO_4$	100 mM
	DMSO	10%
Maltose-Yeast extract-Malt extract media (MYM)	Maltose	2 g/L
	Yeast extract	4 g/L
	Malt extract	10 g/L
	H_2O:ddH_2O	1:1
	Trace Element	2 mL/L (added after autoclaving and sterile filtration)

3.2.2 Solid media

LB/LBoN-Agar	Tryptone	10 g/L
	Yeast extract	5 g/L
	NaCl	5 g/L
	Bacto-Agar	18 g/L
MYM-Agar	Maltose	2 g/L
	Yeast extract	4 g/L
	Malt extract	10 g/L
	Bacto-Agar	20 g/L
	H_2O:ddH_2O	1:1
	Trace Element	2mL/L
Soya Flour-Mannitol (SFM)-Agar	Soy Flour	20 g/L
	Mannitol	20 g/L
	Bacto-Agar	20 g/L
Nutrient Agar (NA)	Nutrient Agar (Roth)	23 g/L

MacConkey-Agar

The production of the MacConkey agar plates was performed using the MacConkey Agar obtained from Roth and Difco and based on manufacturer's specifications. The MacConkey agar was sterilized via the process of autoclaving and, if provided by Difco, supplemented with 1% maltose.

3.2.3 Media supplements

Tab. 3.1 List of utilized media supplements

Solutions	Composition
Ampicillin (Amp)	stock concentration 100 mg/mL; final concentration 100 µg/mL
Apramycin (Apra)	stock concentration 100 mg/mL; final concentration 100 µg/mL
Chloramphenicol	stock concentration 100 mg/mL; final concentration 100 µg/mL
Hygromycin B (Hyg)	stock concentration 50 mg/mL; final concentration 22 µg/mL in liquid medium and 18 µg/mL on solid medium
IPTG stock solution	100 mM IPTG
Kanamycin (Kan)	stock concentration 50mg/mL; final concentration 50 µg/mL
Nalidixic acid (Nal)	stock concentration 100 mg/mL; final concentration 100 µg/mL
Trace Element	$ZnCl_2$; $CuCl_2$; $Na_2B_4O_7$;$FeCl_2$; $MnCl_2$; $(NH_4)_6Mo_7O_{24}$ (End concentration of 0.2% in MYM medium (Kieser et al., 2000)

3.3 Bacterial strains and plasmids

All bacterial strains (Table 6.4 and 6.5), bacteriophages (Table 6.6) and plasmids (Table 6.7, 6.8, 6.9 and 6.10) used in this thesis are listed with their references in the appendix.

3.4 Microbiological methods

3.4.1 Sterilization

Unless stated otherwise, sterilization of reaction tubes, pipette tips as well as liquid and solid media took place via autoclaving for 20 min at 121 °C and 1 bar. Heat stable glassware was dry heat sterilized for 8 h at 180 °C. Thermo-sensitive media supplements and buffers were sterile-filtered using cellulose filters obtained by Roth (pore size 0.22 µm) and added at the flame to the autoclaved and at max. 50 °C cooled down media. All solutions relevant for the isolation and analysis of the RNA samples were solved in ddH_2O supplemented with 0.1% DEPC, stirred for 12 h under the hood and autoclaved in order to eliminate ribonucleases (RNases).

3.4.2 Cultivation

Unless otherwise stated, *E. coli* strains were cultivated in LB liquid culture and on LB agar as solid medium at 28 °C or 37 °C and *S. venezuelae* strains were cultivated in MYM liquid culture and on MYM and NA agar as solid media at 30 °C under aerobic conditions by cultivation of the flasks at 170 rpm. Baffled flasks were used to avoid clumping of the mycelium of *S. venezuelae* liquid cultures.

3.4.3 Determination of the cell density in liquid cultures

The cell density in liquid cultures was determined photo-metrically measuring the optical density at a wavelength of 578 nm ($OD_{578\ nm}$). Sterile media was taken as a negative control. The samples of interest were diluted in sterile media in order to ensure the measured value to stay within the linear correlation area between the amount of cells and the optical density. Actual cell densities were calculated via the dilution factor.

3.4.4 SV1-based transduction of *S. venezuelae*

Transduction is another pathway of horizontal gene transfer and describes the injection of foreign DNA e.g. by bacteriophages like SV1 phages into the host bacterium *S. venezuelae* (Das & Dash, 2015). In this study transduction was utilized to transfer an antibiotic resistance cassette integrated in the genome of *S. venezuelae* in a fresh genomic background. Therefore, the appropriate phage lysate was needed.

Enrichment of SV1 phages was performed by mixing 0.5 µL SV1 wild type phages, 100 µL LB, 3 µL *S. venezuelae* wild type spores and 800 µL NA soft agar, pouring this suspension on LB

plates and incubation overnight (oN) at 30 °C. As a negative control, an approach, containing only the SV1 wild type phages was treated likewise. After 24 h plates were overlaid with 2.5 mL LB and incubated oN at 4 °C. Afterwards, the supernatant was harvested using a syringe with a filter (pore size 0.45 µm) and stored in glass screw cap tubes at 4 °C.

The so gained phage lysate was utilized for further production of phage lysates with distinct mutated target genes. Therefore, dilution series of the SV1 wild type phage lysate (10^{-1} to 10^{-5}) were generated. 100 µL of each dilution step was mixed with 4 mL melted NA soft agar (max. 30 °C) and 10 µL spores of the *S. venezuelae* strain, containing the mutation of interest (undiluted spore stock) was added. This suspension was plated on NA agar plates, containing 0.5% glucose, 10 mM $MgSO_4$ and 10 mM $Ca(NO_3)_2$. An approach with equal volume of LB medium instead of the diluted phage lysate served as a negative control. Plates were incubated oN at 30 °C, overlaid, phage lysate was harvested and stored as described above for the wild type lysate.

The so gained mutant phage lysate was utilized for transduction. Therefore, 100 µL phage lysate, containing the antibiotic cassette integrated at the locus of the gene of interest, was mixed with 10 µL spores of the recipient *S. venezuelae* strain and plated onto MYM agar. Plates were incubated oN at room temperature (RT), overlaid with 20 µL of a 50 mg/mL solution of the antibiotic, associated with the resistance cassette, in 2 mL sterile H_2O, dried under sterile conditions and incubated at 30 °C until colonies became visible. Those transductants were verified by re-striking them twice on NA plates with appropriate antibiotics, following phenotypic analysis on MYM plates to identify repressor mutants. Finally spore or mycelium stocks, depending on the nature of the strain, were generated as described in Section 3.4.7.

3.4.5 Generation of chromosomal knockout mutants via PCR-targeting

For chromosomal deletion, target genes were replaced with an antibiotic resistance cassette on a cosmid via the λ RED recombinase system. Therefore, the corresponding resistance cassette was amplified via PCR (apramycin from pIJ773). The utilized primers were designed to amplify the fragment, flanking a 39 bp long sequence homolog to the up- and downstream of the gene of interest. Electrocompetent cells were generated from the *E. coli* BW25113 strain, previously described in Datsenko & Wanner (2000), containing the λ RED plasmid, pIJ790, as described in Section 3.5.8, hence the heat sensitivity of the pIJ790 incubation took place at 30 °C.

These cells were further transformed with the cosmid, containing the gene of interest and prepared for another transformation with 100 ng PCR product (see above). The successful exchange of the gene of interest with the antibiotic resistance cassette via the λ RED recombinase system was verified with colony PCR or gDNA isolated from transformants. Positive tested cosmids were transferred via electroporation in *E. coli* ET12567, containing pUZ8002, previously described in Paget et al. (1999), that is used for conjugation in *S. venezuelae*. Successful conjugation and the loss of the antibiotic resistance cassette that belongs to the cosmid, resulting from two recombination events, were verified by striking out on NA selection medium and PCR.

3.4.6 Construction of Δ*cdgC* complementing strains

For complementation analysis of Δ*cdgC* with *cdgC*, pSVOJ1, containing *cdgC* under the control of its native promoter was introduced into the phage integration site ΦBT1 of *S. venezuelae cdgC* G658A/G659L/D660L by conjugation and the strain was named as SVSN55. For immunodetection, the gene sequence of *cdgC* under the control of its native promoter was cloned into the p3xFLAG plasmid, previously described in Al-Bassam et al. (2018). The localization of the upstream included carboxy-terminal (C-terminal), triple FLAG (MDYKDHDGDYKDHDIDYKDDDDK) affinity tag sequence, created the plasmid named pSVSN-27. To ensure the presence of the native promoter approximately 300 bp upstream the open reading frame of *cdgC*, it was amplified using the primers AA and AB[1]. This and the similar created plasmids pSVSL-4, pSVSL-11 and pSVSL-5 were each introduced by conjugation into *S. venezuelae cdgC* G658A/G659L/D660L by conjugation resulting in strains named SVSN64, SVSN65 and SVSN66, respectively.

3.4.7 Generation of spore and mycelium stocks

S. venezuelae strains were stored by generation of spore or, if the strain is lacking the ability to sporulate, mycelium stocks. The strains were plated comprehensively onto MYM plates and incubated for two days at 30 °C. For spore harvest, 2 mL 20% glycerol in ddH_2O were spread on the plates with a cotton pad and the absorbed spore suspension was collected via a syringe. Spores were transferred into 1.5 mL cryo screw cap tubes and stored at −80 °C. To generate mycelium stocks the strains were incubated as described in Section 3.4.2 in 20 mL liquid MYM medium oN. Five mL of this oN culture were harvested in 15 mL tubes for 15 min at 5000 rpm and the supernatant was discarded. The pellet was resuspended in 500 µL 20% Glycerin in ddH_2O, transferred in 1.5 mL cryo screw cap tubes and stored at −20 °C.

3.4.8 Storage of strains, bacteriophage lysates and spore stocks

For short term storage on solid medium, bacterial strains were stored at 4 °C for max. five days. For long term storage, *E. coli* strains were grown in liquid culture, harvested following resuspension of the pellet in dimethylsulfoxid (DMSO; final concentration: 7%) and storage at −80 °C. For conservation, *S. venezuelae* strains were incubated at 30 °C on MYM agar until the entrance into sporulation phase and spore stocks were harvested and stored as described in Section 3.4.7.

3.4.9 Determination of the spore titer of *S. venezuelae*

To ensure that all experiments with *S. venezuelae* were inoculated with a distinct amount of bacteria in the same state of the cell cycle, spore titers of each strain were determined. A dilution series of each spore stock was generated in 20% glycerol, followed by appropriate dilutions on NA agar and incubation for two days at 30 °C. The colony forming units (CFU) were counted and the spore titer was calculated, including the dilution factor in CFU/µL volume of the undiluted spore stocks.

[1] named "5187-HindIII-pMS82-f" and "sven15_5080_XhoI_r" in Al-Bassam et al. (2018)

3.4.10 Phenotypic analysis of macrocolonies on solid medium

For phenotypic analysis of each *S. venezuelae* strain, macrocolonies were grown on MYM agar plates as sporulation inducing medium. For cultivation of the macrocolonies on solid medium, a 12 µL drop of a $2 \cdot 10^5$ dilutions of each spore stock were placed on MYM plates and incubated for five days at 30 °C. The colonies were documented at distinct time points under a binocular microscope using the same adjustments each time.

3.4.11 Coverslip impressions

Macrocolonies of *S. venezuelae*, grown on MYM solid medium, were prepared for the microscopic analysis of spores and hyphae using the coverslip impression technique. Therefore, the coverslip was pressed firmly on the colonies to transfer cells on an agarose coated microscope slide.

3.4.12 Phase contrast and confocal microscopy

Samples were harvested from solid medium, as described in Section 3.4.11, while in case of liquid culture 10 µL were collected and dropped on a microscopic slide. The drop was incubated for a couple of minutes at RT, followed by placing a coverslip on top. These prepared microscope slides were analyzed with phase contrast and confocal microscopy. Phase contrast images were taken at 100-fold enlargement directly followed by a fluorescent image captured with a fluorescent filter and an exposure time of 800 ms. Used channels were „TL Phase 3“ and „mCherry“. Images were all post-edited in the same manner using "Adobe Photoshop" and arranged with "Adobe Illustrator".

3.5 Molecular biological methods

3.5.1 Utilized kits

- Kit for isolation of the genomic DNA from bacteria (innuPREP Bacteria DNA Kit): Analytik Jena, Jena
- Kit for plasmid preparation in small scale (innuPREP Plasmid Mini Kit 2.0): Analytik Jena, Jena
- Kits for purification of DNA from agarose gels (Monarch® DNA Gel Extraction Kit): New England Biolabs
- Kit for purification of PCR- or restriction digest-samples (PCR Purification Kit): (Monarch® PCR & DNA Cleanup Kit): New England Biolabs
- Kit for total RNA isolation (SV Total RNA Isolation Kit): Promega
- Kit for qRT-PCR detection (SensiFAST SYBR No-ROX One-Step Kit): Bioline

3.5.2 Utilized oligonucleotides

All utilized oligonucleotides with their references are listed in Table 6.11, 6.12 and 6.13 in the appendix and were ordered from Metabion International AG.

3.5.3 Polymerase chain reaction (PCR)

The amplification of DNA fragments for cloning or sequencing was performed via PCR using either chromosomal DNA, plasmid DNA or lysed bacterial suspension as a template. Restriction sites, point mutations or other DNA sequences needed for further usage were inserted or added to the gene fragment by using appropriated primers (see Table 6.11). PCR reactions were performed in either 25 µL or 60 µL of total volume (see Table 3.2) using either Q5 or Opti-Taq polymerase modified after Sambrook et al. (1989). The PCR profile was modified individually based on manufacturer's specifications for each reaction.

Tab. 3.2 Composition of a standard PCR

Reagent	Amount
Template	2 ng gDNA; 0.5 µL plasmid; 1 µL bacteria suspension
5'- and 3'Primer	0.3 µM
dNTPs	0.5 mM
5× Polymerase buffer	1×
DNA polymerase	1.25 U
ddH_2O	rest volume

3.5.4 Restriction digest

To prepare a ligation of a DNA fragment in a vector or to verify the success afterwards (control digest), PCR products and target-vectors were equipped with distinct restriction sites. Therefore, the purified DNA fragment and the vector were incubated with the same restriction enzymes, according to the manufacturer's protocol, whose restriction sites laid in the target-vector and added via the primers to the PCR products. The reaction samples contained the corresponding restriction enzymes in the appropriated reaction buffer and incubated for 1-2 h at 37 °C. The purification of the products was performed with the "PCR purification" kit based on manufacturer's specifications in case of preparative restriction digest of PCR products and target-vectors samples and control digest samples via agarose gel electrophoresis. The latter showed success of the ligation with a DNA band pattern and positive tested clones were sequenced by the company LGC.

3.5.5 Agarose gel electrophoresis

To analyze the DNA fragments by means of length of their nucleotide strands gel electrophoresis was performed in 0.8-2.5% agarose gels (1% (w/v) agarose in 1xTAE buffer (see 50 ×TAE in Table 6.3). Samples were mixed with 6xDNA loading buffer (see Table 6.3) and loaded in the

agarose gel pockets. Gels, containing the samples in electrophoresis chambers filled with 1xTAE buffer were exposed to 90 V constant direct voltage. Hence the negative loading of the nucleic acid molecule, DNA was pulled along the applied power to the anode. The size-dependent lead time of the DNA strands through the agarose gel causes a horizontal fractionation. GelRED intercalated in a dye bath (0.007% (w/v) GelRED in ddH_2O) with the DNA, causing it to be visible under UV light. For further utilization after a PCR or a restriction digest, DNA bands were cut out of the agarose gel and purified with the help of the Monarch® DNA Gel Extraction Kits (NEB).

3.5.6 Ligation

Enzymatic catalyzed reactions linking two DNA fragments via their ends is described as ligation. The ends of the DNA fragments, which were processed during a restriction digest (see Section 3.5.4), show 4 bp single strand overlaps (*sticky-end*) or no overlaps (*blunt-end*) specific for each restriction enzyme. *Blunt-ends* can be linked sequence independently during the ligation reaction, whereas *sticky-end* sequences must complement each other. If this holds true, formation of phosphodiester bindings between the 3'-OH and the 5'-phosphate end of the DNA fragments were catalyzed by utilization of the T4 DNA ligase. Ligation reactions were performed using the T4 DNA Ligase (NEB) (ligation reaction composition see Table 3.3) and incubating them in a thermocycler (140× at 10 °C, then at 30 °C for 30 s) or at 4 °C for up to two days.

Tab. 3.3 Composition of a standard ligation

Reagent	Amount
PCR-product, digested	10 µL
Plasmid, digested	1 µL
T4 ligase buffer	3 µL
T4 ligase	1 µL
ddH_2O	Rest volume

3.5.7 TSS transformation

Plasmid DNA was transferred in recipient *E. coli* strains either with the help of the TSS transformation (only plasmids transformable with low efficiency) or with electroporation (plasmids or PCR products transformable with high efficiency). The TSS transformation of already purified plasmid DNA took place, according to Chung et al. (1989). Two mL LB medium were inoculated with the recipient *E. coli* strain and incubated for 2 h at 28 °C or 37 °C under shaking conditions until a slight opacity ($OD_{578\ nm}$ 0.3 - 0.4, logarithmic growth) was observed. Cells were mixed 1:1 with 2× TSS and 1-2 µL plasmid and incubated for 30 min on ice. Afterwards, samples were incubated for 1 h at 28 °C or 37 °C under shaking conditions and plated onto appropriated selection plates.

3.5.8 Preparation of electrocompetent *E. coli* cells

For preparation of the recipient *E. coli* strain for electrotransformation, the according strain (see Table 6.5) was cultivated oN in 5 mL LB medium at 37 °C under shaking conditions. The oN culture was used to inoculate the main culture using a 1:100 dilution. The main culture was incubated in LB medium at either 28 °C or 37 °C under shaking conditions up to 0.5 $OD_{578\ nm}$. Subsequently the cells were incubated on ice for 30 min, centrifuged (15 min, 4 °C, 7000 rpm), the supernatant discarded and the pellets washed via several resuspension (in dH_2O and 10% glycerol) and centrifugation steps. Finally, the cells were suspended 200-500× concentrated relative to the start volume in 10% glycerol, dispensed and stored at −80 °C.

3.5.9 Electrotransformation

For electroporation, 50 µL of the electrocompetent recipient strain (see Section 3.5.8) were mixed with 1-10 µL DNA or ligation sample. After transferring the sample to a pre-cooled electroporation cuvette (Biorad), 2.5 kV power were applied for 4 ms with the electroporator Gene Pulser Xcell (Biorad). After electroporation, the cells were immediately picked up in 500 µL LB medium and incubated for 1 h at either 28 °C or 37 °C before plating them onto appropriate selection plates.

3.5.10 RNA isolation

Macrocolonies of the relevant *S. venezuelae* strains were created, as described in Section 3.4.10, and incubated for 30 h at 30 °C. Biomass from three macrocolonies was pooled, resuspended in 200 µL ice-cold stop solution (5% phenol, pH 4.3, solved in 98% ethanol, Roth) and centrifuged for 10 min at 4 °C and 14800 rpm to remove the supernatant. The cell pellets were stored at −80 °C until the RNA isolation. Pellets were resuspended in 700 µL RLA buffer (Promega) and divided into two 350 µL fractions. RNA isolation was continued with one of the fractions, while the other was stored at −80 °C as spare, by adding 352 µL Phenol (Roth, RNA, pH 4.3) and 88 µL Chloroform:Isoamyl alcohol 24:1 (AppliChem). The suspension was then transferred into tubes with Lysing Matrix B (MP Biomedicals), following lysis using a FastPrep-24™ 5G Instrument (MP Biomedicals; 5 pulses, 30 s of intensity 6.0 m/s, with 1 min intervals). Subsequently, the cell crude was pelleted by centrifugation for 15 min at 4 °C at 14000 rpm, the supernatant was transferred into a new reaction tube and this whole step was repeated. The lysates were mixed with RNA Dilution buffer (Promega) in a 1:2 volume ratio (350 µL : 690 µL) and incubated at 70 °C for 3 min. 395 µL 98% ethanol were added and the RNA isolation was further performed using the SV Total RNA Isolation Kit after the manufacturer's protocol (Promega). Elution was performed with 100 µL RNase free water (Promega) and the RNA samples were additionally treated with DNase I treatment (Turbo DNA-free, Ambion) according to the instructions in the manual. RNA quantity and quality were analyzed using NanoDrop 2000 (Thermo Scientific) and Bioanalyzer 2100 (Agilent) software.

3.5.11 qRT-PCR

To quantify the amount of transcripts of a gene of interest in a distinct strain relative to the control strain, qRT-PCR was performed using the SensiFAST SYBR No-ROX One-Step Kit (Bioline). 2 µL of isolated RNA samples, described in Section 3.5.10, were adjusted to a concentration of 10 µg/µL and used in three technical replicates of each gene in every run. Distinct qRT-PCR primers (melting temperature 60 °C, final concentration 250 nM) amplifying a fragment of 70-150 bp of the target genes (*bldM*, *bldN*, *chpC*, *chpE*, *chpH*, *cdgA*, *cdgB*, *cdgC*, *cdgE*, *cdgF*, *rmdA* and *rmdB*) and the reference gene *hrdB* were used. For normalization, primer efficiency was tested by generating a standard curve using chromosomal DNA. For each primer pair, melting curve analysis was performed, confirming the production of a specific single product. qRT-PCR was run on a CFX Connect™ real time system (Bio-Rad) using sealed 96-well PCR plates (BioRad). PCR products were amplified according to the following protocol: 45 °C 20 min, 95 °C 5 min, then 35 cycles at 95 °C 10 s, 60 °C 20 s and 72 °C 10 s. The melting curves were generated from 65 °C to 95 °C with 0.5 °C increments and experiments were repeated at least three times independently. The resulting mean starting quantity (SQ) values were averaged and the fold difference was calculated by the standard curve method using the formulas below and then converted the values into $\log_2$-fold change:

$$\text{Fold difference} = \frac{(E_{\text{target}})^{\Delta C_{\text{t target}}}}{(E_{\text{normalizer}})^{\Delta C_{\text{t normalizer}}}}$$

$$E = 10^{-1/slope}$$

$$\Delta C_{\text{t target}} = C_{\text{t GOI}^c} - C_{\text{t GOI}^s}$$

$$\Delta C_{\text{t normalizer}} = C_{\text{t norm}^c} - C_{\text{t norm}^s}$$

where

E and *slope* denote the efficiency and first derivative of the standard curve,
C_{t} denotes the cycle threshold,
GOI or *target* denotes the gene of interest,
normalizer or norm denotes the reference gene (in this study *hrdB*),
c denotes the calibrator sample (in this case *S. venezuelae* WT) and
s denotes the test sample (here Δ*cdgC*).

3.6 Protein biochemical methods

3.6.1 Cell fractionation

For immunodetection, *S. venezuelae* cells were grown in MYM and samples of 2 mL were taken every 2 h. Samples were harvested (2 mL per sample), washed and resuspended in 1xPBS (see Table 6.3) with cOmplete protease inhibitor cocktail tablets, EDTA-free (Roche) except for immunodetection of FtsZ-Ypet. Here samples were treated, as described in Schlimpert et al. (2017). Cells were resuspended in the respective lysis buffer, homogenized using a BeadBeater (Biozym; six cycles at 6.00 m/s; 30 s pulse; 60 s interval) and cell debris was centrifuged at 14800 rpm for 10 min at 4 °C. Total protein concentration was determined using the Bradford Assay (Roth) and respectively adjusted to 1 mg/mL.

3.6.2 SDS-Polyacrylamide gel electrophoresis (SDS-PAGE)

For molecular weight-dependent separation of proteins, acrylamide gels (see Table 3.4) were used modified after Laemmli (1970). Therefore, protein samples were mixed with SDS sample buffer (see Table 6.3 in the appendix; final concentration 1×) and heated before loading. Membrane proteins were incubated 10 min at 70 °C and cytosolic proteins at 95 °C. The appropriate amount of total protein was loaded on a SDS gel and proteins were separated with 25 mA per gel.

Tab. 3.4 Composition of acrylamide solutions for production of stacking and running gels (5 × 10 cm).

Reagents	Stacking gel	Running gel		
Acrylamide concentration	4%	10%	12%	15%
Gel buffer Tris·HCl pH 8.8 0.4% SDS	-	1.25 mL		
Gel buffer Tris·HCl pH 6.8 0.8% SDS	0.625 mL	-		
Acrylamide	0.325 mL	1.5 mL	2 mL	2.5 mL
H_2O	1.535 mL	2.225 mL	1.725 mL	1.225 mL
10% Ammonium persulphate (APS)	17 µL	50 µL		
Tetramethylethylenediamine	10 µL	5 µL		

3.6.3 Immunoblot analysis (Western Blot)

Specific immunodetection of proteins was performed via Western blotting. After an electrophoretic separation via SDS-PAGE (see Section 3.6.2), proteins were transferred on a PVDF membrane with the help of a blotting apparatus (Biorad). In advance of the transfer, the membrane was equilibrated in ethanol, H_2O and trans blot buffer (see Table 6.3) and placed, free of air bubbles, on the SDS gel. Gel and membrane were inserted between Whatman papers (Roth) soaked in transblot buffer. The transfer was performed for 90 min at 100 V and maximum current strength in cold transblot buffer. Unspecific binding sites were blocked by incubation of the membrane either for 2 h at RT or oN at 4 °C with milk protein in TBSTM (5% milk powder in TBST, see Table 6.3). Then the incubation with primary and secondary antibody (see Table 3.5) was performed for 2 h at RT or oN at 4 °C, each disrupted by three washing steps in TBST. Then visualization was realized, in this study via chemiluminescence (BioRad) based on manufacturer's specifications and documentation with a CCD camera.

Tab. 3.5 Utilized antibodies and their final concentrations

Detected peptide	Primary antibody (dilution)	Secondary antibody (dilution)
BldD	α-BldD-tag (1:10,000)	α-Rabbit (1:10,000)
BldM	α-BldM-tag (1:10,000)	
BldN	α-BldN-tag (1:10,000)	
RsiG	α-RsiG-tag (1:10,000)	
WhiG	α-WhiG-tag (1:10,000)	
CdgA/B/C/E-FLAG	α-FLAG-tag (1:10,000)	α-Mouse (1:10,000)
Ypet	α-GFP(1:3,000)	

3.6.4 Protein overexpression and purification

Plasmids for overexpression of cytosolic part (ΔTM), the `GGDEF` domain, the `EAL` domain and the cytosolic part without the `EAL` domain of *cdgC* (ΔTM-Δ`EAL`), were generated using PCR with oligonucleotides listed in Table 6.11 and either genomic DNA, the cosmid PI-C11 or pSVOJ1 (Al-Bassam et al., 2018) as templates. All gene sequences of interest were cloned into pET15b (Novagen), containing the IPTG inducible T7 promoter and an amino-terminal (N-terminal) 6× `His` tag. The resulting plasmids were named pSVSN1-4 (see Table 6.8 for description). Plasmids were transferred in *E. coli* Rosetta (Novagen) and the culture was incubated at 37 °C, until they reached an $OD_{578\,nm}$ of 0.6. Expression was induced with 50 µM IPTG, following incubation at 16 °C oN. The cells were harvested for 15 min at 4 °C and 6000 g and pellets stored at −20 °C until the purification proceeded. For purification, the cell pellets were thawed on ice, resuspended in 35 mL lysis buffer (50 mM Tris·HCl, pH 8.0; 500 mM NaCl; 20 mM imidazole; 1 mM $MgCl_2$; 5 mM β-mercaptoethanol; 0.1% Triton X 100; 5% glycerol and cOmplete Protease Inhibitor Cocktail Tablets (Roche)) and lysed by 5× passage through a Frenchpress. After centrifugation for 40 min at 4 °C and 17000 rpm, soluble fractions were used for native protein purification of 6xHis-CdgC-`GGDEF`, -`EAL`, -ΔTM and ΔTM-Δ`EAL`, PleD* and PdeH (as positive controls) using Ni-NTA chromatography following standard protocols (Quiagen) at RT. Pre-cooled lysis buffer was used for several washing steps and high concentrations of imidazole were used in an elution buffer (50 mM Tris·HCl, pH 8; 300 mM NaCl; 250 mM imidazole; 1 mM β-mercaptoethanol and 10% glycerol) to oust the 6xHis-tagged proteins from the Ni-NTA matrix in five steps of 1 mL each. Prior activity assays, the purified protein was dialysed against a modified cyclase reaction buffer (25 mM Tris·HCl, pH 7.5; 100 mM NaCl; 10 mM $MnCl_2$; 5 mM β-mercaptoethanol; 5% glycerol) at 4 °C for 4 h. Determination of protein concentrations were performed via SDS-PAGE (see Section 3.6.2) against a standard curve of low molecular weight marker, coomassie staining and analysis using a CCD camera and the software ImageTL.

3.6.5 Enzymatic DGC and PDE activity assays

For the analysis of the enzymatic activity of purified variants of CdgC *in vitro*, PDE and DGC assays after Christen et al. (2005) and Weber et al. (2006) were performed with slight modifications. Therefore, 1 µM purified protein in cyclase reaction buffer (25 mM Tris·HCl, pH 7.5; 100 mM NaCl; 10 mM $MnCl_2$; 5 mM β-mercaptoethanol; 5% glycerol) was incubated

with 4.16 nM [α^{32}P]GTP (Hartmann Analytic GmbH) or 2.08 nM [α^{32}P]c-di-GMP (Hartmann Analytic GmbH) at 30 °C for 1-3 h. The reaction was stopped by adding 5 µL 0.5 M EDTA pH 8 to equal volume of reaction mixture, followed by heating the samples to 95 °C for 5 min. PleD*, a constitutive active DGC from *C. crescentus* (Paul et al., 2004), was added as positive control in DGC assays. PdeH from *E. coli* (Pesavento et al., 2008) served as positive control in PDE assays. Samples were separated by thin layer chromatography on Polygram CEL 300 PEI cellulose TLC plates (Macherey–Nagel) incubated in 1:1.5 (v/v) saturated NH_4SO_4 and 1.5 M KH_2PO_4, pH 3.6. The plates were dried and exposed on a Phosphor Imaging Screen (GE), which was then scanned by Typhoon Scanner FLA 7000 (GE).

3.6.6 UV-crosslink

To analyze the ability of variants of purified CdgC peptide to bind GTP and c-di-GMP UV-crosslinks were performed. Cytosolic variants of CdgC, described and purified as in Section 3.6.4 (4 µg protein in 20 µL end volume), were mixed with radio-labeled GTP ([α^{32}P]GTP; 3000 Ci/mmol) or c-di-GMP (c-di-([α^{32}P]GMP; 6000 Ci/mmol) and first incubated for 15 min at 30 °C, following 4 min for irradiation at 365 nm and maximum intensity in the pre-cooled UV-crosslinker BLX 365 (Peqlab). Samples were analyzed via SDS-PAGE (see Section 3.6.2) and gels were exposed on a Phosphor Imaging Screen (GE), which was then scanned by Typhoon Scanner FLA 7000 (GE).

3.6.7 Analysis of protein-protein interactions

Bacterial Two-Hybrid assay after Karimova et al. (1998)

The analysis of protein-protein interactions of *S. venezuelae* proteins *in vivo* was performed with the bacterial two-hybrid system after Karimova et al. (1998) in *E. coli* W3110Δ*cya*. This method is based on the restoration of the cAMP-dependent regulation cascade, controlling i.a. the degradation of alternative carbon sources. The T18 and T25 subunits of the adenylate cyclase from *Bordetella pertussis* were introduced in a *E. coli* K-12 strain carrying a *cyaA* deletion, which is unable to synthesize cAMP via co-transformation of the plasmids pKT25 or pKNT25 and pUT18 or pUT18C. These plasmids (see Table 6.9) were cloned using primers described in Table 6.11 to encode gene sequences of fusion proteins of T18 or T25 and one of the proteins of interest. Interaction between both proteins of interest led to physical proximity and interaction of the T18 and T25 sub-units, restoring the enzymatic activity. Formation of cAMP and its binding of the transcription regulator CRP enabled the degradation of alternative carbon sources like lactose and maltose. Transformants were selected on LB agar, containing Amp, Kan and 5-Bromo-4-chloro-3-indolyl-β-D-galactopyranoside (X-Gal). Three equal sized colonies were picked per combination, suspended in 1 mL 1× PBS (see Table 6.3), 5 µL of this bacterial suspension placed onto MacConkey, containing 1% maltose, 1% lactose or both, Amp and Kan and incubated for 24, 43, 90 or 108 h at 26 °C.

Pulldown assays

To identify protein-protein interactions in the *S. venezuelae* strain background pulldown assays were performed against FLAG-tagged CdgC, which was expressed under the control of its native promoter from the phage integration site ΦBT1 of *S. venezuelae* Δ*cdgC*. This strain, along with the *S. venezuelae* wild type as a negative control, was cultivated in MYM medium for 20 h at 30 °C and at 170 rpm and, afterwards, harvested for 20 min at 4 °C and 10000 rpm.

The pellet was washed in 20 mL 1× PBS (see Table 6.3), containing cOmplete Protease Inhibitor Cocktail Tablets (Roche) and resuspended in 25 mL TBS buffer (see Table 6.3). The cells were lysed in lysis buffer (50 mM Tris·HCl, pH 7.5; 150 mM NaCl; 1 mM EDTA; 0.8% Triton and cOmplete Protease Inhibitor Cocktail Tablets (Roche)), passing 5× though a french press. The cell debris were pelleted by centrifugation for 10 min at 5000 rpm and 4 °C in a swing rotor. The total protein concentration was analyzed using a Bradford assay and equal amounts of protein were utilized to purify CdgC-FLAG and its interacting proteins via a FLAG affinity matrix. The affinity matrix was activated with three column volumes 0.1 M glycine, pH 3.5. The cell lysate was passed 3× through a column, collected and stored at −20 °C. Afterwards, the matrix was washed with five column volumes of TBS buffer (see Table 6.3). 500 µL of 100 µg/mL FLAG-Peptide were added to the matrix, which was incubated for 30 min on ice before elution. Eluates were boiled for 10 min at 95 °C (to analyze cytosolic proteins) or at 70 °C (to analyze membrane proteins), separated via SDS-PAGE (see Section 3.6.2) and analyzed using immunodetection using antibodies against BldD, BldM, BldN, RsiG, WhiG and FLAG-Tag (as a positive control).

3.7 Databases and bioinformatic analyses

During the development of this research project, the following databases and software were used to obtain and analyze information about gene sequences:

- Adobe Illustrator CC 2018
- Adobe Photoshop CC 2018
- ChemDraw Std 12.0
- Fiji (**F**iji **i**s **j**ust **I**mageJ)
- NCBI (`www.ncbi.nlm.nih.gov`)
- NEB Tm Calculator (version 1.13.0)
- Serial Cloner (version 2.6.1)
- SnapGene Viewer (version 3.3.1)
- StrepDB (`strepdb.streptomyces.org.uk`)
- Zeiss Zen Blue 2

Chapter 4

Results

4.1 The composite GGDEF-EAL protein CdgC is an active diguanylate cyclase

This thesis focuses on the detailed characterization of the GGDEF-EAL protein CdgC, which plays a major role in the coordination of the developmental life cycle in *S. venezuelae*. Preliminary data indicated that CdgC is one of four developmental c-di-GMP turnover proteins (Al-Bassam et al., 2018). Its deletion causes precocious sporulation without aerial hyphae formation (see Fig. 1.10 on page 20). With this striking phenotype, the *cdgC* mutant resembles the deletion strain of the developmental master regulator BldD as well as a strain overexpressing the *E. coli* PDE PdeH. These observations suggest that CdgC plays a key role in the c-di-GMP-dependent developmental regulation in *S. venezuelae*.

This thesis focuses on the molecular function of CdgC. Bioinformatic analyses of the domain architecture of the 1039 amino acids long protein predicted ten N-terminal transmembrane domains anchoring the protein at the membrane (Tsirigos et al., 2015). The following cytosolic protein fraction contains a PAS-PAC domain, a conserved GGDEF domain and a degenerate EAL (EAL_{deg}) domain (see Fig. 4.1 A). The GGDEF domain of CdgC contains a conserved A-site with a GGDEF motif and all conserved residues that are essential for binding GTP via its guanine molecule, Mg^{2+} coordination and catalysis (see Fig. 4.1 B). Like the majority of active DGCs, CdgC carries a RxxD (R649/D652) in close proximity to the A-site, forming the inhibitory site (I-site). This suggests that CdgC is able to bind GTP as well as c-di-GMP at the GGDEF domain and to synthesize c-di-GMP.

The EAL domain of CdgC is degenerate in that it lacks all conserved residues that are essential for catalysis, carrying an alanine instead of a threonine at position 885 and an aspartic acid instead of a glutamic acid at position 971 (see Fig. 4.1 C). Together with the missing EAL motif, a PDE activity of the EAL domain of CdgC seems very unlikely. On the other hand, the EAL domain might still fulfill a regulatory function in CdgC by binding c-di-GMP since it lacks only one aspartic acid (D935) for c-di-GMP binding, while the other three residues are conserved.

In the following, the ability of CdgC to bind GTP and c-di-GMP, as well as its enzymatic activity, shall be verified biochemically.

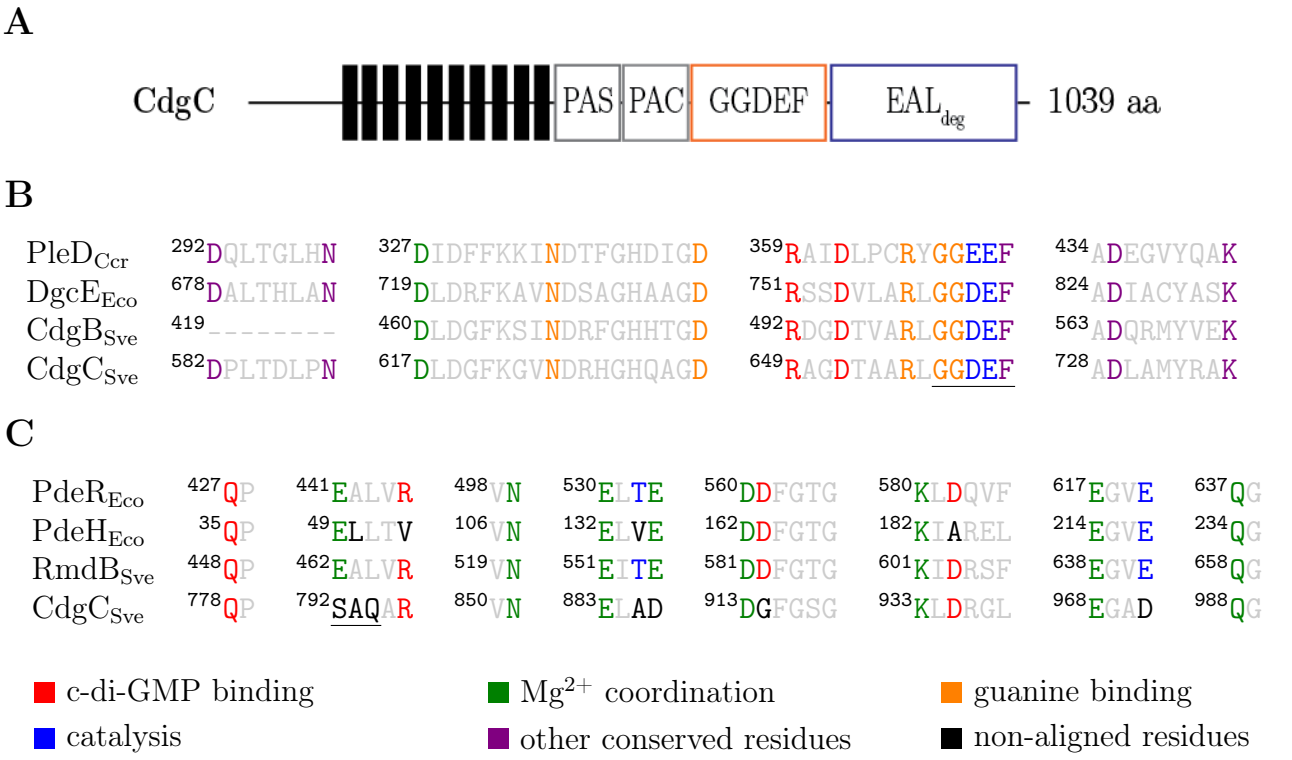

Fig. 4.1 Domain organization (A) and conservation of active site amino acid residues in the GGDEF (B) and EAL (C) domains in CdgC. (A) Bioinformatic software like TOPCONS and SMART predicts that CdgC contains ten transmembrane domains (black bars), a sensory PAS-PAC domain (gray boxes), a GGDEF domain (red box) as well as an EAL domain (blue box) (Tsirigos et al., 2015; Letunic & Bork, 2017; Letunic et al., 2020). The sequence analyses shown in (B) and (C) were generated with the help of Clustal Omega (Sievers et al., 2011). Conserved residues were highlighted in color according to their postulated function in c-di-GMP (red), Mg^{2+} coordination (green) or guanine binding (orange) as well as catalysis (blue) as postulated by Rao et al. (2008) for PDEs and by Schirmer (2016) collected for DGCs. Further conserved residues (violet) and residues deviating from the conserved signature (black) are shown (Schirmer, 2016). Sequences of the GGDEF domain containing proteins *C. crescentus* NA1000 PleD, *E. coli* K-12 DgcE as well as *S. venezuelae* CdgB (Sven15_3942) and CdgC (Sven15_5080) are shown in (B). Sequences of the EAL domain containing proteins *E. coli* K-12 PdeR and PdeH as well as *S. venezuelae* RmdB (Sven15_5058) and CdgC (Sven15_5080) are shown in (C).

4.1.1 Cytosolic CdgC binds GTP and c-di-GMP *in vitro*

Composite GGDEF-EAL proteins like CdgC might bind to GTP and c-di-GMP both at the conserved GGDEF domain and the EAL_{deg} domain with the latter potentially functioning as a sensory domain. This is especially likely since the EAL domain lacks only one aspartic acid of four residues involved in c-di-GMP binding (see Fig. 4.1). UV-crosslink assays were used to test the ability of the single domains of CdgC to bind GTP and c-di-GMP *in vitro* after Christen et al. (2005). Herein, the single GGDEF (pSVSN-4) and EAL (pSVSN-3) domains, as well as the cytosolic fraction of *cdgC* with (pSVSN-2) and without the EAL domain (pSVSN-1), were cloned under the control of an IPTG inducible T7 promoter and fused to a 6× His tag. These plasmids were introduced and overexpressed in *E. coli* Rosetta (DE3). Cells were harvested and the proteins purified via the nickel affinity chromatography. The purified proteins were irradiated for 20 min at a wavelength of 254 nm, separated via SDS-PAGE and visualized using immunodetection against the 6× His tag.

The results, illustrated in Fig. 4.2, show that the cytosolic CdgC with and without the EAL domain produced one radio-labeled band when incubated with c-di-GMP but several with GTP. Comparing the bands with the expected protein sizes and considering the general ability of the domain to bind the tested ligand, the band pattern indicates that band 1 is CdgC protein without transmembrane domains (68 kDa). This protein shows binding of GTP at the GGDEF domain and c-di-GMP, either at the I-site of the GGDEF domain or at the EAL domain. Band 2, 3 and 4 ran very close together and contain the PAS-PAC-GGDEF peptide of CdgC (expected to run at about 37 kDa) with modifications in the presence of the 6× His tag and linkers. While all three variants bind GTP at the GGDEF domain, only one of them appears to bind c-di-GMP. As this protein variant does not contain the EAL domain, c-di-GMP has to bind at the I-site of the GGDEF domain. Band 5 equals the size of the PAC-GGDEF domain (25 kDa) and binds only GTP at the GGDEF domain. The bands 3-5 appear as bands of lower molecular weight when analyzing cytosolic CdgC with and without the EAL domain, suggesting them to be degradation products. In contrast, single GGDEF and EAL domains show binding to neither GTP nor c-di-GMP. As a positive control for GTP binding at its A-site, PleD* showed a very weak band at the expected height of about 50 kDa (Christen et al., 2005) while the negative control, BldD, showed no radio-labeled protein band, providing evidence that the assay works methodically.

Taken together, these results reveal that CdgC is able to bind c-di-GMP, most likely at the I-site of the GGDEF domain, and GTP at the GGDEF domain independent from the presence of the EAL domain. This allows the hypothesis that CdgC might have an enzymatically active GGDEF domain regulated by a c-di-GMP binding I-site that shall be analyzed in the following.

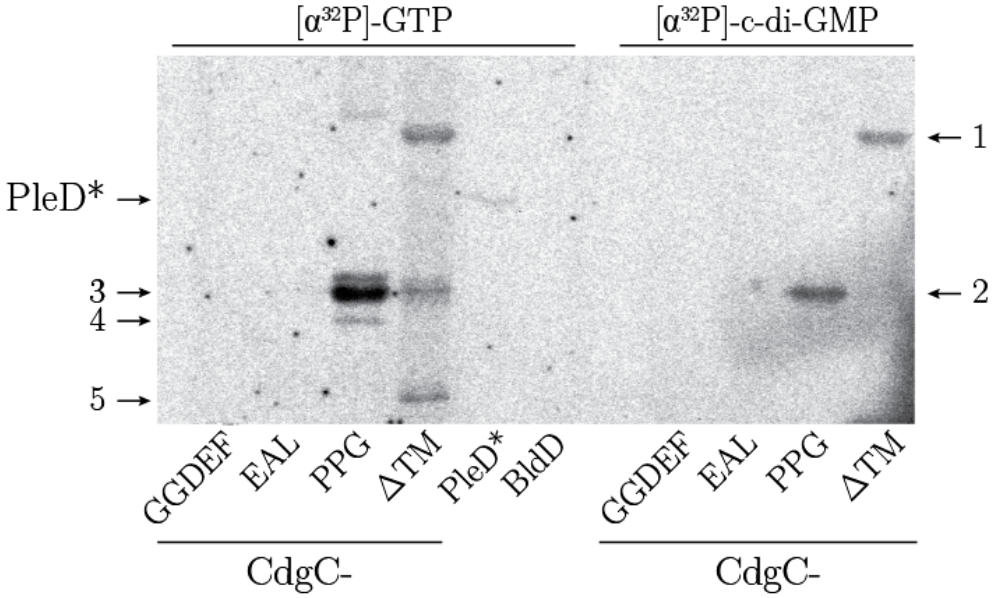

Fig. 4.2 The cytosolic fraction of CdgC binds GTP and c-di-GMP independent of the presence of the EAL domain. Binding of second messengers was investigated using purified variants of the cytosolic fraction of CdgC, incubated for 15 min at 30 °C with radio-labeled GTP ([α^{32}P]GTP; 3000 Ci/mmol) and c-di-GMP (c-di-[α^{32}P]GMP; 6000 Ci/mmol), irradiated for 4 min with UV light using an *in vitro* UV-crosslink and visualized via SDS-PAGE. PleD* served as a positive and BldD as a negative control. 1 - CdgC without the transmembrane domains; 2 - ΔTMΔEAL-CdgC; 3 - ΔTMΔEAL-CdgC without the 6× His tag; 4 - ΔTMΔEAL-CdgC without 6× His tag and linker domain; 5 - only the PAC and GGDEF domain

4.1.2 CdgC shows *in vitro* diguanylate cyclase activity

The domain architecture of CdgC features a conserved `GGDEF` domain suggesting a DGC activity. According to the sequence analysis (see Fig. 4.1), it can be assumed that the `EAL` domain is enzymatically inactive. Nevertheless, a direct biochemical verification of the enzymatic activity of CdgC is still missing. To remedy this, activity assays for DGC and PDE were performed. To this end, the purified proteins (see Section 4.1.1) were incubated in an appropriate buffer with radio-labelled c-di-GMP and GTP, respectively, for up to 3 h, as described in Section 3.6.5. The results are shown in Fig. 4.3 and 4.4. The *in vitro* enzymatic assays verified the DGC activity of CdgC with no enzymatic or binding activity of the isolated `EAL` domain, indicated by UV-crosslink assays *in vitro* (see Fig. 4.2).

In the DGC assays, the `GGDEF` domain alone was not able to synthesize c-di-GMP even after 3 h incubation, unless combined with the PAS-PAC domain and, even more pronounced, when complemented by the `EAL` domain (see Fig. 4.3). The spot observed at the expected height of c-di-GMP became more intense with increased incubation time. The *C. cresentus* DGC PleD served as a positive control, showing complete turnover of GTP to c-di-GMP (Chan et al., 2004; Paul et al., 2004). A reaction mixture with buffer instead of protein served as a negative control. In all lanes, except for the controls, the spot for GTP lies slightly below that of the negative control. The `GGDEF` domain expressed alone most likely fails to fold and dimerize properly. The PAS-PAC and `EAL` domains seem to facilitate the synthesis of c-di-GMP from GTP, probably by supporting the dimerization or folding of the protein.

In the PDE assays, none of the CdgC variants containing the `EAL` domain showed a significant and, proportionally to a prolonged incubation time increasing degradation of c-di-GMP (see Fig. 4.4). With increased incubation time, neither an intensification of the spot at the expected height of linear pGpG, nor a weakening of the c-di-GMP spot could be observed in presence of the `EAL` domain alone. This suggests an artificial linearization caused by the increased temperature. Additionally, the peptide variant of CdgC, lacking only the transmembrane anchor, did not show this spot at all. The *E. coli* PDE PdeH served as a positive control and showed complete degradation of c-di-GMP (Pesavento et al., 2008). A reaction mixture with buffer instead of protein served as a negative control.

Altogether, these experiments showed that CdgC is an active DGC *in vitro*, lacking any significant PDE activity. This raises the question for the impact of this DGC activity on the physiological role of CdgC in *S. venezuelae*.

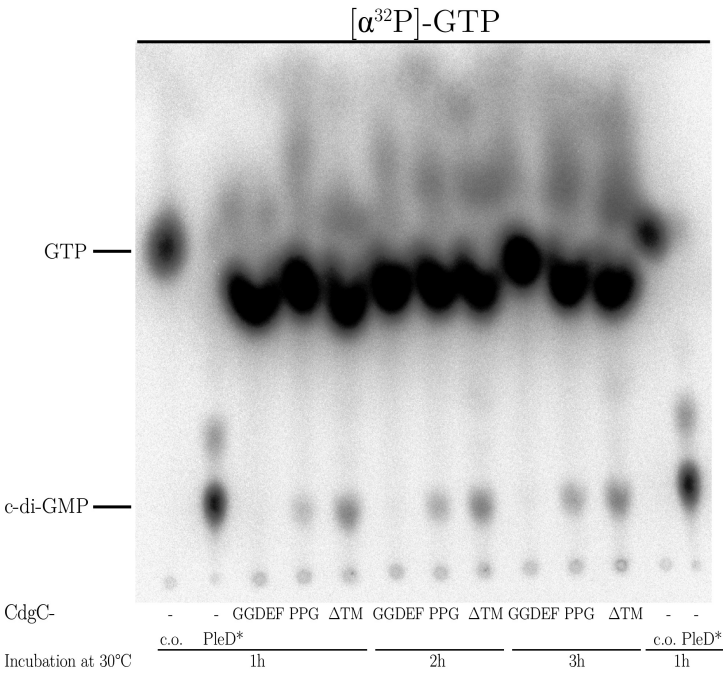

Fig. 4.3 CdgC shows DGC activity *in vitro*. Synthesis of c-di-GMP from GTP was verified using purified variants of the cytosolic fraction of CdgC, incubated in an *in vitro* DGC assay with 83 nM radio-labeled GTP ([α^{32}P]GTP; 3000 Ci/mmol) for up to 3 h and visualized via thin-layer chromatography with exposure on IP plates. This figure was modified with permission after Al-Bassam et al. (2018); published in Frontiers of Microbiology under the CC BY license Attribution 4.0 International License. c.o. - protein-free negative control; PleD* - positive control; `GGDEF` - only the `GGDEF` domain; ΔTM - CdgC without the transmembrane domains; PPG - ΔTMΔ`EAL` - CdgC

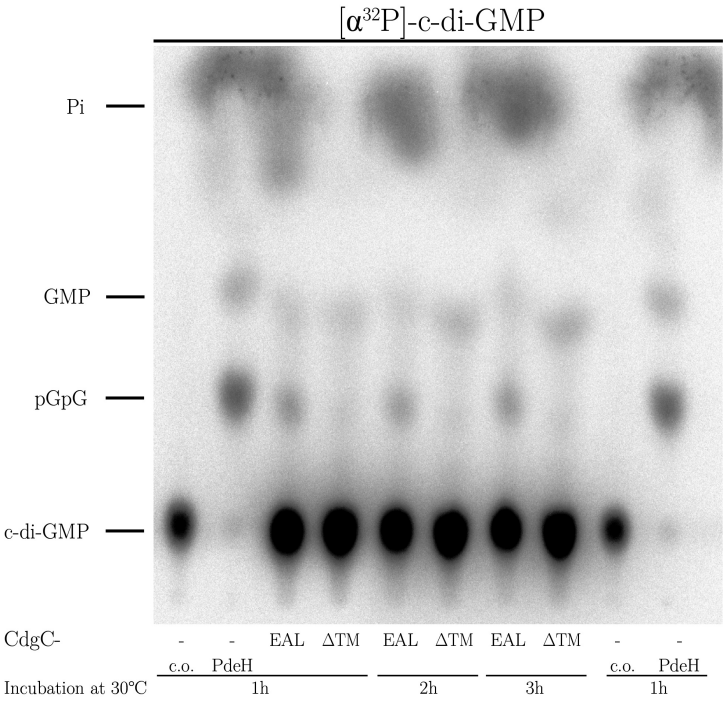

Fig. 4.4 CdgC does not show PDE activity *in vitro*. Radio-labeled c-di-GMP was synthesized with the constitutively active DGC PleD* and [α^{32}P]GTP (Paul et al., 2004). Degradation of c-di-GMP was assayed using purified variants of the cytosolic fraction of CdgC, incubated in an *in vitro* PDE assay with 83 nM radio-labeled c-di-GMP (c-di-[α^{32}P]GMP; 6000 Ci/mmol) for up to 3 h and visualized via thin-layer chromatography with exposure on IP plates. c.o. - protein-free negative control; PdeH - positive control; `EAL` - only the `EAL` domain; ΔTM - CdgC without the transmembrane domains

4.1.3 The A-site of the GGDEF domain in CdgC is essential for its *in vivo* function

Deletion of *cdgC* affects the morphology of *S. venezuelae*, resulting in a remarkable and unique hypersporulation phenotype that skips the formation of aerial hyphae (see Fig. 1.10 on page 20). This characteristic phenotypic alteration with its gray, flat colony morphology can be used as a readout for the essentiality of CdgC domains and motifs for their biological function. The confirmed DGC activity of the conserved GGDEF domain of CdgC (see Section 4.1.2, Fig. 4.3) encouraged the question whether c-di-GMP synthesis is the main biological function of CdgC, causing its morphological impact on the development of *S. venezuelae*.

Phenotypic analyses of macrocolonies were performed to address the *in vivo* function of CdgC. Herein, the A-site was mutagenized from a GGDEF to ALLEF motif at the chromosomal locus of *cdgC*. Analysis on MYM agar revealed that the resulting strain *cdgC*$^{\text{ALLEF}}$ was phenotypically indistinguishable from the *cdgC* knockout strain (see Fig. 4.5). Both mutants failed to form aerial mycelium, remained gray on MYM plates and showed precocious sporulation.

In his bachelor thesis, J. Müller generated *cdgC* under the control of its native promoter and cloned it into the integrative pMS82 vector. The resulting pSVOJ1 plasmid was introduced by conjugation into the Δ*cdgC* mutant and, as part of this PhD study, into *S. venezuelae* *cdgC*$^{\text{ALLEF}}$. In contrast to the empty vector pMS82, all aspects of the *S. venezuelae* *cdgC* deletion mutant were fully complemented in *trans* by a wild type copy of *cdgC* introduced into the ΦBT1 integration site of both mutants as illustrated in Fig. 4.5. (Al-Bassam et al., 2018)

During her project module, A.-B. Klatt analyzed whether the developmental phenotype, resulting from the *cdgC* deletion can be suppressed by a heterologous DGC. To this end, CdgB

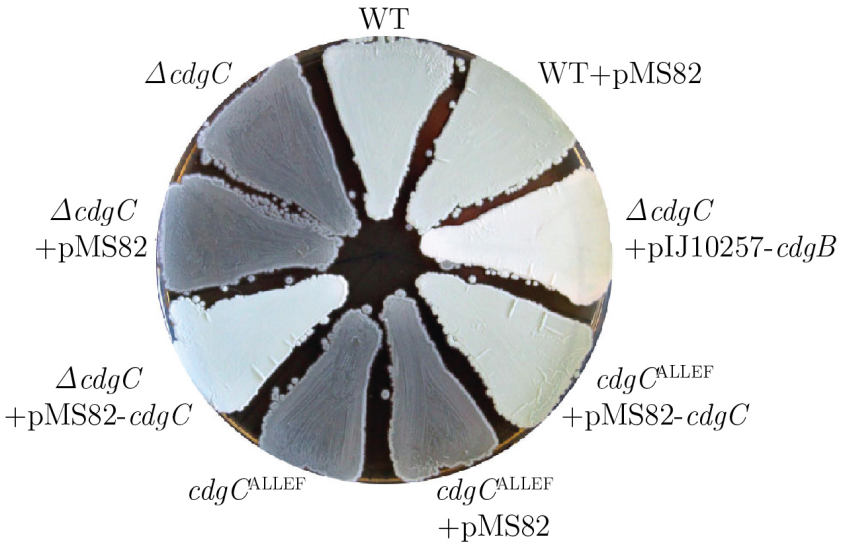

Fig. 4.5 CdgC activity is mainly dependent on its GGDEF motif. Macrocolonies of *S. venezuelae* WT, Δ*cdgC* and *cdgC*$^{\text{ALLEF}}$ alone and with pMS82 with and without *cdgC* integrated as well as Δ*cdgC* overexpressing CdgB (pIJ10257-*cdgB*) were created through drip of 12 µL $2 \cdot 10^5$ CFU/µL spores on MYM agar, plates incubated and documented after 3 d at 30 °C. This figure was modified with permission after Al-Bassam et al. (2018); published in Frontiers of Microbiology under the CC BY license Attribution 4.0 International License.

from *S. coelicolor* was overexpressed using pIJ10350, a derivative of the integrative pIJ10257 vector containing *cdgB*, under control of the strong constitutive *ermE** promoter, as described by Tran et al. (2011). Results verified that the hypersporulation phenotype can be partially suppressed by overexpressing the *S. coelicolor* CdgB (see Fig. 4.5), suggesting that altered c-di-GMP levels are the driving factor of the hypersporulation phenotype in the absence of *cdgC*. Nevertheless, Δ*cdgC* overexpressing CdgB cannot form mature spores that would result in the characteristic green pigmentation of *S. venezuelae*. Instead, the strain shows a white colony surface even after five days of incubation. This observation could be caused either by CdgB producing altered levels of c-di-GMP to contribute to the intracellular pool or by a protein-specific role of CdgC in the cell cycle progression that additional c-di-GMP, synthesized by an overexpressed heterologous DGC, does not complement. These phenotypic analyses showed that the `GGDEF` A-site of CdgC plays a key role in the biological function and additionally suggests a secondary protein-specific role of this protein (Al-Bassam et al., 2018).

4.2 The membrane protein CdgC accumulates along the cell cycle

Grown in liquid medium under laboratory conditions, *S. venezuelae*, as opposed to *S. coelicolor*, is able to undergo the whole cell cycle including sporulation (Bush et al., 2017). To this end, *S. venezuelae* wild type initiates fragmentation of the vegetative hyphae after approximately 14 h of growth, upon transition to spore formation. CdgC is one of the four c-di-GMP turnover proteins that show a morphological effect. Its presence and location at different stages and under different conditions of growth may shed light on its developmental effect. Thus, a C-terminally FLAG-tagged allele of *cdgC* was cloned under the control of its native promoter on the integrative vector pIJ10770 (p3xFLAG-*cdgC*) and integrated into the ΦBT1 integration locus of the *cdgC* deletion mutant. The physiological function of the CdgC-FLAG allele was validated phenotypically via complementation assays (see Fig. 6.1 on page 103 in the appendix).

4.2.1 CdgC-FLAG is located in the membrane fraction

Bioinformatics software like TOPCONS, used for consensus prediction of membrane protein topology, predicts that CdgC contains ten transmembrane helices and that it is therefore integrated into the cell membrane (Tsirigos et al., 2015). This fundamentally important characteristic has been verified by immunodetection of CdgC-FLAG after cell fractionation. For that, Δ*cdgC*+p3xFLAG-*cdgC* was cultivated for 20 h in MYM liquid culture. Whole cell extracts were produced by centrifuging a 5 mL sample for 10 min at 5000 rpm. Cell lysates were prepared (see Section 3.6.1 on page 33) and separated into soluble and membrane fraction using ultracentrifugation for 30 min at 66,000 rpm. Samples from the whole cell lysate, the soluble and the membrane fraction (20 µg total protein per fraction) were separated via SDS-PAGE and immunodetection was carried out using the anti-FLAG antibody, detecting CdgC-FLAG against both, the whole cell extract and the membrane fraction, validating its location in the cell membrane (see Fig. 4.6).

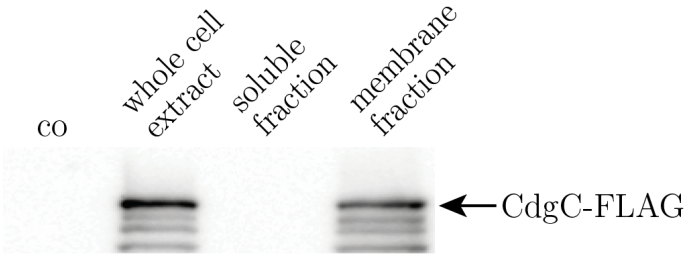

Fig. 4.6 CdgC is a membrane protein. The membrane-bound location of CdgC was experimentally verified by cultivating the FLAG-tagged *cdgC* allele expressed from the ΦBT1 integration site in the *cdgC* mutant (Δ*cdgC*+p3xFLAG-*cdgC*) strain for 20 h in MYM liquid culture and 5 mL samples were harvested by centrifugation for 10 min at 5000 rpm. Whole cell extracts were obtained, as described in Section 3.6.1 on page 33 and a sample was taken for the analysis. Ultracentrifugation for 30 min at 66,000 rpm separated the cytosolic from the membrane fraction and a sample of the supernatant was taken for the analysis. The membrane fraction was washed twice, resuspended in 100 µL 1xPBS containing cOmplete Protease Inhibitor Cocktail Tablets (Roche) and 20 µg total protein per fraction were separated via SDS-PAGE. Immunodetection was performed using the anti-FLAG antibody and chemiluminescence. This figure was modified with permission after Al-Bassam et al. (2018); published in Frontiers of Microbiology under the CC BY license Attribution 4.0 International License. co - membrane fraction of *S. venezuelae* WT (negative control)

4.2.2 Accumulating CdgC-FLAG shows a degradation pattern

Apart from the enzymatic activity of a protein, its temporal expression pattern and, therefore, presence in the cell, determines its physiological function to a major extent. On a transcriptional level, already published time-course microarray data showed accumulation of *cdgC* transcripts along the life cycle, reaching its peak during the sporulation phase. These data were generated taking samples during submerged sporulation. (Bibb et al., 2012) Later on, the data set was processed with quantile normalization and median polishing using the RMA method by Al-Bassam et al. (2018). Immunodetection assays of the Δ*cdgC*+p3xFLAG-*cdgC* complementation strain was performed to detect the presence of CdgC during development. Therefor, seven samples were taken at 8, 10, 12, 14, 16, 18, and 20 h of growth, spanning the complete morphological differentiation states of the bacterium. The results indicated that CdgC accumulates in liquid culture, showing a number of putative degradation bands (see Fig. 4.7).

Comparing the bands with the expected protein sizes and considering the C-terminal location of the detected FLAG tag, the band pattern indicates that band 1 is the full-size CdgC protein, whereas band 2 runs at the size of CdgC cut between the third and fourth transmembrane domain. Band 3 contains the PAS-`GGDEF-EAL` peptide of CdgC (expected to run at about 56 kDa), band 4 equals the size of the `GGDEF-EAL` domain (51 kDa) and band 6 equals the size of the `EAL` domain only (∼31 kDa). Since band 5 also appears in the negative control (*S. venezuelae* wild type after 20 h incubation), it was considered unspecific. Despite the degradation pattern, the results validate the accumulation of *cdgC* transcripts observed by Al-Bassam et al. (2018) on a posttranslational level in liquid culture.

Altogether, the Western blot analyses depicted that CdgC-FLAG accumulates along the life cycle and shows a degradation pattern that shall be further characterized in the following.

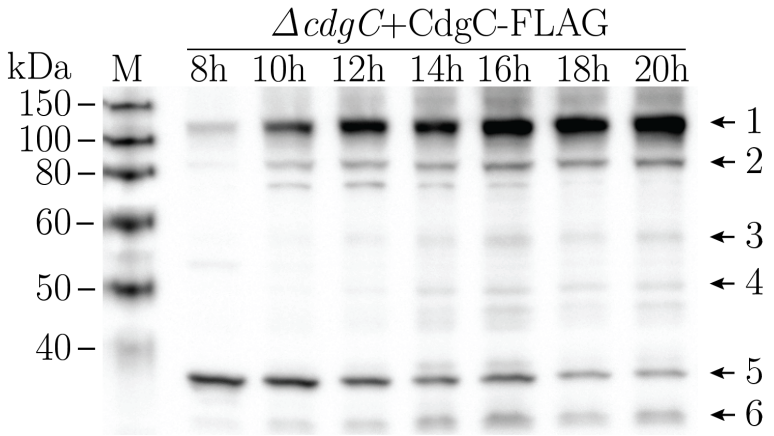

Fig. 4.7 CdgC-FLAG accumulates along the life cycle in liquid culture. The presence of CdgC-FLAG was determined by expressing it from the ΦBT1 integration locus in the *cdgC* deletion mutant. The strain was cultivated for 20 h in MYM liquid culture and samples were harvested every 2 h, starting at 8 h . A total protein amount of 5 µg per sample was separated via SDS-PAGE. Immunodetection was performed using the anti-FLAG antibody. 1 - full-size CdgC-FLAG; 2 - CdgC lacking the first three transmembrane domains; 3 - CdgC-PAC-`GGDEF-EAL`; 4 - CdgC-`GGDEF-EAL`; 5 - unspecific; 6 - CdgC-`EAL`; M - enhanced chemiluminescence marker

4.2.3 Proteolytic processing of CdgC-FLAG

The expression of CdgC-FLAG along the life cycle, with a continually more intensive degradation pattern shown in Section 4.2.2, indicates proteolytic regulation to process or inactivate the protein. Proteolytic regulation can impact the cellular protein level as well as its functionality, raising the question whether a specific protease causes the degradation pattern of CdgC.

To tackle this question, a number of deletion strains of individual proteases in *S. venezuelae* were sent from the John Innes Centre (JIC, Norwich, UK) and conjugated with p3xFLAG-*cdgC* for immunodetection. The strains were cultivated under standard conditions in MYM liquid culture at 30 °C and 170 rpm (see Section 3.4.2 on page 25). Based on the degradation pattern of CdgC, samples were taken 18 h after the start of the incubation. The total protein concentration was determined via Bradford assay (Roth) and 15 µg of total protein were loaded per sample, separated via SDS-PAGE and detected against the anti-FLAG antibody. *S. venezuelae* wild type without the CdgC-FLAG construct served as a negative control.

No decrease in the degradation pattern could be observed in the results, indicating that none of the tested proteases has a specific role in degradation of CdgC (see Fig. 4.8). CdgC-FLAG expressed in Δ*rip1* and Δ*rip3* showed a weaker expression than in the other strain, which might be due to global transcriptomic changes in the absence of those regulatory proteases. Both of them encode zinc metalloproteases and Rip1 is membrane associated (StrepDB). A band at about 40 kDa observed in all samples including the negative control and as band 5 in Fig. 4.7 seems to be unspecific.

Taken together, none of the tested proteases plays a specific role in the regulatory degradation of CdgC, suggesting that either an untested protease or an interplay between several proteases controls the presence or activity of CdgC in *S. venezuelae*.

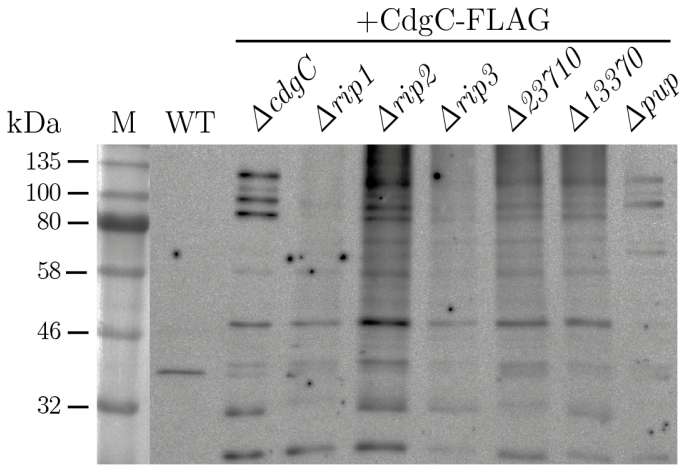

Fig. 4.8 The proteolytical processing of CdgC-FLAG does not seem to be specifically influenced by the proteases Rip1-3, Vnz23710, Vnz13370 or Pup. Protein samples were harvested from *S. venezuelae* WT, Δ*cdgC* as well as Δ*cdgC*, Δ*rip1*, Δ*rip2*, Δ*rip3*, Δ*vnz23710*, Δ*vnz13370* and Δ*pup* conjugated with p3xFLAG-*cdgC* for the immunodetection against CdgC-FLAG protein after 18 h at 30 °C and 170 rpm in MYM liquid culture inoculated with an initial spore concentration of 10^6 CFU/mL. A total protein amount of 10 µg per sample was separated via SDS-PAGE. M - color prestained marker

4.3 BldD represses the transcription of CdgC

Having characterized the expression pattern and posttranslational degradation of CdgC, this section shall focus on the transcriptional regulation of the protein. Recent studies revealed that the developmental master regulator BldD specifically binds the promoter regions of the DGC encoding genes *cdgA*, *cdgB*, *cdgC* and *cdgE*. Leading to the hypothesis that a negative feedback loop in which c-di-GMP enables BldD to form stable dimers for efficient binding of the DNA at this target genes' promoter regions (Tschowri et al., 2014). According to this hypothesis, the repression of the mentioned DGCs would result in less c-di-GMP synthesis and a negative feedback on its own activity. Inactivating BldD is necessary for the cells to shift from the vegetative into the stationary phase. Electrophoretic mobility shift assays (EMSA), used to analyze protein-DNA or protein-RNA interactions, verified BldD binding to the promoter region of *cdgC* (Haist et al., 2020).

As described in Section 1.4 on page 10, BldD assembles a tetramer of c-di-GMP in a sequential mechanism (Tschowri et al., 2014; Schumacher et al., 2017). In the process, one c-di-GMP dimer binds the so-called motif 2 (`RXXD`) in the BldD CTD of up to two monomers of BldD. As a result, a flexible, dimerized intermediate $BldD_2$(c-di-GMP)$_2$ is formed. This intermediate state is quite unstable and unable to bind DNA efficiently. Binding of a second c-di-GMP dimer at the second c-di-GMP binding motif 1 (`RXD`) stabilizes a $BldD_2$(c-di-GMP)$_4$ confirmation, which successfully binds DNA and acts as a repressor.

To verify the regulatory feedback hypothesis of BldD involving CdgC, the expression of CdgC-FLAG shall be analyzed in a strain in which BldD does not act as a repressor. A BldD knockout strain shows severe growth deficiency and abundant suppressor mutants. In conclusion, the strain is unfit for planned analyses, as suppressor mutants could influence the CdgC-FLAG

expression in a non BldD-related manner. A strain containing a *bldD* allele with a D116A point mutation (BldD_D116A) in the c-di-GMP binding residues in the motif 1 of the CTD was used instead. This point mutation traps the BldD-c-di-GMP complex in the intermediate non DNA binding $BldD_2$(c-di-GMP)$_4$ state. (Schumacher et al., 2017) Here, protein samples were harvested from *S. venezuelae* wild type and BldD_D116A, both conjugated with p3xFLAG-*cdgC*, after 12, 24 and 36 h at 30 °C on MYM solid culture that had been inoculated with an initial spore concentration of 10^6 CFU/mL. The total protein concentration was determined via Bradford assay (Roth) and 20 µg total protein amount per fraction were separated via SDS-PAGE. After the Western blot, the PVDF membrane was stained with Ponceau S for 5 min at RT, documented as a loading control (see Fig. 6.2 on page 103 in the appendix), stripped by incubation for 1 min in 0.1 M NaOH and used for the immunodetection against the CdgC-FLAG. The expression of the CdgC-FLAG in WT+p3xFLAG-*cdgC* served as an approximate value for the native CdgC presence in this state of development, because like BldD_D116A it still contains the chromosomal *cdgC* allele at its native locus. A protein sample taken from *S. venezuelae* wild type after 20 h of incubation served as a negative control. Comparing immunodetection of CdgC-FLAG indicates a more prominent expression of CdgC-FLAG in a strain containing the DNA binding insufficient *bldD* allele (see Fig. 4.9). An unspecific band was identified in all samples at about 35 kDa. This experiment hints at a negative regulatory effect of BldD on the expression of CdgC, supporting the hypothesis of a negative feedback loop and the enhanced expression of CdgC observed in *S. ghanaensis* Δ*bldD* compared to the wild type (Tschowri et al., 2014; Nuzzo et al., 2020).

Altogether, the results suggest an enhanced expression of CdgC when BldD is inactive supporting the *in vivo* ChIP-seq analysis and EMSAs that indicated *cdgC* to be a direct BldD-target gene (Tschowri et al., 2014; Haist et al., 2020).

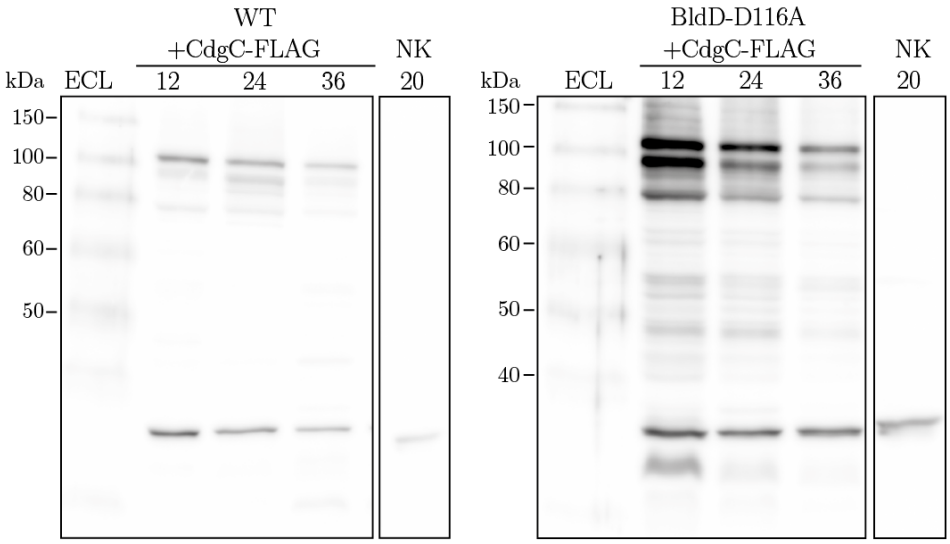

Fig. 4.9 CdgC-FLAG is more stably present in a strain with a DNA binding insufficient BldD allele. Protein samples were harvested from *S. venezuelae* WT and BldD_D116A conjugated with p3xFLAG-*cdgC* for the immunodetection against CdgC-FLAG after 12, 24 and 36 h at 30 °C on MYM solid culture inoculated with an initial spore concentration of 10^6 CFU/mL. *S. venezuelae* WT incubated for 20 h served as a negative control. A total protein amount of 20 µg per sample was separated via SDS-PAGE. ECL - enhanced chemiluminescence marker

4.4 CdgC controls the expression of other c-di-GMP turnover proteins

Phenotypic analyses (described in Section 4.1.3) and *in vitro* enzymatic activity assays (described in Section 4.1.2) provide evidence for a DGC activity of CdgC. The former analyses revealed that a *cdgC* mutant and *cdgC*$^{\texttt{ALLEF}}$ result in the same hypersporulation phenotype (see Fig. 4.5). This indicates that the DGC activity is the main function of CdgC. Furthermore, the strong reminiscence between the hypersporulation phenotype of the *cdgC* mutant and the low c-di-GMP phenotypic manifestation of both to-date identified c-di-GMP effector binding proteins suggest that CdgC is one of the pivotal DGCs in *S. venezuelae*. As a result, the cellular c-di-GMP levels in Δ*cdgC* were expected to be significantly lower than in the wild type. In nucleotide extraction assays performed on samples taken from liquid culture (J. Haist, unpublished) c-di-GMP levels in the wild type declined from 8 h to a minimum at 14 h and then accelerated rapidly (see Fig. 4.10 A). Contrary to the expectations, c-di-GMP levels in Δ*cdgC* showed no significant deviation from the wild type after 8 and 10 h of incubation, followed by a dramatic rise that even surpassed the increasing wild type levels, particularly in the late phases of the experiment (see Fig. 4.10). On solid medium, the differences in c-di-GMP levels are not as pronounced, tending towards an equilibrium at around 5 pmol/mg wet weight as the experiment progresses with decreasing levels in Δ*cdgC* during sampling (see Fig. 4.10 B).

These unexpectedly high c-di-GMP levels in Δ*cdgC* compared to the wild type suggest that the absence of *cdgC* impacts the expression and activity of other c-di-GMP turnover enzymes, which shall be investigated in the following.

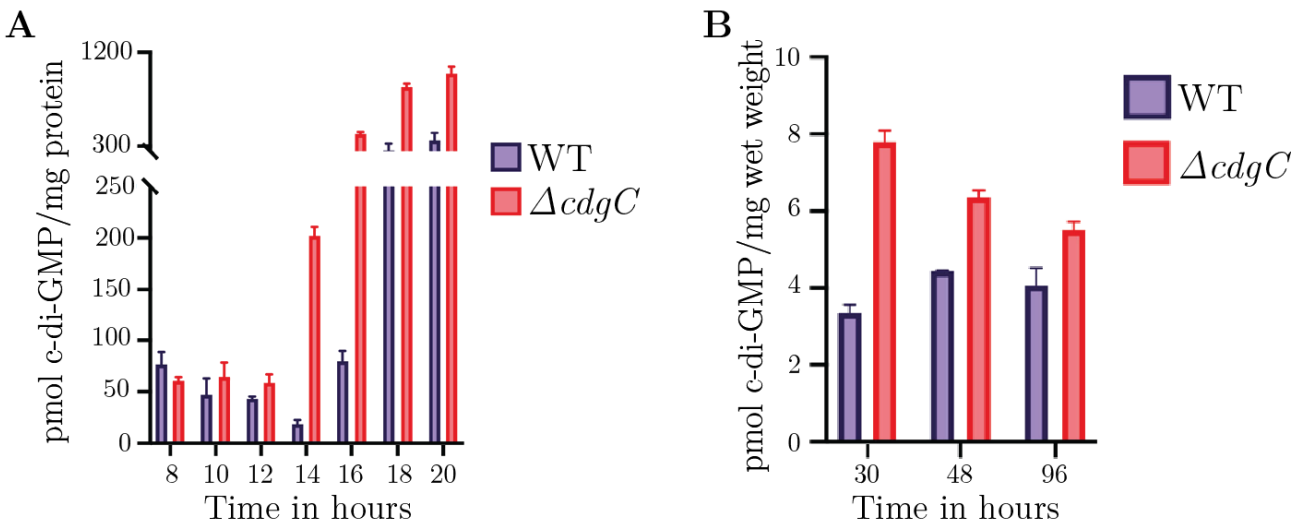

Fig. 4.10 Chromosomal deletion of *cdgC* results in elevated c-di-GMP levels in the later phases of development (performed by J. Haist, unpublished). (A) Incubation took place in MYM liquid culture and samples were harvested (each 5 mL volume) starting after 8 h of incubation at 30 °C and 170 rpm every 2 h for 10 h. (B) On solid MYM medium, samples were harvested after 30, 48 and 96 h of incubation at 30 °C.

4.4.1 A *cdgB cdgC* double mutant is branching deficient

The previous considerations led to the assumption that an upregulated DGC might cause the increased c-di-GMP levels in the *cdgC* mutant compared to the wild type. If this hypothesis is correct, then the double mutant, resulting from deleting this relevant DGC in Δ*cdgC*, would be expected to show reduced cellular c-di-GMP levels compared to Δ*cdgC*.

So far, all knockout mutants of c-di-GMP turnover proteins were realized by λ RED mediated recombination with an Apra resistance cassette (disruption cassette) for gene disruption (Al-Bassam et al., 2018) and are, therefore, not combinable by transduction to generate double mutants. FLP-mediated excision of the disruption cassette is a long and time consuming procedure and, thus, ill-advised as a first approach. As for CdgC, the *cdgC*$^{\texttt{ALLEF}}$ point mutation is enzymatically inactive, behaved like the *cdgC* knockout mutant in all previous experiments and carries no resistance cassette. Since DGCs like CdgC do not usually act as transcription factors themselves, the DGC activity of CdgC was considered especially relevant and the enzymatically inactivated *cdgC*$^{\texttt{ALLEF}}$ strain suitable as an equivalent to the *cdgC* knockout mutant in this approach.

Therefore, double mutants were generated via transduction of the *cdgC*$^{\texttt{ALLEF}}$ strain with a phage lysate of Δ*cdgA*, Δ*cdgB*, Δ*cdgE* and Δ*cdgF*, respectively, as described in Section 3.4.4 on page 25. CdgD was omitted from this experiment, since previous data detected barely any protein present in the cells under the given laboratory conditions (Al-Bassam et al., 2018). After a phenotypical analysis of these strains, their cellular c-di-GMP levels should be measured via nucleotide extraction, as described by Haist et al. (2020) to identify the DGC whose absence might cause the double mutant to show significantly lower c-di-GMP levels than Δ*cdgC*.

First, the morphological impact of the double mutants on the phenotype of *S. venezuelae* shall be analyzed. Therefor, macrocolonies of these strains were created for phenotypic analysis through drip of 12 µL $2 \cdot 10^5$ CFU/µL spores on MYM agar and plates were incubated for 4 d at 30 °C. These growing macrocolonies were documented every 24 h under the binocular microscope (Zeiss). After four days, the collected images were edited with Adobe Photoshop and arranged using Adobe Illustrator. The results are shown in Fig. 4.11.

The simultaneous inactivation of CdgC and CdgA resulted in a darker gray hypersporulation phenotype with radial ridges. Additional deletion of *cdgE* or *cdgF* in *cdgC*$^{\texttt{ALLEF}}$ led to a very similar phenotype, which did not significantly alter from the hypersporulation phenotype of the *cdgC* deletion and the *cdgC*$^{\texttt{ALLEF}}$ point mutation. In contrast, the strain in which CdgB and CdgC are both inactivated has the most astonishing phenotype with a bright beige colony and pronounced wrinkling.

Since these macroscopic analyses allow no conclusions on the ability of these strains to sporulate, they were cultivated along with the corresponding control strains in MYM liquid culture at 30 °C and 170 rpm and examined under the microscope every 2 h from 12 h until 20 h after the inoculation. Samples were prepared for microscopy, as described in Section 3.4.12 on page 28, using the single deletion strains as corresponding control strains. The results of the double mutants are shown in Fig. 4.12, while the corresponding microscopic images of the control strains are shown in Fig. 6.3 on page 104 in the appendix.

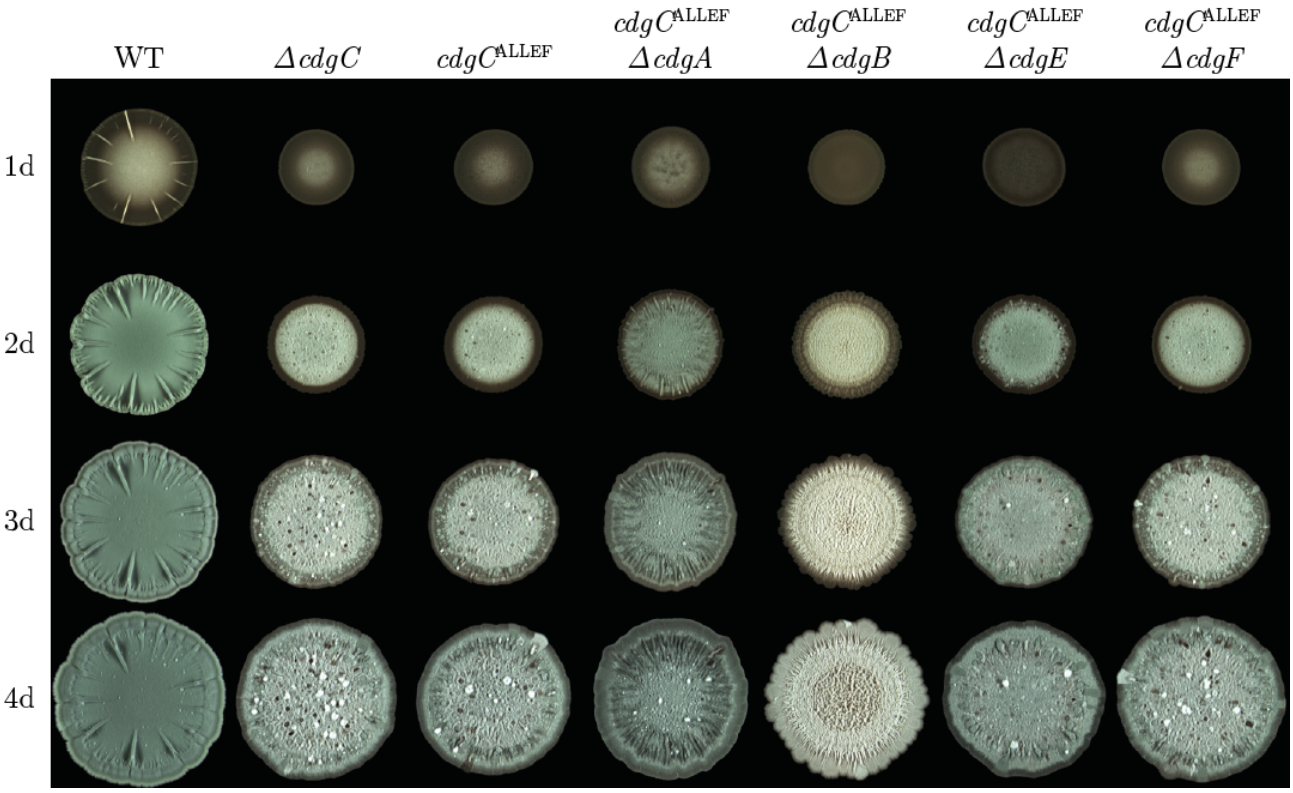

Fig. 4.11 The simultaneous enzymatic inactivity of CdgB and CdgC results in a unique phenotype unlike the hypersporulation. Macrocolonies of *S. venezuelae* WT, Δ*cdgC*, *cdgC*$^{\text{ALLEF}}$, *cdgC*$^{\text{ALLEF}}$Δ*cdgA*, *cdgC*$^{\text{ALLEF}}$Δ*cdgB*, *cdgC*$^{\text{ALLEF}}$Δ*cdgE* and *cdgC*$^{\text{ALLEF}}$Δ*cdgF* were created through drip of 12 µL $2 \cdot 10^5$ CFU/µL spores on MYM agar and plates were incubated for 4 d at 30 °C. The documentation took place every 24 h.

The results of the development of the double mutants with *cdgA*, *cdgE* and *cdgF*, respectively, in *cdgC*$^{\text{ALLEF}}$ basically match those of the single *cdgC* deletion strain (see Fig. 4.12). In contrast, the simultaneous inactivity of CdgB and CdgC resulted, again, in a unique phenotype: the spores seem distinctly enlarged and the strain germinates in radial hyphae, which seem to be inhibited in their apical growth and branching. This phenotype differentiated only marginally during sampling in liquid culture. The density of the colonies hints against a growth defect that blocks the cells after germination and inhibits apical growth and branching.

For a first approach to extract and measure c-di-GMP from these double mutants, their corresponding DGC knockout mutants, *cdgC*$^{\text{ALLEF}}$ and the wild type strains were cultivated in MYM liquid culture for 20 h at 30 °C and 170 rpm. The incubation time was chosen, because c-di-GMP levels in Δ*cdgC* showed the highest deviation from the wild type, according to the previous nucleotide extraction assays performed by J. Haist (see Fig. 4.10 A). Unfortunately, the resulting data could not be analyzed and, therefore, the assay needs to be repeated in the future.

Altogether, the phenotypic analysis of *cdgC*$^{\text{ALLEF}}$Δ*cdgB* revealed the most striking phenotype of all generated double mutants. It showed a bright beige colony phenotype with enhanced wrinkling. Microscopic analysis revealed enlarged spores, germination in radial hyphae with a defect in apical growth and branching, though the density of the colonies contradicts a general growth defect that blocks the cells after germination.

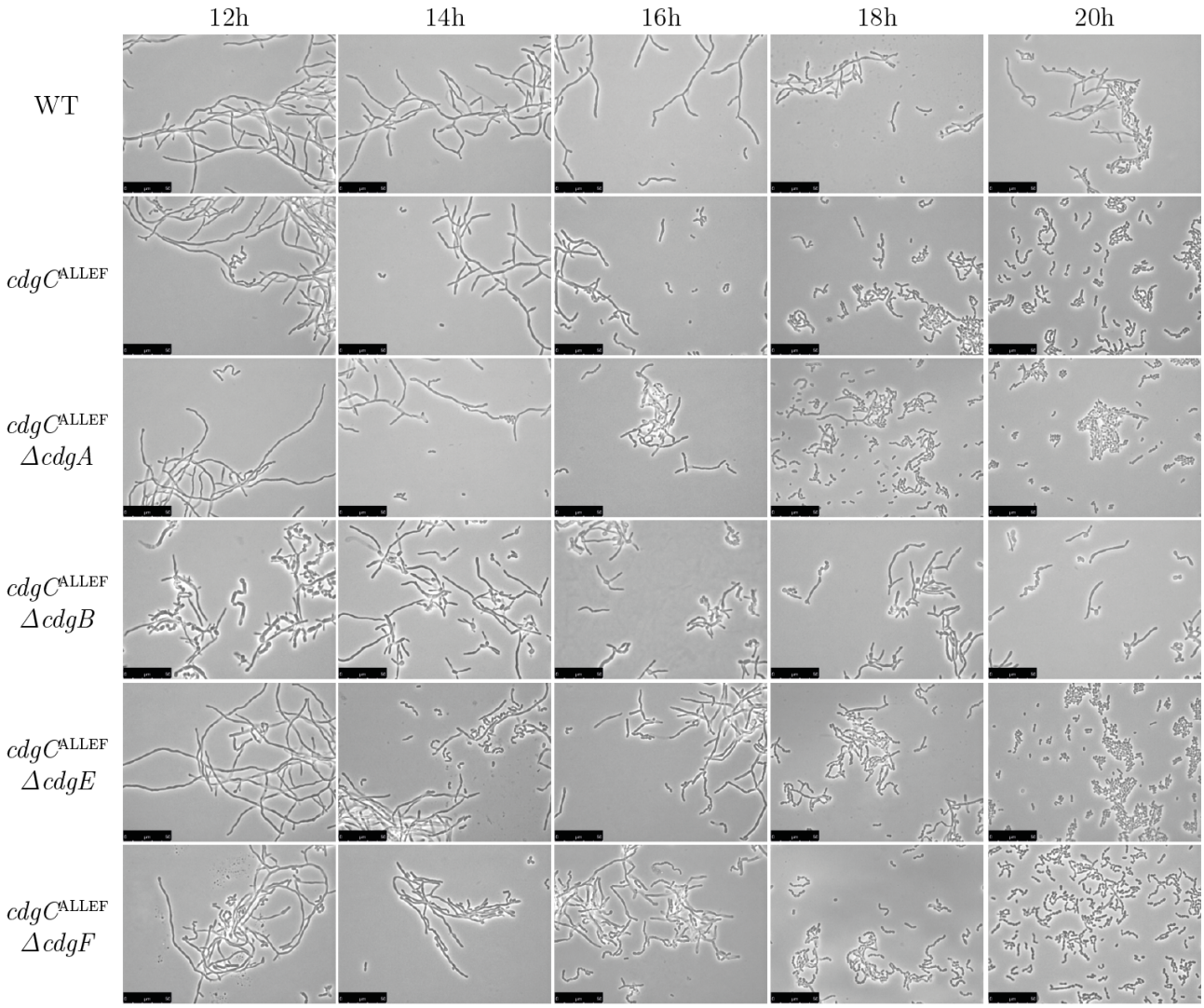

Fig. 4.12 The simultaneous enzymatic inactivity of CdgB and CdgC results in enlarged spores and an apparent inhibition of apical growth as well as branching of the mycelium. *S. venezuelae* WT, Δ*cdgC*, *cdgC*$^{\texttt{ALLEF}}$, *cdgC*$^{\texttt{ALLEF}}$Δ*cdgA*, *cdgC*$^{\texttt{ALLEF}}$Δ*cdgB*, *cdgC*$^{\texttt{ALLEF}}$Δ*cdgE* and *cdgC*$^{\texttt{ALLEF}}$Δ*cdgF* were inoculated in MYM liquid culture to a spore concentration of 10^6 CFU/mL respectively. Incubation took place at 30 °C and 170 rpm and samples were harvested every 2 h from 12 to 20 h. Microscopic images were documented under a 100× phase contrast objective.

4.4.2 The DGC activity of CdgC effects the expression of other DGCs

As discussed in Section 4.3, the expression of CdgC seems to be increased in the BldD_D116A point mutant. The encoded BldD variant is unable to bind the second c-di-GMP dimer, form a stable $BldD_2$(c-di-GMP)$_4$ dimer and, thus, to act as an active repressor (Schumacher et al., 2017). Together with the EMSAs, confirming *in vitro* binding of BldD to the promoter region of *cdgC* (Haist et al., 2020), this suggests that the transcription of *cdgC* might be inhibited by BldD via a negative feedback loop. Following this hypothesis, the absence of CdgC would initially reduce c-di-GMP levels directly after germination. These decreased c-di-GMP levels would inactivate BldD as a repressor and might, thus, increase the transcription of BldD-dependent DGCs. Increased DGC levels and activity could then boost c-di-GMP levels. The nucleotide extraction data showing increased c-di-GMP in the *cdgC* mutant compared to the wild type support this

hypothesis (see Fig. 4.10). Together, these results and the suggested negative feedback loop of BldD on several DGCs raised the hypothesis that the DGC activity of CdgC causes changes in cellular c-di-GMP levels. These changes might influence the dimerization (Elliot et al., 2003) and DNA-binding of BldD and, thereby, the expression of other BldD-controlled DGCs.

To analyze the influence of CdgC on the expression of the other DGCs, strains were generated that, besides the enzymatically inactive CdgC, contain the FLAG-tagged version of CdgA, CdgB or CdgE, respectively, on the integrative p3xFLAG vector. These strains were inoculated with an initial spore concentration of 10^6 CFU/mL, cultivated together with the respective complementation strains in MYM liquid culture at 30 °C and 170 rpm and protein samples were harvested after 20 h of incubation. The total protein concentration was determined via Bradford assay (Roth) and distinct total protein amounts (CdgA-FLAG = 25 µg, CdgB-FLAG = 10 µg, CdgE-FLAG = 15 µg) were separated via SDS-PAGE and analyzed via immunodetection against an anti-FLAG antibody. The results of the immunodetection against the anti-FLAG antibody with *cdgC*$^{\texttt{ALLEF}}$ as a negative control are presented in Fig. 4.13.

These results show that CdgA-FLAG is barely detectable in the *cdgC*$^{\texttt{ALLEF}}$ point mutant, while the expression of CdgB- and CdgE-FLAG seems to be significantly enhanced, compared to the complementation strains. This is particularly surprising, since all three genes are BldD-dependently regulated. Furthermore, the absence of detectable CdgE-FLAG in the CdgE complementation strain casts doubt on the employed methods.

Taken together, these results fail to support the hypothesis that the DGC activity of CdgC impacts the expression of BldD-dependent DGCs in a c-di-GMP-dependent negative feedback loop. To exclude an impact of posttranslational regulation on the observed expression levels, further studies shall be analyzing the transcription levels of c-di-GMP turnover proteins in the *cdgC* mutant compared to the wild type.

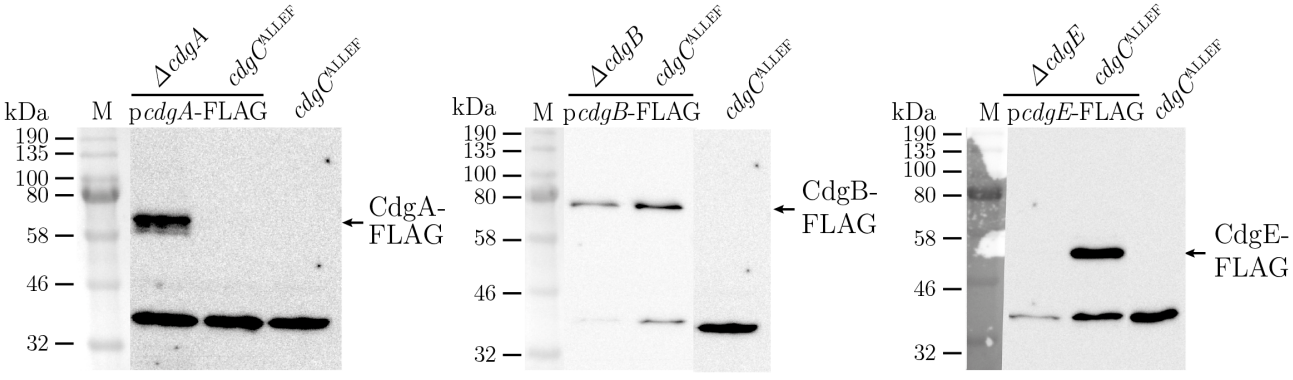

Fig. 4.13 The DGC activity of CdgC influences the expression of some DGCs heterogeneously. Protein samples for the immunodetection against the FLAG tag were harvested from *S. venezuelae* WT, *cdgC*$^{\texttt{ALLEF}}$, *cdgC*$^{\texttt{ALLEF}}$+p3xFLAG-*cdgA*, Δ*cdgA*+p3xFLAG-*cdgA*, *cdgC*$^{\texttt{ALLEF}}$+p3xFLAG-*cdgB*, Δ*cdgB*+p3xFLAG-*cdgB*, *cdgC*$^{\texttt{ALLEF}}$+p3xFLAG-*cdgE* and Δ*cdgE*+p3xFLAG-*cdgE* after 20 h at 30 °C and 170 rpm in MYM liquid culture inoculated in MYM liquid culture to a spore concentration of 10^6 CFU/mL respectively. Distinct total protein amounts were loaded (CdgA-FLAG = 25 µg, CdgB-FLAG = 10 µg, CdgE-FLAG = 15 µg), analyzed via SDS-PAGE and immunodetection was performed against an anti-FLAG antibody. The bands specific for the FLAG-tagged DGC were indicated with a labelled arrow. M - color prestained marker

4.4.3 Differential transcription of c-di-GMP turnover protein encoding genes in Δ*cdgC*

As discussed above, the elevated c-di-GMP levels in the *cdgC* mutant compared to the wild type indicate an impact of CdgC on the expression of other c-di-GMP turnover proteins. Either an upregulation of a DGC, resulting in an increased c-di-GMP synthesis, or downregulation of a PDE, leading to a decreased c-di-GMP hydrolysis, may be responsible for causing this rise of cellular c-di-GMP levels. RNA-seq data showed that *cdgB* and *rmdA* are upregulated in Δ*cdgC* compared to the wild type, while *cdgF* is downregulated (J. Haist, unpublished).

To verify the RNA-seq data and identify the corresponding gene, encoding the c-di-GMP turnover enzyme that might be responsible for the observed increase in c-di-GMP levels in Δ*cdgC*, their transcript levels were analyzed via quantitative Real Time-PCR (qRT-PCR) compared to the wild type. For this analysis, DGC-encoding genes *cdgA*, *cdgB*, *cdgE* and *cdgF* as well as PDE-encoding genes *rmdA* and *rmdB* were considered relevant for testing. Evidence of the DGC activity has been provided for CdgA and CdgB in *S. coelicolor* as well as for CdgE in *S. venezuelae* (Den Hengst et al., 2010; Tran et al., 2011; Haist et al., 2020). CdgF is a composite protein, containing both a conserved `GGDEF` and a conserved `EAL` domain in tandem and may be a bifunctional protein. The PDE activity of the composite `GGDEF-EAL` proteins RmdA and RmdB has been demonstrated experimentally in *S. coelicolor* and, recently, in *S. venezuelae*, where RmdA showed additional DGC activity *in vitro* (Hull et al., 2012; Haist et al., 2020). CdgD was omitted from this experiment, since previous data detected barely any protein under the tested laboratory conditions (Al-Bassam et al., 2018).

For this assay, primers were designed that (1) amplify a fragment of 70-150 bp, (2) bind nowhere else in the genome, (3) form no hairpin-structures or dimers and (4) melt at approximately 60 °C. Efficient template binding of these primers was verified using genomic DNA (dilution series coming from 20 ng) as a template, skipping the reverse transcription of RNA to cDNA. RNA was isolated from samples of *S. venezuelae* wild type and Δ*cdgC* strains, grown on MYM agar at 30 °C, harvested after 30 h and isolated, as described in Section 3.5.10 on page 31. Subsequently, all RNA samples were adjusted to a concentration of 10 ng/µL and 2 µL RNA (20 ng) were used per reaction mix to perform qRT-PCRs for each primer pair in technical triplets and the assay was reproduced at least three times. Controls were carried along for each primer pair using nucleotide-free water instead of RNA. The qRT-PCR was performed using the SensiFAST SYBR No-ROX One-Step Kit (Bioline) and the program described in Section 3.5.11 on page 32.

The results are presented as $\log_2$-fold changes and a value > 1 or < -1 was considered significant (see Fig. 4.14). With these guidelines in mind, the transcription amounts of *cdgA* and *cdgE* do not change significantly in Δ*cdgC* compared to the wild type. The results indicated furthermore that the transcription of *cdgF* is upregulated in Δ*cdgC*, while *cdgB* as well as the PDEs *rmdA* and *rmdB* are downregulated.

Altogether, these results indicate that upregulation of the bifunctional protein CdgF, together with a downregulation of both active PDEs RmdA and RmdB, causes the rise in cellular c-di-GMP levels in Δ*cdgC*. However, the downregulation of CdgB in Δ*cdgC* might combat this effect.

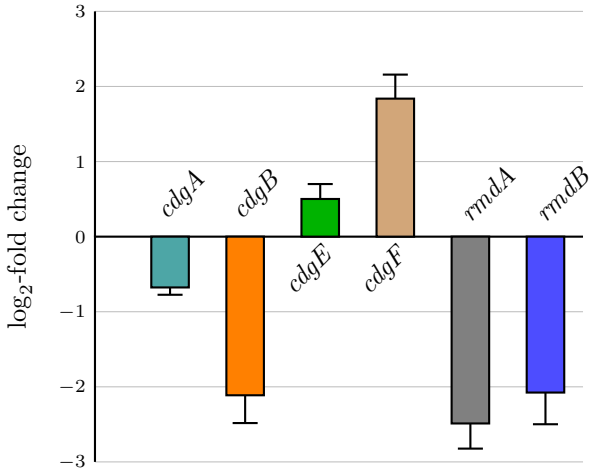

Fig. 4.14 Differential expression of genes encoding c-di-GMP turnover enzymes in Δ*cdgC*. Transcription values of the DGCs *cdgA*, *cdgB*, *cdgE*, *cdgF* and the PDEs *rmdA* and *rmdB* in Δ*cdgC* compared to the WT were quantified via qRT-PCR analysis performed with RNA samples isolated via SV Total RNA Isolation Kit (Promega) harvested after 30 h incubation at 30 °C on MYM agar at least three times with three technical replicates per experiment. Calculations of the expression values relative to the accumulation of the constitutively expressed *hrdB* (encoding the housekeeping σ factor in *Streptomyces*) reference mRNA and normalized to WT value. $\log_2$-fold change > 1 or < -1 was considered significant. Presented data are the mean of three technical replicates ±standard deviation. This figure was modified with permission after Haist et al. (2020); published in Molecular Microbiology under the CC BY license Attribution 4.0 International License.

4.5 FtsZ is upregulated in the DGC mutants

Looking into the morphological details of the alterations caused by the deletion of *cdgB* and *cdgC* in contrast to the wild type, it strikes that, despite huge phenotypic differences, both DGC mutants change the timing of spore formation. This could be due to changes in the expression pattern of genes involved in DNA segregation, cell division and cell wall remodeling. RNA-seq data revealed enhanced transcription of multiple of those genes in Δ*cdgC* compared to the wild type (Haist et al., 2020). Thusly, the three *Streptomyces mreB*-like genes *mreB*, *vnz35885* and *mbl*, as well as *mreC* show enhanced expression in Δ*cdgC*. During spore formation, MreB, Mbl, and MreC play a pivotal role in enhancing the stress resistance of spores via the synthesis of a thickened spore wall (Heichlinger et al., 2011; Kleinschnitz et al., 2011). Accordingly, the majority of genes are only altered in Δ*cdgC*, such as *ssgE*, whose translation product times the spore dissociation (Noens et al., 2005). Among the few shared targets that are also upregulated in Δ*cdgB* is *ssgB*, encoding a protein involved in the assembly of FtsZ rings at the cell division site and direct target gene of the homodimeric BldM transcriptional regulator (Willemse et al., 2011).

Recall from Section 1.2 on page 3 that the synchronous septation of multinucleoid *Streptomyces* hyphae into unigenomic prespore compartments at the onset of sporulation requires the polymerization of the conserved tubulin-like GTPase FtsZ into filaments forming the Z-rings (McCormick et al., 1994; Lutkenhaus & Addinall, 1997). These structures are located in proximity to the membrane, recruiting additional cell division proteins (Jakimowicz et al., 2005; Haeusser & Margolin, 2016). In *S. coelicolor* and *S. venezuelae*, reflecting its distinct requirements in the life cycle, *ftsZ*-expression is regulated by three promoters: a vegetative, a reproductive and

a BldD-dependent promoter region (Flärdh et al., 2000; Haist et al., 2020) (described in Detail in Section 1.4 on page 15). The third, BldD-dependent promoter bridges FtsZ expression to the cellular c-di-GMP level on the level of transcriptional regulation. Thus, $BldD_2$(c-di-GMP)$_4$ binds directly to the *ftsZ* promoter region in both *S. coelicolor* and *S. venezuelae* at a conserved site (Tschowri et al., 2014; Den Hengst et al., 2010).

These preliminary considerations lead to the expectation that transcription levels of *ftsZ* increase in the precociously sporulating *cdgB* and *cdgC* mutants, but RNA-seq provided no significant alterations in *ftsZ* expression (Haist et al., 2020). A possible explanation is that the sporulation of these strains was already completed, when harvested for RNA-isolation from MYM solid medium after 30 h of growth. This raised the question whether the detection of the *ftsZ* expression at an earlier incubation time point would paint a different picture. To address this hypothesis, a confocal microscopic approach was chosen in order to detect an FtsZ-Ypet fusion protein. Herein, its expression and accumulation to Z-rings appear particularly obvious as ladder-like structures, indicating the future septation site.

For a quantitative evaluation, confocal microscopy was combined with immunodetection. Therefor, an *ftsZ-ypet* translational fusion, cloned under the control of its native promoter on the pSS5 plasmid (Schlimpert et al., 2017), was introduced in *S. venezuelae* wild type, Δ*cdgB* and Δ*cdgC* at the ΦBT1 site. Effects of the additional FtsZ allele on the morphology of the strains were excluded phenotypically via macrocolony assays (see Fig. 6.4 on page 105 in the appendix). Afterwards, the strains were grown in liquid MYM medium at 30 °C. After 12 hour of growth, the wild type was in the vegetative phase, resulting in the detection of faint FtsZ-YPet signal while, in Δ*cdgB* and Δ*cdgC*, enhanced expression of the FtsZ-Ypet fusion protein was observed (see Fig. 4.15). To exclude autofluorescence as a cause for the observed signals, wild type, Δ*cdgB* and Δ*cdgC* were carried along as negative controls (see Fig. 6.5 on page 105 in the appendix).

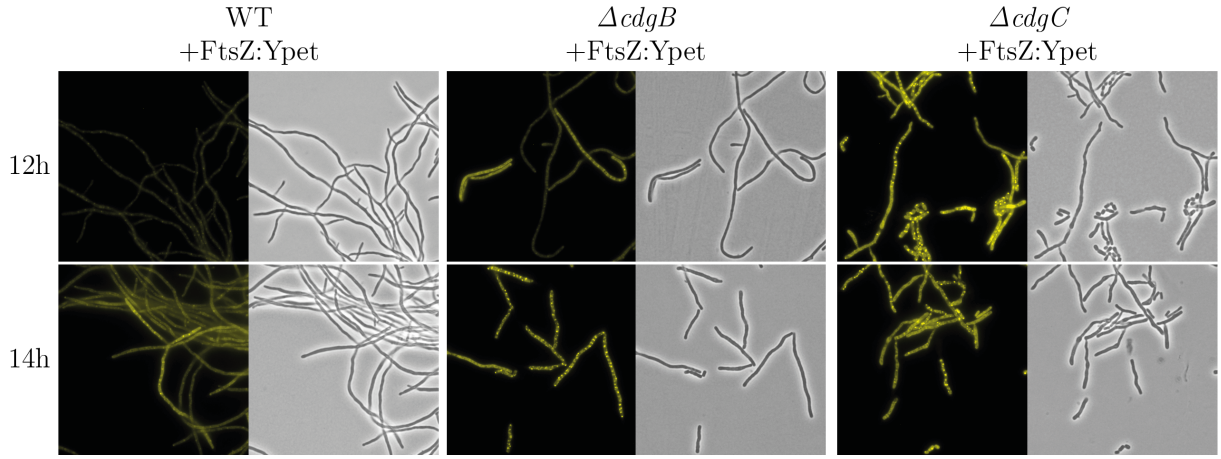

Fig. 4.15 CdgB and CdgC influence the formation of FtsZ-dependent Z-ring ladders. Confocal microscopic analysis of the expression pattern of an FtsZ:Ypet fusion protein under the control of its native promoter (pSS5) integrated into *S. venezuelae* WT, Δ*cdgB* and Δ*cdgC* respectively. These strains were inoculated in MYM liquid culture to a spore concentration of 10^6 CFU/mL. Incubation took place at 30 °C and 170 rpm and samples were harvested after 12 and 14 h. Microscopic images were documented under a 100× phase contrast objective with or without a Ypet filter. This figure was modified with permission after Haist et al. (2020); published in Molecular Microbiology under the CC BY license Attribution 4.0 International License.

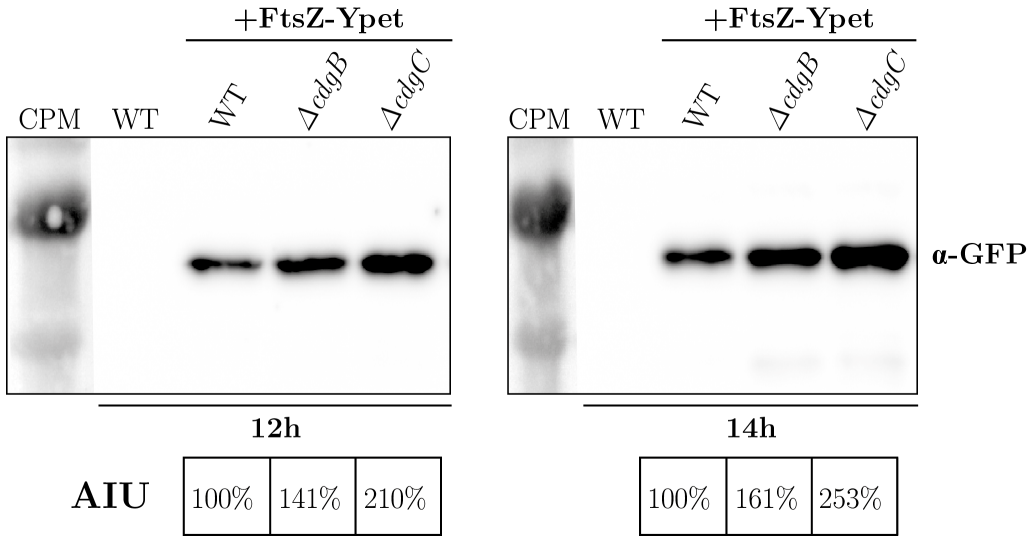

Fig. 4.16 CdgB and CdgC influence the expression of FtsZ. Immunodetection of an FtsZ:Ypet fusion protein expressed under the control of its native promoter (pSS5) and integrated into *S. venezuelae* WT, Δ*cdgB* and Δ*cdgC* respectively. For the Western blot analysis, the strains were inoculated in MYM liquid culture to an initial spore concentration of 10^6 CFU/mL respectively. Incubation took place at 30 °C and 170 rpm and samples were harvested after 12 and 14 h. A total protein amount of 14 µg per sample was separated via SDS-PAGE. This figure was modified with permission after Haist et al. (2020); published in Molecular Microbiology under the CC BY license Attribution 4.0 International License. CPM - color prestained marker; αGFP - anti-GFP antibody

As the phase contrast pictures of the two DGC mutants already showed fragmentation of the hyphae, it comes as no surprise that plenty of Z-ring ladders were observed, indicating ongoing sporulation septation. This observation is particularly pronounced in the already sporulating Δ*cdgC* strain. Another sample batch, taken after 14 h, revealed Z-ring ladders in all three strains although the differences in cell cycle progression were still remarkable (see Fig. 4.15).

For semi-quantitative analysis of the FtsZ-Ypet expression in the two DGC mutants compared to wild type, samples taken in parallel to those for confocal microscopy, described above, were prepared for immunodetection, as described by Schlimpert et al. (2017). The total protein concentration was determined via Bradford assay (Roth) and 15 µg total protein were loaded per sample. The only deviation from this procedure is the addition of 2,2,2-Trichloroethanol (TCE) to the SDS gel solution for protein visualization, as described by Ladner et al. (2004). The resulting fluorescent visible staining of proteins was used for loading controls that are shown in Fig. 6.6 on page 106 in the appendix. An anti-GFP antibody, also sensitive to the YPet protein, served as the primary antibody. The ImageQuantTL software was used to determine the arbitrary units (AIU; ratio of the band intensity relative to the wild type, set for 100%) for quantification. The results of the Western blot (see Fig. 4.16) verified the expected elevation of FtsZ-YPet relative to the wild type in Δ*cdgB* (around 150%) and, even more pronounced, in Δ*cdgC* (over 200%).

Altogether, the increased FtsZ levels in the *cdgC* mutant are coherent with the upregulation of several other genes involved in sporulation septation. The very similar yet slightly delayed effect observed in the *cdgB* mutant hints at partially overlapping influences of both genes on the timing of sporulation initiation in *S. venezuelae*.

4.6 The composition of the hydrophobic coat is altered in the *cdgC* mutant

Phenotypic analyses indicate that CdgC impacts the location and timing of spore formation, resulting in a protein-specific, DGC activity-dependent flat, gray colony phenotype that shows precocious sporulation in the deletion mutant, called hypersporulation. Hydrophobicity assays were performed to analyze whether the phenotype is caused by a deficiency in the hydrophobic coat that enables the aerial mycelium to break the air-water interface at the surface of the colony. For this, equal amounts of spores of *S. venezuelae* wild type and Δ*cdgC* were plated onto MYM agar and incubated for 50 h at 30 °C. The assay was performed through drip of 50 µL ddH_2O. Formation of distinct droplets in *S. venezuelae* wild type showed an intact hydrophobic surface while the water spread diffusely over the surface of the *cdgC* deletion mutant, proving the absence of a functioning hydrophobic coat surrounding the aerial mycelium (see Fig. 4.17).

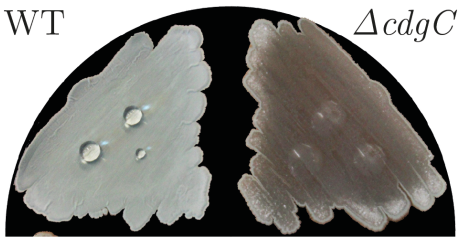

Fig. 4.17 Deletion of *cdgC* results in a hydrophilic colony surface. For the hydrophobicity assay 12 µL $2 \cdot 10^5$ spores of *S. venezuelae* WT and Δ*cdgC* were plated onto MYM agar and incubated for 50 h at 30 °C. The assay was performed through drip of 50 µL ddH_2O.

Recall from Section 1.2 on page 3 that the hydrophobic sheath that coats the outer surface of aerial hyphae consists primary of chaplins and rodlins (Claessen et al., 2003; Elliot et al., 2003). The genome of *S. venezuelae* encodes seven chaplin (*chpB-H*) and three rodlin genes (*rdlA-C*). The former are characterized by the highly conserved, hydrophobic chaplin domain whose abundance in the protein determines their classification in long chaplin proteins (ChpB-C), containing two chaplin domains, and short chaplin protein (ChpE-H, one chaplin domain) with a single chaplin domain (Elliot et al., 2003). In the absence of rodlin genes, the chaplin proteins self-assemble to form fibrils in *S. coelicolor*. The rodlin proteins seem to align these fibrils, resulting in the rodlet layer (Claessen et al., 2004). As their deletion does not alter the developmental progression of *S. coelicolor*, the rodlin proteins are considered non-essential (Claessen et al., 2002). Therefore, it is conceivable that changes in the chaplin-composition might inhibit the formation of the hydrophobic coat and, hence, the aerial mycelium, resulting in the location of sporulation initiation in the vegetative mycelium.

Their expression is controlled by the extracytoplasmic function (ECF) σ factor BldN that also controls the expression of the transcriptional developmental regulator BldM (Bibb et al., 2012). The latter was shown to act as a homodimer in the early sporulation phase, activating the *ssgAB* genes involved in recruiting the cell division machinery. In the late sporulation phase, it forms heterodimers with WhiI to activate the expression of the *whiE* genes and *smeA-ssfA* involved in chromosome segregation (Al-Bassam et al., 2014; Ausmees et al., 2007). Both BldN

and BldM are direct BldD-target genes, leading to the hypothesis that deleting any DGC would increase their expression indirectly via BldD inactivation (Schumacher et al., 2017; Elliot et al., 2001; Yan et al., 2020). Surprisingly, RNA-Seq analysis of *S. venezuelae* Δ*cdgC* compared to the wild type performed by J. Haist showed a decrease in expression of *bldN* and all chaplin genes except *chpB* and *chpD*, which showed no significant alterations (Haist et al., 2020). These data shall be validated in the following via qRT-PCR analysis.

4.6.1 CdgC affects the transcription of *bldN*, *bldM* & several *chp* genes

The unexpected decrease in expression of major players involved in the formation of the hydrophobic sheath in the *cdgC* mutant relative to *S. venezuelae* wild type indicated by RNA-seq data (Haist et al., 2020) prompted a verification via an alternative technique. Here, qRT-PCR of *bldN*, *bldM* and the representative, downregulated chaplin genes *chpC*, *chpE* and *chpH* were used for this attempt. For this, primers were designed, amplified and tested for their binding efficiency, as described in Section 4.4. Subsequently, all RNA samples were adjusted to a concentration of 10 ng/µL and 2 µL RNA (20 ng) was used per reaction mix to perform qRT-PCRs for each primer-pair in technical triplets and the assay was reproduced at least three times. Controls were carried along for each primer-pair using nucleotide-free water instead of RNA. The qRT-PCR was performed using the SensiFAST SYBR No-ROX One-Step Kit (Bioline) and the program described in Section 3.5.11 on page 32. The results of the qRT-PCRs support the tendency suggested by the RNA-seq data. Transcript levels of *bldN*, *bldM* and the tested chaplin genes (*chpC*, *chpE* and *chpH*) are downregulated in the absence of CdgC, even though the $\log_2$-fold change of *bldM* only slightly exceeds the defined threshold for significance (see Fig. 4.18).

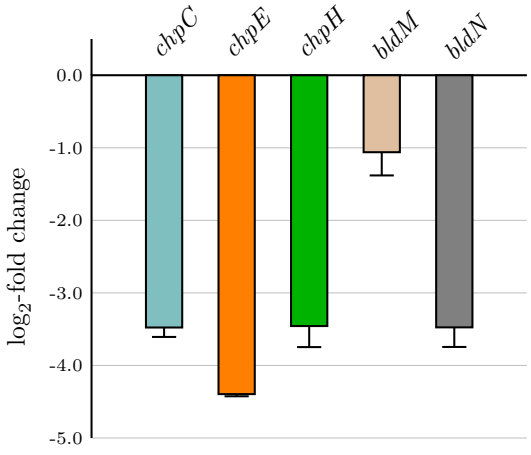

Fig. 4.18 The transcription of *bldM*, *bldN*, *chpC*, *chpE* and *chpH* is downregulated in Δ*cdgC* compared to the WT. Transcription values were quantified via qRT-PCR analysis performed with RNA samples isolated via SV Total RNA Isolation Kit (Promega) harvested after 30 h of incubation at 30 °C on MYM agar at least three times with three technical replicates per experiment. Calculations of the expression values relative to the accumulation of the constitutively expressed *hrdB* reference mRNA (encoding the housekeeping σ factor in *Streptomyces*) and normalized to WT value. $\log_2$-fold change > 1 or < -1 was considered significant. Presented data are the mean of three technical replicates ±standard deviation. This figure was modified with permission after Haist et al. (2020); published in Molecular Microbiology under the CC BY license Attribution 4.0 International License.

4.6.2 Overexpressing ChpC/ChpE rescues aerial mycelium in Δ*cdgC*

As mentioned above, the absence of CdgC results in hypersporulation without aerial hyphae formation and decreased transcription levels of all tested chaplin genes as well as the gene encoding their regulatory σ^{BldN} and its target gene *bldM*. These changes in the chaplin composition could inhibit the formation of the hydrophobic coat and, thus, the aerial mycelium, resulting in the initiation of the sporulation in the vegetative mycelium. Hence, it would be interesting to investigate whether increased chaplin expression levels could influence the CdgC-dependent timing and location of sporulation initiation.

Overexpression of single chaplin genes in *S. venezuelae* was achieved by cloning them each under the control of the constitutively active *ermE** promoter on the integrative pMS82 vector. In case of *chpD* and *chpF*, *ermE** promoter and gene sequence were synthesized *de novo* (GeneScript). For phenotypic analysis, macrocolonies of these strains were generated, as described in Section 3.4.10 on page 28, and incubated for four days at 30 °C. Documentation

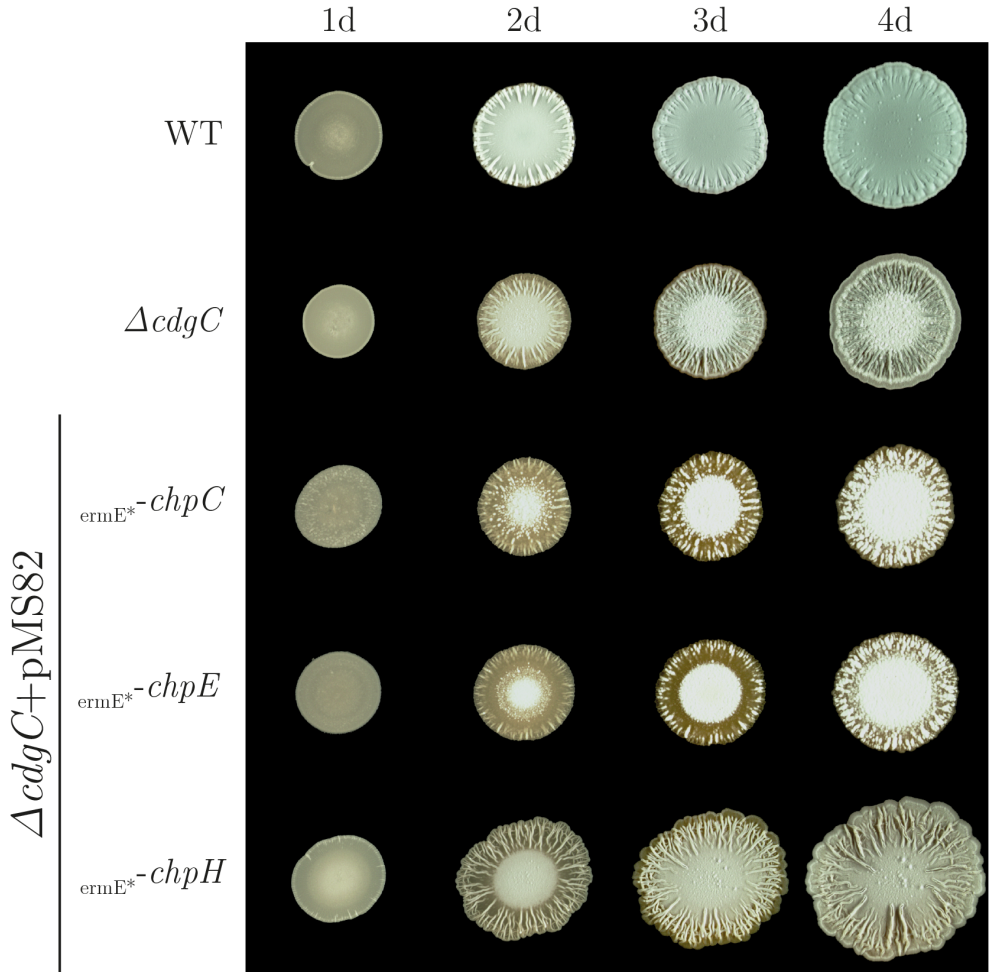

Fig. 4.19 Overexpression of neither ChpC nor ChpE is sufficient to complement hypersporulation, but partially restores formation of aerial hyphae in Δ*cdgC*. *chpC*, *chpE* and *chpH* were individually expressed from the integrative pMS82 vector controlled by the constitutive *ermE** promoter in Δ*cdgC*. Macrocolonies of these strains as well as *S. venezuelae* WT and Δ*cdgC*, serving as control, were created through a drip of 12 µL $2 \cdot 10^5$ CFU µL^{-1} spores on MYM agar and plates were incubated for 4 d at 30 °C. The documentation took place every 24 h. This figure was modified with permission after Haist et al. (2020); published in Molecular Microbiology under the CC BY license Attribution 4.0 International License.

took place every 24 h under the binocular microscope. The results of the overexpression of ChpC, ChpE and ChpH are shown in Fig. 4.19, while those of ChpB, ChpD and ChpF are presented in Fig. 6.7 on page 107 in the appendix.

Overexpressing individual chaplin genes in Δ*cdgC* partially restored the wild type phenotype only for ChpC and ChpE. These colonies developed the white and fuzzy surface typical for aerial hyphae formation, but did not turn green even after prolonged incubation. However, overexpressing ChpH resulted in a hypersporulation phenotype with larger colony size and enhanced radial wrinkling compared to Δ*cdgC*. No visible phenotypic alterations were caused by overexpressing ChpB, ChpD or ChpF. *S. venezuelae* wild type and Δ*cdgC* served for comparing the observed phenotypes and these strains with the empty vector served as control strains to verify that it has no effect on the phenotype.

Altogether, phenotypical analysis unveiled that individual overexpression of none of the tested chaplin genes was sufficient to completely restore aerial mycelium formation to the *cdgC* mutant. This leads to the assumption that the well-orchestrated expression of several chaplin genes is necessary to overcome this developmental defect (Di Berardo et al., 2008).

4.6.3 Overexpressing BldM or BldM restores the functionality of the hydrophobic coat in Δ*cdgC*

Since the overexpression of no single chaplin is sufficient to complement hypersporulation, a putative regulatory role of CdgC further *upstream* the gene cascade should be tested. The σ^{BldN} controls the expression of all *chp* and *rdl* genes as well as *bldM*. It was assumed, that the overexpression of *bldN* would result in a synchronized increase in the expression of multiple hydrophobins. This raises the question of whether the overexpression of BldN (and thereby indirectly all chaplins and rodlins) or BldM (and thereby indirectly SsgA and SsgB, which recruit FtsZ to future cell division sites) could complement the disability to form aerial hyphae.

To investigate this question, overexpression plasmids of BldM and BldN were constructed, as described above for the chaplins, under the control of the constitutively active *ermE** promoter and introduced into *S. venezuelae* wild type and Δ*cdgC*. These strains were used to perform phenotypic complementation assays and hydrophobicity assays shown in Fig. 4.20 (Δ*cdgC*) and in Fig. 6.8 on page 108 in the appendix (wild type).

The resulting macrocolonies show hypersporulation with slightly larger colony size, darker gray color and enhanced wrinkling in the *cdgC* knockout background (see Fig. 4.20 A). Additionally, the hydrophobicity assay shows enhanced hydrophobicity compared to Δ*cdgC* only (see Fig. 4.20 B). Introducing the overexpression constructs of BldM and BldN in *S. venezuelae* wild type results in slightly accelerated sporulation with green coloring, which is already visible after 24 h, but did not alter the phenotype in any other, significant way.

Taken together, these results indicate that the overexpression of BldN enhances the expression of the chaplin proteins, restoring the hydrophobic coat. Contrary to the expectations, this did not restore the aerial hyphae formation and, therefore, the wild type phenotype.

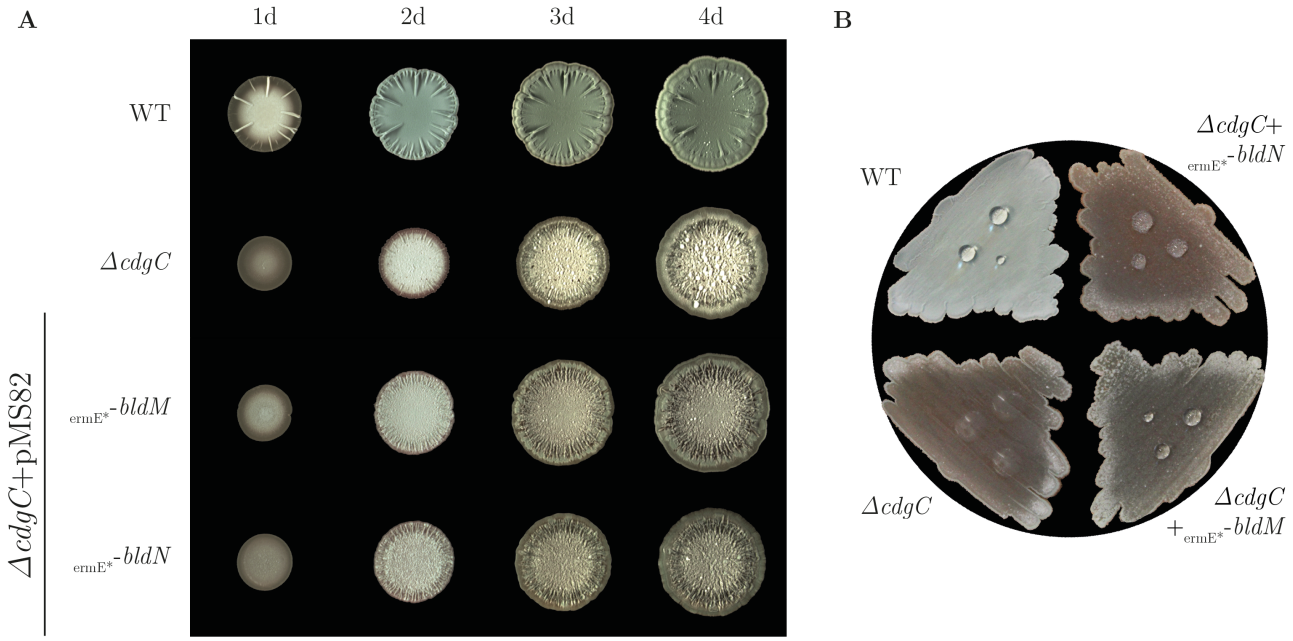

Fig. 4.20 Overexpression of neither BldN nor BldM is sufficient to complement the hypersporulation phenotype, but partially restores the hydrophobicity in Δ*cdgC*. (A) Macrocolonies of *S. venezuelae* WT and Δ*cdgC*, Δ*cdgC*+pMS82-$_{ermE*}$-*bldM/N* were created through drip of 12 µL $2 \cdot 10^5$ CFU/µL spores on MYM agar and plates were incubated for 5 d at 30 °C. The documentation took place every 24 h. (B) For the hydrophobicity assay 12 µL $2 \cdot 10^5$ spores of the above mentioned strains were plated onto MYM agar and incubated for 50 h at 30 °C. The assay was performed through drip of 50 µL ddH_2O.

4.7 CdgC interacts with itself and three putative membrane proteins

4.7.1 CdgC forms homooligomers

Dimerization of DGCs like CdgC is essential to synthesize c-di-GMP from two GTP molecules, each bound by one monomer, resulting in symmetrical phosphodiester bonds (Paul et al., 2007). Promotion of dimerization by their sensory domains could, therefore, be a manner of activation (Römling et al., 2013). The *in vitro* DGC assays indicated that the `GGDEF` domain of CdgC alone is unable to synthesize c-di-GMP, contrasting variants containing the sensory PAS-PAC and `EAL` domains. Ergo, it would be interesting to verify the homooligomerization of CdgC and to determine the supporting domains.

In vivo protein-protein interaction assays like BTH assays after Karimova et al. (1998) (see Section 3.6.7 on page 35) were performed, cloning the genes encoding the peptides of interest on the complementary BTH plasmids. These plasmids were transferred by co-transformation into *E. coli* W3110 Δ*cyaA* cells. The transformed clones were selected on LB agar supplemented with Kan, Amp and XGal. Three colonies per tested combination were resuspended in 1 mL 1xPBS, 5 µL bacterial suspension dropped on MacConkey agar supplemented with 1% maltose or lactose, Amp and Kan and incubated at 26 °C for 90 and 43 h, respectively. Interactions of the fusion proteins complement the *cyaA* deletion, enabling the fermentation of the added carbon source. MacConkey medium contains the pH indicator phenol red that is turned red by the acidification.

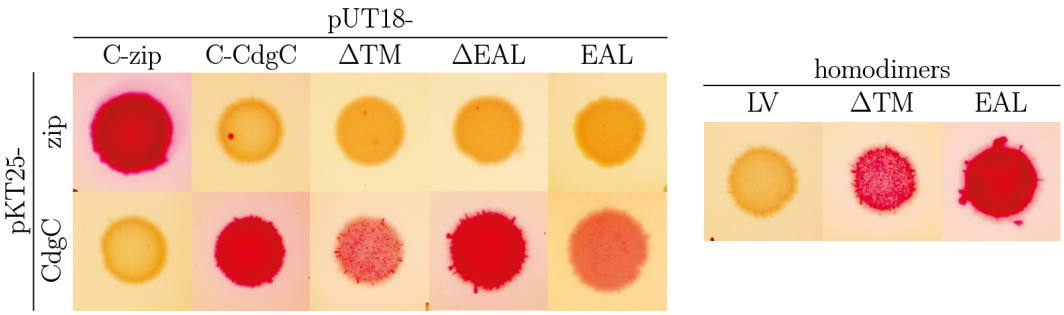

Fig. 4.21 CdgC shows self-interaction supported by the transmembrane anchor and the `EAL` domain. *In vivo* protein-protein interaction assays after Karimova et al. (1998). Fusion proteins of different variants of CdgC on complementary BTH plasmids (T25 N-terminally and T18 C-terminally of the peptide of interest) were co-expressed in *E. coli* W3110 Δ*cyaA*. Three colonies per tested combination were suspended in 1 mL 1xPBS, 5 µL bacterial suspension dropped on MacConkey (Difco, 1% maltose + Amp + Kan) and incubated at 26 °C for 90 h. Interactions of the fusion proteins complement the *cyaA* deletion, enabling the fermentation of the added carbon source. By adding phenol red as a pH indicator, acidification is visible. zip-zip - dimerization of the leucine zipper region of the yeast protein GCN4 (positive control); LV-LV - empty vector combination pKT25 - pUT18 (negative control); C-CdgC - CdgC on pUT18C; ΔTM-CdgC - without the ten transmembrane domains; CdgC-`EAL` - `EAL` domain only; Δ`EAL`-CdgC - without the `EAL` domain

Previous experience with the media revealed alterations in the identified interactions between lactose and maltose as a carbon source, so both media were tested. Representative examples of positive interactions on maltose containing medium, incubated for 90 h, are shown in Fig. 4.21. Further tested interactions of CdgC and its variants both on maltose containing medium for 90 h and on lactose containing medium, incubated for 43 h, are shown in Fig. 6.9 on page 108 in the appendix.

These results suggest that CdgC full-size forms homooligomers on both maltose and lactose. Furthermore, it interacts with its peptide variants that lack the `EAL` domain on maltose containing medium. CdgC full-size also shows interactions with its peptide variants that lack the transmembrane anchor, on maltose and lactose, as well as with the `EAL` domain alone, on maltose only, but significantly weaker considering the lighter red color after 90 h of incubation. In contrast, the `EAL` domain alone shows a dark red color that is associated with strong homooligomerization, on maltose. The peptide variants that lack the transmembrane anchor show a red color similar to the interaction with the full-size CdgC on maltose.

Altogether, BTH assays revealed that CdgC forms homooligomers, supported by its membrane anchor and `EAL` domain.

4.7.2 CdgC does not interact with BldD

Direct protein-protein interactions, more precisely homooligomerization, is essential for the enzymatic activity of DGCs like CdgC. In many bacterial species like *S. venezuelae*, these c-di-GMP turnover enzymes are redundantly present. In those species, direct protein-protein interactions of c-di-GMP turnover proteins with each other and their effector components are a criterion that indicates local c-di-GMP signaling (Sarenko et al., 2017). The DGC CdgC was already shown to fulfill another of the three criteria that define local c-di-GMP signaling:

a specific knockout phenotype (see Fig. 1.10 on page 20). One of the two so far identified c-di-GMP effector proteins, BldD, represses the sporulation cascade during the vegetative phase. Its deletion results in a hypersporulation phenotype that resembles the *cdgC* mutant described before, which is unique among the deletion mutants of the other c-di-GMP turnover proteins (Tschowri et al., 2014). Furthermore, nucleotide extraction analysis revealed surprisingly increased cellular c-di-GMP levels in Δ*cdgC* compared to the wild type for nearly all tested time points, in liquid culture as well as on solid medium, casting doubt on a correlation between c-di-GMP levels and the hypersporulation phenotype of the *cdgC* mutant. This lack of correlation between c-di-GMP levels and biofilm formation morphology was also observed in *E. coli* and, hence, indicates local c-di-GMP signaling (Sarenko et al., 2017; Richter et al., 2020). Therefore, it seems likely that alterations in local c-di-GMP pools affect the regulation of *S. venezuelae* development. Thus, CdgC could also feed into a local c-di-GMP pool sensed by BldD. If CdgC and BldD are linked via local signaling, they likely would show direct protein-protein interactions, which were investigated by performing BTH assays.

The BTH assays were performed, as described in Section 4.7.1, on maltose and lactose, respectively. The results, shown in Fig. 4.22, provide no evidence for a direct protein-protein interaction of CdgC and BldD, while each of them shows self-interaction. The homooligomerization of CdgC, BldD and the leucine zipper protein of the yeast protein GCN4 served as a positive control, whereas the empty BTH vectors pUT18 and pKT25 were taken as a non interacting combination.

Interfering effects in the *in vivo* interaction assay from the performance in *E. coli* instead of the gene origin *S. venezuelae* were excluded by performing pulldown assays with CdgC-FLAG and BldD using the Δ*cdgC*+p3xFLAG-*cdgC* complementation strain and the wild type as a negative control (see Section 3.6.7 on page 36). The CdgC-FLAG protein, expressed in the Δ*cdgC*+p3xFLAG-*cdgC* complementation strain, was purified over a FLAG-affinity matrix. Samples taken from the whole cell crude and the eluate provided evidence for BldD in an Western blot with a primary antibody against BldD in the lysate but not the eluate (see Fig. 4.23 B). The samples were tested for successful purification of CdgC-FLAG with immunodetection against the FLAG antibody, validating its enhanced presence in the eluate, but not the cell lysate (see Fig. 4.23 A). Further bands at about 34 and over 60 kDa match oligomeric states of BldD, regarding their size, but since these samples have been incubated in SDS-containing buffer at 95 °C for 20 min they are most likely unspecific. The lack of CdgC-FLAG detectable in the lysate is unexpected, but might be due to the lower concentration of total protein here. Furthermore, CdgC-FLAG is purified over a FLAG-affinity matrix during the assay, which enhances its concentration in the eluate and, thus, in the sample significantly. These factors might cause a lower protein amount of CdgC-FLAG in the lysate sample, than detectable by the Western blot. The CdgC-FLAG detected in the eluate showed a strong degradation pattern similar to the one described in Section 4.2.2.

Taken together, CdgC and BldD did not show any direct protein-protein-interactions in BTH or pulldown assays.

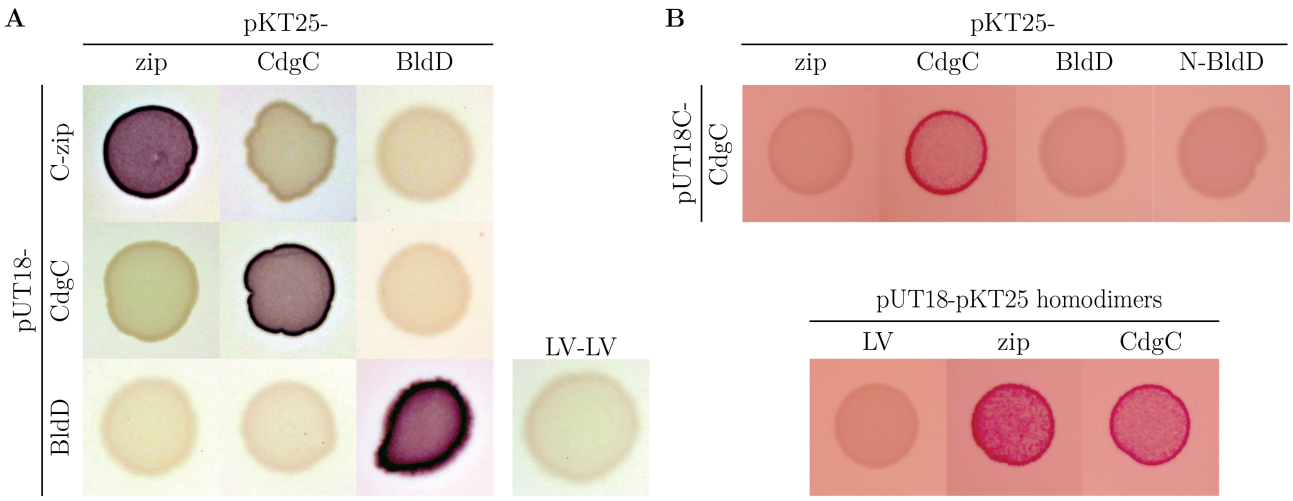

Fig. 4.22 CdgC does not show direct protein-protein interaction with BldD. *In vivo* protein-protein interaction assays after Karimova et al. (1998). Fusion proteins on complementary BTH plasmids (A and B bottom: pKT25 and pUT18 of the peptide of interest; B top: pKT25 and pUT18C of the peptide of interest) were co-expressed in *E. coli* W3110 Δ*cyaA*. Three colonies per tested combination were suspended in 1 mL 1xPBS, 5 µL bacterial suspension dropped on MacConkey (A: Roth, 1% maltose + 1% lactose + Amp + Kan; B: Difco, 1% lactose + Amp + Kan) and incubated for (A) 24 h or (B) 29 h at 26 °C. Interactions of the fusion proteins complement the *cyaA* deletion, enabling the fermentation of the added carbon source. By adding phenol red as a pH indicator, acidification is visible. zip-zip - dimerization of the leucine zipper region of the yeast protein GCN4 (positive control); LV-LV - empty vector combination pKT25 - pUT18 (negative control); N-BldD - pKNT25-BldD

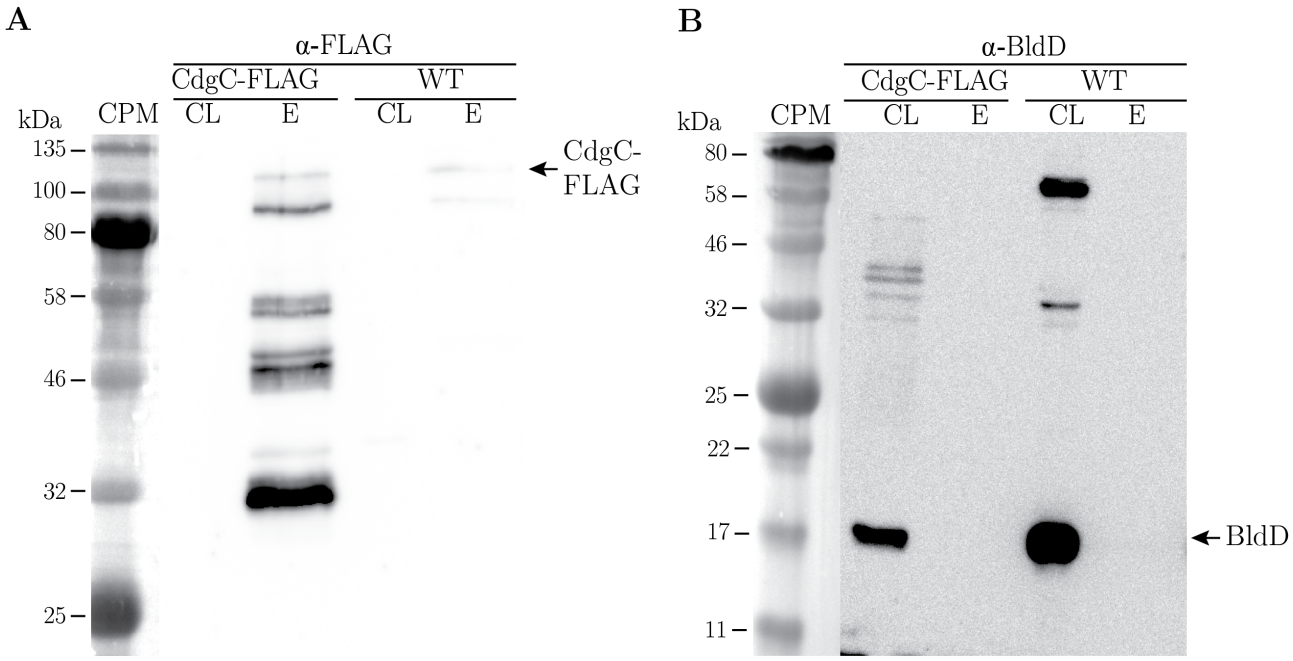

Fig. 4.23 CdgC does not influence developmental regulation via interaction with BldD. *In vivo* protein-protein interaction of CdgC-FLAG with BldD was tested with pulldown assays harvesting cells of the complemented strain Δ*cdgC*+pcdgC-FLAG (CdgC-FLAG). Lysed cells were further purified with an anti-FLAG affinity matrix and analysed with SDS-PAGE and immunodetection against (A) the anti-FLAG (αFLAG) or (B) a protein-specific BldD (αBldD) antibody. The protein-specific bands are indicated by labelled arrows. *S. venezuelae* WT, treated likewise, was used as a negative control. CL - cell lysate; E - eluate; CPM - color prestained marker

4.7.3 CdgC shows no interaction with the RsiG-WhiG complex

Another candidate for local c-di-GMP signaling is the newly identified c-di-GMP effector protein, anti-σ RsiG that is armed by c-di-GMP to effectively interact with its corresponding σ factor WhiG (Gallagher et al., 2020). This binding inhibits the σ^{WhiG} induced expression of over 100 late sporulation genes via its direct target genes *whiH* and *whiI* (Bush et al., 2013). The expression of the former is only partially *whiG*-dependent, but the latter is activated by σ^{WhiG} exclusively (Gallagher et al., 2020). RNA-seq data indicated upregulated transcription levels of *whiI* in Δ*cdgC*. Together with a strong similarity between the phenotype of Δ*cdgC* and a WhiG overexpression strain, this indicates that altered c-di-GMP levels caused by the absence of CdgC and an unbalanced WhiG-RsiG ratio have highly similar consequences for cell morphology (Gallagher et al., 2020). These observations might be caused by CdgC feeding the local c-di-GMP pool that supports RsiG-WhiG-complex formation. To check for further indicators supporting this hypothesis, BTH assays, performed, as described in Section 4.7.1, as well as pulldown assays against protein-specific antibodies, as described in Section 4.7.2, were performed to test for direct protein-protein interactions between CdgC and RsiG or WhiG, respectively.

Representative results of the BTH assays are shown in Fig. 4.24, all further tested combinations can be found in Fig. 6.10 (shown on page 109 in the appendix) and the results of the pulldown assays are shown in Fig. 4.25. None of these experiments provided evidence for an interaction of CdgC with RsiG or WhiG. BTH assays validated the interaction between RsiG and WhiG in several plasmid combinations (see Fig. 4.24 for a representative collection of tested combinations). The Western blots against RsiG showed one prominent and several faint bands that are considered unspecific, since they are also present in the eluate of the wild type (see Fig. 4.25 A). The Western blot against WhiG provides evidence that the primary WhiG antibody lacks specificity as it detected several, most likely unspecific bands in the cell lysates among one that might be the RsiG-WhiG complex (see Fig. 4.25 B).

Altogether, CdgC did not show any direct protein-protein-interactions with either RsiG or WhiG in BTH or pulldown assays. Looking further into details of the above mentioned RNA-seq data reveals that *whiI* is also upregulated in Δ*cdgB*, but downregulated in both Δ*rmdA* and Δ*rmdB* (Haist et al., 2020). This indirect evidence of altered σ^{WhiG} activity hints towards a strictly c-di-GMP-mediated modulation by the tested DGCs and PDEs.

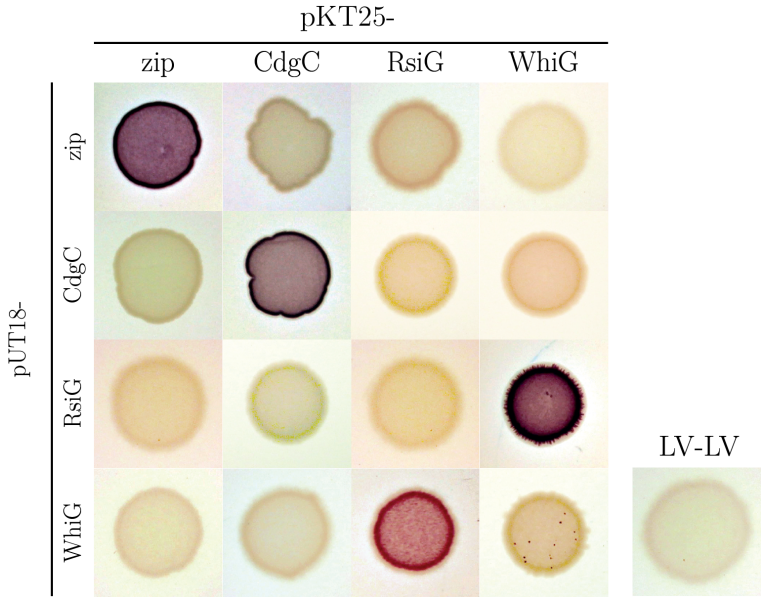

Fig. 4.24 CdgC does not show direct protein-protein interaction with RsiG or WhiG. *In vivo* protein-protein interaction assays after Karimova et al. (1998). Fusion proteins on complementary BTH plasmids (pKT25 and pUT18 of the peptide of interest) were co-expressed in *E. coli* W3110 Δ*cyaA*. Three colonies per tested combination were suspended in 1 mL 1xPBS, 5 µL bacterial suspension dropped on MacConkey (Roth, 1% maltose + 1% lactose + Amp + Kan) and incubated at 26 °C for 24 h. Interactions of the fusion proteins complement the *cyaA* deletion, enabling the fermentation of the added carbon source. By adding phenol red as a pH indicator, acidification is visible. zip-zip - dimerization of the leucine zipper region of the yeast protein GCN4 (positive control); LV-LV - empty vector combination pKT25 - pUT18 (negative control)

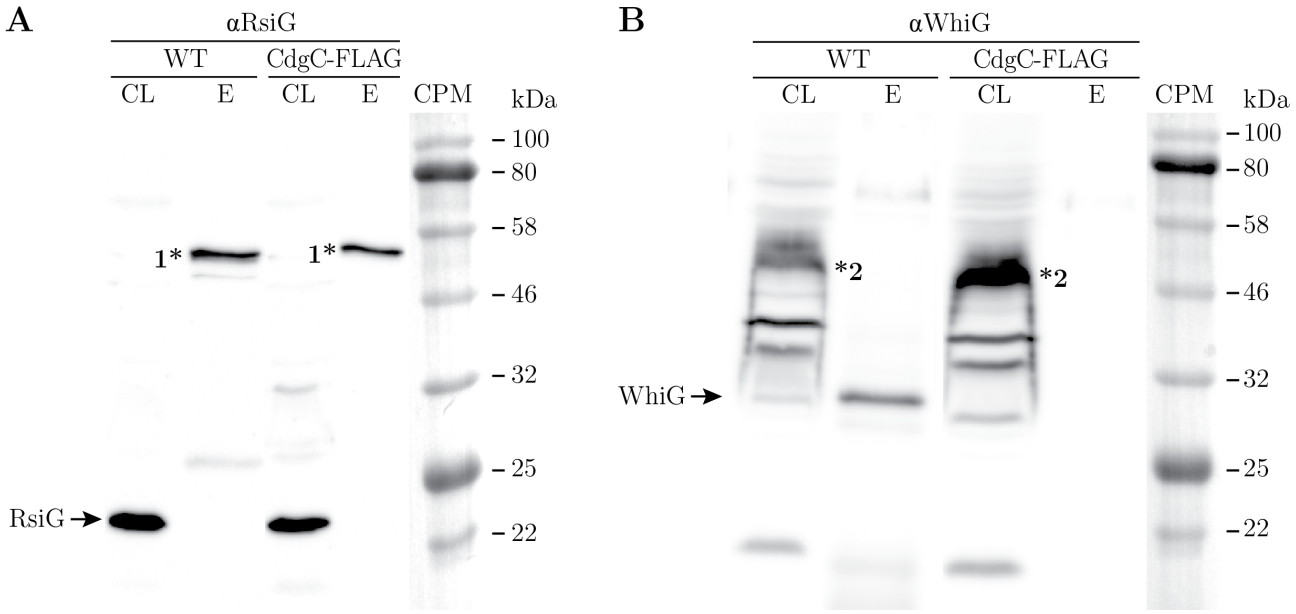

Fig. 4.25 CdgC does not seem to influence the complex formation of RsiG and WhiG. *In vivo* protein-protein interaction assay of CdgC-FLAG with RsiG and WhiG were tested via pulldown assays, harvesting cells of the complementation strain Δ*cdgC*+pcdgC-FLAG (CdgC-FLAG). Lysed cells were purified with an anti-FLAG affinity matrix and analyzed with SDS-PAGE and immunodetection against (A) RsiG (αRsiG) or (B) WhiG (αWhiG) antibody. The protein-specific bands are indicated by labeled arrows. *S. venezuelae* WT, treated likewise, was used as a negative control. CL - cell lysate; E - eluate; CPM - color prestained marker; *1 - specific band; *2 - potential band of the WhiG-RsiG complex

4.7.4 CdgC does not interact with σ^{BldN}

The chromosomal deletion of *cdgC* resulted in reduced expression of most chaplins and rodlins (confirmed via qRT-PCR for *chpC*, *chpE* and *chpH*) as well as their regulating σ factor BldN (see Section 4.6). The resulting deficiency in the hydrophobic coat inhibits the escape of the hyphae from their aqueous environment into the air to form the aerial mycelium initiating the reproductive phase. One can derive the hypothesis that this deficiency causes the sporulation by bypassing aerial mycelium formation. This hypothesis was supported by the partial restoration of the *S. venezuelae* wild type phenotype by respective overexpression of the single ChpC and ChpE protein (see Fig. 4.19). However, this could not be observed by overexpressing σ^{BldN} resulting in slightly enhanced surface hydrophobicity but no restore of the wild type phenotype in Δ*cdgC* (see Fig. 4.20). This indicated a posttranslational sequestration by its anti-σ RsbN, which the tested increase in *bldN* transcripts is not able to compensate in the absence of CdgC. As the chaplin genes seemed to be such a pronounced group of target genes of CdgC, one hypothesis is that a co-localization of CdgC with BldN or its anti-sigma factor RsbN causes this altered expression of *chp* and *rdl* genes. To verify this, BTH assays were performed, as described in Section 4.7.1, on maltose and lactose, respectively.

The results, shown in Fig. 4.26, do not provide any evidence for a direct protein-protein interaction of CdgC with either BldN or RsbN. The direct protein-protein interaction between BldN and RsbN as well as the dimerization of CdgC was validated. These interactions, together with the homodimerization of the leucine zipper of the yeast protein GCN4 served, as a positive control for the assays and the functionality of the fusion constructs.

The results of the BTH assays were verified via pulldown assays (performed as described in Section 3.6.7 on page 36). The resulting eluates of *S. venezuelae* wild type and Δ*cdgC*, conjugated with p3xFLAG-*cdgC*, were tested via immunodetection against protein-specific antibodies for the presence of BldN. The results of these Western blots, shown in Fig. 4.27, indicate no interaction of CdgC with BldN. The Western blot of BldN revealed no bands in the eluate lanes, but several for the cell lysate samples. Previously performed Western blots of BldN in *S. venezuelae*, performed by J. Wiese, showed two bands between 22 and 25 kDa. These two bands are also present in the cell lysate of *S. venezuelae* wild type (see Fig. 4.27 B *1 & *2) and one of them (*2) in the CdgC-FLAG complementation strain together with a potential degradation band (*3). Additionally, both lanes show a strong band at around 32 kDa. In *S. coelicolor*, the expression of BldN initiates with the translation of a proprotein (Pro-σ^{BldN}, 35 kDa), undergoing a proteolytic maturation to the physiologically active ECF σ factor σ^{BldN} (28 kDa) (Bibb & Buttner, 2003). All annotations of BldN in *S. venezuelae* predict a protein size of about 28 kDa indicating that the additional band might be the Pro-σ^{BldN} protein that also undergoes a proteolytic processing to its active version.

Altogether, CdgC did not show any direct protein-protein-interactions with BldN neither in BTH nor in pulldown assays.

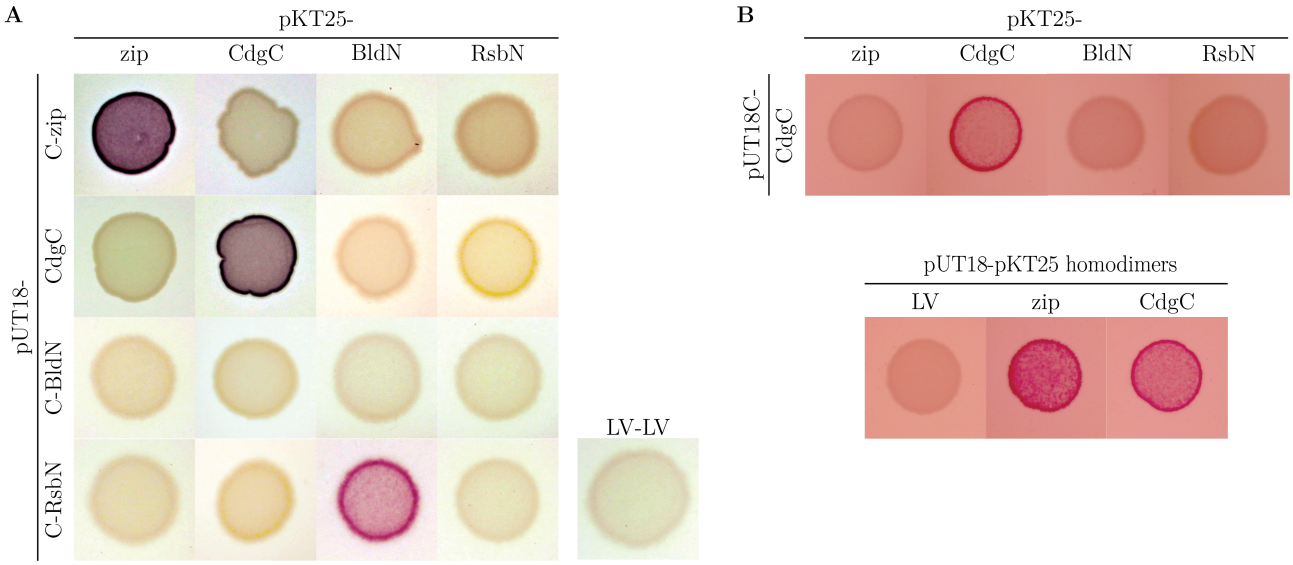

Fig. 4.26 CdgC does not influence the hydrophobin levels via direct protein-protein interactions with BldN or RsbN. *In vivo* protein-protein interaction assays after Karimova et al. (1998). Fusion proteins on complementary BTH plasmids (A: T25 N- and T18 C-terminally of the peptide of interest; B: T25 N-terminally, T18 C-terminally and T18C N-terminally of the peptide of interest) were co-expressed in *E. coli* W3110 Δ*cyaA*. Three colonies per tested combination were suspended in 1 mL 1xPBS, 5 µL bacterial suspension dropped on MacConkey (A: Roth, 1% maltose + 1% lactose + Amp + Kan; B: Difco, 1% lactose + Amp + Kan) and incubated for (A) 24 h or (B) 29 h at 26 °C. Interactions of the fusion proteins complement the *cyaA* deletion, enabling the fermentation of the added carbon source. By adding phenol red as a pH indicator, acidification is visible. zip-zip - dimerization of the leucine zipper region of the yeast protein GCN4 (positive control); LV-LV - empty vector combination pKT25 - pUT18 (negative control)

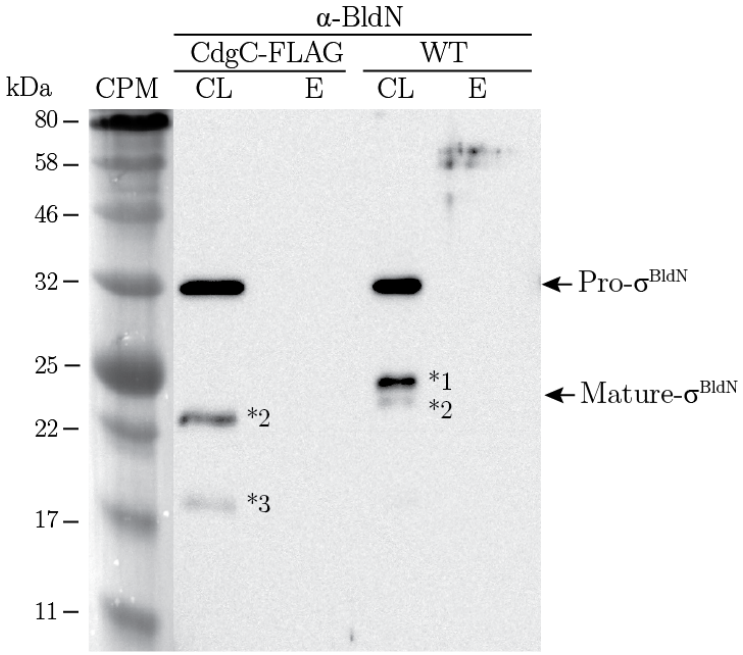

Fig. 4.27 CdgC does not bind BldN *in vivo*. Pulldown assays of CdgC-FLAG with BldN were performed, harvesting cells of the complementation strain Δ*cdgC*+p*cdgC*-FLAG (CdgC-FLAG). Lysed cells were purified with an anti-FLAG affinity matrix and analyzed with SDS-PAGE and immunodetection against BldN (αBldN) antibody. The protein-specific bands are indicated by labelled arrows. Furthermore discussed bands are indicated with numbered stars (*). *S. venezuelae* WT, treated likewise, was used as a negative control. CL - cell lysate; E - eluate; CPM - color prestained marker

4.7.5 CdgC interacts with three membrane-bound proteins

Besides the specific testing of promising candidates for direct protein-protein interactions with CdgC, the *S. venezuelae* proteome was screened for interaction partners in an unbiased manner. BTH-screenings were performed with a BTH genomic library provided by the laboratory of M. Buttner and constructed by BIO S&T (Saint-Laurent, Québec, Canada). Therefore, genomic DNA from *S. venezuelae* was sonified to shear it, end-repaired and cloned into pUT18C vectors, that had been digested with the restriction enzyme SmaI. On the pUT18C vector, the multiple cloning site is located downstream of the sequence encoding the T18 subunit of the adenylate cyclase, thus in frame fusions are only necessary at one end of the cloned insert, in contrast to N-terminal fusions. This BTH pUT18C-library was tested against *cdgC* on the pKT25 vector. Plasmids were co-transformed in *E. coli* W3110 Δ*cyaA*.

These screenings yielded six candidates, three of which were highlighted by sequencing of the interacting plasmids of the pUT18C library as potential interaction partners of CdgC, while the other three were not in frame. Furthermore, bioinformatic analysis identified them as the putative membrane proteins Vnz07170/YjcH, Vnz08595 and Vnz15770. The candidates were cloned on pUT18 and pKT25 and co-transformed with CdgC on the complementary BTH plasmid in *E. coli* W3110 Δ*cyaA* to verify these interactions. The analysis with the addition of maltose and lactose, respectively, was established on the observation that some interactions resulted only with one of the two carbon sources in a red coloration. A representative set of the tested BTH interactions on maltose, confirming the interaction of all three proteins with CdgC, is depicted in Fig. 4.28, further combinations on maltose and lactose can be found in Fig. 6.11 on page 110 in the appendix.

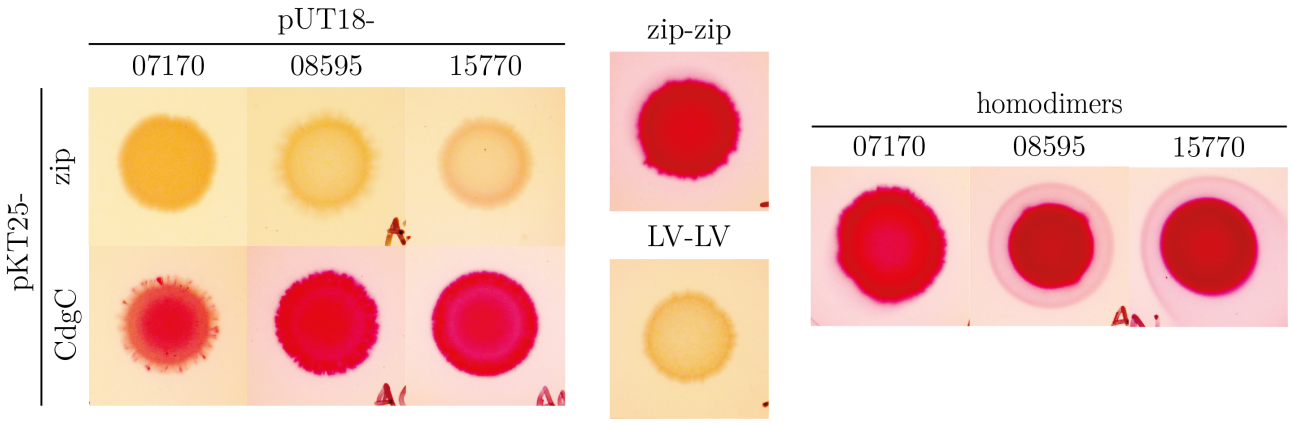

Fig. 4.28 CdgC interacts with Vnz07170, Vnz08595 and Vnz15770, which form homodimers, respectively. *In vivo* protein-protein interaction assays after Karimova et al. (1998). Fusion proteins on complementary BTH plasmids (T25 N-terminally and T18 C-terminally of the peptide of interest) were co-expressed in *E. coli* W3110 Δ*cyaA*. Three colonies per tested combination were suspended in 1 mL 1xPBS, 5 µL bacterial suspension dropped on MacConkey (Difco, 1% maltose + Amp + Kan) and incubated at 26 °C for 108 h. Interactions of the fusion proteins complement the *cyaA* deletion, enabling the fermentation of the added carbon source. By adding phenol red as a pH indicator, acidification is visible. zip-zip - dimerization of the leucine zipper region of the yeast protein GCN4 (positive control); LV-LV - empty vector combination pKT25 - pUT18 (negative control)

During her master thesis, V. Riebe discovered that the membrane anchor of CdgC plays an essential role in these interactions, since cytosolic CdgC interacts with none of these proteins. Vnz08595, a membrane protein, showed the strongest interaction with CdgC in all tested combinations and on both carbon sources. Its ortholog in *S. coelicolor*, Sco2097, interacts with the cell division complex and impacts the coordination of the Z-ring formation in the early reproductive phase (Kleinschnitz et al., 2011).

Taken together, interactions have been observed between CdgC and the potential membrane proteins Vnz07170/YjcH, Vnz08595/Sco2097 and Vnz15770. As Vnz08595 showed the strongest interaction with CdgC, it shall be characterized in more detail in the following.

4.8 The effect of Vnz08595 on sporulation septation

As discussed in Section 4.7, Vnz08595 interacts with CdgC via direct protein-protein interaction. Its ortholog in *S. coelicolor*, Sco2097, plays an important role in the cell division and influences the spore wall synthesis *S. coelicolor* (Kleinschnitz et al., 2011). Orthologs of Sco2097 are conserved in many actinomycetes where its encoding genes are located next or near the "division and cell wall" (dcw) gene cluster (Mingorance et al., 2004; Kleinschnitz et al., 2011). This gene cluster contains i.a. FtsZ, whose expression and assembly were shown above to be c-di-GMP-mediated influenced by CdgC (see Fig. 4.15 and 4.16). Altogether, these findings distill Vnz08595 as the most promising candidate of the three CdgC interaction partners for further characterization. The question was, if Vnz08595 plays a similar role in spore wall synthesis as its ortholog in *S. coelicolor*, Sco2097, and how this role is played out in the context of CdgC.

These questions were approached by generating chromosomal deletions of the gene in presence of enzymatically active (Δ*vnz08595*) and inactivated CdgC (*cdgC*^{ALLEF}Δ *vnz08595*). The choice of the *cdgC*^{ALLEF} instead of Δ*cdgC* was based on methodological considerations. Both mutants, Δ*cdgC* and Δ*vnz08595* were created by recombination with an Apra resistance cassette, making it impossible to combine these single mutations via transduction in a double mutant strain. Hence, a different approach was chosen, combining the *cdgC*$^{\mathrm{ALLEF}}$ point mutant (known to be morphologically identical with the *cdgC* mutant) with the *vnz08595* deletion via PCR-targeting (see Section 3.4.5 on page 26).

The resulting phenotype was initially analyzed in macrocolony assays, performed as described in Section 3.4.10 on page 28. During incubation for four days at 30 °C, the developmental progression of each strain was documented every 24 h under a binocular microscope, images were edited with Adobe Photoshop and arranged with Adobe Illustrator. The knockout phenotype of *vnz08595* highly resembled the wild type phenotype, while *cdgC*^{ALLEF}Δ *vnz08595* shifted the phenotype from the classical hypersporulation phenotype of Δ*cdgC* to a slightly larger and dark gray colony morphology with more pronounced radial ridges (see Fig. 4.29) reminiscent of the *cdgC*^{ALLEF}Δ*cdgA* mutant (see Fig. 4.11).

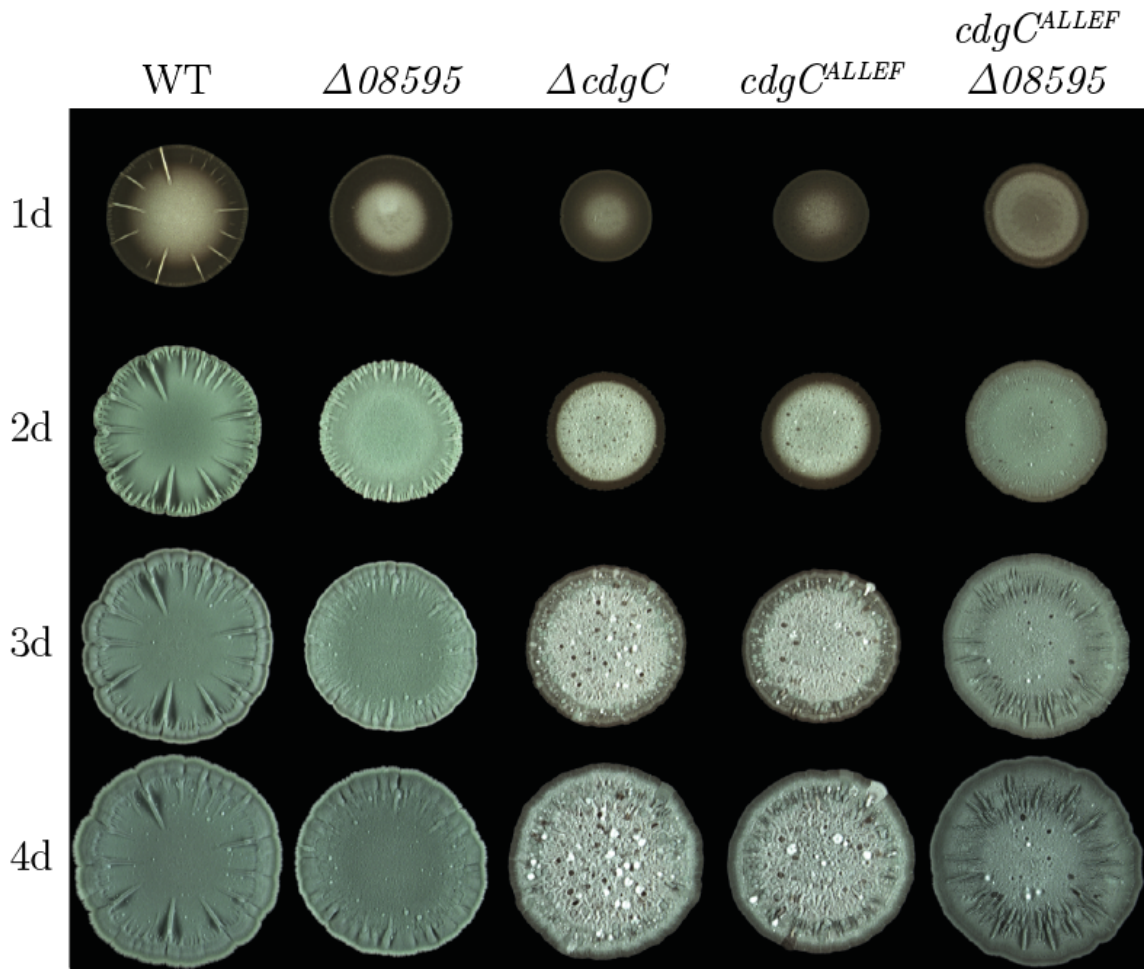

Fig. 4.29 Phenotypic analyses of Δ*vnz08595* in WT and the *cdgC*$^{\mathbf{ALLEF}}$ strain reveal a slight decelerating effect. Macrocolonies of *S. venezuelae* WT, Δ*vnz08595*, Δ*cdgC*, *cdgC*$^{\mathbf{ALLEF}}$ and *cdgC*$^{\mathbf{ALLEF}}$Δ*vnz08595* were created through drip of 12 µL $2 \cdot 10^5$ CFU/µL spores on MYM agar and plates were incubated for 4 d at 30 °C. The documentation took place every 24 h.

Microscopic examinations of the generated strains grown in liquid culture were performed to analyze the influence of the deletion of *vnz08595* on the developmental morphology and sporulation. Samples taken after 12-20 h incubation at 30 °C and 170 rpm were documented every 2 h under a 100× objective with phase contrast. The results of the microscopy showed that the deletion of *vnz08595* resulted in a slight delay in the cell cycle progression in both background strains (see Fig. 4.30). This is in contrast to studies known from *S. coelicolor*, indicating premature germination of the *sco2097* deletion strain (Kleinschnitz et al., 2011).

In order to further characterize the impact of Vnz08595 on the cell division machinery, the expression of the cell division protein FtsZ was detected using an FtsZ-Ypet fusion protein in Δ*vnz08595*. To address this hypothesis, a confocal microscopic approach was chosen inspired by Schlimpert et al. (2017), detecting the presence of an FtsZ-Ypet fusion protein. Herein, its expression and accumulation to Z-rings appear particularly obvious as ladder-like structures indicating the future septation site. For a semi-quantitative evaluation, confocal microscopy was combined with immunodetection. Therefore, an *ftsZ-ypet* translational fusion, under the control of its native promoter on the pSS5 plasmid (Schlimpert et al., 2017), was introduced

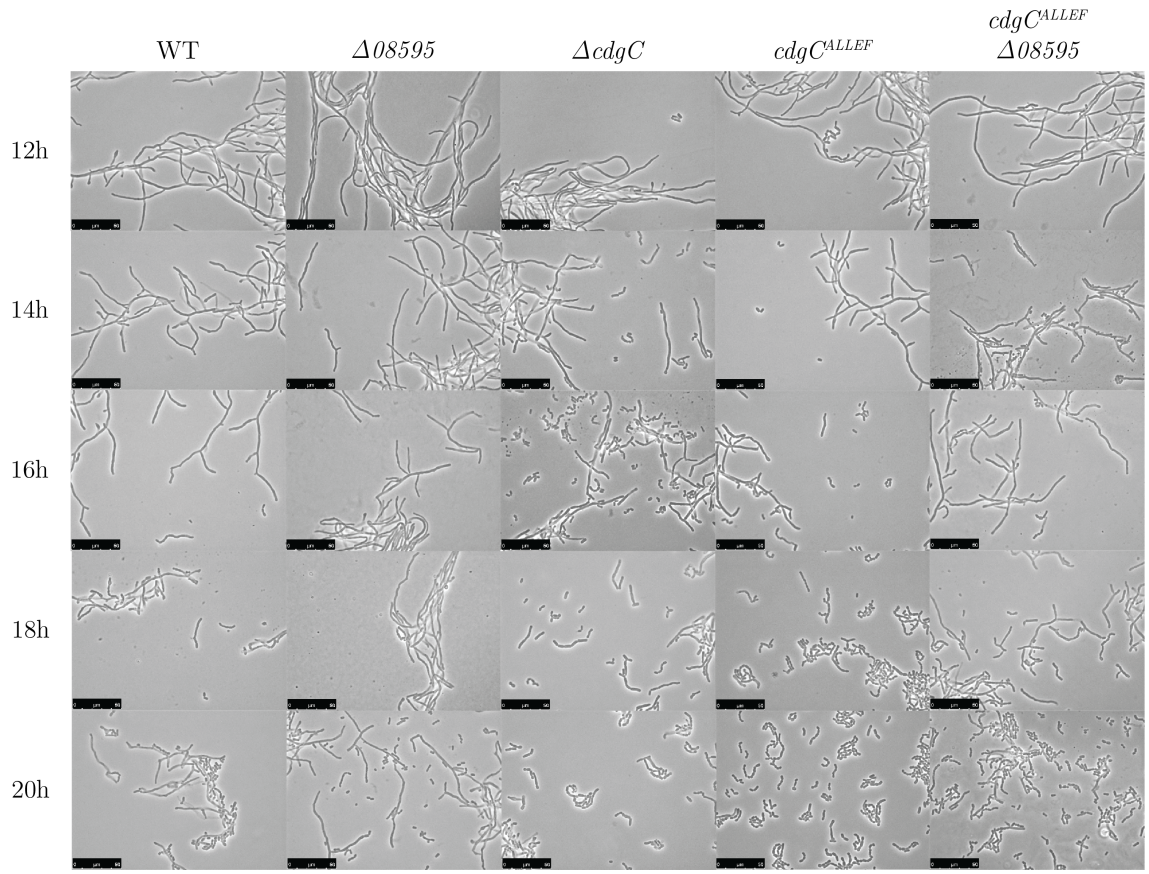

Fig. 4.30 Microscopic analyses of Δ*vnz08595* in WT and the *cdgC*$^{\mathbf{ALLEF}}$ strain confirm a slight decelerating effect. *S. venezuelae* WT, Δ*vnz08595*, Δ*cdgC*, *cdgC*$^{\mathbf{ALLEF}}$ and *cdgC*$^{\mathbf{ALLEF}}$Δ*vnz08595* were inoculated in MYM liquid culture to a spore concentration of 10^6 CFU/mL respectively. Incubation took place at 30 °C and 170 rpm and samples were harvested every 2 h from 12 to 20 h. Microscopic images were documented under a 100× phase contrast objective.

into *S. venezuelae* wild type, Δ*cdgC* and Δ*vnz08595* at the ΦBT1 site. Effects of the additional FtsZ allele on the morphology of the strain was excluded phenotypically via macrocolony assays (see Fig. 6.12 on page 110 in the appendix). The strains were grown in liquid MYM medium at 30 °C and 170 rpm and samples taken every 2 h from 12 to 18 h were examined via confocal microscopy, as described in Section 3.4.12 on page 28. *S. venezuelae* wild type conjugated with pSS5 served as a positive control for the physiological expression of FtsZ. The results of this experiment are shown in Fig. 4.31. To exclude autofluorescence as a cause for the observed signals, wild type samples without pSS5, treated likewise, were used as negative controls (see Fig. 6.13 on page 111 in the appendix).

After growing for 12 h, WT and Δ*vnz08595* were in the vegetative phase, resulting in the detection of faint FtsZ-YPet signal while in the *cdgC* mutant background, enhanced expression of the FtsZ-YPet fusion with pronounced Z-ring ladders were observed (see Fig. 4.31). The latter had already been shown in Fig. 4.15. Therefore, it was unsurprising that plenty of Z-ring ladders were observed, indicating ongoing sporulation septation as the phase contrast pictures already showed fragmentation of the hyphae. These pronounced Z-ring ladders appeared after 14 h in the wild type background and after 16 h in the *vnz08595* mutant, confirming the deceleration in cell cycle progression caused by the absence of Vnz08595 which was already observed in Fig. 4.29 and 4.30.

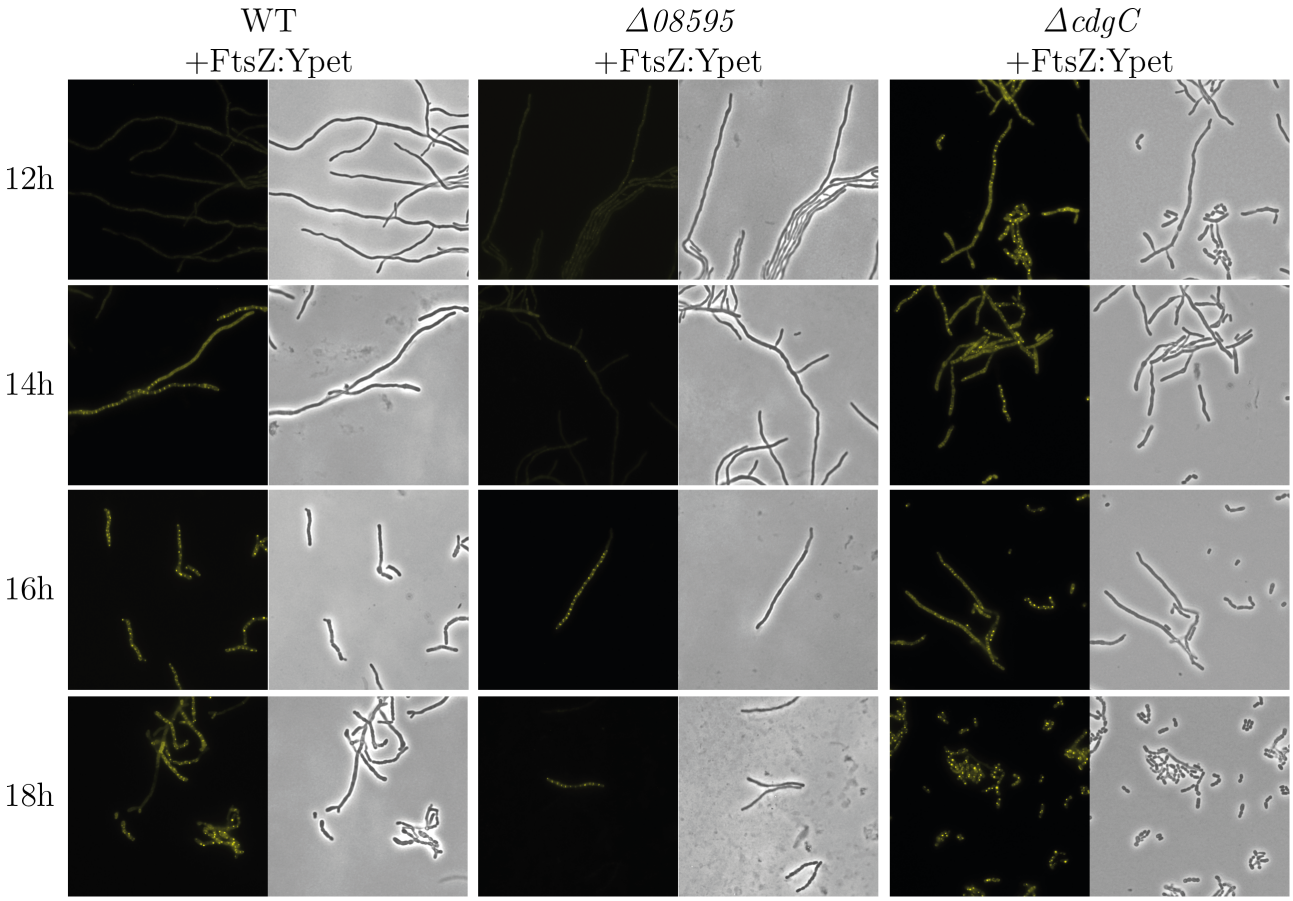

Fig. 4.31 The formation of FtsZ-dependent Z-rings seems to be delayed in the absence of Vnz08595 and increased in the absence of CdgC. Confocal microscopic analysis of the expression pattern of an FtsZ:Ypet fusion protein under the control of its native promoter integrated into *S. venezuelae* WT, Δ*vnz08595* and Δ*cdgC*, respectively. Microscopic analyses were performed with *S. venezuelae* WT+pSS5, Δ*vnz08595*+pSS5 and Δ*cdgC*+pSS5, which were inoculated in MYM liquid culture to a spore concentration of 10^6 CFU/mL, respectively. Incubation took place at 30 °C and 170 rpm and samples were harvested from 12 to 18 h every 2 h. Microscopic images were documented under a 100× phase contrast objective with or without a Ypet filter.

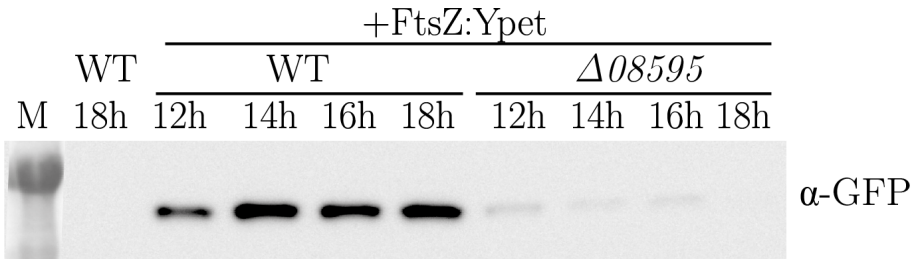

Fig. 4.32 Vnz08595 influences the formation of FtsZ-dependent Z-rings. Immunodetection of the expression pattern of an FtsZ:Ypet fusion protein under the control of its native promoter (pSS5) integrated into *S. venezuelae* WT and Δ*vnz08595*, respectively. The strains were inoculated in MYM liquid culture to a spore concentration of 10^6 CFU/mL, respectively. Incubation took place at 30 °C and 170 rpm and samples were harvested from every 2 h 12 to 18 h. *S. venezuelae* WT incubated for 18 h served as a negative control. A total protein amount of 15 µg per sample was separated via SDS-PAGE. M - color prestained marker; αGFP - anti-GFP antibody

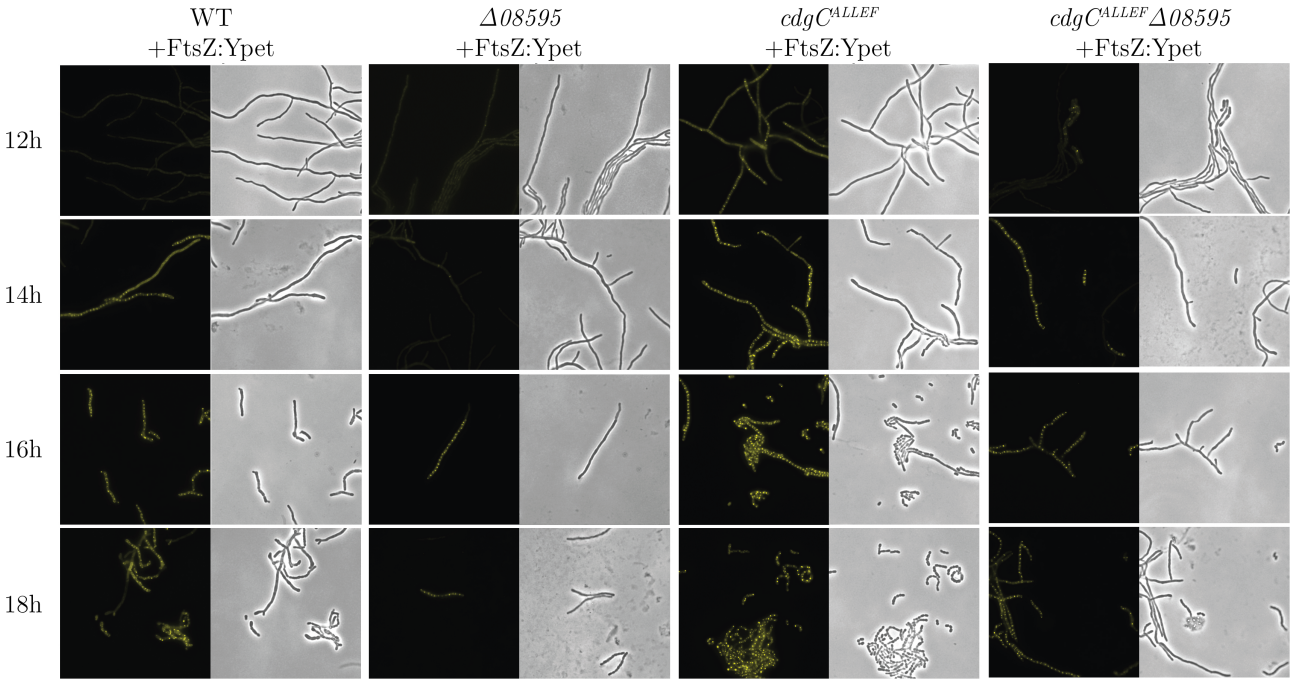

Fig. 4.33 The delay in the formation of Z-rings in the absence of Vnz08595 seem to be counterbalanced in *cdgC*^{ALLEF}. Confocal microscopic analysis of the expression pattern of an FtsZ:Ypet fusion protein under the control of its native promoter integrated into *S. venezuelae* WT, the *vnz08595* deletion strain and a strain containing an enzymatically inactive version of *cdgC* as well as the combination of the latter two alleles in one strain background. Microscopic analyses were performed with *S. venezuelae* WT+pSS5, Δ*vnz08595*+pSS5, *cdgC*^{ALLEF}+pSS5 and *cdgC*^{ALLEF}Δ*vnz08595* which were inoculated in MYM liquid culture to a spore concentration of 10^6 CFU/mL, respectively. Incubation took place at 30 °C and 170 rpm and samples were harvested from every 2 h 12 to 18 h. Microscopic images were documented under a 100× phase contrast objective with or without a Ypet filter.

For semi-quantitative analysis of the FtsZ-Ypet expression in the *vnz08595* mutant compared to wild type, samples taken in parallel to those for confocal microscopy described above were prepared for immunodetection, as described by Schlimpert et al. (2017). The total protein concentration was determined via Bradford assay (Roth) and 15 µg total protein were loaded per sample. The only deviation from this procedure is the addition of TCE to the SDS gel solution for protein visualization, as described by Ladner et al. (2004). The resulting fluorescent visible staining of proteins was used for loading controls that are shown in Fig. 6.14 on page 111 in the appendix. An anti-GFP antibody, also sensitive for the YPet protein, served as the primary antibody. The results of the Western blot (see Fig. 4.32) verified the expected decrease of FtsZ:YPet expression in Δ*vnz08595* relative to the wild type.

As the results so far indicate, CdgC shows direct protein-protein interactions with Vnz08595. They seem to influence the cell cycle progression in adverse ways, raising the question whether their effects compensate one another. To address this hypothesis, an *ftsZ-ypet* translational fusion, under the control of its native promoter on the pSS5 plasmid (Schlimpert et al., 2017), was introduced into *S. venezuelae* wild type, *cdgC*^{ALLEF}, Δ*vnz08595* and the *cdgC*^{ALLEF}Δ*vnz08595* double knockout strain at the ΦBT1 site. This ensured that the control strain with pSS5, introduced in the *cdgC*^{ALLEF} point mutant, shows the same enhanced FtsZ expression and accumu-

lation to Z-rings as Δ*cdgC*+pSS5 depicted in Fig. 4.15. For a quantitative evaluation, confocal microscopy was combined with immunodetection. Effects of the additional FtsZ allele on the morphology of the strain were excluded phenotypically via macrocolony assays (see Fig. 6.12 on page 110 in the appendix). The strains were grown in liquid MYM medium at 30 °C and 170 rpm and samples were taken every 2 h from 12 to 18 h and examined via confocal microscopy, as described in Section 3.4.12 on page 28. *S. venezuelae* WT+FtsZ:Ypet served as a positive control for the physiological expression of FtsZ. The results of this experiment are shown in Fig. 4.33.

After 12 h of growth, the wild type, Δ*vnz08595* and the *cdgC*$^{\texttt{ALLEF}}$Δ*vnz08595* double knockout strain were in the vegetative phase, resulting in the detection of faint FtsZ-YPet signal, while enhanced expression of the FtsZ-YPet fusion with pronounced Z-ring ladders were observed in the *cdgC*$^{\texttt{ALLEF}}$ point mutant background (see Fig. 4.33). The latter resembles the phenotype in Δ*cdgC*+pSS5 (see Fig. 4.15 and 4.31) and matches the expectations. Plenty of Z-ring ladders were observed, indicating ongoing sporulation septation in line with the phase contrast pictures already showing fragmentation of the hyphae. These pronounced Z-ring ladders appeared after 14 h in the wild type and double knockout strain background and after 16 h in the *vnz08595* mutant, supporting the hypothesis that the effects of CdgC and Vnz08595 on cell cycle progression in *S. venezuelae* compensate one another.

Altogether, Vnz08595 seems to influence the developmental morphology and the expression of FtsZ-dependent Z-rings at the onset of sporulation in *S. venezuelae* in ways adverse to CdgC. The *vnz08595* mutant shows delayed cell cycle progression and reduced FtsZ expression compared to the wild type that can be compensated by additional inactivation of CdgC.

Chapter 5

Discussion and Outlook

5.1 CdgC - a major diguanylate cyclase in *S. venezuelae*?

In *Streptomyces*, c-di-GMP impacts the coordinated progression through the life cycle at two stages: the initiation of reproductive growth and spore formation. The first described c-di-GMP effector protein and developmental master regulator BldD binds tetrameric c-di-GMP at its CTD enabling dimerization and stabilising the dimeric DNA binding form of BldD (Tschowri et al., 2014; Schumacher et al., 2017). Thereby, altered c-di-GMP availability results in the initiation of the sporulation cascade, while still enabling RsiG to sequester σ^{WhiG}. In the late reproductive phase, a further decline of the cellular c-di-GMP levels causes RsiG to release σ^{WhiG}, which then forms a holoenzyme with the RNAP, transcribing late sporulation genes (Gallagher et al., 2020).

C-di-GMP turnover. In order to meet these physiological requirements, the cellular c-di-GMP concentration is fine-tuned throughout the life cycle by a dynamic equilibrium between making and braking. This dynamic is calibrated by ten c-di-GMP turnover proteins, encoded in the *S. venezuelae* genome. Each of these proteins has at least one conserved c-di-GMP turnover domain, altering the cellular or local c-di-GMP levels sensed by BldD, the RsiG-σ^{WhiG} complex or further, yet to be discovered c-di-GMP effector proteins. HdgB is the only exception as its `HD-GYP` domain contains a degenerate A-site. Previous research indicated that just four of those ten proteins showed a significant morphological impact: CdgB, CdgC, RmdA and RmdB (see Fig. 1.9 on page 19) (Al-Bassam et al., 2018; Haist et al., 2020).

CdgC domain structure. As a membrane-associated DGC with accessory PAS-PAC and $\mathtt{EAL}_{\mathrm{deg}}$ domain, CdgC is the c-di-GMP turnover protein with one of most complex domain architectures in *S. venezuelae* (Al-Bassam et al., 2018). In *Streptomyces*, PAS-`GGDEF-EAL` domain architecture, most commonly present in other bacterial species, is modified to a PAS-PAC-`GGDEF-EAL` structure found in four of the ten c-di-GMP turnover proteins in *S. venezuelae* (Römling et al., 2013). This thesis sheds first light on the unique and complex role of CdgC in the calibration of c-di-GMP levels and the coordinated progression of the life cycle. The presented knowledge about the function of the enzymatic activity of `GGDEF` and $\mathtt{EAL}_{\mathrm{deg}}$ is discussed below.

5.1.1 The role of the GGDEF- and sensory domains on the dimerization and DGC activity

The domain architecture of CdgC reveals a conserved GGDEF- and a largely degenerate EAL domain. Its knockout mutant shows a specific hypersporulation phenotype associated with c-di-GMP deficiency, as depicted in Fig. 1.10 on page 20 (Al-Bassam et al., 2018). Using *in vitro* DGC and PDE assays performed with purified variants of CdgC that all lack the transmembrane domain, while combining different domains, this thesis illustrates in this thesis, that CdgC has DGC- but no significant PDE activity (see Fig. 4.3 and 4.4 on page 41). Therefore, CdgC is the first biochemically verified c-di-GMP synthesizing protein in *S. venezuelae*.

Of particular note are the tremendous differences in the phenotypic manifestation of developmental alterations in Δ*cdgC* compared to the other developmental DGC mutant Δ*cdgB* (see Fig. 1.9 on page 19). In both cases, the deletion of the encoding gene results in an accelerated cell cycle progression and a precocious sporulation compared to the wild type. While the *cdgB* mutant goes through all distinct stages of *S. venezuelae* development, the *cdgC* mutant takes a shortcut, leading to a precocious onset of sporulation by synchronous sporulation septation events in the vegetative hyphae on the colony surface without aerial hyphae formation (see Fig. 1.10 on page 20).

The key motif GGDEF. The morphological analysis of a *cdgC* allele with an inactivated A-site from GGDEF to ALLEF by point mutations (*cdgC*$^{\text{ALLEF}}$) verified that the intact GGDEF motif is essential for the morphological impact of CdgC (see Fig. 4.5 on page 42). The deletion and point mutation strain were complemented, respectively, via the expression of a *cdgC* allele from the ΦBT1 site, confirming that the effects of the mutants are caused by the inactivation of CdgC. Additionally to the A-site, the GGDEF domain of CdgC also contains a conserved I-site. UV-crosslinks indicated a c-di-GMP binding at the I-site of the GGDEF domain. Hence, an allosteric product inhibition seems likely. *In vitro* enzymatic assays and phenotypic analyses performed with a purified CdgC peptide containing an inactivating point mutation in the I-site would be an interesting approach to investigate a potential allosteric product inhibition.

The CdgC-specific knockout phenotype. Artificially increasing c-di-GMP levels by overexpressing the heterologous cytosolic DGC CdgB from *S. coelicolor* in Δ*cdgC* was shown to be insufficient to restore the wild type phenotype (see Fig. 4.5 on page 42). While, the corresponding strain overcame its deficiency in aerial hyphae formation, though it did not show the green colony pigmentation that is characteristic for the presence of mature spores, even after prolonged incubation. Instead, it was arrested in the early reproductive phase (see Fig. 1.1 B on page 2), indicating aerial hyphae formation prior to spore maturation. This suggests an additional protein-specific function of CdgC beyond its DGC activity. In contrast to CdgC, CdgB is a cytosolic protein containing not only the PAS-PAC-GGDEF domain architecture but, additionally, a GAF domain at the N-terminus. These structural differences, resulting in the perception of other environmental stimuli, could cause functional divergence.

The role of oligomerization. Dimerization of the GGDEF domains is essential for diguanylate cyclases to synthesize c-di-GMP. This dimerization is often mediated by accessory domains in response to various environmental stimuli (Chan et al., 2004; Schirmer & Jenal, 2009). Especially the PAS domain is well-characterized, in combination with the GGDEF domain, to function as a general signaling sensor, mediating dimerization and other protein-protein interactions (Schirmer, 2016). For example, dimerization and enzymatic activity of the GGDEF-EAL domain containing DGC DgcE were shown to be mediated by its multiple PAS domains in *E. coli* (Pfiffer et al., 2019). Another example was revealed by structural analyses of the bifunctional GGDEF-EAL protein RbdA in *Pseudomonas aeruginosa* identifying the PAS domain to majorly promote oligomerization (Liu et al., 2018). In accordance with these examples, *in vitro* DGC assays, performed during this thesis, indicated that GGDEF alone is unable to synthesize c-di-GMP without the presence of the PAS-PAC domain (see Fig. 4.3 on page 41). The *in vitro* DGC activity was even more pronounced in the additional presence of the EAL_{deg} domain, hinting towards a supporting role of these domains for the DGC activity in CdgC (see Fig. 4.3 on page 41).

Using *in vivo* protein interaction studies after Karimova et al. (1998), stable homooligomerization of full-size CdgC was shown during this study (see Fig. 4.21 on page 62). The absence of the transmembrane anchor resulted in significantly weaker, but not completely halted, interaction processes, while CdgC lacking the EAL_{deg} self-interacted like the full-size protein. It is known from other bacteria like *E. coli* that the GGDEF domain alone provides rarely any dimerization capacity on its own (Jenal et al., 2017; Sarenko et al., 2017). Further interaction assays performed with the GGDEF with and without the PAS-PAC domain would be a promising approach for future studies to characterize the impact of the single domains on dimerization of CdgC.

The degenerate EAL domain. Even the isolated EAL_{deg} domain showed weak self interaction during this thesis, suggesting that this domain supports oligomerization of CdgC (see Fig. 4.21 on page 62). Since these *in vivo* interaction assays were performed in the Gram-negative *E. coli* with significantly lower cellular c-di-GMP concentrations than in *S. venezuelae*, they might have their limitations regarding any c-di-GMP-dependent interaction regulation. Therefore, a hypothetical inhibition of CdgC by c-di-GMP binding to its EAL_{deg} domain would be hard to identify during this assay. However, the results indicate only a minor role of the EAL_{deg} in the stabilization of the oligomer.

The transmembrane anchor. Regarding the weaker interaction of CdgC without its transmembrane domains, it is worth noting that previous experiments, performed by V. Riebe during her master studies, indicated an essential role of the transmembrane anchor in the physiological function of CdgC. Her phenotypic analysis showed that $\Delta cdgC$ complemented with FLAG-tagged, cytosolic CdgC (CdgC-ΔTM) failed to restore the wild type phenotype and resembled the *cdgC* knockout and $cdgC^{\text{ALLEF}}$ phenotype. Accordingly, no oligomerization of cytosolic CdgC was observed in BTH assays. However, these experiments were performed with other plasmid combinations on a different medium composition and with significantly shorter incubation times. The latter results contrast the data presented here, but underline the weaker interaction of cytosolic CdgC compared to the full-size CdgC.

Summary. Taken together, CdgC impacts the morphological differentiation in *S. venezuelae* essentially via its DGC activity provided by the GGDEF domain. Additionally, this DGC activity is profoundly supported by the PAS-PAC domain. The oligomerization of CdgC was shown to be supported by its membrane-standing location provided by the transmembrane domain. In future work, it would be interesting to identify the domains that are essential for the formation of stable oligomers using pulldown assays and clarify the functional structure and oligomeric state of CdgC. However, this raises the question for environmental stimuli sensed by the transmembrane anchor or the PAS-PAC domain. A recent study characterized the DGC SSFG_02181 (ortholog of CdgC) in *S. ghanaensis* and provided evidence of heme-binding via the PAS domain of the protein (Nuzzo et al., 2020). Therefore, it would be interesting to test for heme-binding to the PAS domain of CdgC. In the following, the expression and degradation pattern of CdgC are addressed to assess at which stage in the life cycle it might fulfill its physiological function.

5.1.2 CdgC seems to be subject to proteolytic procession by one or several CdgC-specific proteases

Using a FLAG-tagged *cdgC* allele (CdgC-FLAG) expressed under the control of its native promoter, complementing the *cdgC* mutant, the localization of CdgC in the membrane fraction verified the classification of CdgC as a membrane-associated DGC (see Fig. 4.6 on page 44). In addition, microarray data generated by Bibb et al. (2012), predicted an accumulation of *cdgC* along the growth curve in liquid medium, which was confirmed for the protein (see Fig. 4.7 on page 45). The analysis of distinct stages of the life cycle in liquid culture has its limitations regarding the heterogeneous initiation of sporulation within a *S. venezuelae* culture.

The degradation pattern of CdgC. Progression in the *S. venezuelae* life cycle requires eventual inactivation of the developmental repressor BldD as well as release of σ^{WhiG} from RsiG. To this end, c-di-GMP, as a brake of the developmental progression, would have to be "loosened" from its effector proteins. Therefore, an inactivation of CdgC, as an important DGC with a major morphological impact, would be expected. However, no such inactivation was observed on the transcriptional or protein level. On the contrary, CdgC accumulated along the life cycle. (Bibb et al., 2012; Al-Bassam et al., 2018) On the other hand, an intensified degradation pattern of CdgC over time was observed in this thesis. This mechanism of activity regulation in a composite membrane-anchored GGDEF-EAL protein was recently described for the DGC DgcE in *E. coli*, where the contained membrane-associated sensory 1 (MASE1) domain was shown to play a crucial role in proteolysis (Pfiffer et al., 2019). Unfortunately, this work could not identify a CdgC-specific protease by the expression of the CdgC-FLAG allele in distinct protease deletion mutants (see Fig. 4.8 on page 46). It can therefore be assumed that either the CdgC-specific degrading protease was not among the tested or an interplay of several proteases is responsible for the inactivation of CdgC. Whether the proteolytic procession of CdgC actually results in its inactivation and, thus, the reduced c-di-GMP level observed during the transition to the reproductive growth phase and which proteolytic mechanism is involved, remains an exciting project for future research.

Summary. In contrast to the timing of activity indicated by its knockout phenotype, CdgC accumulates throughout the life cycle. However, a tremendous degradation of CdgC throughout the life cycle was observed for C-terminal degradation fragments only, due to the location of the FLAG tag at the protein (see Fig. 4.7 on page 45). Further studies, analyzing the degradation pattern with a C-terminal FLAG tag and another N-terminal tag (for example a Strep tag) could reveal more details about the cleavage sites. Interestingly, it has been observed that the proteolysis of CdgC is independent from the presence of its N-terminal transmembrane anchor (V. Riebe, unpublished). Hence, it seems to be inefficient under the tested conditions, since, for the FLAG-tagged CdgC in the Western blot, the full-size protein was detectable at every time point and accumulated throughout the life cycle (see Fig. 4.7 on page 45). These insights demand a focus on the cellular response caused by the specific *cdgC* knockout mutant in *S. venezuelae*, allowing conclusions about the impact of CdgC on the developmental progression.

5.2 CdgC coordinates the cell cycle progression through c-di-GMP synthesis

After CdgC was proven to exhibit a DGC activity, the question of the physiological function of this DGC in the control of the differentiation from vegetative mycelium to mature spores arose. The deletion of *cdgC* results in a unique hypersporulation phenotype in which the wild type cannot be restored by overexpressing the heterologous DGC CdgB from *S. coelicolor*. These results allow conclusions regarding a protein-specific function of CdgC, despite the major effect of the DGC activity. The morphology of the *cdgC* deletion strain resembles a strain in which cellular c-di-GMP levels are artificially reduced by overexpressing the PDE PdeH from *E. coli* in *S. venezuelae* as well as the low c-di-GMP phenotypic manifestation of both to-date identified c-di-GMP effector binding proteins, BldD and the RsiG-σ^{WhiG} σ-anti-σ complex. This suggests the consideration that CdgC might be involved in a "local" c-di-GMP signaling with either of them.

Local c-di-GMP signaling. The concept of local c-di-GMP signaling describes the spatial proximity of c-di-GMP turnover, sensor and effector proteins, for example by direct protein-protein interactions to larger complexes where local c-di-GMP levels alter in response to environmental signal, without affecting the cellular c-di-GMP concentrations, first described by Lindenberg et al. (2013). Local signaling modules are known from *E. coli* where the interacting DGC-PDE pair, DgcC and PdeK co-localizes with the cellulose synthase complex by directly interacting with the subunit BcsB, establishing a delicately calibrated local c-di-GMP pool in direct proximity of the biosynthesis complex of the biofilm exopolysaccharide pEtN-cellulose (Richter et al., 2020). Extensive interaction analyses were unable to confirm an interaction between CdgC and BldD or the σ^{WhiG}-RsiG complex (see Section 4.7.2 on page 62 and 4.7.3 on page 65). Interestingly, no interactions were observed between CdgC and other c-di-GMP turnover proteins (N. Tschowri, unpublished). Since many described local c-di-GMP signaling modules were shown to contain an interacting, antagonistic DGC-PDE pair, this further contraindicates a role of CdgC in feeding a local c-di-GMP pool (Lindenberg et al., 2013; Sarenko

et al., 2017; Richter et al., 2020). Accordingly, the data presented here do not support the hypothesis that CdgC influences the development of *S. venezuelae* via local signaling with the two investigated c-di-GMP effector proteins. Nonetheless, the unique hypersporulation phenotype of its knockout mutant among the other c-di-GMP turnover proteins in *S. venezuelae* as well as its reminiscence to the low c-di-GMP level states of both so-far identified c-di-GMP effector proteins strongly suggest a major impact of CdgC on the developmental progression. Together, this hints at CdgC as a major global DGC, whose activity is regulated in a dose-dependent manner, rather than altering local c-di-GMP pools sensed by effector compounds.

An interplay between CdgC and BldO? Another interplay that is not investigated in this thesis is between CdgC and BldO. To date, the only identified direct target gene of the transcriptional regulator BldO is *whiB*, encoding WhiB, which is known as the founding member of a family of WhiB-like proteins (Wbl family) carrying an iron-sulphur cluster and fulfilling various regulatory functions in *Streptomyces* (Davis & Chater, 1992; Kormanec & Homerova, 1993; Bush et al., 2017). WhiB forms a heterodimeric transcription regulator with the constitutively present WhiA to activate the expression of circa 240 developmental and sporulation genes like *ftsZ* or *whiG*. In contrast to WhiA, WhiB expression is tightly regulated through inhibition by BldD and BldO, as well as activation by the BldM homodimer, indicating that the accumulation of WhiB constitutes the limiting factor for WhiAB transcriptional activity. As another sovereign transcriptional repressor besides BldD, BldO, whose expression peaks at the onset of sporulation, is regulated by a to-date unknown mechanism and its deletion also results in a hypersporulation phenotype similar to the *cdgC* deletion mutant (Flärdh & McCormick, 2017; Bush et al., 2017). This multi-layered control of developmental genes by BldD and BldO, as well as their similar morphological impact on WhiB, makes the analysis of the potential interplay between BldO and CdgC a promising approach for future research projects on the physiological function of CdgC.

Cellular c-di-GMP levels in Δ*cdgC*. The direct proportionality between CdgC expression and DGC activity on the global cellular level led to the expectation that c-di-GMP levels are reduced in the *cdgC* deletion mutant compared to the wild type. Nucleotide extraction data, performed by J. Haist (Haist et al., 2020), did not validate this hypothesis for the analyzed time points. Unexpectedly, the deletion of *cdgC* seems to result in a significant increase in the cellular c-di-GMP concentration compared to the wild type (see Fig. 4.10 on page 48). This suggests a higher activity of one or more DGCs or a decreased activity of one or more PDEs in absence of CdgC. Previous studies identified the DGCs encoding *cdgA*, *cdgB*, *cdgC* and *cdgE* as direct BldD target genes by *in vivo* ChIP-seq analysis, which was recently confirmed using EMSAs (Tschowri et al., 2014; Schumacher et al., 2017; Haist et al., 2020). The negative feedback hypothesis postulated by Tschowri et al. (2014) suggests that, by sensing c-di-GMP levels, BldD represses the expression of its target DGC-encoding genes, which in turn reduce cellular c-di-GMP levels. Applied to the *cdgC* mutant, it would be possible that the absence of CdgC in the early phase of vegetative growth leads to reduced c-di-GMP levels compared to the wild type after germination. The inactivation of BldD, mediated by a c-di-GMP deficiency,

could lead to an increased expression of the other BldD-dependent DGCs. As a result, higher c-di-GMP levels would come about at later times, as witnessed by the nucleotide extraction analyses. Recent studies in *S. ghanaesis* provided further evidence that BldD is able to sense c-di-GMP levels, controlling the expression of CdgC (Nuzzo et al., 2020).

DGC double mutants were generated to measure their c-di-GMP levels, in hope of identifying the DGC responsible for the increased c-di-GMP level in the absence of CdgC. Herein, a combination of *cdgC*$^{\texttt{ALLEF}}$ and the respective deletion mutant of each of the other DGCs approximates the effect implied by the absence of both genes. Unfortunately, a first attempt to extract and measure c-di-GMP from these strains was not successful, leaving this experiment for future work.

In this context, it is worth considering the aforementioned negative feedback hypothesis, postulating that reduced c-di-GMP levels cause increasing expressions of all BldD-dependent DGCs (CdgA, CdgB, CdgE). However, the expression analyses via immunodetection against these FLAG-tagged DGCs in the *cdgC*$^{\texttt{ALLEF}}$ point mutant compared to the corresponding complementation strain, published by Al-Bassam et al. (2018), remained inconclusive: While the expression of CdgA seemed rather reduced when CdgC is inactive, the expression of CdgB and CdgE was slightly enhanced (see Fig. 4.13 on page 52). However, the almost complete absence of CdgE in the complementation mutant observed in the latter result stands in contrast to published expression patterns of CdgE. Therefore, this experiment needs to be repeated. (Al-Bassam et al., 2018)

Furthermore, RNA-seq analysis, carried out by J. Haist and confirmed in qRT-PCR analyses in the course of this work, did not demonstrate any increase in expression of BldD-dependently expressed DGCs (Haist et al., 2020). RNA-seq data hinted only towards the downregulation of *cdgB* in Δ*cdgC*, confirmed by qRT-PCR. Furthermore, these qRT-PCR analyses detected also a downregulation of *rmdA* and *rmdB* and showed an increased expression of *cdgF*.

CdgF was not identified as a direct BldD target, it contains a 10TM-PAS-PAC-`GGDEF-EAL` domain structure and is one of the least conserved c-di-GMP turnover proteins in streptomycetes (Al-Bassam et al., 2018). In contrast to CdgC, both the `GGDEF` and the `EAL` domains contain all of the conserved amino acids for enzymatic activity. It could thus be a bifunctional protein which, depending on environmental stimuli, has DGC or PDE activity. There are only few examples of truly bifunctional c-di-GMP turnover proteins identified so far. One of them is the bacteriophytochrome BphG1 from *Rhodobacter sphaeroides*. BphG1 posseses a light-dependent switch between DGC and PDE activity, mediated by the PAS-PAC-PHY photosensory module (Tarutina et al., 2006). In *Legionella pneumophila*, the c-di-GMP metabolism is controlled by a RpoS-dependent two-component system whose response regulator is the bifunctional enzyme Lpg0277, mediating the nutrient responsive switch between replicative and stationary phase (Hughes et al., 2019). However, there are currently no enzyme activity assays to identify a possible DGC or PDE activity of CdgF: a deletion of *cdgF* had no influence on the phenotype and only showed weak expression levels under the investigated conditions (Al-Bassam et al., 2018). Thus, a closer examination of this previously neglected DGC, in order to determine its enzyme activity, would be interesting. More details about the active PDE RmdB and the bifunctional RmdA in *Streptomyces* can be found in Hull et al. (2012); Al-Bassam et al. (2018); Haist et al. (2020).

These results suggests that the transcriptional regulation of c-di-GMP turnover enzymes in *S. venezuelae* might be too complex for straight forward cause-effect-hypotheses on the cellular c-di-GMP level. Besides BldD-dependent regulation, the expression of c-di-GMP turnover proteins is controlled by multiple global regulators like the response regulator MtrA, which controls the expression of all direct BldD-(c-di-GMP) targets (*cdgA*, *cdgB*, *cdgC*, and *cdgE*) and shows promoter binding at *cdgF* and *rmdB* (Som et al., 2017a). The DGC CdgB is the only c-di-GMP turnover protein in *S. venezuelae*, that is additionally repressed by the WhiAB transcriptional regulator during later stages of differentiation. Moreover, the BldD target gen *cdgE* was shown to be also a BldC-target gene. (Bush et al., 2013, 2016, 2019) Together, these additional regulatory mechanisms might explain the lack of correlation between altered c-di-GMP levels in the *cdgC* mutant sensed by BldD and the expression of other BldD-dependent DGCs and provide the multilayered transcriptional control necessary for the fine-tuned making and breaking of c-di-GMP in response to various signals.

Summary. Taken together, the cellular c-di-GMP level does not correlate with the opposing hypersporulation phenotype of the *cdgC* knockout mutant. However, this study could not provide any evidence for a role of CdgC in a local c-di-GMP signaling module. Initial attempts to find the c-di-GMP turnover enzyme that is responsible for the high c-di-GMP levels in the *cdgC* mutants, hint towards a combined effect of the upregulation of CdgF, assuming its `GGDEF` domain provides its main enzymatic activity, and the downregulation of the PDE RmdB and the bifunctional RmdA, whose knockout phenotype indicates a major PDE activity. The observed downregulation of the development-specific DGC CdgB seems inconsistent with the high c-di-GMP levels in Δ*cdgC*. In conclusion, the transcriptional regulation of c-di-GMP turnover enzymes in *S. venezuelae* might be too complex and multilayered for straight forward cause-effect-hypotheses verifiable on the cellular c-di-GMP level. This might explain the lack of correlation between altered c-di-GMP levels in the *cdgC* mutant sensed by BldD and the expression of other BldD-dependent DGCs.

5.3 CdgC influences the mode of sporulation via an altered hydrophobin expression

One of the most striking observations in the characterization of CdgC remains the lack of hydrophobicity of the colonies on solid medium and the lack of aerial hyphae formation, which is, normally, a distinct step in the life cycle of *S. venezuelae*. No other c-di-GMP turnover protein has such a strong influence on the constant iteration of the life cycle stages in *Streptomyces*. CdgC influences the expression of the chaplins and rodlins, which make up the hydrophobic layer. On the one hand, it would be conceivable that the changed chaplin composition inhibits the formation of the hydrophobic layer and, thus, aerial hyphae, leading to hypersporulation. On the other hand, it would also be conceivable that the chaplins have an influence on the expression of further sporulation genes and, through this influence, accelerate the formation of spores or

inhibit the formation of pigment substances. RNA-seq data, generated by J. Haist, showed that the transcription of *bldN* as well as almost all *chp* and *rdl* genes encoded in *S. venezuelae* were downregulated in Δ*cdgC* (Haist et al., 2020). These data were confirmed by qRT-PCR data generated over the course of this thesis for *bldN*, *chpC*, *chpE* and *chpH*. This raised the question whether the deficiency in chaplin expression and the associated impairment of the hydrophobic coat, as well as the inability of the hyphae to break through the air-water barrier, is caused solely by the reduced dose of expressed chaplin proteins. Overexpression of individual chaplin proteins in Δ*cdgC* could not restore the wild type phenotype in any case, but the overexpression of ChpC and ChpE were both able to restore aerial hyphae formation (see Fig. 4.19 on page 59). However, this did not result in complete spore maturity with the associated green color.

In an attempt to restore the WT phenotype by simultaneously overexpressing all *chp* and *rdl* genes, their regulating σ^{BldN} was overexpressed in Δ*cdgC*. However, it was shown in this work that overexpression of σ^{BldN} had no significant effect on aerial hyphae formation and only a very weak effect on the hydrophobicity of the colony surface (see Fig. 4.20 on page 61). As σ^{BldN} is subject to posttranslational regulation by its anti-σ RsbN, simply overexpressing *bldN* may not be sufficient to counteract the sequestration by RsbN. Further experiments are needed to verify that the overexpression of *bldN* indeed causes an upregulation of all *chp* and *rdl* genes.

Summary. Taken together, these results paint an unusual picture in which the absence of CdgC leads to a deregulation of the sporulation cascade and apparently influences it in contradicting ways at different points (see Fig. 5.1). The deletion of a major DGC like CdgC is expected to cause a global or local decrease in c-di-GMP. Given that the only identified c-di-GMP effector components so far are BldD and the RsiG-WhiG σ-anti-σ pair, lower c-di-GMP levels are expected to result in an upregulation of their major target genes. In contrast, RNAseq analysis and the results of this thesis showed that some BldD-target genes like *ssgB* or *ftsZ* are upregulated, while *bldH* and *bldN* are downregulated. The results are more consistent regarding σ^{WhiG} target genes, which are all upregulated or equally expressed in the *cdgC* mutant.

5.3.1 Sigma factor competition may explain the Δ*cdgC* transcriptome

A possible explanation for the unexpected transcriptome of Δ*cdgC* may be provided by a common concept of promoter recognition in eubacteria, stating that one housekeeping σ factor (HrdB in *S. venezuelae*) and several alternative σ factors all compete for the same RNAP, developing different strategies to divide the transcriptional capacities among the σ factors and to avoid deleterious effects of the uncontrolled activity of alternative σ factors (Gruber & Gross, 2003; Sun et al., 2017).

In this scenario, the deletion of *cdgC* might result in reduced c-di-GMP concentration at the beginning of the vegetative growth after germination. The low c-di-GMP levels would lead to a partial or complete inactivation of BldD, which would no longer be able to bind to the promoter region of its target genes, and to a premature activation of σ^{WhiG}. This deregulation of the sporulation cascade could bring about a parallel expression of the differentiation stages that

otherwise occur in series and are delicately coordinated. In this case, the otherwise staggered σ factors σ^{BldN} and σ^{WhiG} could become active at the same time and compete with each other for the existing RNAPs.

Both σ^{BldN} and σ^{WhiG} are members of the σ^{70}- type of σ factors, which are classified in several structural groups coming from σ^{70} and its orthologs, mainly housekeeping σ factors containing all four modular regions described for the σ^{70} family (Gruber & Gross, 2003). While group 3 and 4 (e.g. σ^{WhiG}) both lack domain 1, group 3 σ factors like σ^{BldN} additionally lack domain 3, which is associated with the recognition of extended -10 promoters (Gruber & Gross, 2003; Sun et al., 2017). It is conceivable that this causes RNAPs to bind preferably to σ^{WhiG} than to σ^{BldN}. It is not known whether σ^{WhiG} has a higher binding affinity for RNAP than BldN, but the observations from the various expression analyses in $\Delta cdgC$ would allow this conclusion (see Fig. 5.1 for an overview of the differentially expressed compounds of the sporulation cascade in $\Delta cdgC$).

RNA-seq and qRT-PCR confirmed that *bldN* is downregulated in $\Delta cdgC$, whereas *whiG*'s expression is not significantly altered, but its target gene *whiI* is upregulated. Once σ^{WhiG} is

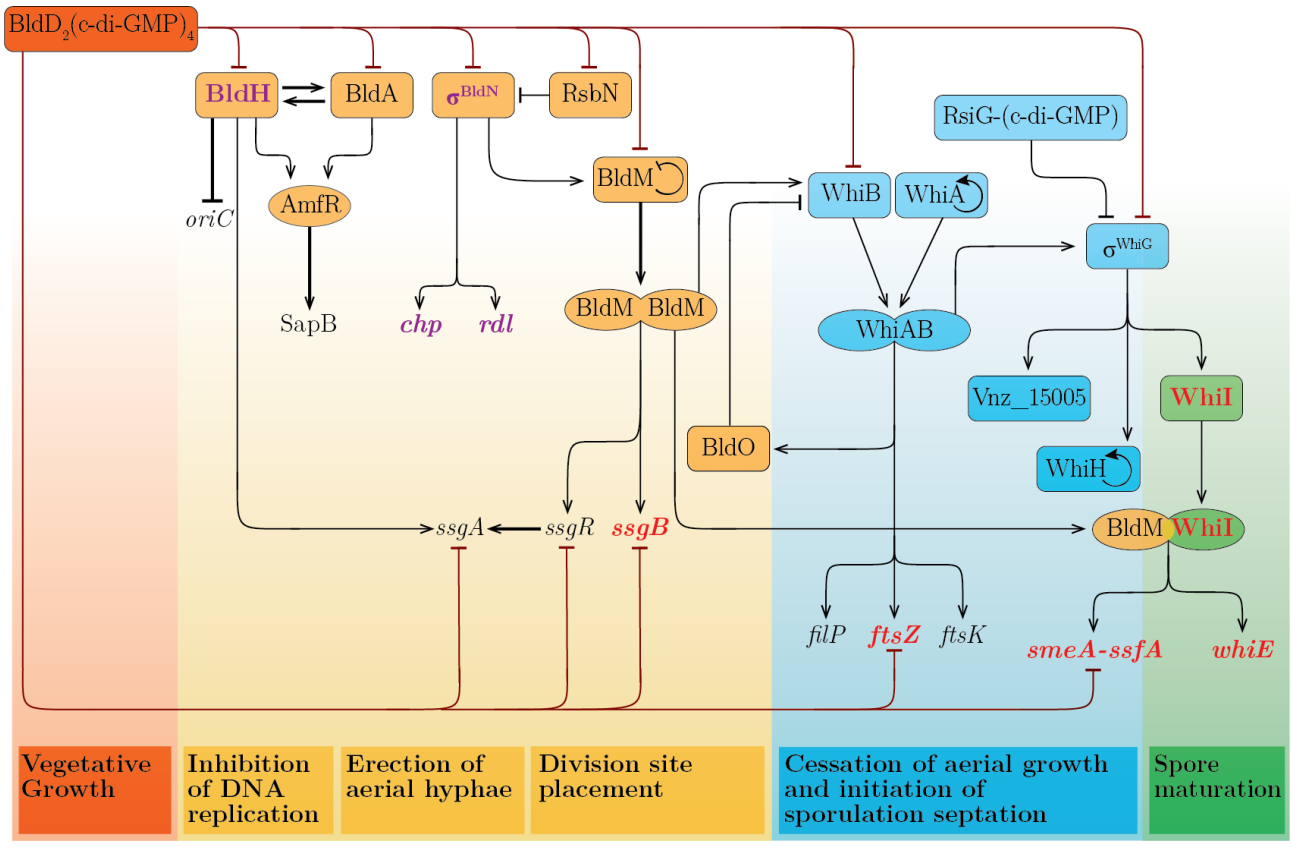

Fig. 5.1 The deletion of *cdgC* impacts the developmental regulatory cascade at different stages (see Fig. 1.7 on page 14 for the situation in the wild type). RNA-seq analyses performed by J. Haist (Haist et al., 2020) as well as qRT-PCRs, Western Blot analyses and confocal microscopy performed during this thesis revealed that the deletion of the major diguanylate cyclase CdgC alters the expression of several key factors in *Streptomyces* development (names of downregulated genes in purple and names of upregulated genes in red). This figure was modified after Bush et al. (2015); published in Nature Reviews Microbiology with license granted at the 4th of January 2021 under the license number: 4982000052251 and is not covered by the CC BY-NC-ND license Attribution-NonCommercial-NoDerivatives 4.0 International License of this thesis. Notice the difference to Fig. 1.7 on page 14 in Section 1.4.

present, c-di-GMP mediates the regulation of its activity by its anti-σ factor RsiG. σ^{BldN} is sequestered by its anti σ factor RsbN until released upon receiving an unknown extracellular stimuli that might or might not occur at this early time point of growth. Finally, a higher affinity of σ^{WhiG} to the RNAP holo enzyme than BldN would make sense regarding the fact, that BldN is normally still present when σ^{WhiG} is released from its anti-σ factor RsiG. Among other things, this would explain why an increase in the expression level of BldN has no effect on the developmental defect of Δ*cdgC*, whereas the overexpression of individual chaplins (under the control of a BldN-independent promoter) does. An alternative explanation is that the anti-σ RsbN keeps σ^{BldN} inactive and neutralizes the effect of increased BldN expression.

In both scenarios, the high c-di-GMP level would result from a combination of increased CdgF DGC activity with simultaneously reduced PDE activity of RmdA. Fig. 5.1 shows the distribution of the components of the sporulation cascade that are up- or downregulated in the expression data for Δ*cdgC*. Note that only two regulators, encoded by direct BldD target genes (BldH and BldN) are actually differentially expressed, but surprisingly, downregulated. The expected increased expression of developmental genes can only be observed in the middle to late phase of differentiation with, for example, the BldM target gene *ssgB* being upregulated (Al-Bassam et al., 2014; Haist et al., 2020). Once expressed, SsgB localizes at the future division sites via a to-date unknown position determination mechanism and recruits FtsZ, initiating the massive septation event at the onset of sporulation (Willemse et al., 2011).

Summary. Altogether, the deletion of *cdgC* seems to deregulate the sensitive developmental cascade far more than any other gene encoding a c-di-GMP turnover protein in *S. venezuelae*. The results is an unexpected transcriptomic pattern, leaving some open questions for future projects. A strong decrease of c-di-GMP levels directly after germination, resulting in a parallel expression of DNA-bound transcriptional regulators that normally act in series, might cause an aberrant σ factor concurrence between the chaplin and rodlin expression regulating σ^{BldN} and the late sporulation gene controlling σ^{WhiG}. Alternatively, σ^{BldN} kept inactive by its anti-σ RsbN keeps could neutralize the effect of increased BldN expression.

5.4 CdgC influences the timing of the sporulation-specific septation event

The tubulin-like FtsZ functions as a highly conserved GTPase by polymerizing into short filaments at the cytoplasmic membrane, forming the cytokinetic Z-rings (Bi & Lutkenhaus, 1991; Löwe & Amos, 1998). Localization of FtsZ to the future septation site initiates the recruitment of further cell division proteins, forming the multi-protein complex named the "divisome" (described in detail in Section 1.2 on page 3). In *S. coelicolor* and *S. venezuelae*, reflecting its distinct requirements in the life cycle, *ftsZ*-expression is regulated by three promoters: a vegetative, a reproductive and a BldD-dependent promoter region (Flärdh et al., 2000; Haist et al., 2020) (described in Detail in Section 1.4 on page 15).

The third, BldD-dependent promoter bridges FtsZ expression to the cellular c-di-GMP level on the level of transcriptional regulation. Thus, $\mathrm{BldD_2(c\text{-}di\text{-}GMP)_4}$ binds directly to the *ftsZ*

promoter region both in *S. coelicolor* and *S. venezuelae* at a conserved site (Tschowri et al., 2014; Den Hengst et al., 2010). It was, therefore, expected to see an upregulation in *ftsZ* transcription levels in the *cdgC* mutant compared to the wild type, but the RNAseq data could not verify this (Haist et al., 2020). Considering that the *cdgC* mutant had already formed spores when harvested for RNA-isolation after 30 h of growth on MYM solid medium, the chosen time point might have been too late in the life cycle to detect changes in *ftsZ* transcription. Using immunodetection and confocal microscopy, it was shown in this work, that the expression of FtsZ is c-di-GMP dependently regulated and, therefore, dramatically upregulated in the *cdgB* mutant and, even more pronounced, in the *cdgC* mutant (see Fig. 4.15 and 4.16 on page 55 and 56).

Since FtsZ expression is repressed by the c-di-GMP effector BldD via direct *ftsZ* promoter binding, the deletion of either *cdgB* or *cdgC* probably leads to its c-di-GMP deficiency mediated dissociation and activation of *ftsZ* expression (Tschowri et al., 2014). Furthermore, *ftsZ* is activated by the transcriptional heterodimer WhiAB, whose activity is limited by expression of the direct BldD target gene *whiB* (Den Hengst et al., 2010). This might add up to the c-di-GMP-mediated enhanced FtsZ expression caused by c-di-GMP deficiency dependent BldD inactivation as well as the c-di-GMP driven inactivation of σ^{WhiG} by its anti-σ RsiG. Regarding the latter, it was shown in *S. coelicolor* that the deletion of *whiG* or one of the two target genes *whiI* and *whiH* results in a weakening or outright elimination of the developmental boost in *ftsZ* transcript levels (Flärdh et al., 2000).

Altogether, *ftsZ* expression provides a less CdgC-specific readout but all the more a profound c-di-GMP-sensitive reporter in *Streptomyces* for all c-di-GMP turnover proteins. Its a morphological impact is triggered by BldD-mediated c-di-GMP-signaling in the vegetative phase as well as RsiG-σ^{WhiG}-sensed c-di-GMP stimuli at the onset of sporulation (Haist et al., 2020).

5.5 The CdgC interactome emphasizes the importance of its membrane-associated location

In an attempt to illuminate the potential protein-specific role of CdgC using a pUT18C-library for BTH screening with CdgC cloned on pKT25, three direct interaction partners of CdgC were identified in this work: Vnz07170/YjcH, Vnz15770 and Vnz08595/Sco2097 (see Fig. 4.28 on page 69). According to the protein domain annotations, all three of them are potential membrane proteins (Letunic & Bork, 2017; Letunic et al., 2020). BTH assays performed by V. Riebe with cytosolic CdgC tested against these three proteins, respectively, revealed no interactions. This indicates that the transmembrane anchor plays an essential role in the observed interactions of CdgC.

Vnz07170. Orthologs of Vnz07170, which contains two putative transmembrane domains and a DUF485 domain, are conserved in *Streptomyces*, but their function remains unclear to date. Structural alignments revealed a match with YjcH (E-value = 0.0034, sequence similarity = 61.4%, jackhmmer, EMBL-EBI) in *E. coli*, co-transcribed with the acetate permease YjcG (Vnz07165) and, therefore, assumed to be associated with acetate dissimilation and transport (Gimenez et al., 2003). Attempts to create a chromosomal deletion of Vnz07170, whose encoding gene is located

in an operon similar to YjcH in *E. coli*, made during this work did not succeed though. It would be interesting to analyze the physiological function of Vnz07170 and its interplay with CdgC by generating the chromosomal deletion. Analyses of the promoter function could characterize the potential operon, associated with acetate transport, encoding *vnz07160* - *vnz07170*. The bioluminescence-providing *luxCDABE* operon from the AT-rich *Photorhabdus luminescens* used as a transcriptional reporter system and described to be synthetically codon-optimized for GC-rich *S. coelicolor* by Craney et al. (2007), might be a useful tool to tackle this characterization. Furthermore, an identification of protein-protein interactions between the proteins encoded in this operon and CdgC could shed light on the functional mechanism behind the identified interaction between Vnz07170 and CdgC.

Vnz15770. The second interaction partner of CdgC also contains two putative transmembrane domains. The *vnz15770* gene is located directly adjacent to *vnz15765*, encoding a potential multidrug ABC transporter and *vnz15760*, encoding an antibiotic ABC transporter permease indicating a function of Vnz15570 in a multidrug efflux transporter system (StrepDB). Structural orthologs can be found in several *Streptomyces* species (e.g. D0Z67_16375 in *S. seoulensis*; E-value = 1.3, sequence similarity = 79.5, jackhmmer, EMBL-EBI) described as potential EamA/RhaT family transporter, the EamA family is also associated with drug/metabolite transport and was termed after the O-acetylserine/cysteine export gene in *E. coli* (Daßler et al., 2000; Franke et al., 2003). Attempts to create a chromosomal deletion of *vnz15770*, whose encoding gene is located in an operon made during this work, did not succeed though. It would be interesting to analyze the physiological function of Vnz15770 and its interplay with CdgC by generating the chromosomal deletion. An identification of the promoter and characterization of the putative *vnz15755* - *vnz15775* operon using a transcriptional reporter fusion as well as the identification of optional interactions between the encoded proteins and CdgC would be promising approaches. If Vnz15770 turns out to be associated to or part of an ABC transporter system together with Vnz15755 and Vnz15775, enzyme activity assays in presence and absence of CdgC using radio-labeled ATP as substrate could provide insights about the impact of CdgC on this potential ABC transporter system.

Vnz08595. The best-analyzed interaction partner of CdgC identified in this thesis is the potential membrane protein Vnz08595 (see Fig. 5.2 C) whose ortholog in *S. coelicolor* (Sco2097) was identified as a morphological protein with a role in spore wall synthesis. Deletion of *sco2097* leads to a similar but less pronounced phenotype then observed for the *mre* (murein formation gene cluster E) cluster genes.

This gene cluster directs peptidoglycan synthesis during sporulation and consists of *mreB*, *mreC*, *mreD*, located in one operon, as well as *pbp2* and *sfr*, which are translationally linked to each other and both controlled by their own promoter, which is involved in the formation of the spore wall synthesizing complex (SSSC) (Burger et al., 2000; Kleinschnitz et al., 2011). Recent studies showed that the actin-like MreB interacts with the transmembrane linker RodZ and the MreB-like protein (Mbl) to determine the locations of the extracytoplasmic cell wall

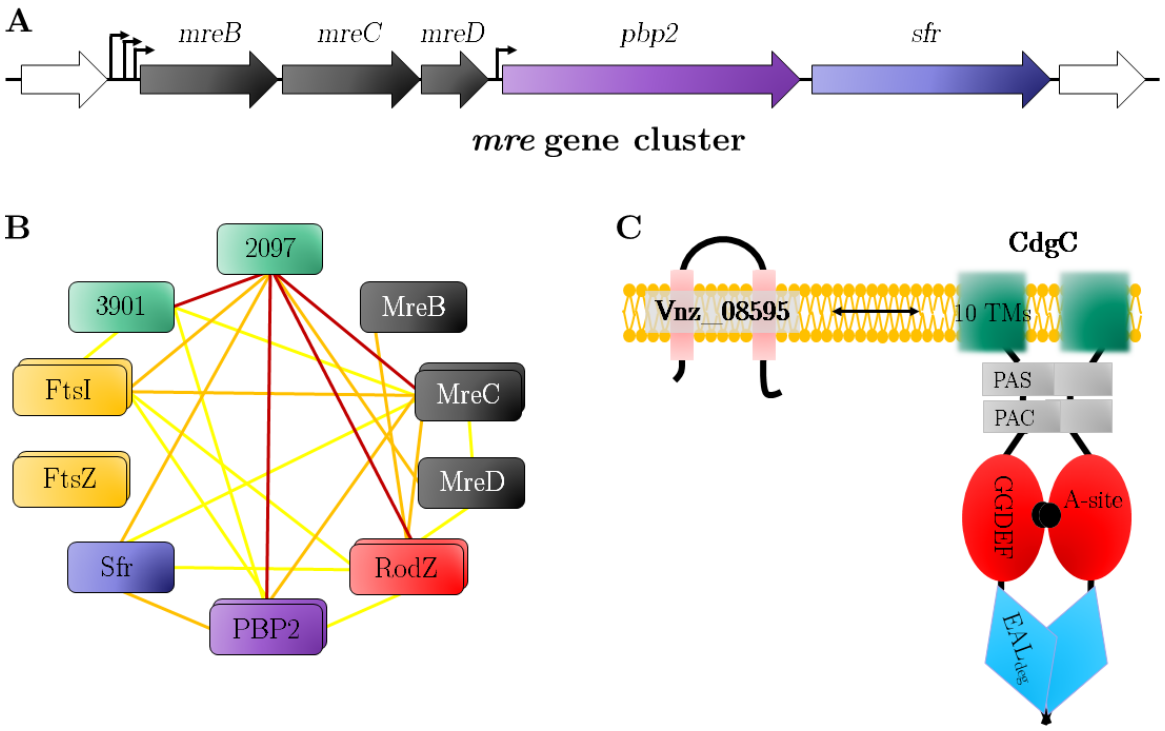

Fig. 5.2 The role of the CdgC interaction partner Vnz08595 in different *Streptomyces* species. (A) Organization of the associated *mre* gene cluster (StrepDB). (B) Schematic model of the selected interactions of components of the putative SSSC with Sco2097 (Vnz08595) based on BTH results from *S. coelicolor*. The connecting lines are colored according to interaction strength (red >1000 units/mg; orange >500 units/mg, 150-500 units/mg). Homodimerisation of the proteins is indicated by double boxes. (C) Protein-protein interaction of CdgC with Vnz08595 (transmembrane domains indicated as pink column) in *S. venezuelae*. Part B was modified with permission after Kleinschnitz et al. (2011); published in Molecular Microbiology with license granted at the 27th of July 2021 under the license number: 5097240970805 © Blackwell Publishing Ltd and is not covered by the CC BY-NC-ND license Attribution-NonCommercial-NoDerivatives 4.0 International License of this thesis. TMs - transmembrane domains of CdgC

synthesis (Vollmer et al., 2019). Furthermore, despite its unknown function, MreC is known to be phosphorylated by the serine/threonine protein kinases (eSTPK) PkaI and PkaH, which indicates that the SSSC might be regulated by protein phosphorylation (Vollmer et al., 2019). Sco2097 interacts with PkaI and several Mre cluster proteins (see Fig. 5.2 A). Identified interactions were particularly pronounced with MreC, RodZ and the penicillin binding protein PBP2, as illustrated in Fig. 5.2 B (Kleinschnitz et al., 2011). No direct interactions between Sco2097 or any members of the Mre cluster and FtsZ were observed, indicating an integration of the spore wall synthesis, as depicted in Fig. 5.2 B (Kleinschnitz et al., 2011).

The deletion of members of the *mre* cluster genes shows (a) enlarged spores, (b) a tendency for premature germination as well as (c) a sensitivity to heat, high osmolarity and cell wall targeting agents. The *sco2097* knockout phenotype deviates from this only because of its elongated spore shape, which was interpreted by Kleinschnitz et al. (2011) as an indicator for a role of Sco2097 in the control of the spore length in *S. coelicolor*. Observations (a) and (b) were also seen in the DGC double mutant $cdgC^{\text{ALLEF}}\Delta cdgB$ in *S. venezuelae*.

Phenotypic analyses of the DGC double mutants revealed that the strain in which both CdgB and CdgC were enzymatically inactivated has the most striking phenotype at colony level and in liquid culture (see Fig. 4.11 and 4.12 on page 50 and 51): the colonies were massively wrinkled, colored beige and by far the most structured. In liquid culture, on the other hand, the strain developed thickened spores that showed limited branching. However, the size and cell density of the macrocolonies contradicted a strong growth deficiency per se. On the microscopic level, the strain strongly resembled several deletion mutants of the *mre* gene cluster (Kleinschnitz et al., 2011). The resemblance of the *cdgC*$^{\texttt{ALLEF}}$Δ*cdgB* double mutant to several knockout phenotypes of this cluster indicates a link of CdgB and CdgC to the SSSC and cell wall synthesis. Furthermore, RNA-seq analysis, performed by J. Haist (Haist et al., 2020), revealed that all *mreB*-like genes (*mreB*, *vnz35885* and *mbl*) were upregulated in Δ*cdgC* as opposed to Δ*cdgB*, which showed no altered transcription of any *mre* genes. These observations underline the difference in heat shock sensitivity observed for these two strains (J. Müller, unpublished) and suggest an interesting role of CdgC in vegetative and sporulation-specific cell division, especially considering the membrane associated location of CdgC, that is worth analyzing in the future.

In contrast to the *sco2097* knockout phenotype, chromosomal deletion of the ortholog gene *vnz08595* in *S. venezuelae* led to a slightly decelerated cell cycle progression with decreased colony size compared to the wild type. Meanwhile, deletion of *vnz08595* in the enzymatically inactive CdgC$^{\texttt{ALLEF}}$ point mutant resulted in the classical hypersporulation phenotype of Δ*cdgC*, slightly shifted to a larger and dark gray colony with more pronounced radial ridges (see Fig. 4.29); this phenotype resembles the *cdgC*$^{\texttt{ALLEF}}$Δ*cdgA* mutant (see Fig. 4.29). In liquid culture, the deletion of *vnz08595* led to a slight delay in differentiation in both background strains, which suggests that the morphological effect of Vnz08595 is independent of CdgC activity (see Fig. 4.30). A Δ*cdgC*Δ*vnz08595* double mutant would help analyze the influence of the presence of CdgC on the impact of Vnz08595. Additionally, the analyses so far could not reproduce the premature germination observed in Δ*sco2097* in *S. coelicolor*, thus requiring further testing.

The gene *vnz08595* and its orthologs are located in proximity of the *dcw* gene cluster, which encodes i.a. *ftsZ* (see Fig. 1.2 on page 5). In order to further narrow down the impact of Vnz08595 on the SSSC and its interaction with the cell division machinery, the expression of the cell division protein FtsZ using an FtsZ-Ypet fusion protein in Δ*vnz08595* shows a significantly lower FtsZ presence compared to the wild type in liquid culture (see Fig. 4.32). Associated therewith, confocal microscopic analyses unveiled a delayed and reduced Z-ring formation (see Fig. 4.31 and 4.32). The generally delayed differentiation indicates a more general non spore wall-specific role of Vnz08595 in differentiation, collaborating with the SSSC during sporulation. This can be deduced, for example, from the interaction of its ortholog *sco2097* with the eukaryotic type serine/threonine kinase (eSTPK) PkaI, suggested to globally impact differentiation besides the SSSC (Ladwig et al., 2015).

Further analyses of the role of Vnz08595 as a CdgC interaction partner in *S. venezuelae* could approximate the aberrant spore wall formation that is observable in the deletion strain of *vnz08595*'s ortholog *sco2097*, to verify the observed sensitivity of the spore to cell wall damaging

agents like vancomycin, SDS (0.5-1%), nalidixic acid or lysozyme (50-100 µg) for Δ*vnz08595*. Additionally, properties of Δ*vnz08595* like heat and osmotic resistance (against NaCl, KCl and sucrose) would be interesting to test.

Finally, it should be noted that all three identified interaction partners of CdgC are potential membrane proteins and, during BTH assays performed by V. Riebe, none of them showed interaction with the cytosolic variant of CdgC. Thus, it is assumed that the membrane anchor of CdgC is essential for these interactions. A potential unspecific co-localization should therefore be investigated by another protein-protein interaction analysis method like pulldown assays.

Summary. Altogether, this study identified three putative membrane proteins as interaction partners of CdgC: Vnz07170, Vnz15770 and Vnz08595. The membrane anchor of CdgC seems to be essential for these interactions. First attempts to characterize Vnz08595 concentrated on its potential impact on cell division and spore wall synthesis, given that its ortholog Sco2097 in *S. coelicolor* interacts with the SSSC. In *S. venezuelae*, Vnz08595 and CdgC seem to influence the developmental cell cycle progression and the expression of the cell division protein FtsZ in adverse ways. Altogether, analyzing the interplay of especially CdgC with the the spore wall synthesizing complex and cell wall stress response is a promising project for future research.

5.6 Conclusion

This study could show that CdgC functions as a major DGC impacting several stages of the complex development network to repress reproductive genes during the vegetative phase in *S. venezuelae*. Deletion of *cdgC* seems to deregulate this sensitive regulation system far more than any other gene encoding a c-di-GMP turnover protein in *S. venezuelae*. The results are a shortened vegetative phase, a deficiency of aerial hyphae formation, correlated with the downregulation of major components of the hydrophobic coat and a precocious sporulation leading to an unexpected transcriptomic pattern, leaving some open questions for future projects. A strong decrease of c-di-GMP levels directly after germination, resulting in a parallel expression of DNA-bound transcriptional regulators that normally act in series, might cause an aberrant σ factor concurrence between the chaplin and rodlin expression regulating σ^{BldN} and the late sporulation gene controlling σ^{WhiG}. This is just one of many possible explanations for the functionality of this c-di-GMP calibrator. The large transmembrane anchor, the PAS-PAC domain and the $\mathtt{EAL}_{\mathrm{deg}}$ domain are promising candidates as potential sensor domain for cellular and external stimuli, influencing not only the dimerization and interaction but maybe also the signal responsive activity of CdgC. Therefore, it will be interesting to further analyze their functions and role.

Chapter 6
Appendix

Tab. 6.1 List of utilized reagents and materials with their corresponding manufacturer

Products	Manufacturer
Acrylamide-Bisacrylamide	Carl Roth
Agarose	Biozym Scientific
Agarose High Resolution	Carl Roth
APS	Carl Roth
Anti-BldD antibody	Sigma Aldrich
Anti-BldN polyclonal (Rabbit)	Matthew Bush, JIC, Norwich, UK
Anti-Flag (Mouse)	Sigma
Anti-Flag®M2 Affinity Gel	Sigma Aldrich
Anti-His (Mouse)	Thermo Scientific
Anti-Mouse-HRP	Thermo Scientific
Anti-Rabbit IgG Horseradish Peroxidase (HRP)	GE Healthcare
Anti-WhiD polyclonal (from rabbit)	Matthew Bush, JIC, Norwich, UK
Anti-WhiG polyclonal (from rabbit)	Matthew Bush, JIC, Norwich, UK
Antibiotics (Amp, Cm, Kan, Hyg)	Carl Roth, σ, Merck
Bacto agar (Difco)	Otto Nord Wald
Bacto-Peptone (Difco)	Otto Nord Wald
Bacto Yeast Extract (Difco)	Otto Nord Wald
Bradford Roti-Quant	Carl Roth
Bradford Roti Nanoquant	Carl Roth
BSA standard	VWR
Blot membrane for protein (Roti-PVDF)	Carl Roth
c-di-GMP	BIOLOG Life Science Institute
Chromatography column frit	Sigma
Coomassie Brilliant Blue R-250	AppliChem
TLC plates for nucleotide fractionation	Macherey-Nagel
Cover slips	VWR
Dialysis membrane DNA	Baack
DNA size marker: 50/100 bp extended	New England Biolabs
DNA marker - GeneRuler 1kb	Thermo Scientific
DNA polymerases (Opti-Taq, Q5)	Roboklon, New England Biolabs
DNase I	AppliChem
dNTP stock solutions	MP Biomedicals
ECL substrates (Western Blot Detection)	BioRad
Electroporation cuvettes	VWR
GelRed	Genaxxon
MacConkey agar (Lactose-containing)	Carl Roth

List of used reagents and materials with their corresponding manufacturer (continued)

Products	Manufacturer
MacConkey agar (Difco)	VWR
Malt extract (Difco)	VWR
Microscope slide	VWR
Nutrient agar	Carl Roth
Ni-NTA	Macherey-Nagel
Oligonucleotide	Metabion
Pierce Silver Stain for Mass Spectrometry	Thermo Scientific
Protease-Inhibitoren	Sigma
Protein Marker LMW	VWR
Protein Marker prestained	NEB
Restriction enzymes & T4 ligase	NEB/Thermo Scientific
SensiFast SYBER no-ROX One-Step Kit	Bioline
TEMED	Carl Roth
X-Gal	Carl Roth

Tab. 6.2 Manufacturers of the utilized devices

Products	Manufacturer
Air incubator (Innova® 44)	New Brunswick Scientific
Autoclave (DX-45; Varioklav 25T)	Systec GmbH; Thermo Fischer Scientific
Bead Beater Homogenizer (BeadBlaster 24)	Biozym
Binocular (AxioCam ICc 3)	Carl Zeiss AG
Block Heater (MB-102 Thermocell mixing block)	Alpha Laboratories
Blotting Apparatur	Bio-Rad, Peqlab
CCD Camera (ECL CHEMOCAM IMAGER)	Intas Pharmaceuticals Limited
Centrifuges	Sorvall Instruments, Eppendorf
Colony counter (Colony Counter-SC6PLUS)	Stuart Equipment, Staffordshire
Elektroporator (Gene Pulser Xcell)	Bio-Rad
ELISA Reader (Model 550)	Bio-Rad
Fluorescence microscope (ZEISS AxioObserver.Z1)/ camera (Axiocam 702 mono)	Carl Zeiss AG
French Press (HTU - DIGI-F-Press)	G. Heinemann Ultraschall- and Labortechnik
UV Camera (Multiimage® II)	Alpha Innotech Corporation
Magnetic Stirrer (RSM-01S)	Phoenix Instrument GmbH
Microcentrifuge (MiniSpin® plus)	Eppendorf AG
NanoDrop	Peqlab
PCR-Thermocycler (Arktik Thermal Cycler)	Thermo Scientific
PhosphoImager (Typhoon FLA-2000G)	GE Healthcare
Photometer (GeneQuant 100)	GE Healthcare
qRT-PCR-Thermocycler "CFX Connect™ real time system"	Bio-Rad
Scale	Carl Roth
Scale, precision (SECURA2102 – 1S)	Sartorius Weighing Technology GmbH
Sterile bench (BioWizard Silver SL-130 Class II)	KOJAIR TECH OY

Tab. 6.3 List of utilized buffers and their composition

Buffer	Composition
10×PBS	1,37 M NaCl;27 mM KCl; 100 M $Na_2HPO_4 \cdot 2\,H_2O$ (with NaOH at pH 7.3); 20 mM KH_2PO_4
50× TAE	40 mM Tris·HCl; 20 mM acetic acid; 1 mM EDTA pH 8.0
6× DNA Loading buffer	0.25% bromphenol blue; 0.25% xylene cyanol; 30% glycerol in 1xTAE
4×SDS Sample buffer	240 mM Tris·HCl pH 6.8; 8% SDS solution; 40% glycerol; 400 mM DTT; 0.02% bromophenol blue
SDS electrophorese buffer	25 mM Tris·HCl; 190 mM glycine; 0.1% SDS
Transblot buffer	25 mM Tris; 192 mM glycine; 20% ethanol
TBS	50 mM Tris·HCl pH 7.5; 150 mM NaCl; 1 mM EDTA pH 8.0; 0.8% Tween-20
TBST	20 mM Tris·HCl pH 7.5;150 mM NaCl; 0.05% Tween-20

Tab. 6.4 List of utilized *S. venezuelae* strains

Strain	Genotype/Description	Utilization	Reference
NRRL B-65442 (*S. venezuelae*)		Wild type	NCBI: NZ_CP018074.1
SVABK-4	*cdgC::apr attB*$_{\Phi BT1}$::pIJ10257_*cdgB*; Apr^R, Hyg^R	Overexpression of $CdgB_{SCO}$ in Δ*cdgC*	Al-Bassam et al. (2018)
SVNT5	*attB*$_{\Phi BT1}$::pMS82; Hyg^R	Empty vector (e.V.)	N. Tschowri
SVNT20	*cdgC::apr*; Apr^R	*cdgC* deletion mutant	Al-Bassam et al. (2018)
SVNT22	*cdgE::apr*; Apr^R	*cdgE* deletion mutant	
SVNT23	*cdgB::apr*; Apr^R	*cdgB* deletion mutant	
SVNT24	*cdgA::apr*; Apr^R	*cdgA* deletion mutant	
SVNT25	*cdgF::apr*; Apr^R	*cdgF* deletion mutant	
SVNT30	*cdgA::apr*; *attB*$_{\Phi BT1}$::p3xFLAG_*cdgA*; Apr^R, Hyg^R	CdgA-FLAG immunodetection	
SVNT37	*cdgE::apr*; *attB*$_{\Phi BT1}$::p3xFLAG_*cdgE*; Apr^R, Hyg^R	CdgE-FLAG immunodetection	
SVSL1	*cdgB::apr attB*$_{\Phi BT1}$::p3xFLAG_*cdgB*; Apr^R, Hyg^R	CdgB-FLAG immunodetection	
SVSN1	*cdgC*(G658A/G659L/D660L); Apr^R	Strain with enzymatically inactive CdgC	This study, Al-Bassam et al. (2018)
SVSN2/3	*cdgC::apr attB*$_{\Phi BT1}$::pMS82_*cdgC*; Hyg^R	Complementation strain of SVNT20	
SVSN6	*cdgC::apr attB*$_{\Phi BT1}$::p3xFLAG_*cdgC*; Hyg^R	Immunodetection of the CT FLAG tag CdgC	
SVSN10	*cdgC*(G658A/G659L/D660L)Δ*vnz08595 attB*$_{\Phi BT1}$::pSS5 (FtsZ:Ypet); Apr^R, Hyg^R	Confocal microscopic imaging for expression analysis of FtsZ in Δ*08595*	This study
SVSN11	*cdgC*(G658A/G659L/D660L) *attB*$_{\Phi BT1}$::pSS5 (FtsZ:Ypet); Apr^R, Hyg^R		

List of utilized *S. venezuelae* strains (continued)

Strain	Genotype/Description	Utilization	Reference
SVSN12	*cdgC*(G658A/G659L/D660L)Δ*vnz08595*; Apr^R	Phenotypic analyses CdgC on Vnz08595	This study
SVSN15	*cdgC*(G658A/G659L/D660L)Δ*cdgF*; Apr^R	Analysis of the DGC double knockout mutant in SVSN1	
SVSN16	*cdgC*(G658A/G659L/D660L)Δ*cdgE*; Apr^R		
SVSN17	*cdgC*(G658A/G659L/D660L)Δ*cdgA*; Apr^R		
SVSN18	Δ*vnz08595* $attB_{\Phi BT1}$::pSS5 (FtsZ:Ypet); Apr^R, Hyg^R	Confocal microscopic imaging for expression analysis of FtsZ in Δ*08595*	
SVSN19	*cdgC*(G658A/G659L/D660L) *cdgA::apr*; Apr^R	Analysis of the DGC double knockout mutant	
SVSN28	$attB_{\Phi BT1}$::pMS82$_{_ermE*}$-*chpB*; Hyg^R	ChpB overexpression	This study, Haist et al. (2020)
SVSN29	*cdgC::apr* $attB_{\Phi BT1}$::pMS82$_{_ermE*}$-*chpB*; Hyg^R		
SVSN30	$attB_{\Phi BT1}$::pMS82$_{_ermE*}$-*chpC*; Hyg^R	ChpC overexpression	
SVSN31	*cdgC::apr* $attB_{\Phi BT1}$::pMS82$_{_ermE*}$-*chpC*; Hyg^R		
SVSN32	$attB_{\Phi BT1}$::pMS82$_{_ermE*}$-*chpD*; Hyg^R	ChpD overexpression	
SVSN33	*cdgC::apr* $attB_{\Phi BT1}$::pMS82$_{_ermE*}$-*chpD*; Hyg^R		
SVSN34	$attB_{\Phi BT1}$::pMS82$_{_ermE*}$-*chpE*; Hyg^R	ChpE overexpression	
SVSN35	*cdgC::apr* $attB_{\Phi BT1}$::pMS82$_{_ermE*}$-*chpE*; Hyg^R		
SVSN36	$attB_{\Phi BT1}$::pMS82$_{_ermE*}$-*chpF*; Hyg^R	ChpF overexpression	
SVSN37	*cdgC::apr* $attB_{\Phi BT1}$::pMS82$_{_ermE*}$-*chpF*; Hyg^R		
SVSN38	$attB_{\Phi BT1}$::pMS82$_{_ermE*}$-*chpH*; Hyg^R	ChpH overexpression	
SVSN39	*cdgC::apr* $attB_{\Phi BT1}$::pMS82$_{_ermE*}$-*chpH*; Hyg^R		
SVSN41	Δ*vnz26460* $attB_{\Phi BT1}$::p3xFLAG_*cdgC*; Apr^R, Hyg^R	Proteolytic analysis of CdgC-FLAG	This study
SVSN42	Δ*vnz09525* $attB_{\Phi BT1}$::p3xFLAG_*cdgC*; Apr^R, Hyg^R		
SVSN43	Δ*vnz06080* $attB_{\Phi BT1}$::p3xFLAG_*cdgC*; Apr^R, Hyg^R		
SVSN44	Δ*vnz23710* $attB_{\Phi BT1}$::p3xFLAG_*cdgC*; Apr^R, Hyg^R		
SVSN45	Δ*vnz13370* $attB_{\Phi BT1}$::p3xFLAG_*cdgC*; Apr^R, Hyg^R		
SVSN45	Δ*vnz06050* $attB_{\Phi BT1}$::p3xFLAG_*cdgC*; Apr^R, Hyg^R		
SVSN51	*cdgC*(G658A/G659L/D660L) $attB_{\Phi BT1}$::p3xFLAG_*cdgE*; Hyg^R	CdgE-FLAG immunodetection	
SVSN52	*cdgC*(G658A/G659L/D660L) $attB_{\Phi BT1}$::p3xFLAG_*cdgB*; Hyg^R	CdgB-FLAG immunodetection	

List of utilized *S. venezuelae* strains (continued)

Strain	Genotype/Description	Utilization	Reference
SVSN55	*cdgC*(G658A/G659L/D660L) $attB_{\Phi BT1}$::pMS82_*cdgC*; Hyg^R	Complementation strain of SVSN1	This study, Al-Bassam et al. (2018)
SVSN56	*cdgC*(G658A/G659L/D660L) $attB_{\Phi BT1}$::pMS82; Hyg^R	Control of SVSN1	
SVSN57	*cdgC::apr* $attB_{\Phi BT1}$::pMS82; $Apra^R$, Hyg^R	Control of SVNT20	
SVSN62	*cdgB::apr* $attB_{\Phi BT1}$*::pSS5 (FtsZ:Ypet)*; Apr^R	Confocal microscopic imaging for expression analysis of FtsZ in Δ*cdgB*	This study
SVSN63	*cdgC::apr* $attB_{\Phi BT1}$::pSS172 *ftsZ:ypet*; Apr^R, Hyg^R	Confocal microscopic imaging for expression analysis of FtsZ in Δ*cdgC*	
SVSN64	$attB_{\Phi BT1}$::pSS170 (e.V.); Hyg^R	Control strain	
SVSN65	*cdgC*(G658A/G659L/D660L) $attB_{\Phi BT1}$::p3xFLAG_*cdgA*; Hyg^R	CdgA-FLAG immunodetection	
SVSN66	*cdgC::apr* $attB_{\Phi BT1}$::pIJ10257$_{ermE*}$-*bldN*; Hyg^R	BldN overexpression	
SVSN67	*cdgC::apr* $attB_{\Phi BT1}$::pIJ10257$_{ermE*}$-*bldM*; Hyg^R	BldM overexpression	
SVSN68	*cdgC::apr* $attB_{\Phi BT1}$::pMS82_*cdgC* (G658A/G659L/D660L); Hyg^R	Used as a *cdgC* complementation strain	
SVSN69	*cdgC::apr* $attB_{\Phi BT1}$::pSS170 (e.V.); Apr^R, Hyg^R	Controll strain	
SVSN70	*bldD::apr* $attB_{\Phi BT1}$::pMS82 (e.V.); Apr^R, Hyg^R		
SVSN73	*vnz08595::apr*; Apr^R	*vnz08595* deletion mutant	
SVSN74	$attB_{\Phi BT1}$::pMS82_*cdgC* (G658A/G659L/D660L); Hyg^R	Complementation strain	
SVSN76	*bldD*(D116A) [SVNT18] $attB_{\Phi BT1}$::pMS82_*cdgC*	Complementation strain in SVNT18	
SVSN77	*bldD*(D116A) [SVNT18] $attB_{\Phi BT1}$::p3xFLAG_*cdgC*	Immunodetection of CdgC-FLAG expression in Δ*bldD*	
SVSN78	*bldD::apr* $attB_{\Phi BT1}$::pMS82_*cdgC* (G658A/G659L/D660L)	Complementation strain in *bldD*	
SVSN79	*bldD::apr* $attB_{\Phi BT1}$::pMS82_*cdgC*		
SVSN80	*bldD*(D116A) [SVNT18] $attB_{\Phi BT1}$::pMS82_*cdgC* (G658A/G659L/D660L)	Complementation strain in SVNT18	
SVSN81	*bldD*(D116A) [SVNT18] $attB_{\Phi BT1}$::pMS82 (e.V.)	Controll strain	
SVSN82	*bldD::apr* $attB_{\Phi BT1}$::p3xFLAG_*cdgC*; Hyg^R	Immunodetection of CdgC-FLAG expression in Δ*bldD*	

List of utilized *S. venezuelae* strains (continued)

Strain	Genotype/Description	Utilization	Reference
SVSN83	*attB*$_{\Phi BT1}$::p3xFLAG_*cdgC*; Hyg^{R}	Immunodetection of CdgC-FLAG expression in WT	This study
SVSN84	*attB*$_{\Phi BT1}$::pIJ10257$_{ermE*}$-*bldM*; Hyg^{R}	BldM overexpression	
SVSN85	*attB*$_{\Phi BT1}$::pIJ10257$_{ermE*}$-*bldN*; Hyg^{R}	BldN overexpression	

Tab. 6.5 List of utilized *E. coli* strains

Strain	Genotype/Description	Utilization	Reference
DH5α	F^{-} *endA1 glnV44 thi-1 recA1 relA1 gyrA96 deoR nupG Φ80dlacZΔM15 Δ(lacZYA-argF)U169, hsdR17(r_K-m_K+), λ-*	Plasmid increase and strain storage	Hanahan et al. (1991)
ET12567/ pUZ8002	F^{-} *dam13::Tn9 dcm6 hsdM hsdR recF143::Tn10 galK2 galT22 ara-14 lacY1 xyl-5 leuB6 thi-1 tonA31 rpsL hisG4 tsx-78 mtl-1 glnV44*	Conjugation in *Streptomyces*	Luo et al. (2014)
W3110	K12 *thyA36 deoC2 IN(rrnD-rrnE)1*	Background strain	Hayashi et al. (2006)
AR388	K12 W3110 *cyaA::scar*	BTH reporter strain	Richter et al. (2020)
Rosetta (DE3)	*F^{-}ompT hsdSB(RB^{-} mB^{-}) gal dcm λ(DE3 [lacI lacUV5-T7 gene 1 ind1 sam7 nin5]) pLysSRARE2 (Cm^{R})*	Overexpression strain for protein purification	Novagen
BL21(DE3) pLysS	*B F^{-} dcm ompT hsdS(rB^{-} mB^{-}) galλ(DE3) [pLysS Cam^{R}]*	Overexpressions strain for protein purification	Stratagen

Tab. 6.6 List of utilized bacteriophages

Lysat	Genotype	Function	Reference
SV1	*S. venezuelae*-WT	transducing phage	laboratory collection
SV1 *cdgA::apr*	*S. venezuelae*, Apr^{R} between *vnz12755* and *vnz12755*	transducing phage for Δ*cdgA*	This study
SV1 *cdgB::apr*	*S. venezuelae*, Apr^{R} between *vnz19915* and *vnz19925*	transducing phage for Δ*cdgB*	
SV1 *cdgE::apr*	*S. venezuelae*, Apr^{R} between *vnz22735* and *vnz22745*	transducing phage for Δ*cdgE*	
SV1 *cdgF::apr*	*S. venezuelae*, Apr^{R} between *vnz02135* and *vnz02145*	transducing phage for Δ*cdgF*	

Tab. 6.7 List of universal plasmids

Plasmid	Description	Reference
pET15b	Overexpression vector with a NT 6xHis tag, Amp^R	Merck
pIJ10770	pMS82 containing an extended Multiple Cloning Site (MCS) lacking the intrinsic apramycin promoter upstream of it; Hyg^R	Schlimpert et al. (2017)
pIJ773	Plasmid amplification template for the Apra-*oriT* cassette for "Redirect" PCR-targeting; Apr^R	Gust et al. (2003)
pMS82	Vector for homologe recombination in Streptomycetes, OriTRP4, $attB_{\Phi BT1}$; Hyg^R	Gregory et al. (2003)
pUZ8002	Helper plasmid, RP4 allele with defective *oriT*, Kan^R	Paget et al. (1999)
p3xFLAG	pIJ10770 with triple Flag Tag downstream of the MCS between XhoI and KpnI sites; Hyg^R	Al-Bassam et al. (2018)

Tab. 6.8 Plasmids for protein overexpression and purification

Plasmid	Description	Reference
pSVSN-1	pET15b_ΔTM-Δ`EAL`-*cdgC*, encodes for the 6xHis-tagged cytosolic CdgC without `EAL` domain	This study
pSVSN-2	pET15b_ΔTM-*cdgC*, encodes for the 6xHis-tagged cytosolic CdgC	This study, Al-Bassam et al. (2018)
pSVSN-3	pET15b_*cdgC*-`EAL`, encodes for the 6xHis-tagged `EAL` domain of CdgC	This study
pSVSN-4	pET15b_*cdgC*-`GGDEF`, encodes for the 6xHis-tagged `GGDEF` domain of CdgC	

Tab. 6.9 Plasmids for the adenylate cyclase activity based Two-Hybrid System

Plasmid	Description	Reference
pIJ10907	pKT25_*whiG*, whole ORF, Kan^R	Gallagher et al. (2020)
pIJ10908	pKNT25_*whiG*, whole ORF, Kan^R	
pIJ10909	pUT18_*whiG*, whole ORF, Amp^R	
pIJ10910	pUT18C_*whiG*, whole ORF, Amp^R	
pIJ10911	pKT25_*rsiG*, whole ORF, Kan^R	
pIJ10912	pUT18_*rsiG*, whole ORF, Amp^R	
pKT25	Expression plasmid for generation of fusion proteins with NT T25 fragment of the adenylate cyclase from *B. pertussens*, Kan^R	Karimova et al. (1998)
pKNT25	Expression plasmid for generation of fusion proteins with CT T25 fragment of the adenylate cyclase from*B. pertussens*, Kan^R	
pUT18	Expression plasmid for generation of fusion proteins with CT T18 fragment of the adenylate cyclase from *B. pertussens*, Amp^R	
pUT18C	Expression plasmid for generation of fusion proteins with NT T18 fragment of the adenylate cyclase from *B. pertussens*, Amp^R	
pKT25_zip	T25 leucine zipper, control plasmid	
pUT18C_zip	T18 leucine zipper, control plasmid	
pKT25_*bldN*	pKT25_*bldN*, whole ORF, Kan^R	JIC, Norwich, UK
pUT18C_*bldN*	pUT18_*bldN*, whole ORF, Amp^R	
pKT25_*rsbN*	pKT25_*rsbN*, whole ORF, Kan^R	
pUT18C_*rsbN*	pUT18_*rsbN*, whole ORF, Amp^R	
pKNT25_*rsiG*	pKNT25_*rsiG*, whole ORF, Kan^R	

Plasmids for the adenylate cyclase activity based Two-Hybrid System (continued)

Plasmid	Description	Reference
pUT18C_*rsiG*	pUT18C_*rsiG*, whole ORF, Amp^R	JIC, Norwich, UK
pSVJK-1	pKT25_*bldD*, whole ORF, Kan^R	J. Krambrich, unpublished
pSVJK-2	pUT18_*bldD*, whole ORF, Amp^R	
pSVNT-21	pKNT25_*bldD*, whole ORF, Kan^R	N. Tschowri, unpublished
pSVSN-8	pUT18_*cdgC*, whole ORF, Amp^R	This study
pSVSN-9	pKT25_*cdgC*, whole ORF, Kan^R	
pSVSN-10	pUT18_*vnz07170*, whole ORF, Amp^R	
pSVSN-11	pKT25_*vnz07170*, whole ORF, Kan^R	
pSVSN-12	pUT18_*vnz08595*, whole ORF, Amp^R	
pSVSN-13	pKT25_*vnz08595*, whole ORF, Kan^R	
pSVSN-14	pUT18_*vnz15770*, whole ORF, Amp^R	
pSVSN-15	pKT25_*vnz15770*, whole ORF, Kan^R	
pSVSN-16	pUT18_*vnz17665*, whole ORF, Amp^R	
pSVSN-17	pKT25_*vnz17665*, whole ORF, Kan^R	
pSVSN-20	pUT18_*cdgC*-`EAL`, `EAL` domain 2230 bp until stop codon, Amp^R	
pSVSN-21	pKT25_*cdgC*-`EAL`, `EAL` domain 2230 bp until stop codon, Kan^R	
pSVSN-22	pUT18_*cdgC*-Δ`EAL`, Start until 2280 bp, Amp^R	
pSVSN-47	pUT18C_*cdgC*, whole ORF, Amp^R	

Tab. 6.10 List of integrative plasmids for conjugation in *Streptomyces*

Plasmid	Description	Reference
pIJ10432	pIJ10257$_{ermE*}$-*bldM*	JIC, Norwich, UK
pIJ10761	pIJ10257$_{ermE*}$-*bldN*	
pSVOJ1	pMS82_*cdgC*, full size under its native promotor	Al-Bassam et al. (2018)
pSS5	pIJ10750-P$_{ftsZ}$-*ftsZ-ypet*, Hyg^R	Schlimpert et al. (2017)
pSVSL4	p3xFLAG_*cdgA*, for analysis of the protein expression of the CT FLAG tag CdgA in *S. venezuelae*	S. Lindenberg; Al-Bassam et al. (2018)
pSVSL5	p3xFLAG_*cdgE*, for analysis of the protein expression of the CT FLAG tag CdgE in *S. venezuelae*	
pSVSL11	p3xFLAG_*cdgB*, for analysis of the protein expression of the CT FLAG tag CdgB in *S. venezuelae*	
pSVSN-27	p3xFLAG_*cdgC*, for immunodetection of the CT FLAG tag CdgC in *S. venezuelae*	This study, Al-Bassam et al. (2018)
pSVSN-38	pMS82$_{ermE*}$-*chpC*, for overexpression of ChpC in *S. venezuelae*	This study, Haist et al. (2020)
pSVSN-39	pMS82$_{ermE*}$-*chpE*, for overexpression of ChpE in *S. venezuelae*	
pSVSN-40	pMS82$_{ermE*}$-*chpH*, for overexpression of ChpH in *S. venezuelae*	
pSVSN-61	pUZ57$_{ermE*}$-*chpD*, synthesis vector for the transport of the inserts	Synthetised by GeneScript
pSVSN-62	pUZ57$_{ermE*}$-*chpF*, synthesis vector for the transport of the inserts	
pSVSN-63	pUZ57$_{ermE*}$-*chpG*, synthesis vector for the transport of the inserts	
pSVSN-65	pMS82$_{ermE*}$-*chpB*, for overexpression of ChpB in *S. venezuelae*	This study, Haist et al. (2020)
pSVSN-66	pMS82$_{ermE*}$-*chpD*, for overexpression of ChpD in *S. venezuelae*	
pSVSN-67	pMS82$_{ermE*}$-*chpF*, for overexpression of ChpF in *S. venezuelae*	
pSVSN-68	pMS82$_{ermE*}$-*chpG*, for overexpression of ChpG in *S. venezuelae*	

Tab. 6.11 List of utilized cloning primers with their base sequences in (5'→ 3'). Restriction site in small capitals.

Primer	fw/rev	Restriction site	Sequence in 5'→ 3' direction	Utilization
AA	fw	HindIII	CAGAAGCTTGAGCCTGTGAACGTCCTC	pSVSN-27
AB	rev	XhoI	GCAGCCTCGAGAGTGGGTGGGACAGGCG	
AN	fw	EcoRI	GACGAGAATTCGTGAAGAACCTCAAGAAGGC	pSVSN-39
AO	rev	BamHI	GACGGATCCGGGTGTCAGCCGTTGA	
AP	fw	EcoRI	GACGAGAATTCATGATCAAGAAGGTCGTCGC	pSVSN-40
AQ	rev	BamHI	GACGGATCCGCGAGGTTCAACGTCA	
AR	fw	EcoRI	GACGAGAATTCGTGGCACTCTTTCGAAGCCGA	pSVSN-38
AS	rev	BamHI	GACGGATCCCTGTGCGTGGTGCGTG	
AT	fw	EcoRV	GACGAGATATCGTGGCACTCTTTCGAAGCCGA	
BY	fw	NdeI	GACCATATGATCATGCTGCTCGACAAC	pSVSN-1 & 2
BZ	rev	XhoI	GACTCTCGAGTTAGACCACCTCGGCCTG	pSVSN-1 & 4
CA	rev	XhoI	CAGTCTCGAGTTCAAGTGGGTGGGACA	pSVSN-2 & 3
CB	fw	NdeI	GACCATATGAAGGACCGCGTCGAGCTC	pSVSN-3
CC	fw	NdeI	GACCATATGGGCCTGATCTTCAACAGC	pSVSN-4
CQ	fw	XbaI	GACCTCTGAGGGTGCCGGACCAGGCC	pSVSN-8 & -9
CR	rev	KpnI	GACGGTACCTCAAGTGGGTGGGACAGGC	pSVSN-9
CS	rev	KpnI	GACGGTACCCGAGTGGGTGGGACAGGCG	pSVSN-8, -22 & -23
CT	fw	XbaI	GACCTCTGAGGATGTCCAGCGAATACGCAAAG	pSVSN-71 & 72
CU	rev	KpnI	GACGGTACCTCAGTTCTCCTCGTGGGC	pSVSN-72
CV	rev	KpnI	GACGGTACCGGTTCTCCTCGTGGGCGAC	pSVSN-71
CW	fw	XbaI	GACCTCTGAGGGTGGCTACCGAAGCAC	pSVSN-10 & -11
CX	rev	BamHI	GACGGATCCCGTGCGTCGGCCTCC	
CY	fw	XbaI	GACCTCTGAGGGTGCCGCTCTCGGAGCAC	pSVSN-12 & -13
CZ	rev	KpnI	GACGGTACCCGGTGGCCGCCGCCC	
DA	fw	XbaI	GACCTCTGAGGGTGAGCGACGAAGAGCAG	pSVSN-14 & -15
DB	rev	KpnI	GACGGTACCCGCTTGCGCTTGGGCTTCTTG	
DC	fw	XbaI	GACCTCTGAGGATGGCACCCGAATCCGG	pSVSN-16 & -17
DD	rev	KpnI	GACGGTACCCGGTTCGTCTCGGCGCCG	
DE	fw	XbaI	GACCTCTGAGGGAGCTCTACGCGCCCCAG	pSVSN-22 & -23

Tab. 6.12 List of utilized sequencing primers with their base sequences in (5'→ 3')

Primer	fw/rev	Sequence in 5'→ 3' direction	Utilization
BR	rev	CCGTAGAGGAAGCAGGAC	gene intern sequencing primer of CdgC
BS	rev	GGAGGCCATGAACGAGGAGAAG	
BT	fw	CTGCTCGACATCGTCCTC	
BU	fw	GAACCGCTCGGCGACCAACAC	
BV	rev	GAACCAGCCGGCGTCGAG	
BW	fw	GACTGGCTCAACGTCGAGTC	
BX	fw	GTGCTCTTCATCGACCTC	

Tab. 6.13 List of utilized primers for quantitative PCR analyses with their base sequences in (5'→ 3')

Primer	Sequence in 5'→ 3' direction	Utilization
*cdgA*_qRT-PCR fw	TCGTACGGGTATGGCAGAACAGG	Expression pattern of the respective gene in Δ*cdgC* compared to wild type
*cdgA*_qRT-PCR rev	GGTGTCGTTGACCGCCTTGAAC	
*cdgB*_qRT-PCR fw	AGCTGCTCGGCGTCATATC	
*cdgB*_qRT-PCR rev	GCACGCTGCATGTTGGAG	
*cdgC*_qRT-PCR fw	AACCACTTCAGGTCACTCGTG	
*cdgC*_qRT-PCR rev	ATGAGCGAGGCCAGTTCGG	
*cdgE*_qRT-PCR fw	TCAAGCGGGTCAACGACAC	
*cdgE*_qRT-PCR rev	ACCGTCAGCAGACAGAACTC	
*cdgF*_qRT-PCR fw	ACCGAACAGCGGAAACTGGAA	
*cdgF*_qRT-PCR rev	ATGCAGGTCAGGGTGGATTC	
*chpC*_qRT-PCR fw	AACGGTGCGGCCATGAATTC	
*chpC*_qRT-PCR rev	CGACGACATTGACCGTGTTTC	
*chpE*_qRT-PCR fw	CGTCCCCGTGAACGTCTC	
*chpE*_qRT-PCR rev	CCGTTGAGGGCGTGGTTG	
*chpH*_qRT-PCR fw	AAGAAGGTCGTCGCTGCTG	
*chpH*_qRT-PCR rev	GGACGACATTGCCCGAGAG	
*hrdB*qRT_F1	TGTTCTGCGCAGCCTCAATC	
*hrdB*qRT_R1	CTCTTCGCTGCGACGCTCTT	
bldM-fw	ATGACATCCGTTCTCGTCTGC	
bldM-rev	AGGACTTCCTCGCCGTTGG	
bldN-fw	ACTTCAAGTCCAGCCGGTTC	
bldN-rev	TTGGAGAGGGACTCCAGGAC	

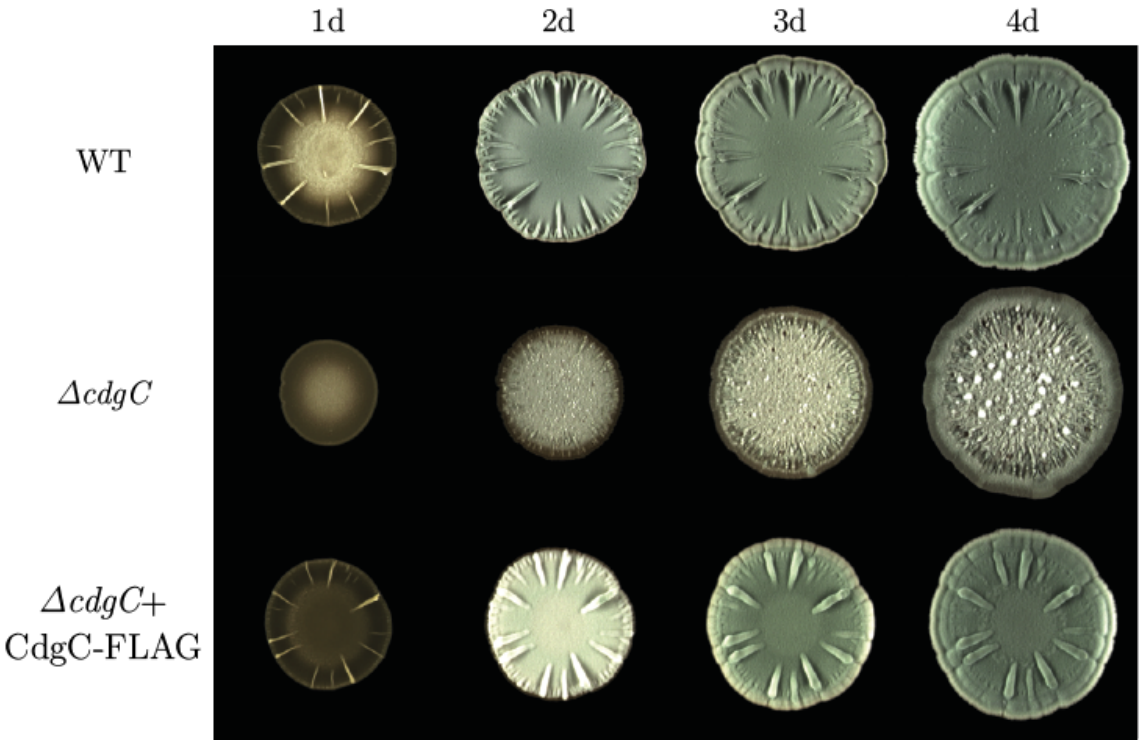

Fig. 6.1 CdgC-FLAG is able to restore the WT phenotype in Δ*cdgC*. Macrocolonies of these strains created through drip of 12 µL $2 \cdot 10^5$ CFU/µL spores on MYM agar and plates were incubated for 4 d at 30 °C. The documentation took place every 24 h.

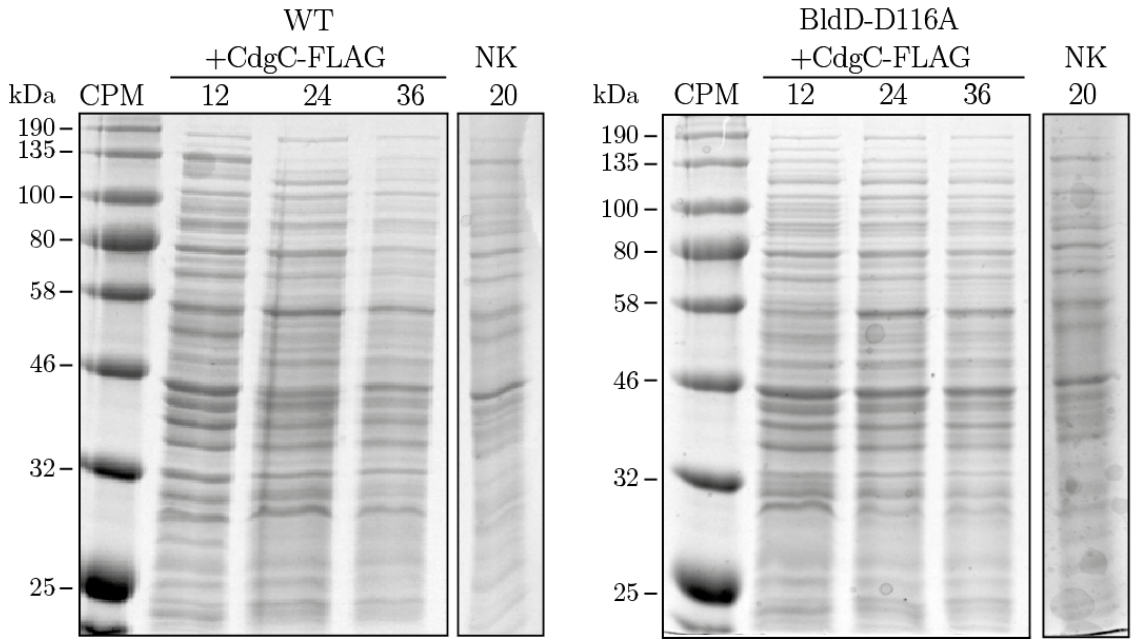

Fig. 6.2 Loading controls for western blot analysis of the expression of CdgC-FLAG in BldD_D116A. Protein samples were harvested from *S. venezuelae* WT and BldD_D116A conjugated with p3xFLAG-*cdgC* for the immunodetection against CdgC-FLAG after 12, 24 and 36 h at 30 °C on MYM solid culture inoculated with an initial spore concentration of 10^6 CFU/mL. *S. venezuelae* WT incubated for 20 h served as a negative control. A total protein amount of 20 µg per sample was separated via SDS-PAGE. CPM - color prestained marker

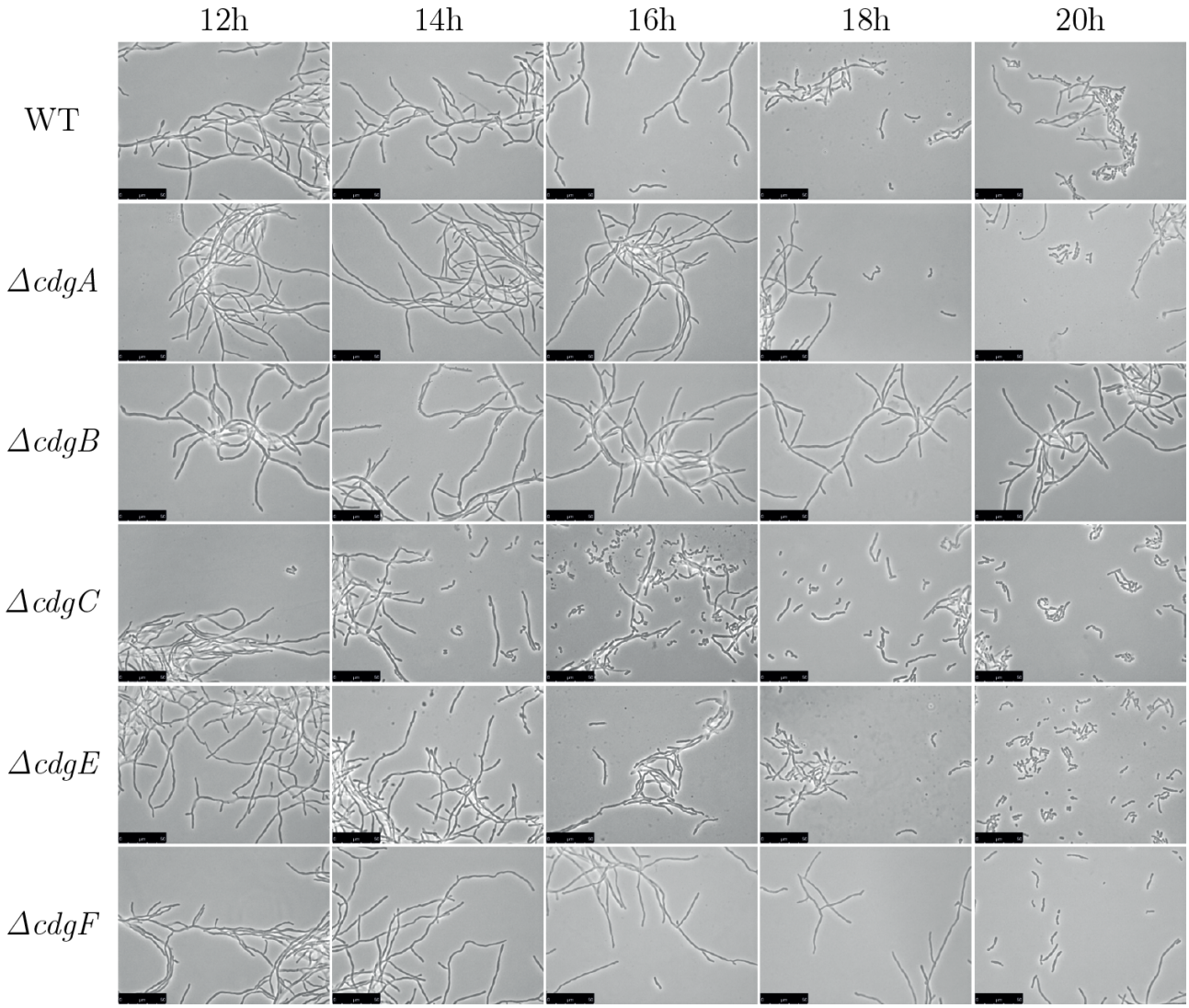

Fig. 6.3 The simultaneous enzymatic inactivity of CdgB and CdgC results in enlarged spores and an apparent inhibition of apical growth as well as branching of the mycelium. *S. venezuelae* WT, Δ*cdgA*, Δ*cdgB*, Δ*cdgC*, Δ*cdgE* and Δ*cdgF* were inoculated in MYM liquid culture to a spore concentration of 10^6 CFU/mL respectively. Incubation took place at 30 °C and 170 rpm and samples were harvested every 2 h from 12 to 20 h. Microscopic images were documented under a 100x phase contrast objective. The black scale indicates a length of 50 µm.

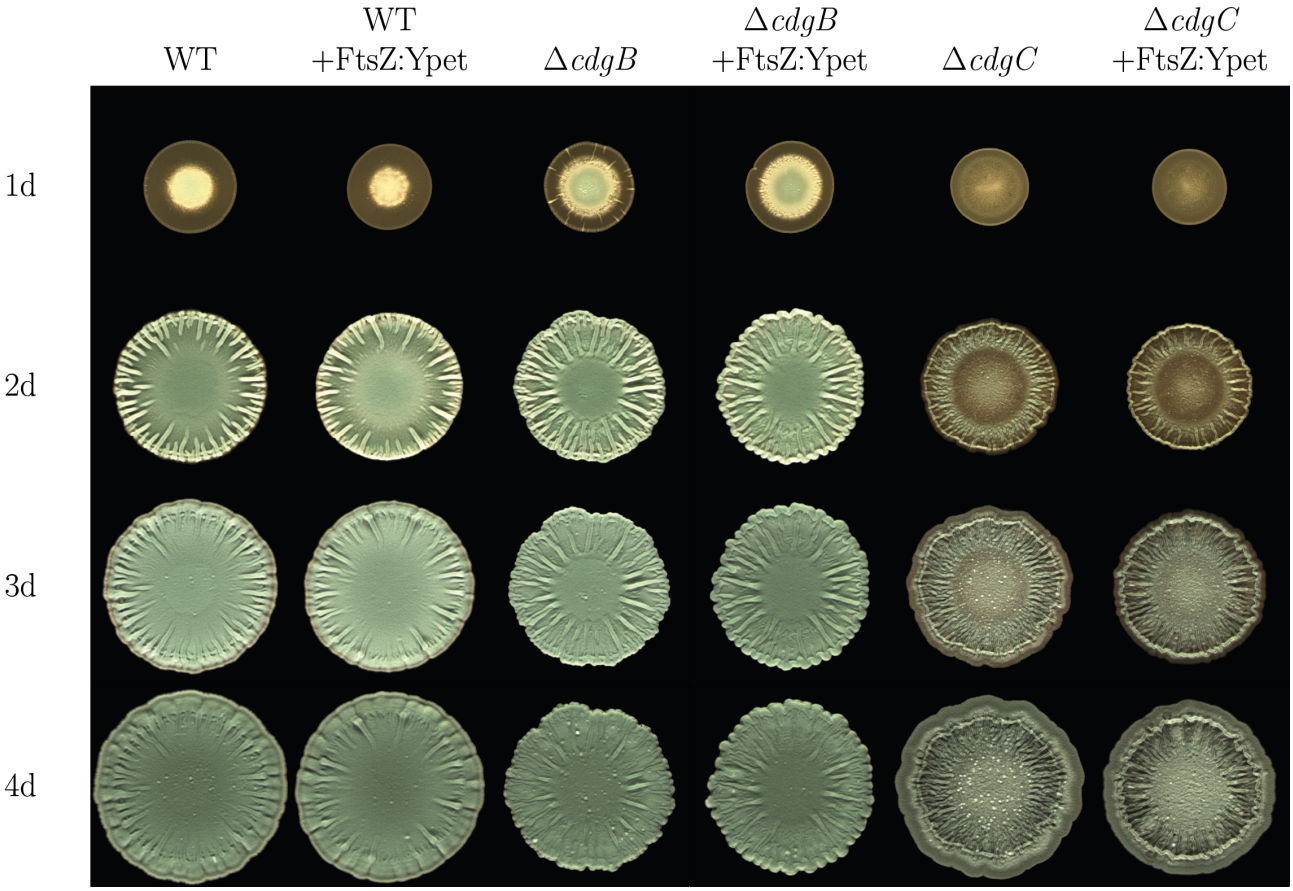

Fig. 6.4 Expression of the FtsZ:YPet fusion does not alter the morphology of Δ*cdgB* or Δ*cdgC*. Macrocolonies of *S. venezuelae* WT, Δ*cdgB* and Δ*cdgC* with and without pSS5 (FtsZ:Ypet) created through drip of 12 µL $2 \cdot 10^5$ CFU/µL spores on MYM agar and plates were incubated for 4 d at 30 °C. The documentation took place every 24 h.

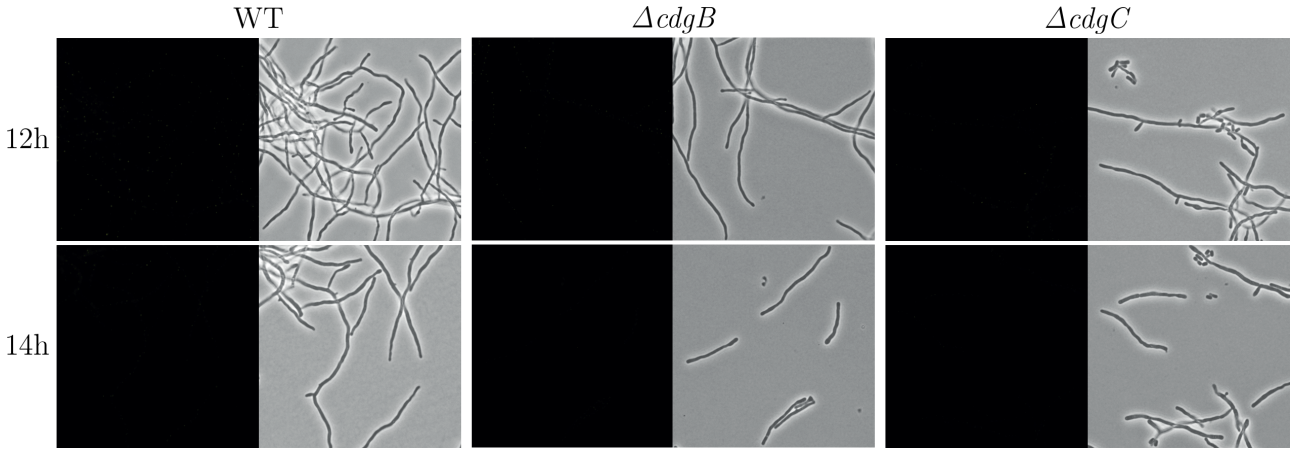

Fig. 6.5 CdgB and CdgC influence the formation of FtsZ-dependent Z-rings. (negative controls) Confocal microscopic analysis of the expression pattern of a FtsZ:Ypet fusion protein under the control of its native promoter integrated into *S. venezuelae* WT, Δ*cdgB* and Δ*cdgC* respectively. *S. venezuelae* strains without plasmid served as a control for autofluorescens at this wavelength and were inoculated in MYM liquid culture to a spore concentration of 10^6 CFU/mL, respectively. Incubation took place at 30 °C and 170 rpm and samples were harvested after 12 and 14 h. Microscopic images were documented under a 100x phase contrast objective with or without a Ypet filter.

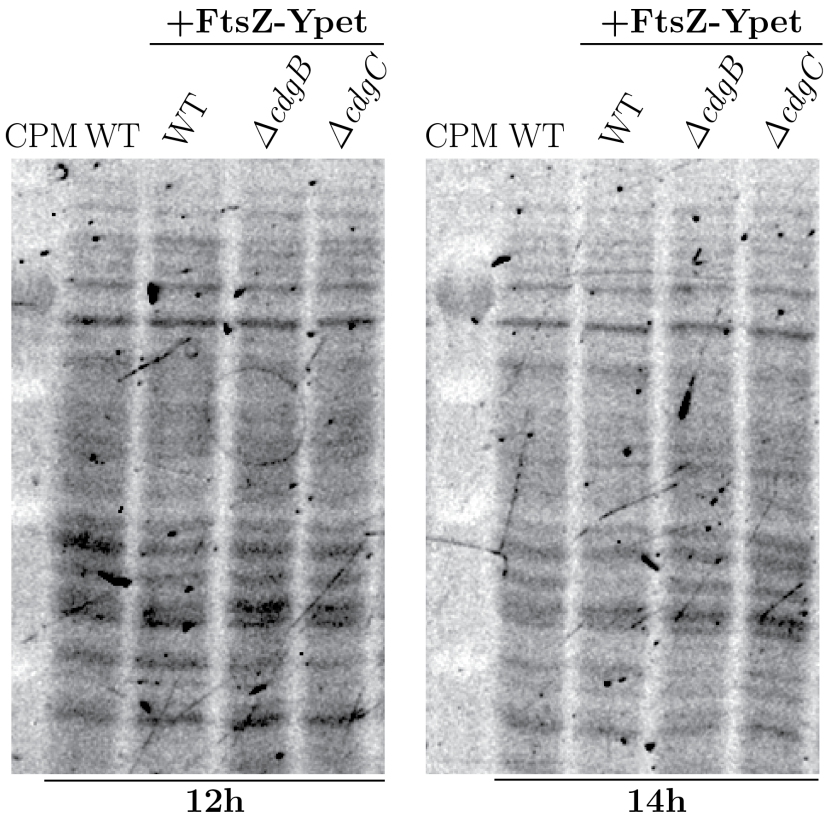

Fig. 6.6 Loading controls for Western blot analysis of the expression pattern of FtsZ:Ypet in Δ*cdgB* and Δ*cdgC*. FtsZ allele C-terminally fused to the Ypet protein cloned under the control of its native promotor on pIJ10750 was introduced into *S. venezuelae* WT, Δ*cdgB* and Δ*cdgC* and expressed from the ΦBT1 integration site. Strains were inoculated in MYM liquid culture to a spore concentration of 10^6 CFU/mL, respectively. Incubation took place at 30 °C and 170 rpm and samples were harvested after 12 and 14 h. Whole cell extracts were prepared as described in Schlimpert et al. (2017). The only deviation from this procedure is the addition of 2,2,2-Trichloroethanol (TCE) to the SDS gel solution for protein visualization as described in Ladner et al. (2004). Proteins were concentrations were determined via Bradford assay (Roth). After loading 14 µg of total protein per sample the cellular FtsZ:Ypet levels were incubated under ultraviolet light for five min processing time to induce a fluorescence emitting reaction of the tryptophan residues in the proteins with trihalocompounds detectable at 300 nm under the Multiimage® II UV camera (Alpha Innotech Corporation). The left part of this figure (12h) was modified with permission after Haist et al. (2020); published in Molecular Microbiology under the CC BY license Attribution 4.0 International License.

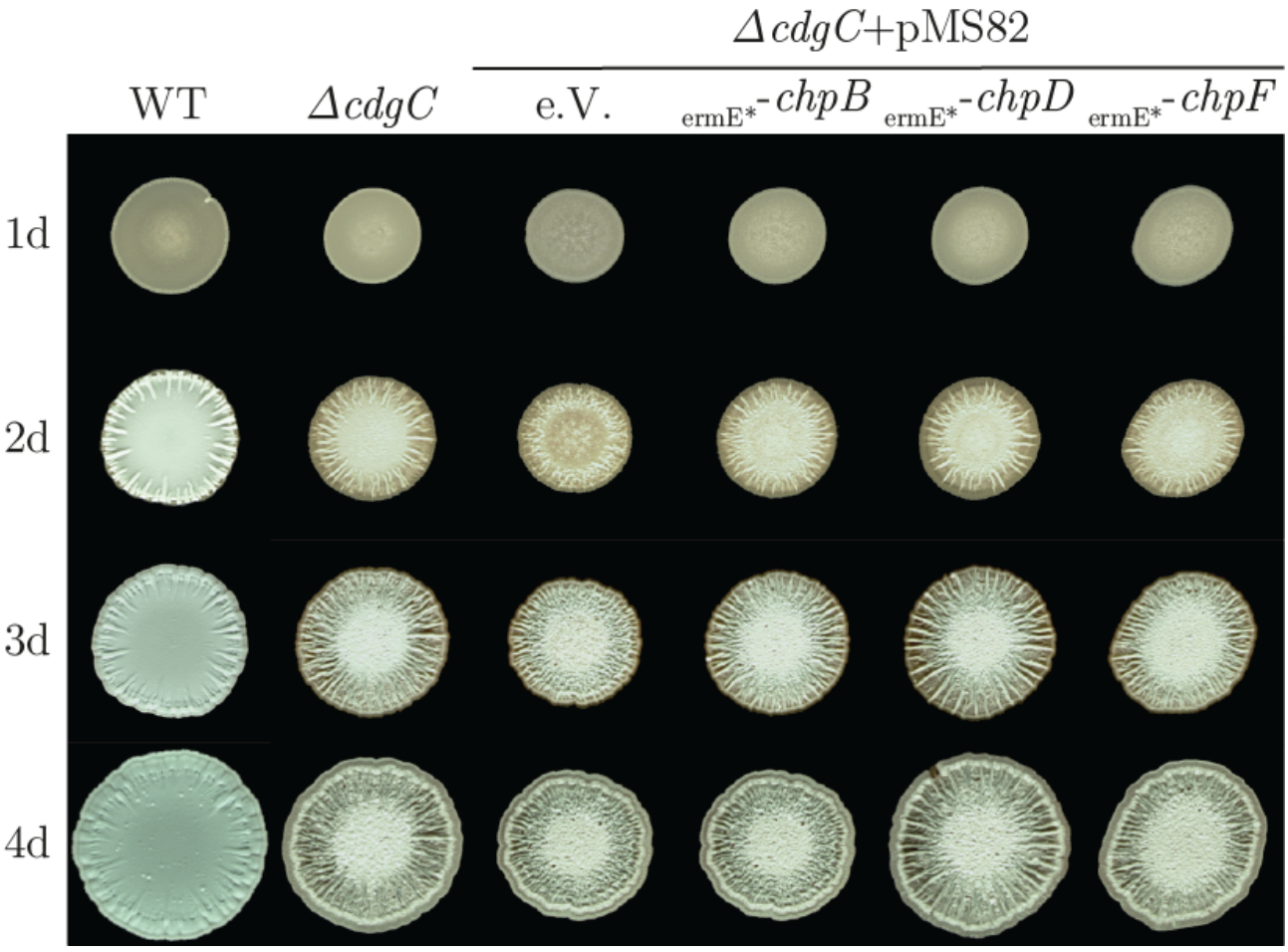

Fig. 6.7 Overexpression of neither ChpB, ChpD nor ChpF is sufficient to complement the hypersporulation in Δ*cdgC*. Macrocolonies of *S. venezuelae* wild type (WT) and Δ*cdgC* as well as Δ*cdgC* with pMS82$_{ermE*}$-*chpB/D/F* respectively were created through drip of 12 µL $2 \cdot 10^5$ CFU/µL spores on MYM agar and plates were incubated for 4 d at 30 °C. The documentation took place every 24 h. This figure was modified with permission after Haist et al. (2020); published in Molecular Microbiology under the CC BY license Attribution 4.0 International License.

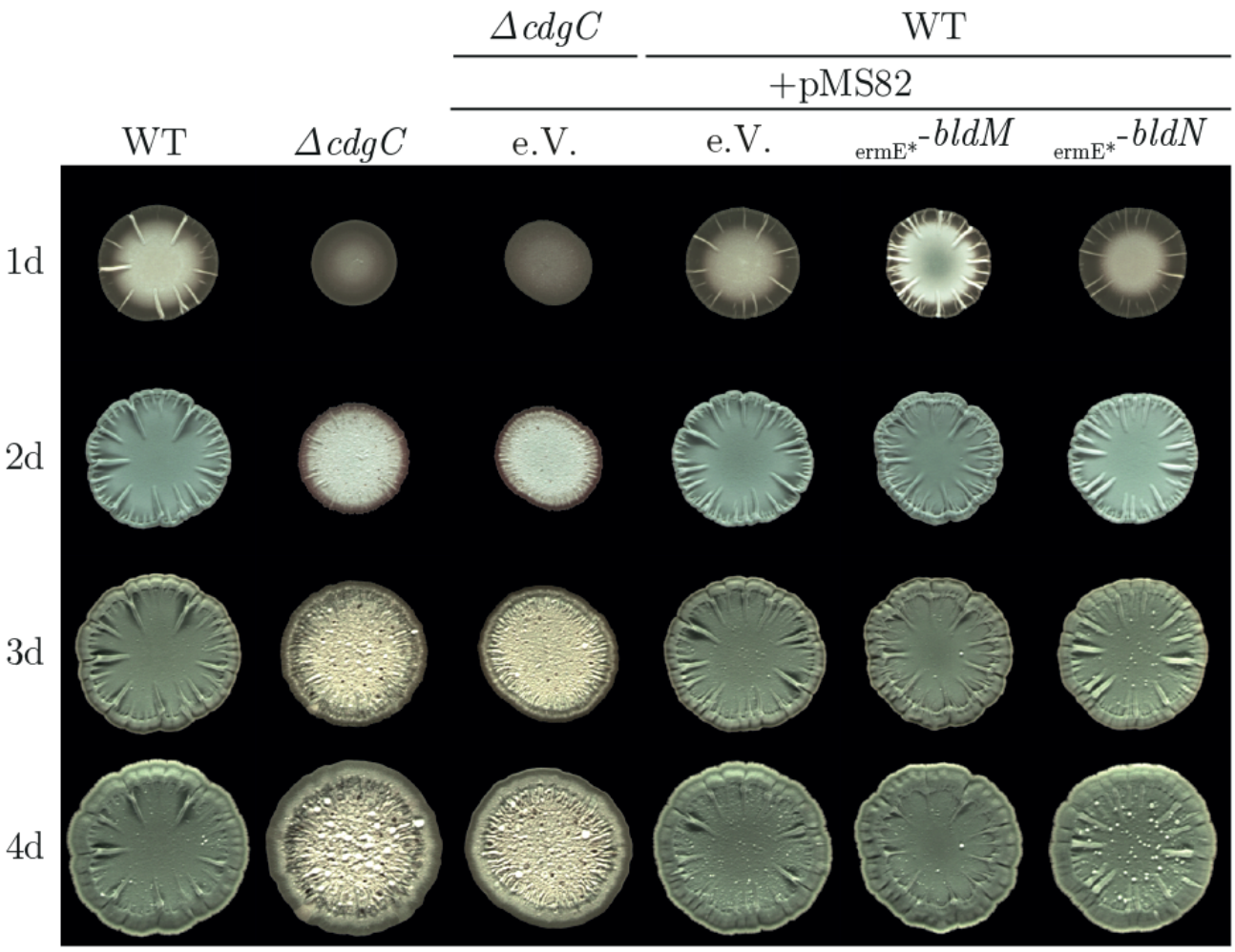

Fig. 6.8 Overexpression of neither BldN nor BldM alters the wild type phenotype significantly. Macrocolonies of *S. venezuelae* WT and Δ*cdgC* as well as the wild type with pMS82_*ermE**-*bldM/N*, respectively, were created through drip of 12 µL $2 \cdot 10^5$ CFU/µL spores on MYM agar and plates were incubated for 4 d at 30 °C. The documentation took place every 24 h.

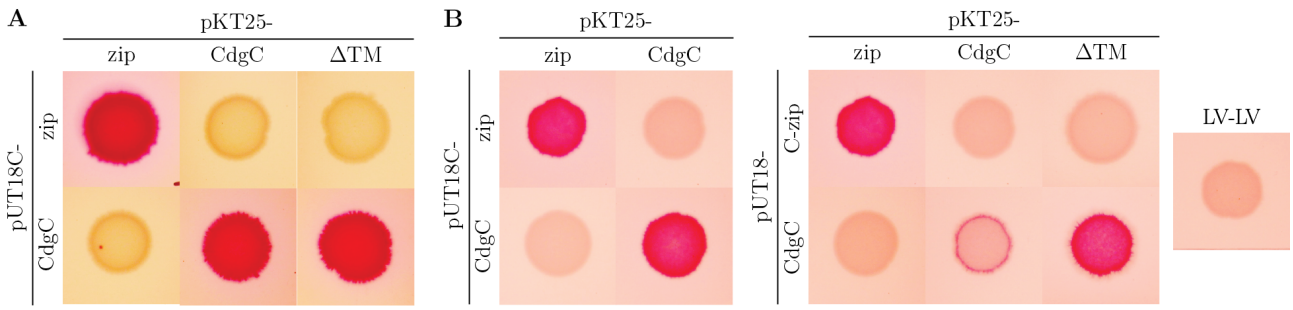

Fig. 6.9 CdgC forms homodimers supported by the transmembrane anchor and the `EAL` domain. *In vivo* protein-protein interaction assays after Karimova et al. (1998). Fusion proteins of different variants of CdgC on complementary BTH plasmids (T25 N-terminally and T18 N- or C-terminally of the peptide of interest) were co-expressed in *E. coli* W3110 Δ*cyaA*. Three colonies per tested combination were suspended in 1 mL 1xPBS, 5 µL bacterial suspension dropped on MacConkey (A: Difco, 1% maltose + Amp + Kan; B: Roth, Amp + Kan) and incubated at 26 °C for (A) 90 or (B) 43 h. Interactions of the fusion proteins complement the *cyaA* deletion, this enables the fermentation of the added carbon source. By adding phenol red as a pH indicator acidification is visible. zip-zip - dimerization of the leucine zipper region of the yeast protein GCN4 (positive control); LV-LV - empty vector combination pKT25 - pUT18 (negative control); ΔTM-CdgC - without the ten transmembrane domains

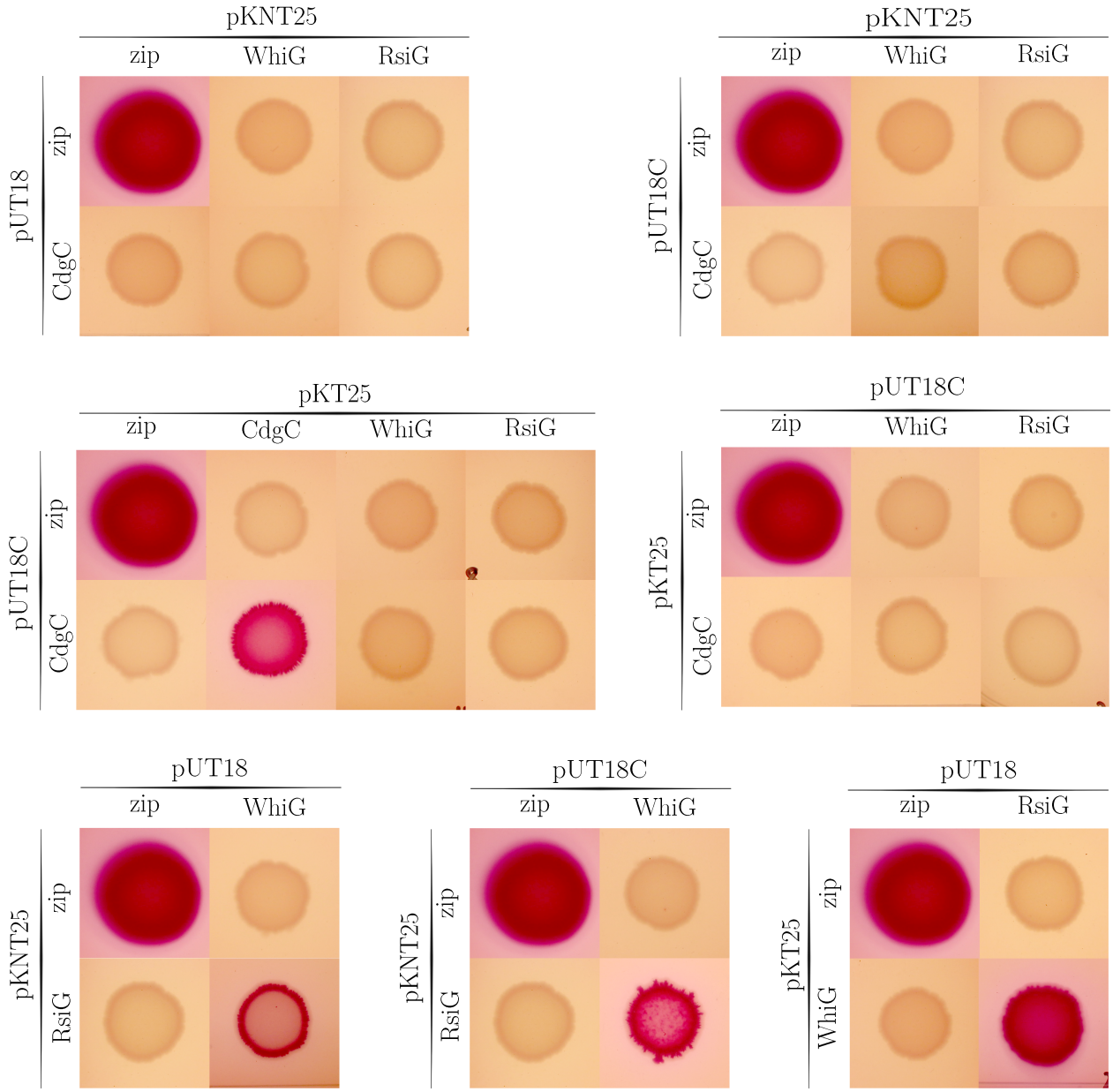

Fig. 6.10 RsiG and WhiG interact with each other, but not with CdgC. *In vivo* protein-protein interaction assays after Karimova et al. (1998). Fusion proteins on complementary BTH plasmids were co-expressed in *E. coli* W3110 Δ*cyaA*. Three colonies per tested combination were suspended in 1 mL 1xPBS, 5 µL bacterial suspension dropped on MacConkey (Difco, 1% maltose + Amp + Kan) and incubated for 108 h at 26 °C. Interactions of the fusion proteins complement the *cyaA* deletion, this enables the fermentation of the added carbon source. By adding phenol red as a pH indicator acidification is visible. zip-zip - dimerization of the leucine zipper region of the yeast protein GCN4 (positive control)

.

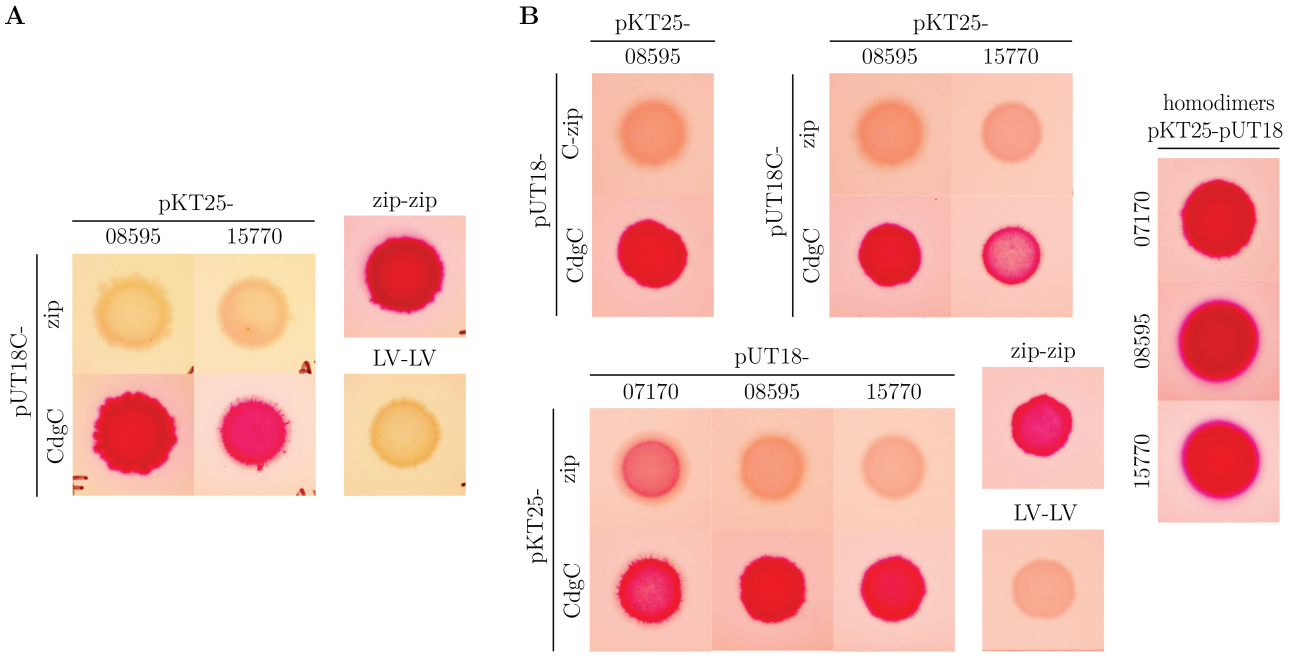

Fig. 6.11 CdgC binds the three membrane proteins Vnz07170, Vnz08595 and Vnz15770, that form homodimers, respectively. *In vivo* protein-protein interaction assays after Karimova et al. (1998). Fusion proteins on complementary BTH plasmids were co-expressed in *E. coli* W3110 Δ*cyaA*. Three colonies per tested combination were suspended in 1 mL 1xPBS, 5 µL bacterial suspension dropped on MacConkey (A: Difco, 1% maltose + Amp + Kan; B: Roth, Amp + Kan) and incubated at 26 °C for (A) 108 or (B) 43 h. Interactions of the fusion proteins complement the *cyaA* deletion, this enables the fermentation of the added carbon source. By adding phenol red as a pH indicator acidification is visible. zip-zip - dimerization of the leucine zipper region of the yeast protein GCN4 (positive control)

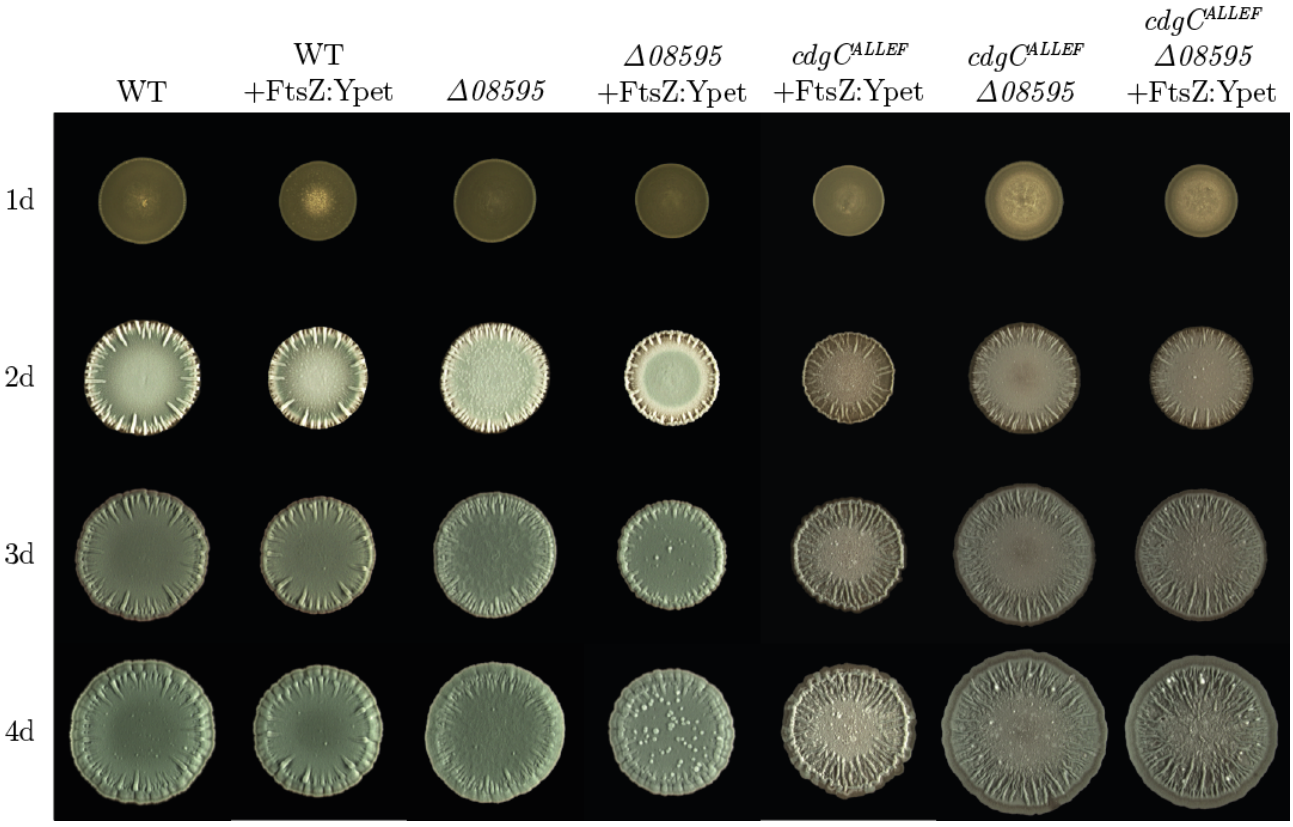

Fig. 6.12 Expression of the FtsZ:YPet fusion does not alter the colony morphology. Macrocolonies of *S. venezuelae* WT, Δ*vnz08595*, Δ*cdgC*, *cdgC*-GGDEF::ALLEF (*cdgC*^{ALLEF}) and *cdgC*-GGDEF::ALLEFΔ*vnz08595* (*cdgC*^{ALLEF}Δ*vnz08595*) with and without pSS5 (FtsZ:Ypet) created through drip of 12 µL $2 \cdot 10^5$ CFU/µL spores on MYM agar and plates were incubated for 4 d at 30 °C. The documentation took place every 24 h.

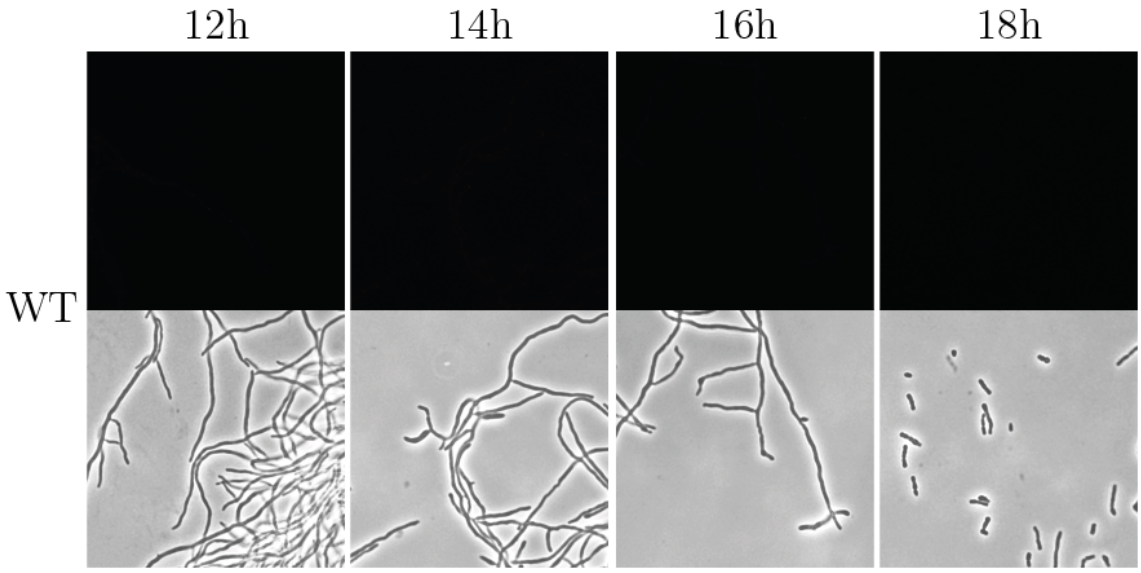

Fig. 6.13 The formation of FtsZ-dependent Z-rings seems to be delayed in the absence of *vnz08595* and increased in the absence of CdgC. (negative control) Confocal microscopic analysis of *S. venezuelae* WT. For the microscopic analysis *S. venezuelae* wild type without plasmid served as a control for autofluorescens at this wavelength and were inoculated in MYM liquid culture to a spore concentration of 10^6 CFU/mL, respectively. Incubation took place at 30 °C and 170 rpm and samples were harvested from 12-18 h every 2 h. Microscopic images were documented under a 100x phase contrast objective with or without a Ypet filter.

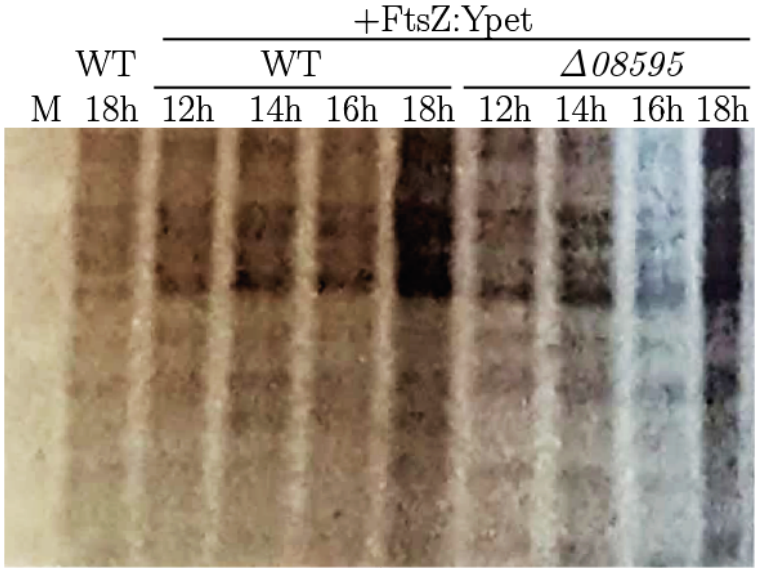

Fig. 6.14 Loading controls for western blot analysis of the expression pattern of FtsZ:Ypet in wildtype and Δ*08595*. FtsZ allele C-terminally fused to the Ypet protein cloned under the control of its native promotor on pIJ10750 was introduced into *S. venezuelae* WT and Δ*08595* and expressed from the ΦBT1 integration site. Strains were inoculated in MYM liquid culture to a spore concentration of 10^6 CFU/mL, respectively. Incubation took place at 30 °C and 170 rpm and samples were harvested after 12, 14, 16 and 18 h. *S. venezuelae* WT incubated for 18 h served as a negative control. Whole cell extracts were prepared as described in Schlimpert et al. (2017). The only deviation from this procedure is the addition of 2,2,2-Trichloroethanol (TCE) to the SDS gel solution for protein visualization as described in Ladner et al. (2004). Proteins were concentrations were determined via Bradford assay (Roth). After loading 15 µg of total protein per sample the cellular FtsZ:Ypet levels were incubated under ultraviolet light for five min processing time to induce a fluorescence emitting reaction of the tryptophan residues in the proteins with trihalocompounds detectable at 300 nm under the Multiimage® II UV camera (Alpha Innotech Corporation).

Bibliography

van der Aart, L. T., Spijksma, G. K., Harms, A., Vollmer, W., Hankemeier, T., & van Wezel, G. P. (2018). High-Resolution Analysis of the Peptidoglycan Composition in *Streptomyces coelicolor*. *Journal of Bacteriology*, *200*(20). American Society for Microbiology Journals.

Al-Bassam, M. M., Bibb, M. J., Bush, M. J., Chandra, G., & Buttner, M. J. (2014). Response Regulator Heterodimer Formation Controls a Key Stage in *Streptomyces* Development. *PLOS Genetics*, *10*(8), 1–11. Public Library of Science.

Al-Bassam, M. M., Haist, J., Neumann, S. A., Lindenberg, S., & Tschowri, N. (2018). Expression Patterns, Genomic Conservation and Input Into Developmental Regulation of the `GGDEF/EAL/HD-GYP` Domain Proteins in *Streptomyces*. *Frontiers in Microbiology*, *9*, 2524. Frontiers Media SA.

Amikam, D., & Galperin, M. Y. (2005). PilZ domain is part of the bacterial c-di-GMP binding protein. *Bioinformatics*, *22*(1), 3–6. Oxford University Press.

Anderl, A., Kolmar, H., & Fuchsbauer, H.-L. (2020). The metal-binding properties of the long chaplin from *Streptomyces mobaraensis*: A bioinformatic and biochemical approach. *Journal of Inorganic Biochemistry*, *202*, 110878. Elsevier B.V.

Ausmees, N., Mayer, R., Weinhouse, H., Volman, G., Amikam, D., Benziman, M., & Lindberg, M. (2001). Genetic data indicate that proteins containing the `GGDEF` domain possess diguanylate cyclase activity. *FEMS Microbiology Letters*, *204*(1), 163–167. Oxford University Press.

Ausmees, N., Wahlstedt, H., Bagchi, S., Elliot, M. A., Buttner, M. J., & Flärdh, K. (2007). SmeA, a small membrane protein with multiple functions in *Streptomyces* sporulation including targeting of a SpoIIIE/FtsK-like protein to cell division septa. *Molecular Microbiology*, *65*(6), 1458–1473. Wiley Online Library.

Bagchi, S., Tomenius, H., Belova, L. M., & Ausmees, N. (2008). Intermediate filament-like proteins in bacteria and a cytoskeletal function in *Streptomyces*. *Molecular Microbiology*, *70*(4), 1037–1050. Wiley Online Library.

Becher, P. G., Verschut, V., Bibb, M. J., Bush, M. J., Molnár, B. P., Barane, E., Al-Bassam, M. M., Chandra, G., Song, L., Challis, G. L., et al. (2020). Developmentally regulated volatiles geosmin and 2-methylisoborneol attract a soil arthropod to *Streptomyces* bacteria promoting spore dispersal. *Nature Microbiology*, *5*(6), 821–829. Springer Nature.

Benach, J., Swaminathan, S. S., Tamayo, R., Handelman, S. K., Folta-Stogniew, E., Ramos, J. E., Forouhar, F., Neely, H., Seetharaman, J., Camilli, A., & Hunt, J. F. (2007). The structural basis of cyclic diguanylate signal transduction by PilZ domains. *The EMBO Journal*, *26*(24), 5153–5166. EMBO Press.

Bentley, S. D., Chater, K. F., Cerden-Tárraga, A.-M., Challis, G. L., Thomson, N. R., James, K. D., Harris, D. E., Quail, M. A., Kieser, H., Harper, D., et al. (2002). Complete genome sequence of the model actinomycete *Streptomyces coelicolor* A3(2). *Nature*, *417*, 141–147. Macmillan Magazines Ltd.

Bi, E., & Lutkenhaus, J. (1991). FtsZ ring structure associated with division in *Escherichia coli*. *Nature*, *354*(6349), 161–4. Nature Publishing Group.

Bibb, M. J., & Buttner, M. J. (2003). The *Streptomyces coelicolor* Developmental Transcription Factor σ^{BldN} is Synthesized as a Proprotein. *Journal of Bacteriology*, *185*(7), 2338–2345. American Society for Microbiology Journals.

Bibb, M. J., Domonkos, A., Chandra, G., & Buttner, M. J. (2012). Expression of the chaplin and rodlin hydrophobic sheath proteins in *Streptomyces venezuelae* is controlled by σ^{BldN} and a cognate anti-sigma factor, RsbN. *Molecular Microbiology*, *84*(6), 1033–1049. Wiley Online Library.

Bobek, J., Halada, P., Angelis, J., Vohradský, J., & Mikulík, K. (2004). Activation and expression of proteins during synchronous germination of aerial spores of *Streptomyces granaticolor*. *PROTEOMICS*, *4*(12), 3864–3880. Wiley Online Library.

Bobek, J., Šmídová, K., & Čihák, M. (2017). A Waking Review: Old and Novel Insights into the Spore Germination in *Streptomyces*. *Frontiers in Microbiology*, *8*, 2205. Frontiers Media SA.

Bokhove, M., Claessen, D., de Jong, W., Dijkhuizen, L., Boekema, E. J., & Oostergetel, G. T. (2013). Chaplins of *Streptomyces coelicolor* self-assemble into two distinct functional amyloids. *Journal of Structural Biology*, *184*(2), 301–309. Elsevier B.V.

Bordeleau, E., Fortier, L.-C., Malouin, F., & Burrus, V. (2011). c-di-GMP Turn-Over in *Clostridium difficile* Is Controlled by a Plethora of Diguanylate Cyclases and Phosphodiesterases. *PLOS Genetics*, *7*(3), 1–12. Public Library of Science.

Boyd, C. D., & O'Toole, G. A. (2012). Second Messenger Regulation of Biofilm Formation: Breakthroughs in Understanding c-di-GMP Effector Systems. *Annual Review of Cell and Developmental Biology*, *28*(1), 439–462. Annual Reviews.

Burger, A., Sichler, K., Kelemen, G., Buttner, M., & Wohlleben, W. (2000). Identification and characterization of the mre gene region of *Streptomyces coelicolor* A3(2). *Molecular and General Genetics MGG*, *263*(6), 1053–60. Springer-Verlag GmbH.

Bush, M. J., Bibb, M. J., Chandra, G., Findlay, K. C., & Buttner, M. J. (2013). Genes Required for Aerial Growth, Cell Division, and Chromosome Segregation Are Targets of WhiA before Sporulation in *Streptomyces venezuelae*. *mBio*, *4*(5). American Society for Microbiology.

Bush, M. J., Chandra, G., Al-Bassam, M. M., Findlay, K. C., & Buttner, M. J. (2019). BldC Delays Entry into Development To Produce a Sustained Period of Vegetative Growth in *Streptomyces venezuelae*. *mBio*, *10*(1). American Society for Microbiology.

Bush, M. J., Chandra, G., Bibb, M. J., Findlay, K. C., & Buttner, M. J. (2016). Genome-Wide Chromatin Immunoprecipitation Sequencing Analysis Shows that WhiB Is a Transcription Factor That Cocontrols Its Regulon with WhiA To Initiate Developmental Cell Division in *Streptomyces*. *mBio*, *7*(2). American Society for Microbiology.

Bush, M. J., Chandra, G., Findlay, K., & Buttner, M. J. (2017). Multi-layered inhibition of *Streptomyces* development: BldO is a dedicated repressor of *whiB*. *Molecular Microbiology*, *104*(5), 700–711. Wiley Online Library.

Bush, M. J., Tschowri, N., Schlimpert, S., Flärdh, K., & Buttner, M. J. (2015). C-di-GMP signalling and the regulation of developmental transitions in Streptomycetes. *Nature Reviews Microbiology*, *13*, 749–760. Macmillan Publishers Limited.

Capstick, D. S., Willey, J. M., Buttner, M. J., & Elliot, M. A. (2007). SapB and the chaplins: connections between morphogenetic proteins in *Streptomyces coelicolor*. *Molecular Microbiology*, *64*(3), 602–613. Wiley Online Library.

Chan, C., Paul, R., Samoray, D., Amiot, N. C., Giese, B., Jenal, U., & Schirmer, T. (2004). Structural basis of activity and allosteric control of diguanylate cyclase. *Proceedings of the National Academy of Sciences*, *101*(49), 17084–17089. National Academy of Sciences.

Chater, K. F. (1972). A Morphological and Genetic Mapping Study of White Colony Mutants of *Streptomyces coelicolor*. *Microbiology*, *72*(1), 9–28. Microbiology Society.

Christen, M., Christen, B., Folcher, M., Schauerte, A., & Jenal, U. (2005). Identification and characterization of a cyclic di-GMP-specific phosphodiesterase and its allosteric control by GTP. *The Journal of Biological Chemistry*, *280*(35), 30829–30837. ASBMB Publications.

Chung, C. T., Niemela, S. L., & Miller, R. H. (1989). One-step preparation of competent *Escherichia coli*: transformation and storage of bacterial cells in the same solution. *Proceedings of the National Academy of Sciences*, *86*(7), 2172–2175. National Academy of Sciences.

Claessen, D., Rink, R., de Jong, W., Siebring, J., de Vreugd, P., Boersma, F. H., Dijkhuizen, L., & Wösten, H. A. (2003). A novel class of secreted hydrophobic proteins is involved in aerial hyphae formation in *Streptomyces coelicolor* by forming amyloid-like fibrils. *Genes & Development*, *17*(14), 1714–1726. Cold Spring Harbor Laboratory Press.

Claessen, D., Rozen, D., Kuipers, O., Søgaard-Andersen, L., & van Wezel, G. P. (2014). Bacterial solutions to multicellularity: a tale of biofilms, filaments and fruiting bodies. *Nature Reviews Microbiology*, *12*, 115–124. Macmillan Publishers Limited.

Claessen, D., Stokroos, I., Deelstra, H. J., Penninga, N. A., Bormann, C., Salas, J. A., Dijkhuizen, L., & Wösten, H. A. B. (2004). The formation of the rodlet layer of streptomycetes is the result of the interplay between rodlins and chaplins. *Molecular Microbiology*, *53*(2), 433–443. Wiley Online Library.

Claessen, D., Wösten, H. A. B., Keulen, G. v., Faber, O. G., Alves, A. M. C. R., Meijer, W. G., & Dijkhuizen, L. (2002). Two novel homologous proteins of *Streptomyces coelicolor* and *Streptomyces lividans* are involved in the formation of the rodlet layer and mediate attachment to a hydrophobic surface. *Molecular Microbiology*, *44*(6), 1483–1492. Wiley Online Library.

Cohen, D., Mechold, U., Nevenzal, H., Yarmiyhu, Y., Randall, T. E., Bay, D. C., Rich, J. D., Parsek, M. R., Kaever, V., Harrison, J. J., & Banin, E. (2015). Oligoribonuclease is a central feature of cyclic diguanylate signaling in *Pseudomonas aeruginosa*. *Proceedings of the National Academy of Sciences*, *112*(36), 11359–11364. National Academy of Sciences.

Craney, A., Hohenauer, T., Xu, Y., Navani, N. K., Li, Y., & Nodwell, J. (2007). A synthetic *luxCDABE* gene cluster optimized for expression in high-GC bacteria. *Nucleic Acids Research*, *35*(6), e46–e46. Oxford University Press.

Das, S., & Dash, H. (2015). *Microbial Biotechnology - A Laboratory Manual for Bacterial Systems*. Springer India.

Datsenko, K. A., & Wanner, B. L. (2000). One-step inactivation of chromosomal genes in *Escherichia coli* K-12 using PCR products. *Proceedings of the National Academy of Sciences*, *97*(12), 6640–6645. National Academy of Sciences.

Davis, N., & Chater, K. (1992). The *Streptomyces coelicolor whiB* gene encodes a small transcription factor-like protein dispensable for growth but essential for sporulation. *Molecular and General Genetics MGG*, *232*, 351–358. Springer Link.

Daßler, T., Maier, T., Winterhalter, C., & Böck, A. (2000). Identification of a major facilitator protein from *Escherichia coli* involved in efflux of metabolites of the cysteine pathway. *Molecular Microbiology*, *36*(5), 1101–1112. Wiley Online Library.

Den Hengst, C. D., Tran, N. T., Bibb, M. J., Chandra, G., Leskiw, B. K., & Buttner, M. J. (2010). Genes essential for morphological development and antibiotic production in *Streptomyces coelicolor* are targets of BldD during vegetative growth. *Molecular Microbiology*, *78*(2), 361–379. Wiley Online Library.

Di Berardo, C., Capstick, D. S., Bibb, M. J., Findlay, K. C., Buttner, M. J., & Elliot, M. A. (2008). Function and Redundancy of the Chaplin Cell Surface Proteins in Aerial Hypha Formation, Rodlet Assembly, and Viability in *Streptomyces coelicolor*. *Journal of Bacteriology*, *190*(17), 5879–5889. American Society for Microbiology Journals.

Ditkowski, B., Holmes, N., Rydzak, J., Donczew, M., Bezulska, M., Ginda, K., Kędzierski, P., Zakrzewska-Czerwińska, J., Kelemen, G. H., & Jakimowicz, D. (2013). Dynamic interplay of ParA with the polarity protein, Scy, coordinates the growth with chromosome segregation in *Streptomyces coelicolor*. *Open Biology*, *3*(3), 130006. Royal Society Publishing.

Dragoš, A., Kovács, Á. T., & Claessen, D. (2017). The Role of Functional Amyloids in Multicellular Growth and Development of Gram-Positive Bacteria. *Biomolecules*, *7*(3). MDPI Publishing.

Duong, A., Capstick, D. S., Di Berardo, C., Findlay, K. C., Hesketh, A., Hong, H.-J., & Elliot, M. A. (2012). Aerial development in *Streptomyces coelicolor* requires sortase activity. *Molecular Microbiology*, *83*(5), 992–1005. Wiley Online Library.

Elliot, M. A., Bibb, M. J., Buttner, M. J., & Leskiw, B. K. (2001). BldD is a direct regulator of key developmental genes in *Streptomyces coelicolor* A3(2). *Molecular Microbiology*, *40*(1), 257–269. Wiley Online Library.

Elliot, M. A., Karoonuthaisiri, N., Huang, J., Bibb, M. J., Cohen, S. N., Kao, C. M., & Buttner, M. J. (2003). The chaplins: a family of hydrophobic cell-surface proteins involved in aerial mycelium formation in *Streptomyces coelicolor*. *Genes & Development*, *17*(14), 1727–1740. Cold Spring Harbor Laboratory Press.

Flärdh, K. (2003). Essential role of DivIVA in polar growth and morphogenesis in *Streptomyces coelicolor* A3(2). *Molecular Microbiology*, *49*(6), 1523–1536. Wiley Online Library.

Flärdh, K., Leibovitz, E., Buttner, M. J., & Chater, K. F. (2000). Generation of a non-sporulating strain of *Streptomyces coelicolor* A3(2) by the manipulation of a developmentally controlled *ftsZ* promoter. *Molecular Microbiology*, *38*(4), 737–749. Wiley Online Library.

Flärdh, K., & McCormick, J. R. (2017). The Streptomyces O-B one connection: a force within layered repression of a key developmental decision. *Molecular Microbiology*, *104*(5), 695–699. Wiley Online Library.

Flärdh, K., Richards, D. M., Hempel, A. M., Howard, M., & Buttner, M. J. (2012). Regulation of apical growth and hyphal branching in *Streptomyces*. *Current Opinion in Microbiology*, *15*(6), 737–743. Elsevier B.V.

Franke, I., Resch, A., Daßler, T., Maier, T., & Böck, A. (2003). YfiK from *Escherichia coli* Promotes Export of O-Acetylserine and Cysteine. *Journal of Bacteriology*, *185*(4), 1161–1166. American Society for Microbiology Journals.

Fröjd, M. J., & Flärdh, K. (2019). Apical assemblies of intermediate filament-like protein FilP are highly dynamic and affect polar growth determinant DivIVA in *Streptomyces venezuelae*. *Molecular Microbiology*, *112*(1), 47–61. Wiley Online Library.

Gallagher, K. A., Schumacher, M. A., Bush, M. J., Bibb, M. J., Chandra, G., Holmes, N. A., Zeng, W., Henderson, M., Zhang, H., Findlay, K. C., Brennan, R. G., & Buttner, M. J. (2020). C-di-GMP Arms an Anti-σ to Control Progression of Multicellular Differentiation in *Streptomyces*. *Molecular Cell*, *77*(3), 586–599. Elsevier B.V.

Germani, F., Nardini, M., De Schutter, A., Cuypers, B., Berghmans, H., Van Hauwaert, M.-L., Bruno, S., Mozzarelli, A., Moens, L., Van Doorslaer, S., Bolognesi, M., Pesce, A., & Dewilde, S. (2020). Structural and Functional Characterization of the Globin-Coupled Sensors of *Azotobacter vinelandii* and *Bordetella pertussis*. *Antioxidants & Redox Signaling*, *32*(6), 378–395. Mary Ann Liebert, Inc., publishers.

Gimenez, R., Nuñez, M. F., Badia, J., Aguilar, J., & Baldoma, L. (2003). The Gene *yjcG*, Cotranscribed with the Gene *acs*, Encodes an Acetate Permease in *Escherichia coli*. *Journal of Bacteriology*, *185*(21), 6448–6455. American Society for Microbiology Journals.

Gregory, M. A., Till, R., & Smith, M. C. M. (2003). Integration Site for *Streptomyces* Phage ΦBT1 and Development of Site-Specific Integrating Vectors. *Journal of Bacteriology*, *185*(17), 5320–5323. American Society for Microbiology Journals.

Gruber, T. M., & Gross, C. A. (2003). Multiple Sigma Subunits and the Partitioning of Bacterial Transcription Space. *Annual Review of Microbiology*, *57*(1), 441–466. Annual Reviews.

Gust, B., Challis, G. L., Fowler, K., Kieser, T., & Chater, K. F. (2003). PCR-targeted *Streptomyces* gene replacement identifies a protein domain needed for biosynthesis of the sesquiterpene soil odor geosmin. *Proceedings of the National Academy of Sciences*, *100*(4), 1541–1546. National Academy of Sciences.

Haeusser, D., & Margolin, W. (2016). Splitsville: structural and functional insights into the dynamic bacterial Z ring. *Nature Reviews Microbiology*, *14*, 305–319. Macmillan Publishers Limited.

Haist, J., Neumann, S. A., Al-Bassam, M. M., Lindenberg, S., Elliot, M. A., & Tschowri, N. (2020). Specialized and shared functions of diguanylate cyclases and phosphodiesterases in *Streptomyces* development. *Molecular Microbiology*, *114*(5), 808–822. Wiley Online Library.

Han, L., Yang, K., Ramalingam, E., Mosher, R. H., & Vining, L. C. (1994). Cloning and characterization of polyketide synthase genes for jadomycin B biosynthesis in *Streptomyces venezuelae* ISP5230. *Microbiology*, *140*(12), 3379–3389. Microbiology Society.

Hanahan, D., Jessee, J., & Bloom, F. R. (1991). Plasmid transformation of *Escherichia coli* and other bacteria. *Methods in enzymology*, *204*, 63—113. Elsevier B.V.

Hardisson, C., Manzanal, M.-B., Salas, J.-A., & Suárez, J.-E. (1978). Fine Structure, Physiology and Biochemistry of Arthrospore Germination in *Streptomyces antibioticus*. *Microbiology*, *105*(2), 203–214. Microbiology Society.

Hayashi, K., Morooka, N., Yamamoto, Y., Fujita, K., Isono, K., Choi, S., Ohtsubo, E., Baba, T., Wanner, B., Mori, H., & Horiuchi, T. (2006). Highly accurate genome sequences of *Escherichia coli* K-12 strains MG1655 and W3110. *Molecular Systems Biology*, *2*(1), 2006.0007. EMBO and Nature Publishing Group.

Hee, C.-S., Habazettl, J., Schmutz, C., Schirmer, T., Jenal, U., & Grzesiek, S. (2020). Intercepting second-messenger signaling by rationally designed peptides sequestering c-di-GMP. *Proceedings of the National Academy of Sciences*, *117*(29), 17211–17220. National Academy of Sciences.

Heichlinger, A., Ammelburg, M., Kleinschnitz, E.-M., Latus, A., Maldener, I., Flärdh, K., Wohlleben, W., & Muth, G. (2011). The MreB-Like Protein Mbl of *Streptomyces coelicolor* A3(2) Depends on MreB for Proper Localization and Contributes to Spore Wall Synthesis. *Journal of Bacteriology*, *193*(7), 1533–1542. American Society for Microbiology Journals.

Hempel, A. M., Wang, S.-b., Letek, M., Gil, J. A., & Flärdh, K. (2008). Assemblies of DivIVA Mark Sites for Hyphal Branching and Can Establish New Zones of Cell Wall Growth in *Streptomyces coelicolor*. *Journal of Bacteriology*, *190*(22), 7579–7583. American Society for Microbiology Journals.

Hengge, R. (2009). Principles of c-di-GMP signalling in bacteria. *Nature Reviews Microbiology*, *7*(4), 263–273. Macmillan Publishers Limited.

Higo, A., Hara, H., Horinouchi, S., & Ohnishi, Y. (2012). Genome-wide Distribution of AdpA, a Global Regulator for Secondary Metabolism and Morphological Differentiation in *Streptomyces*, Revealed the Extent and Complexity of the AdpA Regulatory Network. *DNA Research*, *19*(3), 259–274. Oxford University Press.

Higo, A., Horinouchi, S., & Ohnishi, Y. (2011). Strict regulation of morphological differentiation and secondary metabolism by a positive feedback loop between two global regulators AdpA and BldA in *Streptomyces griseus*. *Molecular Microbiology*, *81*(6), 1607–1622. Wiley Online Library.

Ho, Y.-S. J., Burden, L. M., & Hurley, J. H. (2000). Structure of the GAF domain, a ubiquitous signaling motif and a new class of cyclic GMP receptor. *The EMBO Journal*, *19*(20), 5288–5299. Oxford University Press.

Holmes, N. A., Walshaw, J., Leggett, R. M., Thibessard, A., Dalton, K. A., Gillespie, M. D., Hemmings, A. M., Gust, B., & Kelemen, G. H. (2013). Coiled-coil protein Scy is a key component of a multiprotein assembly controlling polarized growth in *Streptomyces*. *Proceedings of the National Academy of Sciences*, *110*(5), E397–E406. National Academy of Sciences.

Hopwood, D. A. (2007). *Streptomyces in Nature and Medicine: The Antibiotic Makers*. Oxford, New York: Oxford University Press.

Hoskisson, P. A., & Rigali, S. (2009). Chapter 1 Variation in Form and Function: The Helix-Turn-Helix Regulators of the GntR Superfamily. In *Advances in Applied Microbiology*, vol. 69, (pp. 1–22). Academic Press.

Hughes, E. D., Byrne, B. G., & Swanson, M. S. (2019). A Two-Component System That Modulates Cyclic di-GMP Metabolism Promotes *Legionella pneumophila* Differentiation and Viability in Low-Nutrient Conditions. *Journal of Bacteriology*, *201*(17). American Society for Microbiology Journals.

Hull, T. D., Ryu, M.-H., Sullivan, M. J., Johnson, R. C., Klena, N. T., Geiger, R. M., Gomelsky, M., & Bennett, J. A. (2012). Cyclic Di-GMP Phosphodiesterases RmdA and RmdB Are Involved in Regulating Colony Morphology and Development in *Streptomyces coelicolor*. *Journal of Bacteriology*, *194*(17), 4642–4651. American Society for Microbiology Journals.

Jakimowicz, P., Cheesman, M. R., Bishai, W. R., Chater, K. F., Thomson, A. J., & Buttner, M. J. (2005). Evidence That the *Streptomyces* Developmental Protein WhiD, a Member of the WhiB Family, Binds a [4Fe-4S] Cluster. *Journal of Biological Chemistry*, *280*(9), 8309–8315. ASBMB.

Jenal, U., & Malone, J. (2006). Mechanisms of Cyclic-di-GMP Signaling in Bacteria. *Annual Review of Genetics*, *40*(1), 385–407. Annual Reviews.

Jenal, U., Reinders, A., & Lori, C. (2017). Cyclic di-GMP: second messenger extraordinaire. *Nature*, *5*(15), 271–284. Nature Publishing Group.

Jones, S. E., Ho, L., Rees, C. A., Hill, J. E., Nodwell, J. R., & Elliot, M. A. (2017). *Streptomyces* exploration is triggered by fungal interactions and volatile signals. *eLife*, *6*, e21738. eLife Sciences Publications, Ltd.

Jones, S. E., Pham, C. A., McKillip, J., Zambri, M., Carlson, E. E., & Elliot, M. A. (2018). *Streptomyces* volatile compounds influence exploration and microbial community dynamics by altering iron availability. *bioRxiv*. Cold Spring Harbor Laboratory.

de Jong, W., Vijgenboom, E., Dijkhuizen, L., Wösten, H. A., & Claessen, D. (2012). SapB and the rodlins are required for development of *Streptomyces coelicolor* in high osmolarity media. *FEMS Microbiology Letters*, *329*(2), 154–159. Oxford University Press.

Kaczmarczyk, A., Hempel, A. M., von Arx, C., Böhm, R., Dubey, B. N., Nesper, J., Schirmer, T., Hiller, S., & Jenal, U. (2020). Precise timing of transcription by c-di-GMP coordinates cell cycle and morphogenesis in *Caulobacter*. *Nature Communications*, *816*(11). Springer Nature.

Karimova, G., Pidoux, J., Ullmann, A., & Ladant, D. (1998). A bacterial two-hybrid system based on a reconstituted signal transduction pathway. *Proceedings of the National Academy of Sciences*, *95*(10), 5752–5756. National Academy of Sciences.

Kelemen, G. H., Brian, P., Flärdh, K., Chamberlin, L., Chater, K. F., & Buttner, M. J. (1998). Developmental Regulation of Transcription of *whiE*, a Locus Specifying the Polyketide Spore Pigment in *Streptomyces coelicolor* A3(2). *Journal of Bacteriology*, *180*(9), 2515–2521. American Society for Microbiology Journals.

Kieser, T., Bibb, M. J., Buttner, M. J., Chater, K. F., Hopwood, D. A., et al. (2000). *Practical Streptomyces genetics*, vol. 291. John Innes Foundation Norwich.

Kim, I.-K., Lee, C.-J., Kim, M.-K., Kim, J.-M., Kim, J.-H., Yim, H.-S., Cha, S.-S., & Kang, S.-O. (2006). Crystal structure of the DNA-binding domain of BldD, a central regulator of aerial mycelium formation in *Streptomyces coelicolor* A3(2). *Molecular Microbiology*, *60*(5), 1179–1193. Wiley Online Library.

Kleinschnitz, E.-M., Heichlinger, A., Schirner, K., Winkler, J., Latus, A., Maldener, I., Wohlleben, W., & Muth, G. (2011). Proteins encoded by the *mre* gene cluster in *Streptomyces coelicolor* A3(2) cooperate in spore wall synthesis. *Molecular Microbiology*, *79*(5), 1367–1379. Wiley Online Library.

Kois-Ostrowska, A., Strzałka, A., Lipietta, N., Tilley, E., Zakrzewska-Czerwińska, J., Herron, P., & Jakimowicz, D. (2016). Unique Function of the Bacterial Chromosome Segregation Machinery in Apically Growing *Streptomyces* - Targeting the Chromosome to New Hyphal Tubes and its Anchorage at the Tips. *PLOS Genetics*, *12*(12), 1–25. Public Library of Science.

Kormanec, J., & Homerova, D. (1993). *Streptomyces aureofaciens whiB* gene encoding putative transcription factor essential for differentiation. *Nucleic Acids Research*, *21*(10), 2512–2512. Oxford University Press.

Ladner, C. L., Yang, J., Turner, R. J., & Edwards, R. A. (2004). Visible fluorescent detection of proteins in polyacrylamide gels without staining. *Analytical Biochemistry*, *326*(1), 13–20. Elsevier B.V.

Ladwig, N., Franz-Wachtel, M., Hezel, F., Soufi, B., Macek, B., Wohlleben, W., & Muth, G. (2015). Control of Morphological Differentiation of *Streptomyces coelicolor* A3(2) by Phosphorylation of MreC and PBP2. *PLOS ONE*, *10*(4), 1–21. Public Library of Science.

Laemmli, U. K. (1970). Cleavage of structural proteins during the assembly of the head of bacteriophage T4. *Nature*, *227*(5259), 680–5. Nature Publishing Group.

Letunic, I., & Bork, P. (2017). 20 years of the SMART protein domain annotation resource. *Nucleic Acids Research*, *46*(D1), D493–D496. Oxford University Press.

Letunic, I., Khedkar, S., & Bork, P. (2020). SMART: recent updates, new developments and status in 2020. *Nucleic Acids Research*. Oxford University Press.

Li, J., Wang, N., Tang, Y., Cai, X., Xu, Y., Liu, R., Wu, H., & Zhang, B. (2019). Developmental regulator BldD directly regulates lincomycin biosynthesis in *Streptomyces lincolnensis*. *Biochemical and Biophysical Research Communications*, *518*(3), 548–553. Elsevier B.V.

Lindenberg, S., Klauck, G., Pesavento, C., Klauck, E., & Hengge, R. (2013). The EAL domain protein YciR acts as a trigger enzyme in a c-di-GMP signalling cascade in *E. coli* biofilm control. *The EMBO Journal*, *32*(14), 2001–2014. Nature Publishing Group.

Liu, C., Liew, C. W., Wong, Y. H., Tan, S. T., Poh, W. H., Manimekalai, M. S. S., Rajan, S., Xin, L., Liang, Z.-X., Grüber, G., Rice, S. A., & Lescar, J. (2018). Insights into Biofilm Dispersal Regulation from the Crystal Structure of the PAS-GGDEF-EAL Region of RbdA from *Pseudomonas aeruginosa*. *Journal of Bacteriology*, *200*(3). American Society for Microbiology Journals.

Liu, X., Zheng, G., Wang, G., Jiang, W., Li, L., & Lu, Y. (2009). Overexpression of the diguanylate cyclase CdgD blocks developmental transitions and antibiotic biosynthesis in *Streptomyces coelicolor*. *Nature*, *11*(62), 1492–1505. Nature Publishing Group.

Luo, S., Sun, D., Zhu, J., Chen, Z., Wen, Y., & Li, J. (2014). An extracytoplasmic function sigma factor, σ^{25}, differentially regulates avermectin and oligomycin biosynthesis in *Streptomyces avermitilis*. *Applied Microbiology and Biotechnology*, *98*(16), 7097–7112. Springer Link.

Lutkenhaus, J., & Addinall, S. G. (1997). Bacterial cell division and the z ring. *Annual Review of Biochemistry*, *66*(1), 93–116. Annual Reviews.

Löwe, J., & Amos, L. (1998). Crystal structure of the bacterial cell-division protein FtsZ. *Nature*, *391*(6663), 203–206. Macmillan Publishers Ltd.

Ma, Z., Hu, Y., Liao, Z., Xu, J., Xu, X., Bechthold, A., & Yu, X. (2020). Cloning and Overexpression of the Toy Cluster for Titer Improvement of Toyocamycin in *Streptomyces diastatochromogenes*. *Frontiers in Microbiology*, *11*, 2074. Frontiers Media SA.

McCormick, J. R., Su, E. P., Driks, A., & Losick, R. (1994). Growth and viability of *Streptomyces coelicolor* mutant for the cell division gene *ftsZ*. *Molecular Microbiology*, *14*(2), 243–254. Wiley Online Library.

McCormick, J. R., & Flärdh, K. (2012). Signals and regulators that govern *Streptomyces* development. *FEMS Microbiology Reviews*, *36*(1), 206–231. Blackwell Publishing Ltd.

Merrick, M. J. (1976). A morphological and genetic mapping study of bald colony mutants of *Streptomyces coelicolor*. *Journal of General Microbiology*, *96*(2), 299–315. Society for General Microbiology.

Mikulík, K., Bobek, J., Bezoušková, S., Benada, O., & Kofroňvá, O. (2002). Expression of proteins and protein kinase activity during germination of aerial spores of *Streptomyces granaticolor*. *Biochemical and Biophysical Research Communications*, *299*(2), 335–342. Elsevier B.V.

Mingorance, J., Tamames, J., & Vicente, M. (2004). Genomic channeling in bacterial cell division. *Journal of Molecular Recognition*, *17*(5), 481–487. Wiley Online Library.

Muok, A. R., Claessen, D., & Briegel, A. (2020). Microbial piggy-back: how *Streptomyces* spores are transported by motile soil bacteria. *bioRxiv*. Cold Spring Harbor Laboratory.

Sánchez de la Nieta, R., Antoraz, S., Alzate, J. F., Santamaría, R. I., & Díaz, M. (2020). Antibiotic Production and Antibiotic Resistance: The Two Sides of AbrB1/B2, a Two-Component System of *Streptomyces coelicolor*. *Frontiers in Microbiology*, *11*, 2549. Frontiers Media SA.

Noens, E. E. E., Mersinias, V., Traag, B. A., Smith, C. P., Koerten, H. K., & van Wezel, G. P. (2005). SsgA-like proteins determine the fate of peptidoglycan during sporulation of *Streptomyces coelicolor*. *Molecular Microbiology*, *58*(4), 929–944. Wiley Online Library.

Nuzzo, D., Makitrynskyy, R., Tsypik, O., & Bechthold, A. (2020). Cyclic di-GMP cyclase SSFG_02181 from *Streptomyces ghanaensis* ATCC14672 regulates antibiotic biosynthesis and morphological differentiation in streptomycetes. *Scientific Reports*, *10*(1), 12021. Springer Nature.

Ohnishi, Y., Ishikawa, J., Hara, H., Suzuki, H., Ikenoya, M., Ikeda, H., Yamashita, A., Hattori, M., & Horinouchi, S. (2008). Genome Sequence of the Streptomycin-Producing Microorganism *Streptomyces griseus* IFO 13350. *Journal of Bacteriology*, *190*(11), 4050–4060. American Society for Microbiology Journals.

Orr, M. W., Donaldson, G. P., Severin, G. B., Wang, J., Sintim, H. O., Waters, C. M., & Lee, V. T. (2015). Oligoribonuclease is the primary degradative enzyme for pGpG in *Pseudomonas aeruginosa* that is required for cyclic-di-GMP turnover. *Proceedings of the National Academy of Sciences*, *112*(36), E5048–E5057. National Academy of Sciences.

Paget, M. S. B., Chamberlin, L., Atrih, A., Foster, S. J., & Buttner, M. J. (1999). Evidence that the Extracytoplasmic Function Sigma Factor σ^{E} Is Required for Normal Cell Wall Structure in *Streptomyces coelicolor* A3(2). *Journal of Bacteriology*, *181*(1), 204–211. American Society for Microbiology Journals.

Paul, R., Abel, S., Wassmann, P., Beck, A., Heerklotz, H., & Jenal, U. (2007). Activation of the Diguanylate Cyclase PleD by Phosphorylation-mediated Dimerization. *Journal of Biological Chemistry*, *282*(40), 29170–29177. ASBMB.

Paul, R., Weiser, S., Amiot, N., Chan, C., Schirmer, T., Giese, B., & Jenal, U. (2004). Cell cycle-dependent dynamic localization of a bacterial response regulator with a novel diguanylate cyclase output domain. *Genes & Development*, *18*(6), 715–727. Cold Spring Harbor Laboratory Press.

Persson, J., Chater, K. F., & Flärdh, K. (2013). Molecular and cytological analysis of the expression of *Streptomyces* sporulation regulatory gene *whiH*. *FEMS Microbiology Letters*, *341*(2), 96–105. Blackwell Publishing Ltd.

Pesavento, C., Becker, G., Sommerfeldt, N., Possling, A., Tschowri, N., Mehlis, A., & Hengge, R. (2008). Inverse regulatory coordination of motility and curli-mediated adhesion in *Escherichia coli*. *Genes & Development*, *22*(17), 2434–2446. Cold Spring Harbor Laboratory Press.

Pfiffer, V., Sarenko, O., Possling, A., & Hengge, R. (2019). Genetic dissection of *Escherichia coli*'s master diguanylate cyclase DgcE: Role of the N-terminal MASE1 domain and direct signal input from a GTPase partner system. *PLOS Genetics*, *15*(4), 1–28. Public Library of Science.

Ponting, C. P., & Aravind, L. (1997). PAS: a multifunctional domain family comes to light. *Current Biology*, *7*(11), 674–R677. Cell Press.

Pultz, I. S., Christen, M., Kulasekara, H. D., Kennard, A., Kulasekara, B., & Miller, S. I. (2012). The response threshold of *Salmonella* PilZ domain proteins is determined by their binding affinities for c-di-GMP. *Molecular Microbiology*, *86*(6), 1424–1440. Wiley Online Library.

Ramijan, K., Ultee, E., Willemse, J., Zhang, Z., Wondergem, J. A., van der Meij, A., Heinrich, D., Briegel, A., van Wezel, G. P., & Claessen, D. (2018). Stress-induced formation of cell wall-deficient cells in filamentous actinomycetes. *Nature communications*, *9*(1), 1–13. Nature Publishing Group.

Rao, F., Yang, Y., Qi, Y., & Liang, Z.-X. (2008). Catalytic Mechanism of Cyclic Di-GMP-Specific Phosphodiesterase: a Study of the `EAL` Domain-Containing RocR from *Pseudomonas aeruginosa*. *Journal of Bacteriology*, *190*(10), 3622–3631. American Society for Microbiology Journals.

Richter, A. M., Possling, A., Malysheva, N., Yousef, K. P., Herbst, S., von Kleist, M., & Hengge, R. (2020). Local c-di-GMP Signaling in the Control of Synthesis of the *E. coli* Biofilm Exopolysaccharide pEtN-Cellulose. *Journal of Molecular Biology*, *432*(16), 4576–4595. Elsevier B.V.

Rigali, S., Anderssen, S., Naômé, A., & van Wezel, G. P. (2018). Cracking the regulatory code of biosynthetic gene clusters as a strategy for natural product discovery. *Biochemical Pharmacology*, *153*, 24–34. Elsevier B.V.

Ross, P., Mayer, R., & Benziman, M. (1991). Cellulose biosynthesis and function in bacteria. *Microbiology and Molecular Biology Reviews*, *55*(1), 35–58. American Society for Microbiology Journals.

Ross, P., Weinhouse, H., Aloni, Y., Michaeli, D., Weinberger-Ohana, P., Mayer, R., Braun, S., de Vroom, E., van der Marel, G., van Boom, J., & Benziman, M. (1987). Regulation of cellulose synthesis in *Acetobacter xylinum* by cyclic diguanylic acid. *PLOS ONE*, *325*(6101), 1–7. Public Library of Science.

Ruddick, S., & Williams, S. (1972). Studies on the ecology of actinomycetes in soil V. Some factors influencing the dispersal and adsorption of spores in soil. *Soil Biology and Biochemistry*, *4*(1), 93–103. Elsevier B.V.

Ryjenkov, D. A., Simm, R., Römling, U., & Gomelsky, M. (2006). The PilZ Domain Is a Receptor for the Second Messenger c-di-GMP: the PilZ Domain Protein YcgR Controls Motility in Enterobacteria. *Journal of Biological Chemistry*, *281*(41), 30310–30314. ASBMB.

Römling, U., Galperin, M. Y., & Gomelsky, M. (2013). Cyclic di-GMP: the First 25 Years of a Universal Bacterial Second Messenger. *Microbiology and Molecular Biology Reviews*, *77*(1), 1–52. American Society for Microbiology Journals.

Sambrook, J., Fritsch, E. F., & Maniatis, T. (1989). *Molecular cloning: a laboratory manual*. N.Y.: Cold Spring Harbor Laboratory, Cold Spring Harbor.

Sarenko, O., Klauck, G., Wilke, F. M., Pfiffer, V., Richter, A. M., Herbst, S., Kaever, V., & Hengge, R. (2017). More than Enzymes That Make or Break Cyclic Di-GMP—Local Signaling in the Interactome of `GGDEF/EAL` Domain Proteins of *Escherichia coli*. *mBio*, *8*(5). American Society for Microbiology.

Schirmer, T. (2016). C-di-GMP Synthesis: Structural Aspects of Evolution, Catalysis and Regulation. *Journal of Molecular Biology*, *428*(19), 3683–3701. Elsevier B.V.

Schirmer, T., & Jenal, U. (2009). Structural and mechanistic determinants of c-di-GMP signalling. *Nature Reviews Microbiology*, *10*(7), 724–35. Macmillan Publishers Limited.

Schlimpert, S., Wasserstrom, S., Chandra, G., Bibb, M. J., Findlay, K. C., Flärdh, K., & Buttner, M. J. (2017). Two dynamin-like proteins stabilize FtsZ rings during *Streptomyces* sporulation. *Proceedings of the National Academy of Sciences*, *114*(30), E6176–E6183. National Academy of Sciences.

Schumacher, M., Bush, M., Bibb, M., Ramos-León, F., Chandra, G., Zeng, W., & Buttner, M. (2018). The crystal structure of the RsbN–σ^{BldN} complex from *Streptomyces venezuelae* defines a new structural class of anti-σ factor. *Nucleic Acids Research*, *46*(14), 7405–7417. Oxford University Press.

Schumacher, M., Zeng, W., Findlay, K., Buttner, M., Brennan, R., & Tschowri, N. (2017). The *Streptomyces* master regulator BldD binds c-di-GMP sequentially to create a functional BldD_2-$(\text{c-di-GMP})_4$ complex. *Nucleic Acids Research*, *45*(11), 6923–6933. Oxford University Press.

Seipke, R. F., Kaltenpoth, M., & Hutchings, M. I. (2012). *Streptomyces* as symbionts: an emerging and widespread theme? *FEMS Microbiology Reviews*, *36*(4), 862–876. Blackwell Publishing Ltd.

Sexton, D. L., & Tocheva, E. I. (2020). Ultrastructure of Exospore Formation in *Streptomyces* Revealed by Cryo-Electron Tomography. *Frontiers in Microbiology*, *11*, 2378. Frontiers Media SA.

Shyp, V., Dubey, B. N., Böhm, R., Hartl, J., Nesper, J., Vorholt, J. A., Hiller, S., Schirmer, T., & Jenal, U. (2020). Reciprocal growth control by competitive binding of nucleotide second messengers to a metabolic switch in *Caulobacter crescentus*. *Nature Microbiology*, (pp. 1–14). Nature Publishing Group.

Sievers, F., Wilm, A., Dineen, D., Gibson, T. J., Karplus, K., Li, W., Lopez, R., McWilliam, H., Remmert, M., Söding, J., Thompson, J. D., & Higgins, D. G. (2011). Fast, scalable generation of high-quality protein multiple sequence alignments using Clustal Omega. *Molecular Systems Biology*, *7*(1), 539. EMBO and Macmillan Publishers Limited.

Som, N. F., Heine, D., Holmes, N., Knowles, F., Chandra, G., Seipke, R. F., Hoskisson, P. A., Wilkinson, B., & Hutchings, M. I. (2017a). The MtrAB two-component system controls antibiotic production in *Streptomyces coelicolor* A3(2). *Microbiology*, *163*(10), 1415–1419. Microbiology Society.

Som, N. F., Heine, D., Holmes, N. A., Munnoch, J. T., Chandra, G., Seipke, R. F., Hoskisson, P. A., Wilkinson, B., & Hutchings, M. I. (2017b). The Conserved Actinobacterial Two-Component System MtrAB Coordinates Chloramphenicol Production with Sporulation in *Streptomyces venezuelae* NRRL B-65442. *Frontiers in Microbiology*, *8*, 1145. Frontiers Media SA.

Strakova, E., Bobek, J., Zikova, A., & Vohradsky, J. (2013). Global Features of Gene Expression on the Proteome and Transcriptome Levels in *S. coelicolor* during Germination. *PLOS ONE*, *8*(9), 1–14. Public Library of Science.

Sudarsan, N., Lee, E. R., Weinberg, Z., Moy, R. H., Kim, J. N., Link, K. H., & Breaker, R. R. (2008). Riboswitches in Eubacteria Sense the Second Messenger Cyclic Di-GMP. *Science*, *321*(5887), 411–413. American Association for the Advancement of Science.

Sun, D., Liu, C., Zhu, J., & Liu, W. (2017). Connecting Metabolic Pathways: Sigma Factors in *Streptomyces* spp. *Frontiers in Microbiology*, *8*, 2546. Frontiers Media SA.

Tao, W., Yang, A., Deng, Z., & Sun, Y. (2018). CRISPR/Cas9-Based Editing of *Streptomyces* for Discovery, Characterization, and Production of Natural Products. *Frontiers in Microbiology*, *24*(9), 1660. Frontiers Media SA.

Tarutina, M., Ryjenkov, D. A., & Gomelsky, M. (2006). An Unorthodox Bacteriophytochrome from *Rhodobacter sphaeroides* Involved in Turnover of the Second Messenger c-di-GMP. *Journal of Biological Chemistry*, *281*(46), 34751–34758. ASBMB.

Tenconi, E., Traxler, M. F., Hoebreck, C., van Wezel, G. P., & Rigali, S. (2018). Production of Prodiginines Is Part of a Programmed Cell Death Process in *Streptomyces coelicolor*. *Frontiers in Microbiology*, *9*, 1742. Frontiers Media SA.

Tran, N. T., Den Hengst, C. D., Gomez-Escribano, J. P., & Buttner, M. J. (2011). Identification and Characterization of CdgB, a Diguanylate Cyclase Involved in Developmental Processes in *Streptomyces coelicolor*. *Journal of Bacteriology*, *193*(12), 3100–3108. American Society for Microbiology Journals.

Tschowri, N. (2016). Cyclic Dinucleotide-Controlled Regulatory Pathways in *Streptomyces* Species. *Journal of Bacteriology*, *198*(1), 47–54. American Society for Microbiology Journals.

Tschowri, N., Schumacher, M. A., Schlimpert, S., Chinnam, N. B., Findlay, K. C., Brennan, R. G., & Buttner, M. J. (2014). Tetrameric c-di-GMP Mediates Effective Transcription Factor Dimerization to Control *Streptomyces* Development. *Cell*, *158*(5), 1136–1147. CellPress.

Tsirigos, K. D., Peters, C., Shu, N., Käll, L., & Elofsson, A. (2015). The TOPCONS web server for consensus prediction of membrane protein topology and signal peptides. *Nucleic Acids Research*, *43*(W1), W401–W407. Oxford University Press.

Ueda, K., Takano, H., Nishimoto, M., Inaba, H., & Beppu, T. (2005). Dual Transcriptional Control of amfTSBA, Which Regulates the Onset of Cellular Differentiation in *Streptomyces griseus*. *Journal of Bacteriology*, *187*(1), 135–142. American Society for Microbiology Journals.

Ultee, E., van der Aart, L. T., Zhang, L., van Dissel, D., Diebolder, C. A., van Wezel, G. P., Claessen, D., & Briegel, A. (2020). Teichoic acids anchor distinct cell wall lamellae in an apically growing bacterium. *Communications biology*, *3*(314), 1. Nature publishing group.

Valentini, M., & Filloux, A. (2019). Multiple Roles of c-di-GMP Signaling in Bacterial Pathogenesis. *Annual Review of Microbiology*, *73*(1), 387–406. Annual Reviews.

Vasilchenko, A. S., Julian, W. T., Lapchinskaya, O. A., Katrukha, G. S., Sadykova, V. S., & Rogozhin, E. A. (2020). A Novel Peptide Antibiotic Produced by *Streptomyces roseoflavus* Strain INA-Ac-5812 With Directed Activity Against Gram-Positive Bacteria. *Frontiers in Microbiology*, *11*, 2213. Frontiers Media SA.

Vollmer, B., Steblau, N., Ladwig, N., Mayer, C., Macek, B., Mitousis, L., Sigle, S., Walter, A., Wohlleben, W., & Muth, G. (2019). Role of the Streptomyces spore wall synthesizing complex SSSC in differentiation of *Streptomyces coelicolor* A3(2). *International Journal of Medical Microbiology*, *309*(6), 151327. Elsevier B.V.

Vurukonda, S. S. K. P., Giovanardi, D., & Stefani, E. (2018). Plant Growth Promoting and Biocontrol Activity of *Streptomyces* spp. as Endophytes. *International Journal of Molecular Sciences*, *19*(4), 952. MDPI.

Weber, H., Pesavento, C., Possling, A., Tischendorf, G., & Hengge, R. (2006). Cyclic-di-GMP-mediated signaling within the σ^{S} network of *Escherichia coli*. *Molecular Microbiology*, *62*, 1014–1034. Wiley Online Library.

Willemse, J., Borst, J. W., de Waal, E., Bisseling, T., & van Wezel, G. P. (2011). Positive control of cell division: FtsZ is recruited by SsgB during sporulation of *Streptomyces*. *Genes & Development*, *25*(1), 89–99. Cold Spring Harbor Laboratory Press.

Willey, J., Santamaria, R., Guijarro, J., Geistlich, M., & Losick, R. (1991). Extracellular complementation of a developmental mutation implicates a small sporulation protein in aerial mycelium formation by *S. coelicolor*. *Cell*, *65*(4), 641–650. Elsevier.

Wright, E. S., & Vetsigian, K. H. (2019). Stochastic exits from dormancy give rise to heavy-tailed distributions of descendants in bacterial populations. *Molecular Ecology*, *28*(17), 3915–3928. Wiley Online Library.

Xiao, J., & Goley, E. D. (2016). Redefining the roles of the FtsZ-ring in bacterial cytokinesis. *Current Opinion in Microbiology*, *34*, 90–96. Elsevier B.V.

Yagüe, P., Willemse, J., Koning, R. I., Rioseras, B., López-García, M. T., Gonzalez-Quinonez, N., Lopez-Iglesias, C., Shliaha, P. V., Rogowska-Wrzesinska, A., Koster, A. J., et al. (2016). Subcompartmentalization by cross-membranes during early growth of *Streptomyces* hyphae. *Nature Communications*, *7*, 12467. Springer Nature.

Yan, H., Lu, X., Sun, D., Zhuang, S., Chen, Q., Chen, Z., Li, J., & Wen, Y. (2020). BldD, a master developmental repressor, activates antibiotic production in two *Streptomyces* species. *Molecular Microbiology*, *113*(1), 123–142. Wiley Online Library.

Yan, L., Zhang, Q., Virolle, M.-J., & Xu, D. (2017). In conditions of over-expression, WblI, a WhiB-like transcriptional regulator, has a positive impact on the weak antibiotic production of *Streptomyces lividans* TK24. *PLOS ONE*, *12*(3), 1–16. Public Library of Science.

Yang, W., Willemse, J., Sawyer, E., Lou, F., Gong, W., Zhang, H., Gras, S., Claessen, D., & Perrett, S. (2017). The propensity of the bacterial rodlin protein RdlB to form amyloid fibrils determines its function in *Streptomyces coelicolor*. *Scientific Reports*, *17*(7), 42867. Springer Nature.

Zähringer, F., Lacanna, E., Jenal, U., Schirmer, T., & Boehm, A. (2013). Structure and signaling mechanism of a zinc-sensory diguanylate cyclase. *Structure*, *21*(7), 1149–1157. Elsevier.

Selbstständigkeitserklärung

Hiermit versichere ich, dass ich die vorliegende Arbeit selbstständig und lediglich auf der Grundlage der angegebenen Hilfsmittel und Hilfen angefertigt habe.

Ich versichere, dass ich die Grundsätze der Humboldt-Universität zu Berlin zur Sicherung guter wissenschaftlicher Praxis eingehalten habe.

Ich versichere, dass ich mich weder anderwärts um einen Doktorgrad beworben habe noch einen entsprechenden Doktorgrad besitze.

Ich versichere, dass diese Dissertation oder Teile davon nicht bereits bei einer anderen wissenschaftlichen Einrichtung eingereicht, angenommen oder abgelehnt wurden.

Ich versichere, dass keine Zusammenarbeit mit gewerblichen Promotionsberatern stattfand.

Ich versichere, dass ich die dem angestrebten Verfahren zugrunde liegende Promotionsordnung zur Kenntnis genommen habe.

.....

Datum/ Unterschrift